STATISTICAL ANALYSIS OF SINGLE NANOPARTICLE CATALYSIS

A Dissertation

Presented to the Faculty of the Graduate School

of Cornell University

in Partial Fulfillment of the Requirements for the Degree of

Doctor of Philosophy

by

Maicol Arley Ochoa Daza

August 2012

STATISTICAL ANALYSIS OF SINGLE NANOPARTICLE CATALYSIS

Maicol Arley Ochoa Daza, Ph.D.

Cornell University 2012

Single-molecule fluorescence spectroscopy is nowadays one of the most robust experimental techniques when one is to measure local fluctuations of individual molecules. The Chen group at Cornell University has been able to adapt this technique to detect catalytic transformations of resazurin into resorufin on the surface of a single gold nanoparticle. In this experiment, the emission intensity of a single nanoparticle is recorded as a function of time. This trajectory is intrinsically stochastic and two distinct states of different emission intensity are detected. Every state shows random dwell times that are multiexponentially distributed and their mean values depend on the substrate concentration, exhibiting saturation. In addition, memory effects are detected as dwell times are correlated.

In this work we have investigated the chemical basis of the dynamical complexity and the stochastic nature of this system under saturating conditions. To this goal, we have defined constrained mean dwell times and, by studying the difference between constrained and unconstrained mean dwell times, we have found that each active site undergoes internal dynamics, fluctuating among several substates. We have also found that active sites on the surface of a nanoparticle are spatially correlated and, therefore, their fluctuations are correlated. We have also determined that fast activation processes occur through the same reaction path as slow product desorptions, and vice versa. We have obtained a further insight into the internal dynamics of each active site by studying dwell-

time correlation functions. In this way, we demonstrated that every active site fluctuates among no less than three internal substates and, therefore, catalytic transformations occur through no less than three distinct reaction paths. We found that the decay rates of the autocorrelation functions are relative measures of the time scales of two distinct internal processes. For a gold nanoparticle of 6 nm diameter, the time scales of the internal fluctuations are at least one order of magnitude smaller that the time scales of the activation and product desorption processes. We also demonstrated that constrained mean dwell times, together with the dwell-time correlation functions, form a minimum set of statistical indicators that can qualitatively characterize the kinetic mechanism of the catalytic transformations on the nanoparticle surface, including fluctuations and spatial correlation among active sites.

BIOGRAPHICAL SKETCH

Maicol Arley Ochoa Daza was born in Bogotá, Colombia, on March 21st 1983. He obtained a Bachelors in Science with concentration in Chemistry from the Universidad Nacional de Colombia, and a Master of Science with concentration in Mathematics from the same institution. He was admitted in 2007 to the Ph.D program in Chemistry and Chemical Biology at Cornell University and he finished his studies in 2012.

dedicado a Natalia Ochoa

ACKNOWLEDGEMENTS

Foremost, I would like to express my deep gratitude to my adviser Professor Roger Loring, whose encouragement and dedication motivated me to do research in theoretical chemistry. The many discussions with him enlightened me and helped me to overcome the obstacles that I confronted during my graduate research.

I am especially grateful to Professor Peng Chen for his support, guidance and helpful suggestions. He has provided insightful discussions which helped me to define some of my research goals.

I would like to thank Professor Gregory Ezra and Professor Garnet Chan for serving as members of my special committee. I really enjoyed the classes that I took with them and the intellectually stimulating interactions that we had.

I am thankful to the faculty and friends who I met during my time at Cornell. It has been a great privilege to spend several years in the Department of Chemistry and Chemical Biology.

I also want to thank my family and friends for their support during my studies.

Finally, I want to acknowledge support from the National Science Foundation (NSF) through the grants No. CHE0413992 and No. CHE0743299.

TABLE OF CONTENTS

LIST OF FIGURES

CHAPTER 1

ELEMENTS OF SINGLE-MOLECULE KINETIC THEORY

1.1 Single-molecule studies

About twenty years ago, efforts to follow chemical reactions in condensed phases on a single molecule basis became successful. First, Moerner and Kador[34] observed the optical-absorption spectrum of single dopant molecules of pentacene in a p-terphenyl host crystal at liquid-helium temperatures. About the same time, Orrit and Bernard[36] found that, at cryogenic conditions, narrow peaks in the fluorescence-excitation spectrum of a pentacene-doped p-terphenyl crystal stem were generated by single molecules. After this, with the work of Xie [48, 30, 28, 29], Betzig and Chichester[7], Macklin et. al. [31], Ambrose et. al. [2] and others, it became possible to measure the fluorescence emission of individual molecules at room temperature. Around the same time, different techniques for single-molecule manipulation were developed by Ashkin, Dziedzic, Bjorkholm and Chu [3]; Block et al [8]; Smith, Cui and Bustamante [41] and many others. These advancements in the manipulation and detection of individual molecules opened the door to the study of new phenomena that were not accessible by traditional ensemble experiments. In particular Lu, Xun and Xie[29] were able to follow, for the first time, catalytic transformations by a single enzyme as a function of time. This led to the kinetic study of conformational dynamics in enzymes, as well as their subtle differences in catalytic activity: single-molecule enzymology was born. In 2008 Chen and coworkers[51, 49, 11, 52], were able to study the catalytic activity of gold nanoparticles by means of single-molecule fluorescence

spectroscopy. Afterwards, Chen and coworkers have expanded their results to the study of nanoparticle-size effects on the catalytic properties[58], nanoscale electrocatalysis[40], single-nanorod catalysis[57] and catalysis on single silver nanoparticles[21].

Along with the appearance of new experiments, better and novel physical theories are needed. Single-molecule studies have motivated a different sort of chemical kinetics that studies fluctuations instead of ensemble means. To mention a few achievements, Brown [9] and later with Peng, Xie and Zheng[37] have been able to interpret the statistics of the emission of single photons by means of the generating function formalism for single-molecule spectroscopy. Vlad, Moran, Schneider and Ross [45] have studied memory effects and oscillations in single-molecule kinetics for systems with two chemical states by means of correlation functions of the fluorescent signal. In their work they discuss the possible cause of chemical oscillations in single molecule kinetics, showing that the intrinsic dynamics of the molecule, expressed by the fluctuations of the control parameters, may lead to damped oscillations of the correlation functions of the fluorescent signal. Flomenbom and Silbey [17] have introduced a procedure that classifies kinetic schemes that are equivalent in the statistical properties of the single-molecule signal. This procedure partitions the space of kinetic schemes into canonical forms, which constitutes a powerful tool in discriminating among kinetic schemes. Gopich and Szabo[22, 19, 20] have analyzed data from single molecule fluorescence and force spectroscopy experiments from a theoretical perspective, concentrating on the distribution of the number of transitions during a fixed observation time, the distribution of times between transitions, and the corresponding correlation functions. They are able to show how these quantities are related to each other, and their formalism is illustrated by

a detailed analysis of the statistics of catalytic turnovers of enzymes. Taylor, Makarov and Landes [44] developed a method to separete noise and signal in single-molecule fluorescence resonance energy trajectories using wavelet detail thresholding and Bayesian inference. Fisher and Kolomeisky[16, 15] have employed continuum ratchet concepts in the description of motor-protein dynamics, concentrating on discrete kinetic and stochastic models to predict the mean velocity and other observables as a function of an imposed load force, the ATP concentration, and other variables. Akimov and Kolomeisky [26, 1] have used coarse-grained molecular dynamics to analyze single-molecule dynamics of artificial molecular motors and molecular rotors. Cao [10] has defined n-channel models to describe the complexity of single molecule processes, investigating the multiexponential behavior observed in the frequency distribution functions of single fluorescence trajectories. Quantitative measurements of memory effects were initially studied by Cao by means of dwell-time correlation functions[54, 10, 46], intensity correlation functions [46] and also through the number density of single-molecule sequences[55].

While we have witnessed the appearance of many new ideas intended to better explain single molecule measurements, we found that no physical theory is in place to the describe the complete set of observations and phenomena discovered in single nanoparticle catalysis[51, 49, 11, 52]. We find, though, that the conceptual framework of single enzyme catalysis provides a good starting point to build up the physical ideas that at the end will describe the additional complications that catalysis by individual nanoparticles exhibits. To better pose the main questions in Sec. 1.3 that have motivated our study, we will explore in detail the experimental findings of Chen and coworkers [51, 49, 11, 52, 58]. Along with this discussion in Sec. 1.2, we will introduce the basic statistical tools that

are typically employed to extract the physical mechanism responsible for the trajectories observed in single-molecule fluorescence. After, in Sec. 1.4 we will elaborate on the mathematical aspects that have been used to describe single enzyme catalysis, as they will also apply to single nanoparticle catalysis.

1.2 Single nanoparticle catalysis

Chen and coworkers have been successful in studying the catalytic transformation of rezasurin to resorufin, in the presence of NH_2OH and on the surface of gold nanoparticles, by means of single-molecule fluorescence spectroscopy[51]. In their experiments, gold nanoparticles are immobilized on an amine-functionalized, positively charged glass surface. The dispersion of the gold nanoparticles is such that the probability of finding two gold nanoparticles in a square of $1\mu m^2$ area is less than 0.06%. As a solution of substrate molecules (rezasurin) flows over the glass surface with many fixed nanoparticles, the fluorescence intensity signal can be recorded as a function of time. Figure 1.1 presents in a rather simple form the experimental system just described. The wavelength of fluorescence detection is 532 nm and the consistent height of the high level signal indicates that each fluorescence burst comes from a single resorufin molecule. Figure 1.2 is a representation of a typical fluorescence trajectory for this system. In these experiments, the concentration of the reducing agent is fixed to 1 mM. Product formation on the nanoparticle surface appears as an instantaneous increase in the fluorescence signal. A product dissociation from the nanoparticle surface appears as an instantaneous signal decrease. A turnover is any part of the trajectory, starting at a sudden change in the fluorescence intensity, that completes a cycle in the trajectory.

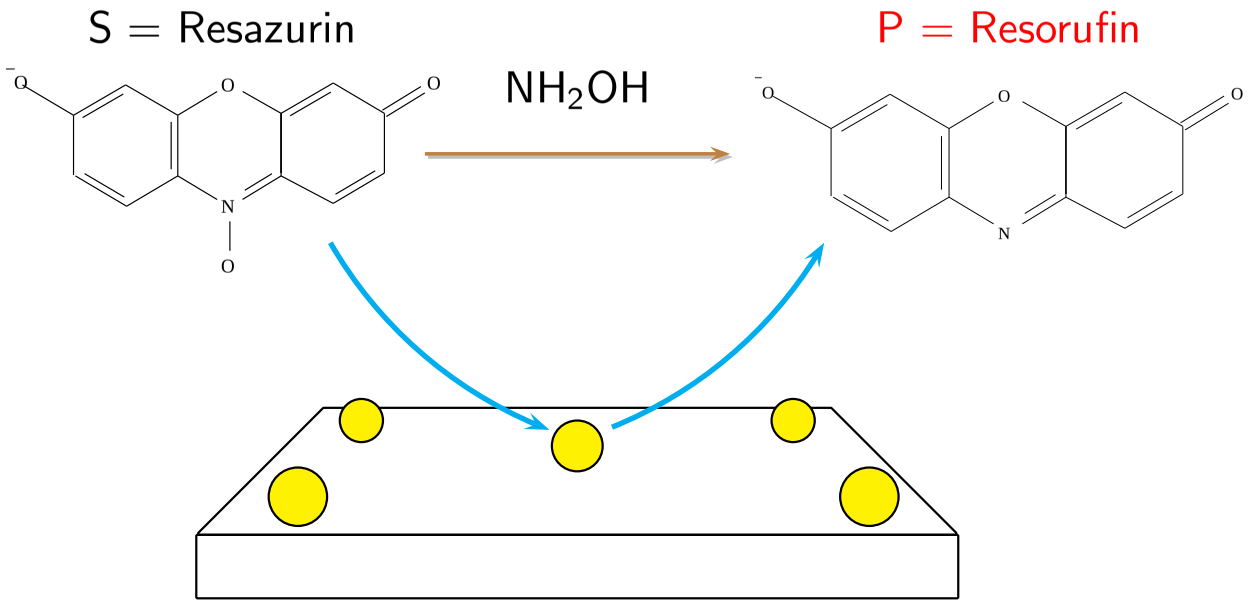

Figure 1.1: Schematic representation of the experimental system studied by Chen and coworkers [51]. Gold nanoparticles are immobilized on an amine-functionalized glass surface, such that they are separated. A solution of rezasurin flows over the nanoparticles, they are adsorbed and transform into resorufin (a fluorescent molecule) on the nanoparticle surface. The reaction occurs in the presence of NH_2OH. Product molecules are eventually desorbed. The fluorescence intensity signal is recorded as a function of time at a given point.

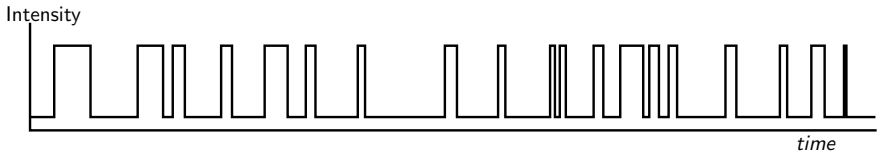

Figure 1.2: A representation of a fluorescence trajectory for transformation of rezasurin to resorufin in a single nanoparticle, after a threshold value in the intensity has been set to determine the high intensity signal and after the background noise has been suppressed. Two different states, one of low intesity and one of high intensity can be differentiated. The dwell times for each state are stochastic.

Several important characteristics of nanoparticles as heterogeneous catalysts are revealed from the inspection of these trajectories. It has been found that for about 1 % of the trajectories, the fluorescence bursts show multiple intensity levels. This indicates the existence of either multiple catalytic sites that can undertake catalysis simultaneously or, docking sites where resorufin molecules can be adsorbed before they are finally desorbed. On the other hand, the number of these multilevel events is very rare and, as an analysis of density of states reveals, we can clearly identify two different states corresponding to different fluorescence intensities. We will refer to the state with low intensity in the fluorescence signal as the *Dark or D* state while the state with high intensity in the fluorescence signal will be called the *Light or L* state. Associated with either of these states one can define their *dwell times*. The time t_D between a sudden decrease and the next sudden increase in the flourescence intensity is a dark dwell time. Similarly, the time t_L between a sudden increase and the next decrease in the intensity is a light dwell time.

One can immediately observe that the dark and light dwell times are stochas-

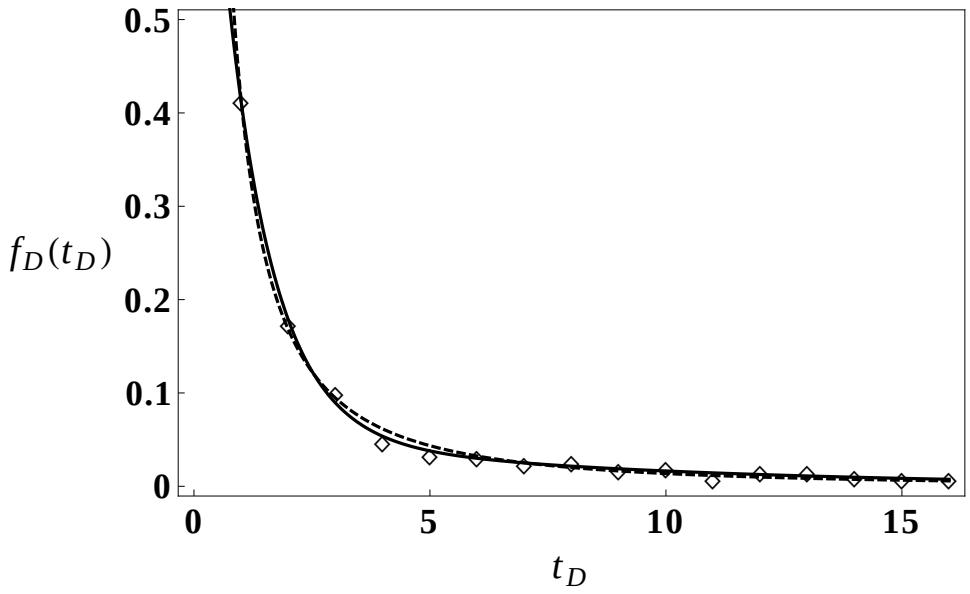

Figure 1.3: Dark-dwell-time density function for a typical fluorescence trajectory for a catalytic transformation on the surface of a single nanoparticle. Experimental data is represented by rhombuses, a biexponential fitting is presented in the solid line and stretched exponential fitting is represented by the dashed line. The form of the biexponential fitted to the experimental data is $0.06\exp(-0.13t_D) + 0.98\exp(-1.00138t_D)$. The form of the stretched exponential fitted to the experimental data is $1.23 \times 10^3 \exp(-8t_D^{0.15})$. Time is given in seconds.

tic variables and we may wonder about the origin of this randomness. In contrast to traditional ensemble kinetic studies, at the single molecule level local fluctuations in the environment can lead to significant differences in the instant dynamical properties. Perhaps the best example of how fluctuations can bring into a stochastic regime a system that is seemingly deterministic is the Brownian motion. In that case, local fluctuations in the location of the molecules surrounding a relatively small cluster of molecules, can instantly take this aggregate out of the equilibrium position to a new place in space. Fluctuations in the local environment are undetectable in ensemble experiments, as they have

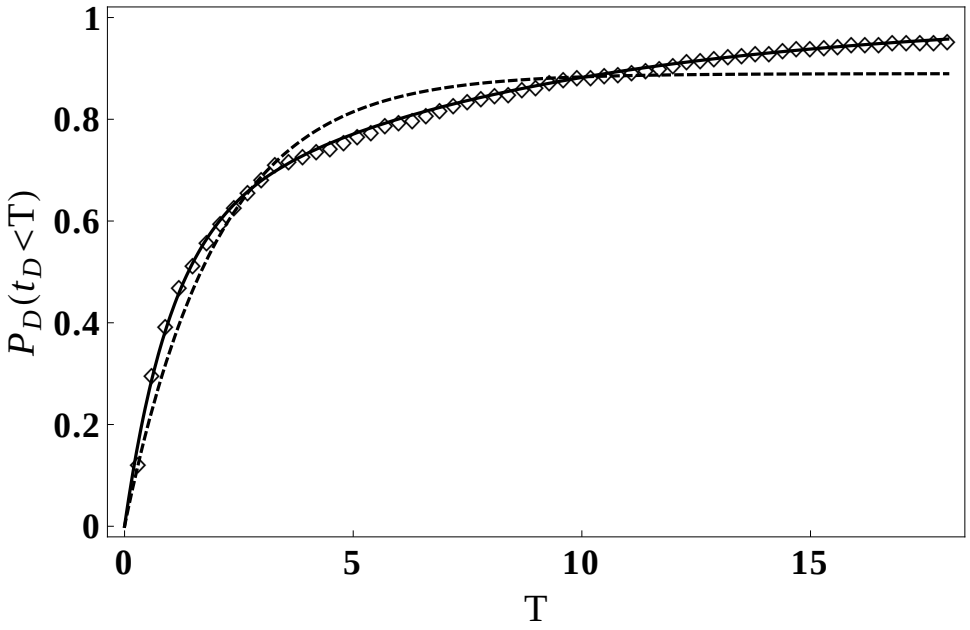

Figure 1.4: Dark-dwell-time cumulative distribution for a typical fluorescence trajectory for a catalytic transformation on the surface of a single nanoparticle. Experimental data is represented by rhombuses, a biexponential fitting is presented in the solid line and the monoexponential fitting is represented by the dashed line. The form of the biexponential fitted to the experimental data is $0.44(1 - \exp(-0.11t_D)) + 0.59(1 - \exp(-0.97t_D))$. The form of the monoexponential fitted to the experimental data is $0.89\exp(-0.495t_D)$. Time is given in seconds.

a mean of zero after averaging over the whole ensemble. This averaging does not take place in a single molecule experiment, and one can expect to see the influence of these fluctuations in the local dynamics. This, of course, provides an advantage and a new challenge. Single molecule experiments open the door to a more systematic understanding of these fluctuations and their effect on dynamics. What the nature of these fluctuations is, depends on the system under study.

We can better characterize the stochastic nature of the set of dwell times for the dark or the light state by calculating their density functions and the mo-

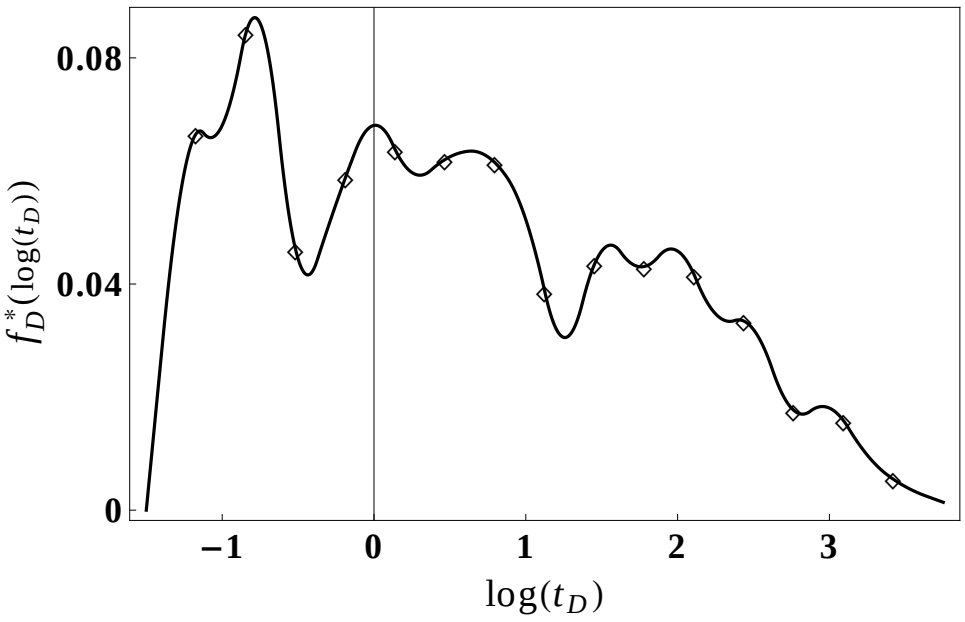

Figure 1.5: Density function for the natural logarithm of the dark dwell times for a typical fluorescence trajectory for a catalytic transformation on the surface of a single nanoparticle. Experimental data is represented by rhombus, as the solid line is a simple interpolation line. Time is given in seconds.

ments associated with them. Experimentally, density functions are obtained from the histogram of dwell times. Figure 1.3 shows the experimental density function for the dark dwell times of the trajectory studied by Xu and Chen[51]. The bin size selected to partition the time line was 1 s, and the value reported at $t_i = 1, \ldots,$ is the ratio of the total number of dwell times that are smaller than t_i and at the same time greater than $t_i - 1$. Fitting these data by a least-squares minimization shows that the density function for the dark dwell times cannot be described by a single exponential function. Instead, a better description of the experimental data is obtained with a biexponential function or with a stretched exponential function. In Fig. 1.3 these fittings are represented by a solid and a dashed line, respectively. This is a noticeable fact, as it is the first indicator of dynamic complexity and internal structure. Before we introduce the ideas

that will support this statement, it is possible to suggest the existence of this complexity by comparing the density function observed with that of a Poisson process. A Poisson variable is a random variable characterized by a monoexponential density function

$$f^{Poisson}(t) = \lambda e^{-\lambda t}, \tag{1.1}$$

for λ positive real[14]. From any density function $f(t)$ one can obtain the cumulative distribution by integration

$$P(t < T) = \int_0^T f(t)dt, \tag{1.2}$$

from which we can derive the relation

$$\frac{dP(t < T)}{dT} = f(T). \tag{1.3}$$

Equation (1.3) tells us that we can derive the density function by solving a differential equation, which presumably also describes the dynamical evolution of our system, as it depends on the statistical properties of the dwell times. The density function for a Poisson process in Eq. (1.1) is the solution of a simple differential equation that is characteristic of systems with very simple dynamics, such us a unimolecular reaction that occurs in one single step. The cumulative distribution of dark dwell times $P(t_D < T)$ is presented in Fig. 1.4 and it is contrasted against monoexponential and a biexponential fits. Cumulative distributions have the nice property that, when calculated from experimental data, the error due to the bin size selected is suppressed, and the T parameter can be varied continuously to obtain as many points as required for a better fitting. We can again state that a biexponential function is an appropriate functional form for the density.

There are other indicators that can be calculated from this trajectory that indicate the existence of dynamical complexity. One of them is the randomness

parameter that has been used in the study of ion channels[30, 39]. This quantity is defined as the ratio between the variance[1] and the square of the mean of a random variable. The first and second moments of the density function in Eq. (1.1) are λ^{-1} and λ^{-2}, respectively. As a consequence, the randomness parameter of this distribution equals 1. On the contrary, we observe that the set of dark dwell times has a variance of $36.7s^2$ and a mean of $3.87s$, and also the set of light dwell times has a variance of $0.36s^2$ and a mean of $0.53s$. Therefore they have a randomness parameter that is different from one supporting the idea that a monoexponential function does not describe the stochastic properties of these dwell times.

Transforming dwell times into new variables can also reveal information that may be encrypted in the experimental trajectory. In this way Xu, Kong and Chen [49] were able to identify two different populations of active sites by studying the variances of t_L^{-1} and t_D^{-1}. Another way to see the multiexponential nature of t_D is achieved by studying the random variable $u_D = \log t_D$. Figure 1.5 shows the frequency plot for the u_D values. Since $P(t_D < T) = P(\log t_D < \log T)$, we can derive the expression for the density function $f^*(u_D)$ for u_D, using Eq. (1.3) and the chain rule. As a result, if $f(t_D)$ is given by Eq. (1.1) then

$$f^{Poisson\,*}(u_D) = e^{u_D}\lambda e^{-\lambda e^{u_D}}, \tag{1.4}$$

and for a multiexponential density function in t_D we will have that $f^*(u)$ is a linear combination of functions of the form in Eq. (1.4). For the set of experimental t_D we find that for the density function of u_D, a linear combination of *three* functions of the form in Eq. (1.4) is required to have good qualitative agreement with the experimental data. Equation (1.4) has a gaussian-like form with only

[1]The variance of is given by the difference between the mean value of t^2 and the square of the mean value of t.

one maximum and we can differentiate three local maxima.

The experimental trajectory in consideration was recorded for a substrate concentration $[S]$ of 1.2 μM [51]. By studying similar trajectories at different concentrations[51], it was possible to determine that both the mean dark dwell time and the mean light dwell time depend on the concentration following a Langmuir - Hinshelwood mechanism[51, 50]. In fact, the mean values of t_D and t_L, $\bar{t}_D$ and $\bar{t}_L$, exhibit saturation kinetics similar to the one observed for the same quantities in single-molecule enzymology[30]. More precisely,

$$\frac{1}{\bar{t}_D} = \frac{c_1[S]}{c_2 + [S]}, \tag{1.5}$$

$$\frac{1}{\bar{t}_L} = \frac{c_3[S]}{c_4 + [S]}, \tag{1.6}$$

where the constants c_1, c_2, c_3 and c_4 are given in terms of the rate constants of the kinetic model proposed by Xu, Kong and Chen [51]. Independent of the explicit form of these constants, Eqs. (1.5) and (1.6) show that these mean values achieve a substrate-independent value for a large value of $[S]$, in which case we say that the system is in saturating conditions. The concentration of $1.2\mu M$ of rezasurin is a saturating concentration for gold nanoparticles of 6 nm diameter.

Another interesting characteristic of the fluorescence trajectories is that they exhibit memory: dark dwell times as well as light dwell times are autocorrelated[51]. The experimental correlation plots for this trajectory are presented in Fig. 1.6. Here C_D denotes the dark-dwell-time correlation function, C_L the one corresponding to light dwell times and, C_{LD} and C_{DL} are the crosscorrelation functions. We observe that, first, C_D and C_L are positive and decay with different rates. Also, C_{LD} and C_{DL} are very close to zero and we can say that t_D and t_L are uncorrelated. What exactly these observations about the correlation functions mean, in terms of the chemical and physical properties of the nanopar-

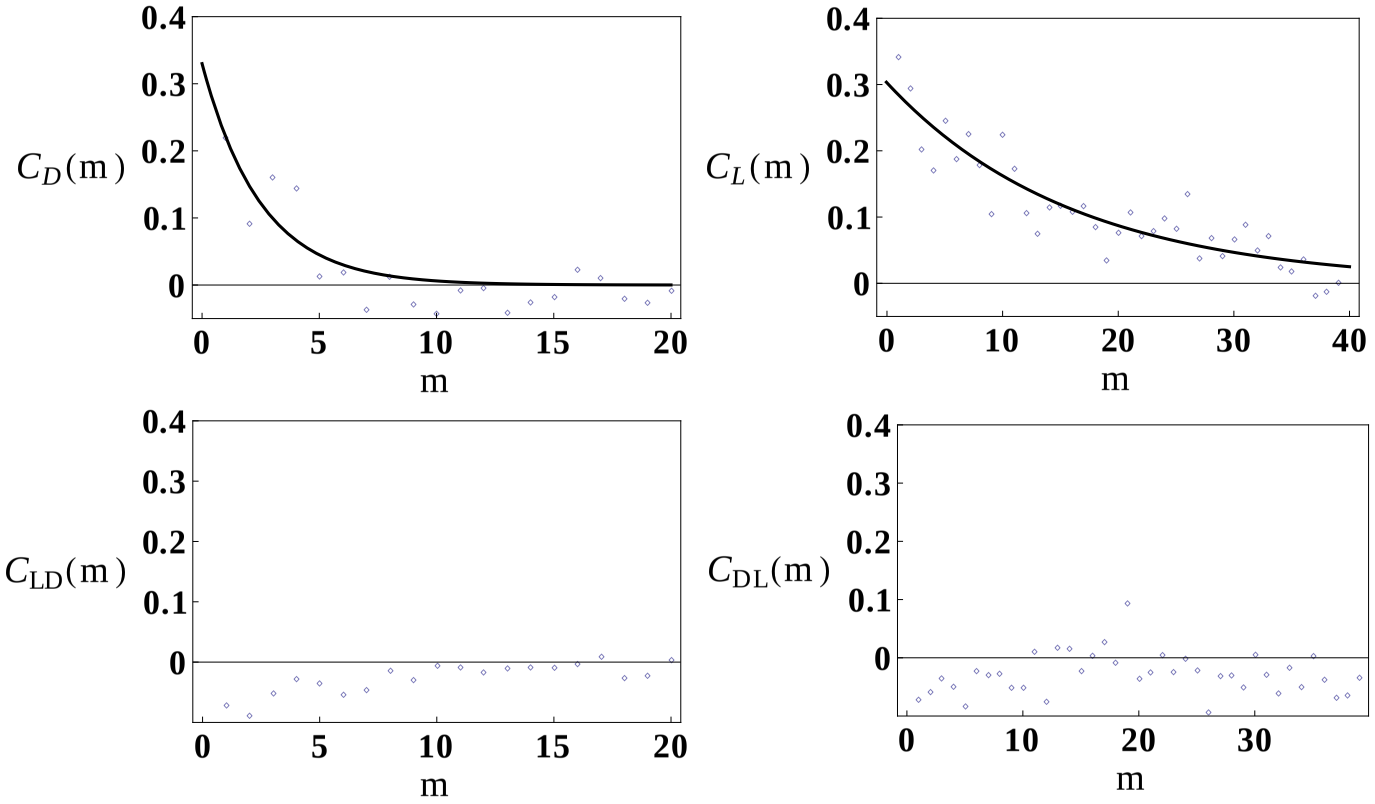

Figure 1.6: Experimental correlation functions for the single-nanoparticle catalytic conversion of resazurin to resorufin, on a nanoparticle of 6 nm diameter. C_D is the dark autocorrelation function, C_L is the light autocorrelation function and C_{LD} and C_{DL} are cross-correlation functions for these two times. m is the number of turnovers separating the two events in consideration.

ticle and the catalyzed reaction, is one of the questions we will address in the present work (see Chapter 3).

At this point, we have described enough about the phenomenology of the experiment to state several questions. As they will serve to define the direction and the scope of this work, we will formulate them in a separate section.

1.3 Questions arising from single nanoparticle catalysis

1. What is the correct expression for the dwell-time density functions? Certainly, they are not Poisson density functions in general. While we can fit data to functions such as stretched exponentials, multiexponential functions arise naturally in a theory that describes single-molecule and ensemble kinetics by similar and compatible rules. The compatibility condition, that we will study in Sec. 1.4, is the idea behind the development of the general theory of single-molecule dynamics[30, 10, 20].
2. What is the set of observables, as functions of the dwell times, that provides more information about the heterogeneity in the nanoparticle? In addition to the density functions and the means, we can define several other quantities to explore the information content of the trajectories. In the following chapters we will study several statistical indicators that reveal qualitative properties that, to our knowledge, have not been reported before.
3. How different is the catalytic activity of a catalyst with a single active site, such as an enzyme, and one with multiple active sites, such as a nanoparticle? Should we expect to observe cooperative effects or correlation among

active sites in a nanoparticle? If so, how can this correlation among active sites be determined? We will find answers to these questions in Chapters 2 and Chapter 3.

4. What does it mean that trajectories exhibit positive autocorrelation, but they do not have crosscorrelation? What information is carried by the rates of decay of C_D and C_L? Cao[10] and also Gopich and Szabo[20], have found that for a few simple kinetic models, the rate of decay of the autocorrelation functions is equal to the ratio between the rate constants of internal transformations and the rate constants of reaction [55] (Equation (32) in this reference). In light of this result, we initially conclude that the internal dynamics of these nanoparticles must be significantly slower than the time scale associated with the reaction and desorption process[51]. We will address these questions in Chapter 3.

5. Can we characterize the mechanism for the catalytic transformation of rezasurin to resorufin on the surface of a nanoparticle at a single nanoparticle level? Substrate-concentration dependence of $\bar{t}_D$ and $\bar{t}_L$ suggested that the catalytic transformation occurs in several steps and several paths, including a substrate-assisted desorption step. While we can only detect two different states in the trajectory, statistical properties of the dwell times can only be explained assuming the existence of substates within the same state and, in this way, every state should experience internal dynamics. How many substates are required to describe the correlation properties of the correlation function together with any other quantity we can define in terms of dwell times? Is it possible to characterize, at least qualitatively, the set of parameters that define the internal processes just by analyzing a single trajectory?

In order to find answers, total or partial, to the above questions, we will define several indicators. First, we must review the basic ideas of the kinetic theory of single-molecule processes that are relevant for the present study. That is our goal in the next section.

1.4 Single molecule kinetics

The time evolution of a chemical process for an ensemble of molecules is given by the solution to differential equations for the concentration of each species. Tracking the same process in a small part of the ensemble, of dimensions comparable to the size of a molecule, will show continuous fluctuations in the number of molecules detected in that region even after the system has reached equilibrium. For a region of the dimensions of the size of just one molecule, concentration of a species will then fluctuate between zero and the inverse of this tiny volume. In this scenario, the concentration $[S]$ of a chemical species S is equivalent to the probability P of observing one molecule of S at a given time. As a consequence, the probability of this event must be determined by the same rules that determine the change in time of the concentration. Put another way, in a region of atomic or molecular dimensions, where at most one molecule can be detected; the probability of observing a molecule varies in time as the concentration does according to the rules of macroscopic kinetics. Therefore, the equations of evolution for P and C should be the same. This is the natural correspondence between single-molecule and macroscopic kinetics.

For a single molecule, such as an enzyme, that can be captured by specific interactions in the small region under study, chemical transformations should

correspond to a sequence of unimolecular steps[2]. Cao and coworkers[10, 54] have defined and studied n-channel models to describe the complexity of single molecule processes and they have implemented different techniques from the theory of stochastic process to analyze experimental trajectories. n-channel models are kinetic schemes with two states, one dark and one light, each one of them with a manifold of n substates . A channel is a reaction path connecting two conformers from different states. As a consequence, an n-channel system couples every substate with one in the complementary state by means of a reaction path.

In Fig. 1.7 we present a typical two-channel model. Notice that every transformation has a rate constant associated. We use k_D, k_L, d and l to denote rate constants as explained in the caption of Fig. 1.7. Since every transition between two states is a unimolecular process, the differential equations that describe the change in time of the probability of observing each state are linear. For the two channel system in Fig. 1.7 we can define the matrices

$$\mathsf{K}_D = \begin{pmatrix} k_{D_1} & 0 \\ 0 & k_{D_2} \end{pmatrix}, \tag{1.7}$$

$$\mathsf{K}_L = \begin{pmatrix} k_{L_1} & 0 \\ 0 & k_{L_2} \end{pmatrix}, \tag{1.8}$$

$$\Gamma_D = \begin{pmatrix} d_{21} & -d_{12} \\ -d_{21} & d_{12} \end{pmatrix}, \tag{1.9}$$

$$\Gamma_L = \begin{pmatrix} l_{21} & -l_{12} \\ -l_{21} & l_{12} \end{pmatrix}. \tag{1.10}$$

[2]Bimolecular elementary steps may be included. However if other molecules are allowed to freely diffuse and there is a continuous supply of them, we can consider this process as a pseudo-first-order process.

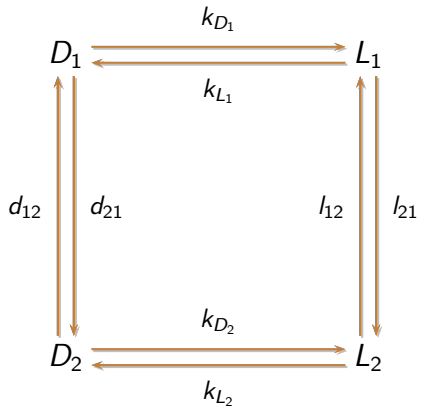

Figure 1.7: An example of a two-channel model. Dark substates are represented by a D, light substates by L. Rate constants for the internal transformation from the $D_i(L_j)$ to the D_j (L_j) substates are represented by d_{ij} (l_{ij}). Reaction rate constants are represented by k_{D_i} and k_{L_i}.

In terms of these, the differential equation for the time evolution of the probabilities ρ_{D_1}, ρ_{D_2}, ρ_{L_1} and ρ_{L_2}, is

$$\frac{d}{dt}|p(t)\rangle = -\begin{pmatrix} \Gamma_D + \mathsf{K}_D & -\mathsf{K}_L \\ -\mathsf{K}_D & \Gamma_L + \mathsf{K}_L \end{pmatrix}|p(t)\rangle, \tag{1.11}$$

where $|p(t)\rangle = (\rho_{D_1}(t), \rho_{D_2}(t), \rho_{L_1}(t), \rho_{L_2}(t))^T$ is the total vector of substate probabilities. In addition, if we define $\langle 1| = (1,1,1,1)$ then the equality $\langle 1|p(t)\rangle = 1$ must always hold. The last statement is the condition of probability conservation.

Fluorescence trajectories differentiate between dark and light states, but do

not detect every substate or internal transformation. Thus, it is important to determine the equations for the evolution for each state. Equation (1.11) together with the condition of probability conservation are sufficient to determine such equations, as we will illustrate below.

The solution of Eq. (1.11) is a vector $|p(t)\rangle$ that for a given time T, carries the probabilities of observing each substate, depending on an initial condition $|p(0)\rangle$. For an increasing sequence of times $\{0, T_1, T_2, T_3, \dots\}$, the sequence of vectors $|p(0)\rangle, |p(T_1)\rangle, |p(T_2)\rangle, \dots$ defines a Markov process[24, 56], since one can take $|p(T_i)\rangle$ as the initial condition for the calculation of $|p(T_{i+1})\rangle$, instead of $|p(0)\rangle$. From this Markov process, one can find the expression for the evolution of the system in an interval of time, say $(0, T)$, with the condition that, for example, no transition from any dark substate to the light state occurs. In this way we can find the dynamic equations for the dark state. The technique that we are trying to sketch here, involves the observation of all finite partitions of the interval $(0, T)$ into an increasing sequence of times $0 \leq T_i \leq T$, in a limit process similar to the one implemented in the definition of the Riemannian integral. At the end, one assigns the minimum value of all possible partitions to the dark vector state in the interval $(0, T)$. At the end, this procedure generates a Markov process that is continuous in time from a Markov process that is discrete in time.

The disadvantage of the above procedure is not only that it requires a good understanding of the mathematical details of many concepts of Markov process and measure theory, but also that we have to go through the same procedure from the beginning to the end for every kinetic scheme. Alternatively, Cao[10, 54] has found a different approach for the determination of the equations of evolution of each state, that has all the properties demanded by the

exact solution[56], with the additional advantage of providing at once the dynamics for each state and for every n-channel system. Since we will adopt Cao's mathematical formulation of single-molecule kinetics in this work, we will now review the main elements of this theory. For another alternative solution see [20].

The two channel system in Fig. 1.7 can be studied by means of the independent contributions from the subsystems

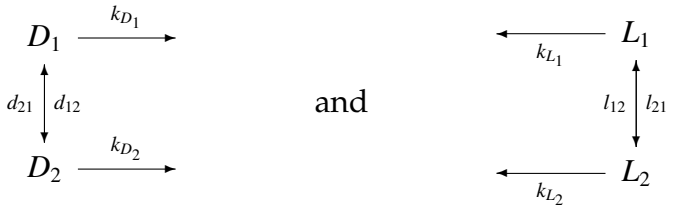

(1.12)

We now let $|p_D(t)\rangle = (\rho_{D_1}, \rho_{D_2})^T$ and $|p_L(t)\rangle = (\rho_{L_1}, \rho_{L_2})^T$ be the probability vectors for the dark and light state, respectively. In the dark state, the kinetic scheme in the right in Eq. (1.12) describes all possible events that can take place. Similarly, the kinetic scheme in the left in Eq. (1.12) describes all possible events in the light state. The dynamic equations for the dark and light state are

$$\frac{d}{dt}|p_D(t)\rangle = -(\mathsf{K}_D + \Gamma_D)|p_D(t)\rangle, \tag{1.13}$$

$$\frac{d}{dt}|p_L(t)\rangle = -(\mathsf{K}_L + \Gamma_L)|p_L(t)\rangle, \tag{1.14}$$

from which we obtain the solutions

$$|p_D(t)\rangle = e^{-(\mathsf{K}_D+\Gamma_D)t}|p_D(0)\rangle, \tag{1.15}$$

$$|p_L(t)\rangle = e^{-(\mathsf{K}_L+\Gamma_L)t}|p_L(0)\rangle. \tag{1.16}$$

We define the dark and light Green functions as follows

$$\mathsf{g}_\mathsf{D}(t) = e^{-(\mathsf{K}_D+\Gamma_D)t}, \tag{1.17}$$

$$\mathsf{g}_\mathsf{L}(t) = e^{-(\mathsf{K}_L+\Gamma_L)t}. \tag{1.18}$$

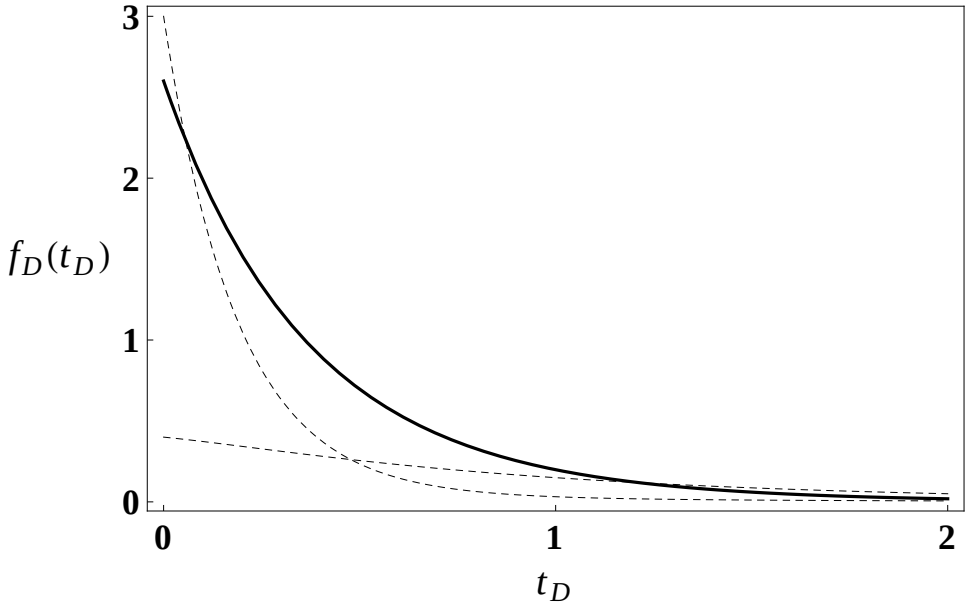

Figure 1.8: The solid line shows the dark-dwell-time density function $f_D(t_D)$ for a two-channel system with rate constants $k_{D_1} = 1, k_{D_2} = 5, k_{L_1} = 2, k_{L_2} = 3, l_{12} = l_{21} = d_{21} = 0.1$ and $d_{12} = 1/3$ in units of k_{D_1}. The biexponential form of $f_D(t_D)$ is illustrated by the dashed plots that represent the two monoexponential functions that add to give $f_D(t_D)$ as predicted by Eq. (1.27).

The dark-dwell-time density function is derived from Eqs. (1.3), (1.13) and (1.15). As a result,

$$f_D(t_D) = \langle 1|\mathsf{K}_D \mathsf{g}_D(t_D)|p_D(0)\rangle, \tag{1.19}$$

and similarly, the set of light dwell times

$$f_L(t_L) = \langle 1|\mathsf{K}_L \mathsf{g}_L(t_L)|p_L(0)\rangle. \tag{1.20}$$

$|p_D(0)\rangle$ and $|p_L(0)\rangle$ are determined from the stationary solutions to Eq. (1.11). If $|p_D^{eq}\rangle$ and $|p_L^{eq}\rangle$ are the state probability vectors at equilibrium, then

$$\begin{pmatrix} |p_D(0)\rangle \\ |p_L(0)\rangle \end{pmatrix} = \mathcal{N}^{-1} \begin{pmatrix} \mathsf{K}_L|p_L^{eq}\rangle \\ \mathsf{K}_D|p_D^{eq}\rangle \end{pmatrix} \tag{1.21}$$

where $\mathcal{N} = \langle 1|\mathsf{K}_L|p_L^{eq}\rangle$ is the normalization constant. These initial conditions can be interpreted as the stationary fluxes from the L state to the D state, and vice versa. We notice that the equilibrium probabilities $|p_D^{eq}\rangle$ and $|p_L^{eq}\rangle$ obey the following equalities

$$(\mathsf{K}_D + \Gamma_D)|p_D^{eq}\rangle = \mathsf{K}_L|p_L^{eq}\rangle, \tag{1.22}$$

$$\mathsf{K}_D|p_D^{eq}\rangle = (\mathsf{K}_L + \Gamma_L)|p_L^{eq}\rangle. \tag{1.23}$$

In addition, the identities

$$\langle 1|\Gamma_D = \langle 0|, \tag{1.24}$$

$$\langle 1|\Gamma_L = \langle 0|, \tag{1.25}$$

together with Eqs. (1.22) and (1.23) imply that

$$\mathcal{N} = \langle 1|\mathsf{K}_D|p_D^{eq}\rangle = \langle 1|\mathsf{K}_L|p_D^{eq}\rangle. \tag{1.26}$$

Thus, Eqs. (1.19),(1.20) and (1.21) lead to the following expressions for the dark and light density functions:

$$f_D(t_D) = \frac{\langle 1|\mathsf{K}_D\mathsf{g}_\mathsf{D}(t_D)\mathsf{K}_L|p_L^{eq}\rangle}{\langle 1|\mathsf{K}_D|p_D^{eq}\rangle}, \tag{1.27}$$

$$f_L(t_L) = \frac{\langle 1|\mathsf{K}_L\mathsf{g}_\mathsf{L}(t_L)\mathsf{K}_D|p_D^{eq}\rangle}{\langle 1|\mathsf{K}_L|p_L^{eq}\rangle}. \tag{1.28}$$

Equations (1.27) and (1.28) for an n-channel model show that in general $f_D(t_D)$ and $f_L(t_L)$ are multiexponential. In particular, for a two-channel model density functions are biexponential. In Fig. 1.8, we illustrate this fact for a specific model.

The mean dark dwell time $\bar{t}_D$, and the variance σ_D^2 are calculated from Eq.

(1.27), as follows

$$\bar{t}_D = \int_0^\infty dt_D t_D f_D(t_D) \tag{1.29}$$

$$= \frac{\langle 1|p_D^{eq}\rangle}{\langle 1|\mathsf{K}_D|p_D^{eq}\rangle}, \tag{1.30}$$

$$\sigma_D^2 = \overline{t_D^2} - \overline{t_D}^2 \tag{1.31}$$

$$= 2\frac{\langle 1|(\mathsf{K}_D + \Gamma_D)^{-1}|p_D^{eq}\rangle}{\langle 1|\mathsf{K}_D|p_D^{eq}\rangle}. \tag{1.32}$$

with similar expressions for $\bar{t}_L$ and σ_L^2. An interesting fact should be noted from Eq. (1.30), for a two channel system:

$$\frac{1}{\bar{t}_D} = x_1 k_{D_1} + x_2 k_{D_2} \tag{1.33}$$

where $x_i = \rho_{D_i}/(\rho_{D_1} + \rho_{D_2})$. Therefore, the inverse value of the mean dark dwell time is a mean value of the reaction rate constants leading to a transition from the dark to the light state. Notice that the result in Eq. (1.33) can be generalized to any n-channel system and as a consequence, this statement is also general.

A final note on the density functions in Eqs. (1.27) and (1.28), comes from the fact that they can be generated by differentiation from the following functions:

$$g_D(t_D) = \frac{\langle 1|\mathsf{g}_\mathsf{D}(t_D)|p_D^{eq}\rangle}{\langle 1|\mathsf{K}_D|p_D^{eq}\rangle}, \tag{1.34}$$

$$g_L(t_L) = \frac{\langle 1|\mathsf{g}_\mathsf{L}(t_L)|p_L^{eq}\rangle}{\langle 1|\mathsf{K}_L|p_L^{eq}\rangle}. \tag{1.35}$$

Thus,

$$f_D(t_D) = \frac{d^2}{dt_D^2} g_D(t_D), \tag{1.36}$$

$$f_L(t_L) = \frac{d^2}{dt_L^2} g_L(t_L). \tag{1.37}$$

In addition, observe that $g_D(0) = \bar{t}_D$ and $g_L(0) = \bar{t}_L$, as $\mathsf{g}_\mathsf{D}(0) = I = \mathsf{g}_\mathsf{L}(0)$, where I is the identity matrix of dimension n.

1.5 Conclusion

Throughout this Chapter, we have revisited different single-molecule studies that occurred prior to the investigations in single-nanoparticle catalysis. In all these experiments, dynamic heterogeneity has been reported and we have illustrated how this heterogeneity is discovered in single nanoparticle catalysis. In particular, we analyzed the multiexponential nature of the density functions of the dark and light dwell times, as recorded in a typical fluorescence trajectory. We also found that dwell times are autocorrelated. Questions about the chemistry and physics responsible for the statistical properties of these dwell times were posed. n-channel systems and single-molecule kinetics were introduced, and they allowed us to explain the multiexponential behavior of the density functions in terms of the existence of multiple reaction paths. These ideas describe the dynamics of a catalyst with one active site. In contrast, nanoparticles are catalysts with multiple active sites and multiple docking sites. As a consequence, we need to formulate a theory that accounts for the existence of multiple active sites to describe catalysis in individual nanoparticles.

CHAPTER 2

CONSTRAINED MEAN DWELL TIMES

One of our main conclusions in Chapter 1 was that the inverse values of $\bar{t}_D$ and $\bar{t}_L$ are mean values of the rate constants of reaction $\bar{k}_D$ and desorption $\bar{k}_L$, respectively (see Eq. 1.33). This average in the reaction rate constants is in general different from their arithmetic mean, since the mean value is calculated as a weighted sum of reaction rate constants and the weighting factors are proportional to the equilibrium probabilities of each substate (see again Eq. (1.33)). A general assumption in the interpretation of single molecule trajectories is that this mean value of the reaction rate constants is exactly the same value than one can measure in an equivalent macroscopic experiment. If mean values in the dwell times provide direct information of the value of the reaction rate constants, then calculating several means, in many different ways, for the same collection of dwell times, will unfold the heterogeneity of these rate constants. Inventing new forms to compute these means, such that we understand and control how they discern among different reaction paths or ponder the reaction rate constants is a valuable enterprise.

In this Chapter we will introduce a new family of dwell time means: the constrained mean dwell times. In brief, they are conditional expectations of the stochastic dark or light dwell times. A constraint is introduced in the calculation of the mean value of a dwell time: a dwell time from the collection that defines the trajectory is to be considered in the computation of its mean only if it fulfills a condition on its immediately preceding event. In this work the condition or constraint will be either of two kinds. The first sort of constraint essentially rejects any dwell time that occurs after a very slow event. The second sort of

constraint rejects the complementary set of times. Slow and fast events will be defined in terms of a time gap or a threshold time T. We will make more precise these definitions in the subsequent sections.

We will start our discussion in Sec. 2.1 by introducing density functions for two consecutive events that occur in a single active site. These elements will be used in Sec. 2.2 to define the constrained mean dwell times for one active site. Catalysts, such as nanoparticles, may have multiple active sites that, during the course of many catalytic transformations, contribute to the trajectory. Mean values may also be sensitive not only to the number of active sites or the rate constant values, but also to synergistic effects among different active sites. We study in Sec. 2.3 and Sec. 2.4 systems with many identical active sites. In Sec. 2.3, we assume that they are all independent while in Sec. 2.4 we construct a simple model for many active sites that are correlated. Models with both correlated and independent active sites will be discussed in Sec. 2.5. Finally, we investigate the constrained mean dwell times for the catalytic transformation discussed in Chapter 1 as they compare to our models.

2.1 Joint density functions for a single n-channel system

In this section we introduce density functions for dwell times that occur in sequence along a single-molecule fluorescence trajectory. As in Chapter 1, we assume that the single-molecule trajectory has only two distinct states. These functions are multidimensional, with one parameter per each dwell time in the sequence. In order to build up some chemical intuition in our definition, we start by remembering from Eqs. (1.15) and (1.17), that the $n \times n$ matrix $\mathsf{g}_{\mathsf{D}}(t) = e^{-(\mathsf{K}_D+\Gamma_D)t}$ is the evolution matrix for the vector of probabilities for the

dark substates when the system is in such a state. In Chapter 1, we defined in Eq. (1.27) the dark dwell-time density function $f_D(t)$ by

$$f_D(t) = \frac{1}{\langle 1|\mathsf{K}_D|p_D^{eq}\rangle}\langle 1|\mathsf{K}_D\mathsf{g}_\mathsf{D}(t)\mathsf{K}_L|p_L^{eq}\rangle,$$

where $|p_D^{eq}\rangle$ is the vector of equilibrium probabilities for the substates in the dark state and $\mathcal{N} = \langle 1|\mathsf{K}_D|p_D^{eq}\rangle = \langle 1|\mathsf{K}_L|p_L^{eq}\rangle$ as we found in Eq. (1.26). We interpreted $f_D(t)$ as the sum of the elements of the propagated vector of initial probabilities for the dark state under the action of the evolution operator $\mathsf{g}_\mathsf{D}(t)$ during an interval of time of length t and, right after an instantaneous transition to the light state (as suggested by the matrix K_D in Eq. (1.7)).

An event is a sudden change in the signal detected, corresponding to a change in state. Events are of two kinds: $D \to L$ or $L \to D$. For a sequence of events, as for example $D \to L \to \cdots \to D \to L$, Cao ([10]) has defined the multidimensional density functions for their dwell-times $t_{D_1}, t_{L_1}, \ldots, t_{D_m}, t_{L_m}$ by the expression

$$f_{(DL)^m}(t_{D_1}, t_{L_2}, \ldots, t_{D_m}, t_{L_m+1}) = \frac{1}{\mathcal{N}}\langle 1|\prod_{i=1}^{m}\mathsf{K}_D\mathsf{g}_\mathsf{D}(t_{D_i})\mathsf{K}_L\mathsf{g}_\mathsf{L}(t_{L_{i+1}})\mathsf{K}_D|p_D\rangle. \tag{2.1}$$

One can verify that the marginal probabilities are

$$f_D(t_{D_i}) = \int_0^\infty dt_{D_1}\int_0^\infty dt_{L_1}\ldots\int_0^\infty dt_{L_{i-1}}\int_0^\infty dt_{L_i}\ldots\int_0^\infty dt_{L_m} f_{(DL)^m}(t_{D_1}, t_{L_1}, \ldots, t_{D_m}, t_{L_m}), \tag{2.2}$$

and also that

$$\int_0^\infty dt_{D_1}\int_0^\infty dt_{L_1}\ldots\int_0^\infty dt_{L_i}\ldots\int_0^\infty dt_{L_m} f_{(DL)^m}(t_{D_1}, t_{L_1}, \ldots, t_{D_m}, t_{L_m}) = 1, \tag{2.3}$$

employing the rules that we derived in Chapter 1. In particular, for two consecutive times we have

$$f_{DL}(t_{D_1}, t_{L_2}) = \frac{1}{\langle 1|\mathsf{K}_D|p_D\rangle}\langle 1|\mathsf{K}_L\mathsf{g}_\mathsf{L}(t_{L_1})\mathsf{K}_D\mathsf{g}_\mathsf{D}(t_{D_1})\mathsf{K}_L|p_L\rangle, \tag{2.4}$$

$$f_{LD}(t_{L_1}, t_{D_2}) = \frac{1}{\langle 1|\mathsf{K}_L|p_L\rangle}\langle 1|\mathsf{K}_D\mathsf{g}_\mathsf{D}(t_{D_1})\mathsf{K}_L\mathsf{g}_\mathsf{L}(t_{L_1})\mathsf{K}_D|p_D\rangle. \tag{2.5}$$

The density function in Eq. (2.1), and in particular Eq. (2.4) and Eq. (2.5) can be described as a sum of the elements of the propagated initial vector along the corresponding sequence of events, each one during a time interval t_{D_i} or t_{L_i} depending on the state. Our choice of the initial conditions $\mathcal{N}^{-1}\,\mathsf{K}_D|p_D\rangle$ and $\mathcal{N}^{-1}\,\mathsf{K}_L|p_L\rangle$, is based on the idea that if we screen a sequence of events along the trajectory (time average) that process is equivalent to taking as our initial point the equilibrium probabilities (space average). Put it other way, we assume that the system is ergodic and that in the long run of the experiment, the trajectory samples all possible initial conditions in a way that is proportional to the equilibrium probabilities of each state.

Cao [10, 54] has extensively studied the properties of these joint density functions as indicators of complex chemical schemes. In the next section, we will make use of them to define the constrained mean dwell times as conditional expectations. The reader should notice that if t_L and t_D are independent, then we should have $f_{LD}(t_L, t_D) = f_L(t_L)f_D(t_D)$. We anticipate that our analysis of the constrained mean dwell times will show that, in general, t_L and t_D are not independent. As it will turn out, it will be useful to consider an additional pair of functions, the generating functions g_{DL} and g_{LD}, that are associated with these joint density functions by means of a simple operation. The generation functions in consideration are defined as follows

$$g_{DL}(t_{D_1}, t_{L_2}) = \frac{1}{\langle 1|\mathsf{K}_D|p_D\rangle}\langle 1|\mathsf{g}_\mathsf{L}(t_{L_2})\mathsf{K}_D\mathsf{g}_\mathsf{D}(t_{D_1})|p_D\rangle, \tag{2.6}$$

$$g_{LD}(t_{L_1}, t_{D_2}) = \frac{1}{\langle 1|\mathsf{K}_L|p_L\rangle}\langle 1|\mathsf{g}_\mathsf{D}(t_{D_2})\mathsf{K}_L\mathsf{g}_\mathsf{L}(t_{L_1})|p_L\rangle, \tag{2.7}$$

and their connection with the joint density functions in Eq. (2.5) and Eq. (2.4) is

given by:

$$\frac{\partial^2}{\partial t_D \partial t_L} g_{DL}(t_D, t_L) = f_{DL}(t_D, t_L), \tag{2.8}$$

$$\frac{\partial^2}{\partial t_D \partial t_L} g_{LD}(t_L, t_D) = f_{LD}(t_L, t_D). \tag{2.9}$$

The generating functions have the following properties

$$g_{DL}(0, t_L) = g_{LD}(t_L, 0) = -\dot{g}_L(t_L), \tag{2.10}$$

$$g_{DL}(t_D, 0) = g_{LD}(0, t_D) = -\dot{g}_D(t_D). \tag{2.11}$$

where $g_D(t_D)$ and $g_L(t_L)$ have been defined in Eqs. (1.34) and (1.35). These definitions are for a single active site and they will let us define and understand the constrained mean dwell times for this case in the following section.

2.2 Constrained mean dwell times for a single active site

The constrained mean dwell times are a particular class of conditional expectations, they are the mean value of the dark or light dwell times of those dwell times that fulfill a condition that is imposed in the previous light or dark dwell time event, depending on the case. Specifically, we define the functions $\bar{t}_{L<}(T), \bar{t}_{L>}(T), \bar{t}_{D<}(T), \bar{t}_{D<}(T)$ by

$$\bar{t}_{L<}(T) = \frac{\int_0^\infty dt_L t_L \int_0^T dt_D f_{DL}(t_D, t_L)}{\int_0^T dt_D f_D(t_D)}, \tag{2.12}$$

$$\bar{t}_{L>}(T) = \frac{\int_0^\infty dt_L t_L \int_T^\infty dt_D f_{DL}(t_D, t_L)}{\int_T^\infty dt_D f_D(t_D)}, \tag{2.13}$$

$$\bar{t}_{D<}(T) = \frac{\int_0^\infty dt_D t_D \int_0^T dt_L f_{LD}(t_L, t_D)}{\int_0^T dt_L f_L(t_L)}, \tag{2.14}$$

$$\bar{t}_{D>}(T) = \frac{\int_0^\infty dt_D t_D \int_T^\infty dt_L f_{LD}(t_L, t_D)}{\int_T^\infty dt_L f_L(t_L)}, \tag{2.15}$$

and we refer collectively to them as the constrained mean dwell times. The functions $\bar{t}_{L<}(T)$ and $\bar{t}_{L>}(T)$ are two different means for light dwell times. The former is the mean value of all the light dwell times that are preceded by a dark dwell time that is *less than or equal to* a threshold time T. At times, we will refer to these dark times as being short or, corresponding to a fast process. On the other hand, the latter function is the mean value of all the light dwell times that are preceded by a dark dwell time that is *greater than or equal to* a threshold time T. At times, we will refer to these dark times as being long or corresponding to a slow process. The values of these constrained mean light dwell times are therefore dependent on the threshold T, and they have the following asymptotic limits:

$$\bar{t}_{L<}(T) \to \bar{t}_L \text{ as } T \to \infty, \tag{2.16}$$

$$\bar{t}_{L>}(T) \to \bar{t}_L \text{ as } T \to 0, \tag{2.17}$$

which can be expected as in these two limits the constraint is too weak to effectively separate fast and slow processes. In fact, if t_L and t_D are independent, then $\bar{t}_{L<}(T) = \bar{t}_L = \bar{t}_{L>}(T)$ for all values of the threshold T. As we found in Chapter 1, in the absence of internal dynamics in the two states, t_L and t_D are independent. Thus, conformal fluctuations in enzymes should have different values for the constrained means than the unconstrained ones. Similar conclusions can be drawn for the case of the constrained mean dark dwell times $\bar{t}_{D<}(T)$ and $\bar{t}_{D>}(T)$.

This suggests that rather than studying the constrained means by themselves, we must study *the difference* between the constrained and unconstrained means, as they can show the existence of dependence between pairs of adjacent events. As expected from the number of constrained mean dwell times and the expressions in Eq. (2.16) and (2.17) and the equivalent expressions for

dark dwell times, we have four new functions:

$$\Delta\bar{t}_{D<}(T) = \bar{t}_{D<}(T) - \bar{t}_D, \tag{2.18}$$

$$\Delta\bar{t}_{D>}(T) = \bar{t}_{D>}(T) - \bar{t}_D, \tag{2.19}$$

$$\Delta\bar{t}_{L<}(T) = \bar{t}_{L<}(T) - \bar{t}_L, \tag{2.20}$$

$$\Delta\bar{t}_{L>}(T) = \bar{t}_{L>}(T) - \bar{t}_L, \tag{2.21}$$

These are the objects of the present study. Since every constrained mean can define only one of the above $\Delta\bar{t}$ functions, we will refer to the difference between the constrained and the unconstrained mean by the name of the corresponding constrained mean. Besides, as elaborated above, it is the difference between the constrained and the unconstrained mean that is of relevance. These constrained means can reveal interesting patterns in the internal dynamic transformations. In general, they have simple forms in terms of generating functions. For example, from Eq. (2.14) we have

$$\bar{t}_{D<}(T) = \frac{\int_0^\infty t_D dt_D \int_0^T dt_L f_{LD}(t_L, t_D)}{\int_0^T f_L(t_L) dt_L} \tag{2.22}$$

$$= \frac{\int_0^\infty t_D dt_D \int_0^T dt_L \partial_{t_L}\partial_{t_D} g_{LD}(t_L, t_D)}{\int_0^T f_L(t_L) dt_L} \tag{2.23}$$

$$= \frac{\int_0^\infty t_D dt_D \left[\partial_{t_D} g_{LD}(t_L, t_D)\right]_0^T}{\int_0^T f_L(t_L) dt_L} \tag{2.24}$$

$$= \frac{\int_0^\infty t_D dt_D \left[\partial_{t_D} g_{LD}(T, t_D) - \partial_{t_D} g_{LD}(0, t_D)\right]}{\int_0^T f_L(t_L) dt_L} \tag{2.25}$$

$$= \frac{\int_0^\infty dt_D \left[g_{LD}(0, t_D) - g_{LD}(T, t_D)\right]}{\int_0^T f_L(t_L) dt_L} \tag{2.26}$$

$$= \frac{\bar{t}_D - \int_0^\infty dt_D g_{LD}(T, t_D)}{1 + \dot{g}_L(T)}. \tag{2.27}$$

Therefore

$$\Delta\bar{t}_{D<} = \frac{-\bar{t}_D \dot{g}_L(T) - \int_0^\infty dt_D g_{LD}(T, t_D)}{1 + \dot{g}_L(T)}, \tag{2.28}$$

and if we take the opposite constraint we have

$$\Delta\bar{t}_{D>} = \frac{-\bar{t}_D \dot{g}_L(T) - \int_0^\infty dt_D g_{LD}(T, t_D)}{\dot{g}_L(T)}. \tag{2.29}$$

The reader should notice that expressions in Eq. (2.28) and Eq. (2.29) are valid for any n-channel system.

In general, constrained mean dwell times are complex functions whose qualitative properties depend not only on the number of channels or reaction paths in the kinetic scheme, but also in the explicit set of values that all the rate constants can take. As we discussed in Chapter 1, dwell-time correlation functions experimentally determined in enzymes and nanoparticles suggest that internal transformations happen in a different time scale than those transformations leading to a change in the system state. In the presence of multiple substates, we think of a transformation among different states as a mean to prepare the system in a given substate. For instance, a reaction that is catalyzed by an enzyme, should happen through a single conformal configuration and, the enzyme remains in this configuration for some time after the reaction. For a reaction that is catalyzed on the surface of nanoparticle, this transformation occurs at the surface in a particular stable atomic configuration: a nanoparticle substate. A change in substate has to be a process much slower than any state transformation, if memory effects are to be observed. Otherwise, the system will have enough time to relax and transform into different substates almost in a random way, breaking in this way any possible dependence that the next reaction may have on previous events. These ideas serve as motivation to introduce an ideal limit in which the internal transformations are several orders of magnitude slower when compared to the speed of reactions from one state to another. The *static limit*[53, 59] neglects in the evolution of $|p_D\rangle$ and $|p_L\rangle$ the

contribution that on it has the set of internal transformations. More precisely, the Green functions are taken as depending only on the reaction rate constants:

$$e^{-(\mathsf{K}_L+\Gamma_L)t_L} \to e^{-\mathsf{K}_L+t_L}, \tag{2.30}$$

$$e^{-(\mathsf{K}_D+\Gamma_D)t_D} \to e^{-\mathsf{K}_D t_D}. \tag{2.31}$$

Internal transformations are not neglected in the computation of the equilibrium probabilities for each substate. Whenever the rate constants for internal transformations are significantly smaller than the reaction rate constants, we will say that the system is *close to the static limit* or that it obeys the *static limit condition*. We will explore the idea of memory along a trajectory and how this further justifies the study of this limit in Chapter 3.

The simplest scenario for which constrained mean dwell times are not equal to the unconstrained means is the one in which the system has two substates. This corresponds to a two-channel model. In the static limit, Eq. (2.28) and Eq. (2.29), for a two channel model lead to the following expressions for the constrained means in the dark dwell times:

$$\Delta\bar{t}_{D<}(T) = \frac{\rho_{D_1}\rho_{D_2}}{k_{D_1}\rho_{D_1} + k_{D_2}\rho_{D_2}} \frac{(e^{-k_{L_2}T} - e^{-k_{L_1}T})(k_{D_1} - k_{D_2})}{(1 - e^{-k_{L_1}T})k_{L_1}\rho_{L_1} + (1 - e^{-k_{L_2}T})k_{L_2}\rho_{L_2}}, \tag{2.32}$$

$$\Delta\bar{t}_{D>}(T) = \frac{\rho_{D_1}\rho_{D_2}}{k_{D_1}\rho_{D_1} + k_{D_2}\rho_{D_2}} \frac{(e^{-k_{L_2}T} - e^{-k_{L_1}T})(k_{D_2} - k_{D_1})}{e^{-k_{L_1}T}k_{L_1}\rho_{L_1} + e^{-k_{L_2}T}k_{L_2}\rho_{L_2}}. \tag{2.33}$$

We now illustrate how to obtain Eq. (2.32). First, we observe that in the static limit $\mathsf{K}_L|p_L\rangle = \mathsf{K}_D|p_D\rangle$ holds and the generating function $g_{LD}(t_L, t_D)$ is

$$g_{LD}(t_L, t_D) = \frac{1}{k_{D_1}\rho_{D_1} + k_{D_2}\rho_{D_2}}(e^{-k_{D_1}t_D}k_{L_1}e^{-k_{L_1}t_L}\rho_{L_1} + e^{-k_{D_2}t_D}k_{L_2}e^{-k_{L_2}t_L}\rho_{L_2}). \tag{2.34}$$

From this expression we evaluate the following integral

$$\int_0^\infty dt_D g_{LD}(T, t_D) = \frac{1}{k_{D_1}\rho_{D_1} + k_{D_2}\rho_{D_2}}(e^{-k_{L_1}T}\rho_{D_1} + e^{-k_{L_2}T}\rho_{D_2}). \tag{2.35}$$

In addition, we notice that

$$\bar{t}_D \dot{g}_L(T) = -\frac{\rho_{D_1} + \rho_{D_2}}{(k_{D_1}\rho_{D_1} + k_{D_2}\rho_{D_2})^2}(e^{-k_{L_1}T}k_{L_1}\rho_{L_1} + e^{-k_{L_2}T}k_{L_2}\rho_{L_2}), \tag{2.36}$$

and hence

$$-\bar{t}_D \dot{g}_L(T) - \int_0^\infty dt_D g_{LD}(T, t_D) = \frac{1}{(k_{D_1}\rho_{D_1} + k_{D_2}\rho_{D_2})^2}\rho_{D_1}\rho_{D_2}(e^{-k_{L_2}T} - e^{-k_{L_1}T})(k_{D_1} - k_{D_2}). \tag{2.37}$$

What remains is to evaluate of the term in the denominator in Eq. (2.28):

$$1 + \dot{g}_L(T) = \frac{(1 - e^{-k_{L_1}T})k_{L_1}\rho_{L_1} + (1 - e^{-k_{L_2}T})k_{L_2}\rho_{L_2}}{k_{D_1}\rho_{D_1} + k_{D_2}\rho_{D_2}}. \tag{2.38}$$

One can proceed following the same line of argument and derive general expressions for the light constrained means

$$\Delta\bar{t}_{L<} = \frac{-\bar{t}_L \dot{g}_D(T) - \int_0^\infty dt_L g_{DL}(T, t_L)}{1 + \dot{g}_D(T)}, \tag{2.39}$$

$$\Delta\bar{t}_{L>} = \frac{-\bar{t}_L \dot{g}_D(T) - \int_0^\infty dt_L g_{DL}(T, t_L)}{\dot{g}_D(T)}, \tag{2.40}$$

and also expressions for their corresponding static limit:

$$\Delta\bar{t}_{L<}(T) = \frac{\rho_{L_1}\rho_{L_2}}{k_{L_1}\rho_{L_1} + k_{L_2}\rho_{L_2}} \frac{(e^{-k_{D_2}T} - e^{-k_{D_1}T})(k_{L_1} - k_{L_2})}{(1 - e^{-k_{D_1}T})k_{D_1}\rho_{D_1} + (1 - e^{-k_{D_2}T})k_{D_2}\rho_{D_2}}, \tag{2.41}$$

$$\Delta\bar{t}_{L>}(T) = \frac{\rho_{L_1}\rho_{L_2}}{k_{L_1}\rho_{L_1} + k_{L_2}\rho_{L_2}} \frac{(e^{-k_{D_2}T} - e^{-k_{D_1}T})(k_{L_2} - k_{L_1})}{e^{-k_{D_1}T}k_{D_1}\rho_{D_1} + e^{-k_{D_2}T}k_{D_2}\rho_{D_2}}. \tag{2.42}$$

We can now use these results to describe how the rate constants and the mechanism of reaction of a chemical system influence the qualitative properties of these constrained means. First of all, we observe that by definition, $\Delta\bar{t}_{D<}(T)$ and $\Delta\bar{t}_{L<}(T)$ tend to zero as T becomes large. Also, Eq. (2.32) and Eq. (2.41) show that the sign of $\Delta\bar{t}_{D<}$ and $\Delta\bar{t}_{L<}$ is given by the algebraic sign of the product $(k_{L_1} - k_{L_2})(k_{D_2} - k_{D_1})$. As a consequence, the sign of these functions is a measure

of the relative proportion of the four reaction rate constants. For the catalytic transformation by gold nanoparticles, if the reaction on the surface can occur through two different paths (i.e. two different channels) and if one of these reaction paths has the larger reaction rate constant and also the larger rate constant of product desorption, then we should observe that $\Delta\bar{t}_{D<}$ and $\Delta\bar{t}_{L<}$ decay to zero from negative values. On the contrary, if fast reactions and slow desorptions happen through the same channel, then $\Delta\bar{t}_{D<}$ and $\Delta\bar{t}_{L<}$ must decay to zero from positive values.

The asymptotic decay rate of $\Delta\bar{t}_{D<}$ and $\Delta\bar{t}_{L<}$ also carries useful information. For the case of well-separated rate constants for transitions from dark to light and light to dark such that k_D^{big} is significantly bigger than k_D^{small} and also k_L^{big} is significantly bigger than k_L^{small}, $\Delta\bar{t}_{L<}(T)$ approaches zero exponentially with decay constant k_D^{small}. Moreover, for time less than or of the order of $(k_D^{big})^{-1}$, $\bar{t}_L(T)$ selects the sub-population with larger reaction rate, but for times comparable to or larger than $(k_D^{small})^{-1}$, this mean reflects the entire ensemble, and selectivity is lost. Thus, the rate constant for the slower of the two reaction processes may be extracted from the long T dependence of $\Delta\bar{t}_{L<}(T)$. In the same fashion, $\Delta\bar{t}_{D<}$ approaches zero exponentially with decay constant k_L^{small}, with high selectivity for the sub-population with the larger desorption rate when $T < (k_L^{small})^{-1}$.

From Eq. (2.33) and (2.42), it can be asserted that the sign of the constrained means $\Delta\bar{t}_{D>}$ and $\Delta\bar{t}_{L>}$, close to the static limit, is the same for every value of the threshold T and thus, the algebraic sign is determined by the product $(k_{L_1} - k_{L_2})(k_{D_1} - k_{D_2})$. This prediction also tells us that complementary constrained means have different signs. In accordance, if the catalytic transformation on the surface of the nanoparticle can happen through two channels and, fast reactions

and fast desorptions occur through the same channel, then $\Delta\bar{t}_{L>}$ and $\Delta\bar{t}_{D>}$ must be positive. If fast reactions and slow desorptions take place along the same channel then $\Delta\bar{t}_{L>}$ and $\Delta\bar{t}_{D>}$ must be negative.

$\Delta\bar{t}_{D>}(T)$ and $\Delta\bar{t}_{L>}(T)$ tend to zero as T becomes smaller and they approach a finite asymptote for large values of T. In the static limit and for well-separated reaction rate constants, $\Delta\bar{t}_{D<}$ and $\Delta\bar{t}_{L<}$ approach their asymptotes exponentially with decay constants k_L^{big} and k_D^{big}, respectively.

At this point we should illustrate in a numerical example all the properties that we have listed above. Figure 2.1 shows plots for each constrained mean dwell time for two different models of a catalyst with one active site. In both models the active site is assumed to have two substates. The first model, whose constrained means are plotted in Fig. 2.1 in solid lines, has reaction rate constants $k_{D_1} = 0.1, k_{D_2} = 0.01$ and desorption rate constants $k_{L_1} = 10$ and $k_{L_2} = 1$, i.e. fast reactions and slow desorptions occur through one of its channels. On the contrary, the second model, represented in Fig. 2.1 by dashed lines, undergoes fast reactions and fast desorptions through the same channel. We must point out that both models have rate constants for internal transformations that, when compared to the reaction and desorption rate constants, are small and, consequently, these models are close to the static limit. As predicted, for the first model $\Delta\bar{t}_{D<}(T)$ and $\Delta\bar{t}_{L<}(T)$ are positive for every value of T whilst they are negative for the second model. In the same fashion, $\Delta\bar{t}_{D>}(T)$ and $\Delta\bar{t}_{L>}(T)$ are negative functions for the first model and positive for the second. This example typifies the capacity that the constrained mean dwell times have to discern between these two possible scenarios.

Thus far, our understanding of the qualitative properties of the constrained

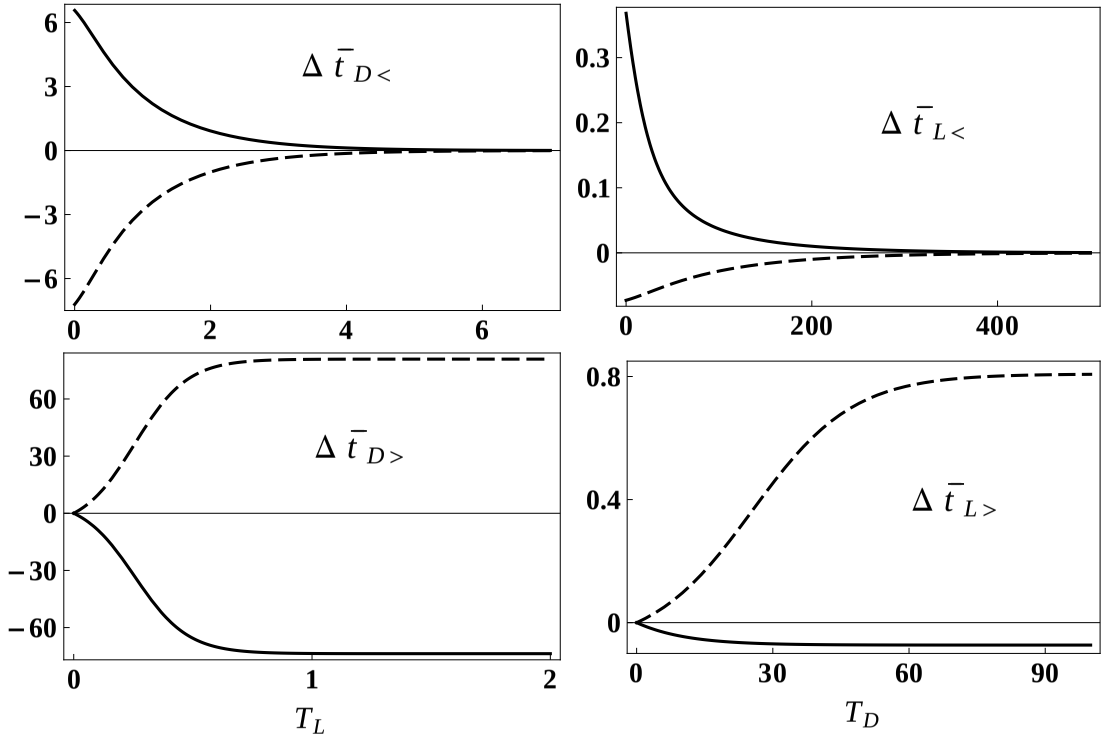

Figure 2.1: Constrained mean dwell times are shown for a catalyst with one active site and two internal states. Differences between constrained and unconstrained mean times are plotted. Solid curves are calculated for reaction rate constants $k_{D_1} = 0.1$ and $k_{D_2} = 0.01$, for product desorption rate constants $k_{L_1} = 1$ and $k_{L_2} = 10$, and for site state changing rate constants $d_{12} = l_{12} = l_{21} = 10^{-4}$ and $d_{21} = 0.01$. Time unit is $k_{L_1}^{-1}$. Dashed curves are calculated for the same parameters, but with interchange of the values of k_{D_1} and k_{D_2}, and $d_{21} = 10^{-4}$.

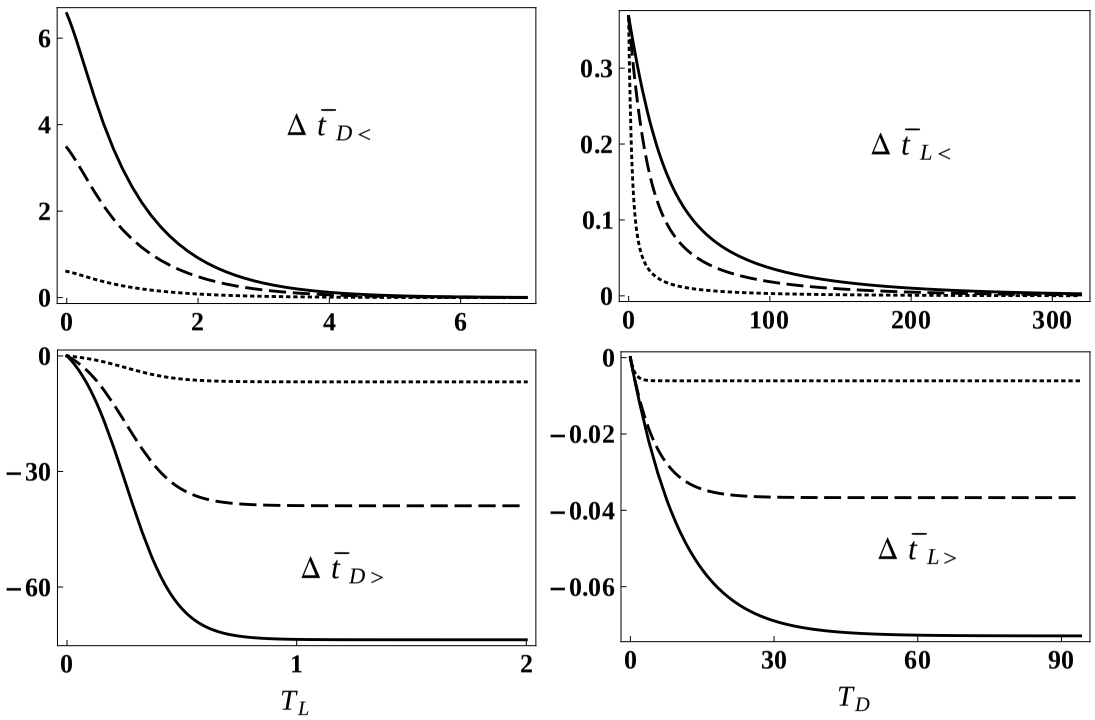

Figure 2.2: Constrained mean dwell times are shown for a catalyst with one active site and two internal states. Differences between constrained and unconstrained mean times are plotted. Rate constants for reaction and desorption have the same values of the solid curves in Fig. 2.1 , $k_{D_1} = 0.1$, $k_{D_2} = 0.01$, $k_{L_1} = 1$, and $k_{L_2} = 10$. Rate constants for changing site substates $d_{12} = l_{12} = l_{21}$ are increased from the value in Fig. 2.1 of 10^{-4} (solid) to 10^{-3} (dashes) to 10^{-2} (dots) and d_{21} increases from 10^{-2} (solid) to 0.1 (dashes) and 1 (dots). Time unit is $k_{L_1}^{-1}$.

mean dwell times is based on their simple form in the static limit in Eq. (2.32), (2.33),(2.41) and (2.42). In Fig. 2.2 we take the model in Fig. 2.1 represented by solid lines, out of the static limit by sequentially increasing the value of the internal rate constants. In Fig. 2.2, d_{12}, l_{12} and l_{21} increase by one order of magnitude from 10^{-4} to 10^{-2} as the curve goes from solid to dotted. The rate constant d_{21} is chosen such that the condition of detailed balance is satisfied. Observe that d_{21} is of the order of magnitude as some of the reaction rate constants in both the dashed and dotted plots and, that even in these two cases our prediction for the qualitative behavior of the constrained means based on the relative proportions of the reaction and desorption rate constants is correct.

Another relevant observation about the model in Fig. 2.2 is that the absolute value of every constrained mean, for a given value of T, decreases as the values of the internal rate constants increase. In order to visualize this trend, it is enough to trace at any point in every panel in Fig. 2.2 a vertical line and compare the intersected values. This is a manifestation of the idea that our capacity of effectively selecting dwell times corresponding to the fastest or slowest channel is affected by the ratio between internal and reaction rate constants. As the internal rates of dynamics increase, the possibility of internal transformations in short times increases and the preparation of our system, achieved by means of the constraint imposed in the preceding dwell time, can be more easily destroyed by such an internal transition. As a consequence the absolute value of the difference between the constrained and the unconstrained mean decreases.

Out of the static limit, the constrained mean dwell times for an active site with two substates can be obtained by considering the spectral decomposition of the matrices $K_L + \Gamma_L$ and $K_D + \Gamma_D$, and by writing the propagator for each

substate in the corresponding basis. After this consideration, the derivation of the general case follows the same line of argument described above for the case of the static limit. An alternative but similar derivation can be found in Eqs. (B.97)-(B.117) in Appendix B.6 in Chapter 3 based on the properties of the turnover matrix. As a result, the constrained mean dwell times, out of the static limit have the general form:

$$\Delta\bar{t}_{D<} = \left(\frac{P_{D2L1}}{\alpha_1\alpha_2}\right)\frac{\left(e^{-\beta_1 T} - e^{-\beta_2 T}\right)(\alpha_2 - \alpha_1)}{(1 - e^{-\beta_1 T})P_{L1} + (1 - e^{-\beta_2 T})P_{L2}}, \tag{2.43}$$

$$\Delta\bar{t}_{D>} = \left(\frac{P_{D2L1}}{\alpha_1\alpha_2}\right)\frac{\left(e^{-\beta_1 T} - e^{-\beta_2 T}\right)(\alpha_1 - \alpha_2)}{e^{-\beta_1 T}P_{L1} + e^{-\beta_2 T}P_{L2}}, \tag{2.44}$$

$$\Delta\bar{t}_{L<} = \left(\frac{P_{L2D1}}{\beta_1\beta_2}\right)\frac{\left(e^{-\alpha_1 T} - e^{-\alpha_2 T}\right)(\beta_2 - \beta_1)}{(1 - e^{-\alpha_1 T})P_{D1} + (1 - e^{-\alpha_2 T})P_{D2}}, \tag{2.45}$$

$$\Delta\bar{t}_{L>} = \left(\frac{P_{L2D1}}{\beta_1\beta_2}\right)\frac{\left(e^{-\alpha_1 T} - e^{-\alpha_2 T}\right)(\beta_1 - \beta_2)}{e^{-\alpha_1 T}P_{D1} + e^{-\alpha_2 T}P_{D2}}, \tag{2.46}$$

where α_1 and α_2 are the eigenvalues of $K_D + \Gamma_D$, and β_1 and β_2 are those of $K_L + \Gamma_L$. Also, P_{D2L1} and P_{L2D1} are factors involving projections into the eigenvectors of these two matrices. Their actual form is given in Appendix B.6. It should be noted that close to the static limit α_i tends to k_{D_i} whereas β_i tends to k_{L_i}. Hence, Eq. (2.43)- (2.46) are indeed more general and can be used to study these functions in different *normal modes of conformal fluctuation*, a concept introduced by Cao[55], to describe the eigenvectors of g_D and g_L (see reference [55] Sec. III C.).

On a final note, one should notice that Eq. (2.43)- (2.46) indicate that even out of the static limit, the constrained means have a definite sign, i.e. they can only be either positive or negative for all T, and that $\Delta\bar{t}_{D<}$ and $\Delta\bar{t}_{L<}$ have the algebraic sign of the product $(\alpha_1 - \alpha_2)(\beta_2 - \beta_1)$. Numerically it has been observed that for certain choices of internal rate constants, far from the static limit and when they are comparable or bigger than the reaction rate constants, the sign of the

products $(\alpha_1 - \alpha_2)(\beta_2 - \beta_1)$ and $(k_{D_1} - k_{D_2})(k_{L_2} - k_{L_1})$ are different and our prediction of the sign based only on the relative values of the reaction rate constants may be violated.

2.3 A catalyst with many independent active sites.

Nanoparticles, as heterogeneous catalysts, have a multitude of active sites on their surface and their catalytic activity can change through dynamic restructuring of the surface metal, either as a spontaneous process or induced by the reaction of adsorbed molecules. Active sites on a single nanoparticle can also be very different in nature, vary in number with time and have their catalytic activity fluctuate as nearby active sites also fluctuate. These observations motivate the study of models for systems with many active sites.

In this section we generalize the model introduced in Sec. 2.2 with a single active site to a system with N independent active sites, each one corresponding to an n-channel system. We will not consider any possible spatial correlation among active sites until Sec. 2.4.

Two states are possible, one of low intensity and one of high intensity in the fluorescence emission. The former is the dark state and the later the light state for the nanoparticle. We will use the word configuration for a substate of the nanoparticle, which in principle corresponds to a collection of substates for each active site. For a single active site, the dark state has n substates and as a consequence, there are n^N possible configurations for the whole nanoparticle in the dark state. The light state admits every possible configuration in which only one active site is in any light substate, while the other active sites are in any of

the dark substates. Thus, we have $N \times n^N$ possible configurations in the light state.

The vector state for the dark state $|P_D(t)\rangle$, is defined as a column vector of dimension n^N all whose elements are products of the form $\rho^{(1)}_{D_{i_1}}(t) \ldots \rho^{(N)}_{D_{i_N}}(t)$ with i_k equal to 1 to n. This product of probabilities corresponds to the probability of one of the possible dark configurations (see Appendix A.1). Alternatively, the dark vector state $|P_D(t)\rangle$ is the direct product of the dark vector states for every single active site:

$$|P_D(t)\rangle = \prod_{j=1}^{N} |p_D^{(j)}(t)\rangle. \tag{2.47}$$

The vector state for the j-th active site $|p_D^{(j)}\rangle$ evolves according to the single site dynamics in Eq. 1.15. The light vector state for the catalyst, when the j-th active site is in the light state $|P_L^{(j)}(t)\rangle$ is a vector of length n^N with elements $\rho^{(1)}_{D_{i_1}}(t) \ldots \rho^{(j)}_{L_{i_j}}(t) \ldots \rho^{(N)}_{D_{i_N}}(t)$. The total light vector state is $|P_L(t)\rangle = \left(|P_L^{(1)}(t)\rangle, \ldots, |P_L^{(N)}(t)\rangle\right)^T$. Alternatively, the light vector state is the direct sum over all the active sites of the direct product of dark vector states for $N-1$ active sites and one light vector state for a single active site:

$$|P_L(t)\rangle = \sum_{i=1}^{N} \prod_{j \neq i}^{N} |p_D^{(j)}(t)\rangle |p_L^{(i)}(t)\rangle. \tag{2.48}$$

Likewise, the total probability vector for the catalyst $|P(t)\rangle$ is:

$$|P(t)\rangle = |P_D(t)\rangle \otimes |P_L(t)\rangle. \tag{2.49}$$

The equation of evolution of $|P(t)\rangle$ can be determined from the equation of motion of every active site, as they are independent. For probability conservation, a restriction in the internal transitions between two light configurations is introduced: during the time that an active site is in the light state, transitions from the dark to the light state and also internal transformations between dark substates

are forbidden for all the other active sites(see Appendix A.1). The differential equation for the time evolution of $|P(t)\rangle$ is

$$|\dot{P}(t)\rangle = -\begin{pmatrix} W_{DD} & -W_{DL} \\ -W_{LD} & W_{LL} \end{pmatrix} |P(t)\rangle. \tag{2.50}$$

The explicit form of the matrices W_{DD}, W_{DL}, W_{LD} and W_{LL} are included in Appendix A.1, along with the details for the derivation of Eq. (2.50). In brief, each of these matrices carries on the rate constants for a given subset of changes in the catalyst configuration. For instance, W_{DD} has as matrix elements the rate constants for every possible internal transformation from a dark to a dark substate, for every active site, and also the reaction rate constants that leads to a change in the state of the nanoparticle.

As a consequence of Eq. (2.50) and (2.49), the following equalities should hold at equilibrium:

$$W_{DD}|P_D^{eq}\rangle = W_{DL}|P_L^{eq}\rangle, \tag{2.51}$$

$$W_{LL}|P_L^{eq}\rangle = W_{LD}|P_D^{eq}\rangle. \tag{2.52}$$

In addition, based on the definition introduced in Appendix A.1 we have

$$\langle 1_{n^N}|W_{DD} = \langle 1_{N\times n^N}|W_{LD}, \tag{2.53}$$

$$\langle 1_{N\times n^N}|W_{LL} = \langle 1_{n^N}|W_{DL}, \tag{2.54}$$

where the vector $\langle 1_A|$ is a row vector of length A, all whose elements are equal to 1. As the length of the vector $\langle 1_A|$ will always be the same as the dimension of the square matrix that is multiplying to its right, in the following we will omit the sub index A in the vector $\langle 1|$, for the sake of simplicity in our notation. With

this convention in mind, we also obtain the following results

$$\langle 1|W_{DD}|P_D^{eq}\rangle = \langle 1|K_D|P_D^{eq}\rangle, \tag{2.55}$$

$$= \sum_{s=1}^{N} \langle 1|K_L^{(s)}|P_L^{(s),eq}\rangle, \tag{2.56}$$

$$= \langle 1|W_{LL}|P_L^{eq}\rangle. \tag{2.57}$$

The dwell-time density functions for the dark and light states are given as functions of the propagation in time of the corresponding probability vectors. These functions are defined as follows

$$F_D(t) = \frac{\langle 1|W_{DD}\mathsf{G}_\mathsf{D}(t)W_{DD}|P_D^{eq}\rangle}{\langle 1|W_{DD}|P_D^{eq}\rangle}, \tag{2.58}$$

$$F_L(t) = \frac{\langle 1|W_{LL}\mathsf{G}_\mathsf{L}(t)W_{LL}|P_L^{eq}\rangle}{\langle 1|W_{LL}|P_L^{eq}\rangle}, \tag{2.59}$$

where

$$\mathsf{G}_\mathsf{D}(t) = e^{-W_{DD}t}, \tag{2.60}$$

$$\mathsf{G}_\mathsf{L}(t) = e^{-W_{LL}t}, \tag{2.61}$$

are the propagators or the Green functions for the dark and light state vectors. In resemblance to the single active site case, we can also define the generating functions for a systems with many active sites

$$G_D(t) = \frac{\langle 1|\mathsf{G}_\mathsf{D}(t)|P_D^{eq}\rangle}{\langle 1|W_{DD}|P_D^{eq}\rangle}, \tag{2.62}$$

$$G_L(t) = \frac{\langle 1|\mathsf{G}_\mathsf{L}(t)|P_L^{eq}\rangle}{\langle 1|W_{LL}|P_L^{eq}\rangle}, \tag{2.63}$$

and they generate the density functions in Eq. (2.58) and (2.59) by differentiation ($F_D(t) = \ddot{G}_D(t)$ and $F_L(t) = \ddot{G}_L(t)$). In addition, $G_D(0) = \bar{t}_D$ and $G_L(0) = \bar{t}_L$. Joint density functions and their corresponding generating functions are defined by

$$F_{DL}(t_D, t_L) = \frac{\langle 1|W_{LL}\mathsf{G}_\mathsf{L}(t_L)W_{LD}\mathsf{G}_\mathsf{D}(t_D)W_{DD}|P_D^{eq}\rangle}{\langle 1|W_{DD}|P_D^{eq}\rangle}, \tag{2.64}$$

$$F_{LD}(t_L, t_D) = \frac{\langle 1|W_{DD}\mathsf{G}_\mathsf{D}(t_D)W_{DL}\mathsf{G}_\mathsf{L}(t_L)W_{LL}|P_L^{eq}\rangle}{\langle 1|W_{LL}|P_L^{eq}\rangle}, \tag{2.65}$$

$$G_{DL}(t_D,t_L) = \frac{\langle 1|\mathsf{G_L}(t_L)W_{LD}\mathsf{G_D}(t_D)|P_D^{eq}\rangle}{\langle 1|W_{DD}|P_D^{eq}\rangle}, \tag{2.66}$$

$$G_{LD}(t_L,t_D) = \frac{\langle 1|\mathsf{G_D}(t_D)W_{DL}\mathsf{G_L}(t_L)|P_L^{eq}\rangle}{\langle 1|W_{LL}|P_L^{eq}\rangle}, \tag{2.67}$$

with

$$\frac{\partial^2}{\partial t_L \partial t_D} G_{DL}(t_D,t_L) = F_{DL}(t_D,t_L), \tag{2.68}$$

$$\frac{\partial^2}{\partial t_L \partial t_D} G_{LD}(t_L,t_D) = F_{LD}(t_L,t_D). \tag{2.69}$$

We stress the similarity in the form that Eq. (2.66)-(2.67) have with those for a single active site, in Eq. (2.6)-(2.7). As a consequence of that similarity, the derivation of the general expressions for the constrained mean dwell times for a set of N independent active sites follows the same line of argument used in the case of a single case. For instance, the mean value of the dark dwell times that happen after a light dwell time than is shorter that a threshold time T, is given by

$$\vec{t}_{D<}^{(N)}(T) = \frac{\int_0^\infty t_D dt_D \int_0^T dt_L F_{LD}(t_L,t_D)}{\int_0^T F_L(t_L)dt_L}, \tag{2.70}$$

$$= \frac{\vec{t}_D^{(N)} - \int_0^\infty dt_D G_{LD}(T,t_D)}{1+\dot{G}_L(T)}. \tag{2.71}$$

where Eq. (2.71) can be obtained by a sequence of steps identical to Eq. (2.23) - (2.27). We will use the superindex (N) in the notation of constrained mean dwell times to specify that they are calculated for models with N active sites. Therefore

$$\Delta\vec{t}_{D<}^{(N)}(T) = \frac{-\vec{t}_D^{(N)}\dot{G}_L(T) - \int_0^\infty dt_D G_{LD}(T,t_D)}{1+\dot{G}_L(T)}, \tag{2.72}$$

and for the opposite constraint we obtain

$$\Delta\vec{t}_{D>}^{(N)}(T) = \frac{-\vec{t}_D^{(N)}\dot{G}_L(T) - \int_0^\infty dt_D G_{LD}(T,t_D)}{\dot{G}_L(T)}. \tag{2.73}$$

In the case of the constrained means of light dwell times we obtain.

$$\Delta\bar{t}_{L<}^{(N)}(T) = \frac{-\bar{t}_L^{(N)}\dot{G}_D(T) - \int_0^\infty dt_L G_{DL}(T,t_L)}{1+\dot{G}_D(T)}, \tag{2.74}$$

$$\Delta\bar{t}_{L>}^{(N)}(T) = \frac{-\bar{t}_L^{(N)}\dot{G}_D(T) - \int_0^\infty dt_L G_{DL}(T,t_L)}{\dot{G}_D(T)}. \tag{2.75}$$

We want to understand how the constrained means, as given by Eq. (2.72) - (2.75), for a catalyst with many active sites compare for different numbers of active sites. In particular, we are interested in understanding how these constrained means compare to the constrained means of a single active site. Our treatment of the problem has not made any assumption about the nature of the active sites, other than imposing that all of them have two states, each one with n substates. For simplicity, we will now assume that all the active sites in the catalyst are chemically identical, i.e. the internal transformations, the reaction and the desorption process have the same set of rate constants for every active site.

For a system with N identical active sites we can write the generating functions in Eq. (2.66)-(2.67) in terms of those corresponding to a single active site (Eq. (2.6) to (2.7)). Notice that K_D and $|p_D^{eq}\rangle$ are the matrix K_D and $|P_D^{eq}\rangle$ in the case $N = 1$ (see Appendix A.1). As derived in the Appendix A.2,

$$\langle 1|W_{DD}|P_D^{eq}\rangle = N\langle 1|\mathsf{K}_D|p_D^{eq}\rangle\langle 1|p_D^{eq}\rangle^{N-1}, \tag{2.76}$$

$$\langle 1|\mathsf{G}_\mathsf{D}(t)|P_D^{eq}\rangle = \langle 1|\mathsf{g}_\mathsf{D}(t)|p_D^{eq}\rangle^N. \tag{2.77}$$

As a consequence, we observe that $\bar{t}_D^{(N)} = \bar{t}_D^{(1)}/N$. In addition

$$\langle 1|W_{LL}|P_L^{eq}\rangle = N\langle 1|\mathsf{K}_L|p_L^{eq}\rangle\langle 1|p_D^{eq}\rangle^{N-1}, \tag{2.78}$$

$$\langle 1|\mathsf{G}_\mathsf{L}(t)|P_L^{eq}\rangle = N\langle 1|\mathsf{g}_\mathsf{L}(t)|p_L^{eq}\rangle\langle 1|p_D^{eq}\rangle^{N-1}, \tag{2.79}$$

implying in this case that $\bar{t}_L^{(N)} = \bar{t}_L^{(1)}$. Observe that Eq. (2.77) suggests that the sum of the elements of the vector resulting from the action of the Green function $\mathsf{G}_\mathsf{D}(t)$

on the state vector $|P_D^{eq}\rangle$ is equivalent to the product of the sum of the elements of the action of the Green function $\mathsf{g_D}(t)$ for each single-active-site vector state $|p_D^{eq}\rangle$. In addition, Eq. (2.79) suggests that the sum of the elements of the vector resulting from the action of the Green function $\mathsf{G_L}(t)$ on the state vector $|P_L^{eq}\rangle$ is equivalent to the sum over all products of a sum of the elements of the action of the Green function $\mathsf{g_L}(t)$ on the unique active site in the light state $|p_L^{eq}\rangle$, and the sums of the elements of the remaining $N-1$ vector states states $|p_D^{eq}\rangle$. Notice that the sum is over all the active sites. Similarly, from Eq. (2.76) and Eq. (2.78), and after noticing that $\langle 1|W_{DD} = \langle 1|K_D$ and also $\langle 1|W_{LL} = \langle 1|K_L$, we can describe the trace of K_D and K_L in terms of their action on individual active sites. For instance, the trace of the action of K_D on the state vector $|P_D^{eq}\rangle$ is equivalent to the sum over all active sites, of the action of the operator K_D on an active site $|p_D^{eq}\rangle$ times the product of the traces of the individual vector states $|p_D^{eq}\rangle$ for the other active sites.

Our previous analysis can be extended to the product of Green functions and other operators, such as those found in the definition of $G_{DL}(t_D, t_L)$ and $G_{LD}(t_L, t_D)$. In these two cases, we discover the function

$$E_D(t) = \frac{\langle 1|\mathsf{g_D}(t)|p_D^{eq}\rangle}{\langle 1|p_D\rangle}, \tag{2.80}$$

in terms of which the relation between the generating functions $G_{DL}(t_D, t_L)$ and $G_{LD}(t_L, t_D)$ for many independent active sites and $g_{DL}(t_D, t_L)$ and $g_{LD}(t_L, t_D)$ for a single active site is given:

$$G_{DL}(t_D, t_L) = g_{DL}(t_D, t_L)E_D(t_D)^{N-1}, \tag{2.81}$$

$$G_{LD}(t_L, t_D) = g_{LD}(t_L, t_D)E_D(t_D)^{N-1}. \tag{2.82}$$

Now we have enough tools to describe how the constrained mean dwell times for many independent active sites change with N. We will illustrate how

the derivation proceeds for the case of $\Delta\vec{t}^{(N)}_{D<}$. Starting with Eq. (2.72) we can derive two different expressions for $\Delta\vec{t}^{(N)}_{D<}$, to wit,

$$\Delta\vec{t}^{(N)}_{D<}(T) = \frac{-\vec{t}^{(1)}_D \dot{g}_L(T)/N - \int_0^\infty dt_D g_{DL}(t_D, t_L)(E_D(t_D))^{N-1}}{1 + \dot{g}_L(T)}, \tag{2.83}$$

and

$$\Delta\vec{t}^{(N)}_{D<}(T) = \frac{\langle 1|(I\vec{t}^{(N)}_D - W^{-1}_{DD})W_{DL}\mathsf{G}_\mathsf{L}(T)|P^{eq}_L\rangle}{\langle 1|(I - \mathsf{G}_\mathsf{L}(T))W_{LL}|P^{eq}_L\rangle}. \tag{2.84}$$

The expression in Eq. (2.83) is directly obtained after replacing Eq. (2.77), (2.79), (2.81) and (2.82) in Eq. (2.72). On the other hand, the expression in Eq. (2.84) is the result of calculating the integrals of the corresponding generating functions (see Appendix A.3).

In the static limit, either Eq. (2.83) or (2.84) lead to the following expression

$$\Delta\bar{t}_{D<}(T) = \frac{(e^{-k_{L_2}T} - e^{-k_{L_1}T})\vec{t}^{(1)}_D k_{L_2}\rho_{L_2}}{N\langle 1|(I - e^{-\mathsf{K}_L T})\mathsf{K}_L|p^{eq}_L\rangle}\left(1 - \frac{N}{\vec{t}^{(1)}_D}\int_0^\infty e^{-k_{D_2}t}E_D(t)^{N-1}dt\right), \tag{2.85}$$

Details of the derivation of Eq. (2.85) are in the Appendix A.4. One should notice that the above expression for $\Delta\bar{t}_{D<}(T)$ in the case $N = 1$ gives the same result in Eq. (2.32). In fact, Eq. (2.85) is valid for every number of independent active sites. If the number of active sites is large we can derive a simpler expression for $\Delta\vec{t}^{(N)}_{D<}(T)$. The function $E_D(t)$ is a weighted mean of an exponential operator. Thus, $(E_D(t))^N$ admits the cumulant expansion

$$(E_D(t_D))^N = e^{-Nt_D/\vec{t}^{(1)}_D}\ (1 + N\sigma^2_w t^2_D/2 + O(t^3_D)), \tag{2.86}$$

with

$$\sigma^2_w = \frac{\langle 1|(\mathsf{K}_D + \Gamma_D)^2|p^{eq}_D\rangle}{\langle 1|p^{eq}_D\rangle} - (\vec{t}^{(1)}_D)^{-2}. \tag{2.87}$$

For large N, the exponential term dominates and, in this case we can replace $(E_D(t_D))^{N-1}$ by $\exp(-Nt_D/\vec{t}^{(1)}_D)$ in Eq. (2.85), which after integration gives a simpler

expression for the N-dependence of $\Delta\vec{t}_{D<}^{(N)}$ for large N, i.e.

$$\Delta\vec{t}_{D<}^{(N)}(T) \sim \left(\frac{\vec{t}_D^{(1)}}{N}\right)^2 \frac{(e^{-k_{L_2}T} - e^{-k_{L_1}T})(k_{D_2} - k_{D_1})k_{D_2}\rho_{D_2}k_{D_1}\rho_{D_1}}{\langle 1|\mathsf{K}_D|p_D^{eq}\rangle\langle 1|(I - e^{-\mathsf{K}_L T})\mathsf{K}_L|p_L^{eq}\rangle}. \tag{2.88}$$

$$= k_{D_1}k_{D_2}\left(\frac{\vec{t}_D^{(1)}}{N}\right)^2 \Delta\vec{t}_{D<}^{(1)}(T). \tag{2.89}$$

The same line of argument adapted to Eq. (2.73), leads to the following expression for the complementary dark constrained mean

$$\Delta\vec{t}_{D>}^{(N)}(T) = -\frac{(e^{-k_{L_2}T} - e^{-k_{L_1}T})\vec{t}_D^{(1)}k_{L_2}\rho_{L_2}}{N\langle 1|e^{-\mathsf{K}_L T}\mathsf{K}_L|p_L^{eq}\rangle}\left(1 - \frac{N}{\vec{t}_D^{(1)}}\int_0^\infty e^{-k_{D_2}t}E_D(t)^{N-1}dt\right), \tag{2.90}$$

and for large N

$$\Delta\vec{t}_{D>}^{(N)}(T) \sim \left(\frac{\vec{t}_D^{(1)}}{N}\right)^2 \frac{(e^{-k_{L_2}T} - e^{-k_{L_1}T})(k_{D_1} - k_{D_2})k_{D_2}\rho_{D_2}k_{D_1}\rho_{D_1}}{\langle 1|\mathsf{K}_D|p_D^{eq}\rangle\langle 1|e^{-\mathsf{K}_L T}\mathsf{K}_L|p_L^{eq}\rangle} \tag{2.91}$$

$$= k_{D_1}k_{D_2}\left(\frac{\vec{t}_D^{(1)}}{N}\right)^2 \Delta\vec{t}_{D>}^{(1)}(T). \tag{2.92}$$

At this point we can draw an interesting conclusion from Eq. (2.89) and Eq. (2.92): $\Delta\vec{t}_{D<}^{(N)}$ and $\Delta\vec{t}_{D>}^{(N)}$ have the same algebraic signs as their single-active-site counterparts, but their amplitude decays as N^{-2} for large N. In Fig. 2.3, we investigate numerically the N-dependence for a catalyst with many active sites, all of them identical to the active site in Fig. 2.1 represented by a solid line. While we expect Eq. (2.89) and Eq. (2.92) to be numerically correct for large N, we see that this prediction is still accurate for small systems with only ten active sites.

Constrained means for light dwell times have a different dependence on N. We consider first $\Delta\vec{t}_{L<}^{(N)}$. From Eq. (2.74), we find two general and equivalent expressions in terms of single-active-site Green functions, that explicitly reflect the dependence of $\Delta\vec{t}_{L<}^{(N)}$ on N

$$\Delta\vec{t}_{L<}^{(N)}(T) = E_D(T)^{N-1}\frac{\langle 1|(I\vec{t}_L^{(1)} - \mathsf{K}_L^{-1})\mathsf{K}_D\mathsf{g}_\mathsf{D}(T)|p_D^{eq}\rangle}{\langle 1|\mathsf{K}_D|p_D^{eq}\rangle - E_D(T)^{N-1}\langle 1|\mathsf{K}_D\mathsf{g}_\mathsf{D}(T)|p_D^{eq}\rangle}, \tag{2.93}$$

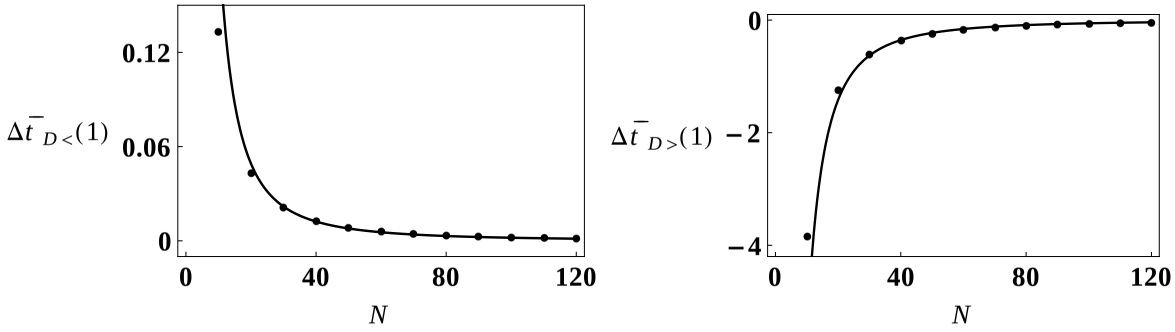

Figure 2.3: Discrete points show constrained mean dwell time differences in the nonfluorescent state at $T_L = 1$ for catalysts with N active sites, each with two internal states. Rate constants for reaction and desorption have the same values of the solid curves in Fig. 2.1 , $k_{D_1} = 0.1$, $k_{D_2} = 0.01$, $k_{L_1} = 1$, and $k_{L_2} = 10$, as do rate constants for changing site states, $d_{12} = l_{12} = l_{21} = 10^{-4}$ and $d_{21} = 0.01$. Solid curves are fits to the form $\propto N^{-2}$. Time unit is $k_{L_1}^{-1}$.

and

$$\Delta\bar{t}_{L<}^{(N)}(T) = E_D(T)^{N-1}\left(\frac{-\bar{t}_L^{(1)}\dot{g}_D(T) - \int_0^\infty dt_L g_{LD}(t_L,T)}{1+(E_D(T))^{N-1}\dot{g}_D(T)}\right). \tag{2.94}$$

Both of these expressions coincide with our prediction in Eq. (2.39) when $N = 1$. For a catalyst with a large number of identical and independent active sites, each one admitting two internal substates and close to the static limit, Eq. (2.93) and Eq. (2.94) become

$$\Delta\bar{t}_{L<}^{(N)}(T) = \frac{e^{-NT/\bar{t}_D}}{\langle 1|\mathsf{K}_L|p_L^{eq}\rangle}\frac{(k_{L_1}-k_{L_2})(e^{-k_{D_1}T}-e^{-k_{D_2}T})}{(1-e^{-k_{D_1}T}e^{-NT/\bar{t}_D})k_{D_1}\rho_{D_1}+(1-e^{-k_{D_2}T}e^{-NT/\bar{t}_D})k_{D_2}\rho_{D_2}}. \tag{2.95}$$

We observe that, in contrast to the case of $Deltat\bar{t}_{D<}^{(N)}(T)$ and $Deltat\bar{t}_{D>}^{(N)}(T)$ in Eqs. (2.89) and (2.89), in the static limit $Deltat\bar{t}_{L<}^{(N)}(T)$ does not exhibit a simple connection with the correspondig constrained mean for a single active site. Moreover, $Deltat\bar{t}_{L<}^{(N)}(T)$ on N in a nontrivial form and the term $e^{-NT/\bar{t}_D}$ will dominate only for large N. In contrast, a striking result emerges from the analysis of Eq. (2.75), namely

$$\Delta\bar{t}_{L>}^{(N)}(T) = \Delta\bar{t}_{L>}^{(1)}(T). \tag{2.96}$$

We infer that the constrained mean light dwell time, when the constraint is to consider only light dwell times that take place after long dark dwell times (i.e. bigger than the threshold value T), does only reflect the dynamic heterogeneity of a single active site and disregards the total number of active sites. Moreover, Eq. (2.96) is valid whether the system is close the static limit or not and, the algebraic sign of both $\Delta\bar{t}_{L<}^{(N)}$ and $\Delta\bar{t}_{L>}^{(N)}$ coincides with the one predicted for a single active site.

Another qualitative characteristic of the constrained mean dwell times that bears information regarding the number of active sites is the rate of decay. We found in Sec. 2.2 that $\Delta\bar{t}_{D<}$ and $\Delta\bar{t}_{L<}$ decay to zero, while $\Delta\bar{t}_{D<}$ and $\Delta\bar{t}_{L<}$ approach

to two different nonzero constants. In the static limit, for a system with two substates, and when the separation of the two reaction rate constants and also between the two desorption rate constants is large, the decay of these functions is exponential, with the decay dominated by one of these rate constants. Explicitly, from Eq. (2.89) and Eq. (2.92) we observe that $\Delta\bar{t}^{(N)}_{D<}(T)$ and $\Delta\bar{t}^{(N)}_{D>}(T)$ have asymptotic decay rates dominated by the rate constants k_L^{small} and k_L^{big}, respectively. On the contrary, from Eq. (2.95) and Eq. (2.96) we find that $\Delta\bar{t}^{(N)}_{L<}(T)$ and $\Delta\bar{t}^{(N)}_{L>}(T)$ have asymptotic decay rates Nk_D^{big} and k_D^{big}, respectively. Notice that in the asymptotic analysis of the constrained means, one has to take in account that $\bar{t}_D \to (k_D^{big})^{-1}$ in the static limit, and with k_D^{small} significantly smaller than k_D^{big}.

The question now is whether we can assert that nanoparticles as heterogeneous catalysts with multiple active sites can be well described by a model with identical and independent active sites. Before we attempt to answer this question, we must investigate what properties the constrained mean dwell times have for a model with many *dependent* active sites. This will be our task in the next section.

2.4 A model for a system with correlated active sites

In the absence of spatial resolution, we introduce correlation among active sites by restricting the number of configurations that the nanoparticle can take. In this way, if one were able to determine the substate of a given single active site, then one could better estimate, if not completely determine, the substate in which other active sites are. Thus, restricting the number of possible configurations is indeed a way to introduce space correlation in our models.

We now present a correlated model for N chemically-identical active sites, each one of which has n-substates. We restrict the number of possible configurations by imposing that in the dark state only configurations that assign to every single active site the same dark substate, say D_i, are accessible. Moreover, admissible light configurations have only one active site in the light state, say in the substate L_i, and every other active site is in the same dark substate (accordingly D_i). Thus, we have n configurations in the dark state and $N \times n$ configurations in the light state. However, as the experiment does not discern between light configurations corresponding to light states occurring in different active sites, light configurations that differ only in the active site that is in the light substate are equivalent. We are therefore led to n distinct configurations in the light state. Consequently, the dark state vector $|P_D\rangle$, is a column vector of dimension n whose i-th element is ρ_{D_i}, which in this case will denote the probability of the ith dark configuration. Also, $|P_L\rangle$ is a vector of dimension n whose i-th element is the ith-light-configuration probability ρ_{L_i}. $|P_L\rangle$ can also be defined as a linear combination of the N equivalent configurations $|P_L^{(j)}\rangle$, where j labels the active site that is in the light state. Finally, we denote by $|P\rangle$ the vector of all substate probabilities that is given by $|P_D\rangle \otimes |P_L\rangle$.

The equations of evolution of $|P\rangle$ can be estimated from the equations of evolution of individual configurations. In order to be able to compare this model with the independent model introduced in Sec. 2.3, we assume that rate constants of reaction and desorption are the same in both models. Although we shall use the same notation for the internal rate constants, the reader should notice that they are different from those of a single active site. The equations for

the evolution of different configurations are

$$\frac{d\rho_{D_k}}{dt} = -\left(Nk_{D_k} + \sum_{r\neq k}^{m} d_{rk}\right)\rho_{D_k} + k_{L_k}\rho_{L_k} + \sum_{r\neq k}^{m} d_{kr}\rho_{D_r}, \tag{2.97}$$

$$\frac{d\rho_{L_k}}{dt} = -\left(k_{L_k} + \sum_{r\neq k}^{m} l_{rk}\right)\rho_{L_k} + Nk_{D_k}\rho_{D_k} + \sum_{r\neq k}^{m} l_{kr}\rho_{L_r}. \tag{2.98}$$

Eq. (2.97) and (2.98) are identical to the equations of evolution for a single active site with reaction rate constants k_{D_k} increased by a factor that is equal to the number of correlated active sites N. Hence, the differential equation of $|P\rangle$ is identical to Eq. (2.50) with the following definition for the matrices W_{DD}, W_{DL}, W_{LD} and W_{LL}

$$W_{DD} = N\mathsf{K}_D + \Gamma_D, \tag{2.99}$$

$$W_{DL} = -\mathsf{K}_L, \tag{2.100}$$

$$W_{LD} = -N\mathsf{K}_D, \tag{2.101}$$

$$W_{LL} = \mathsf{K}_L + \Gamma_L. \tag{2.102}$$

Observe that definitions for many-active-site density functions in Eqs. (2.58), (2.59), (2.64) and (2.65), and their corresponding generating functions in Eqs. (2.62), (2.63), (2.66) and (2.67) are given in terms of general W matrices and do not use the independence hypothesis. Therefore, they can be used along with the definitions in Eq. (2.99) - (2.102) to compute constrained and unconstrained means. In this way we find that mean value of the dwell times are

$$\bar{t}_D^{(N)} = \frac{1}{N}\frac{\langle 1|P_D\rangle}{\langle 1|\mathsf{K}_D|P_D\rangle}, \tag{2.103}$$

$$\bar{t}_L^{(N)} = \frac{\langle 1|P_L\rangle}{\langle 1|\mathsf{K}_L|P_L\rangle}. \tag{2.104}$$

These results are not readily comparable with neither the mean times for a single active site nor those for the independent model. The reason for this, is that $|P_L\rangle$ and $|P_D\rangle$ are rational functions of the number of correlated active sites N. This

may lead to complicated changes in these values for a small number of active sites. However, for large N, the ratios $\frac{\langle 1|P_D\rangle}{\langle 1|\mathsf{K}_D|P_D\rangle}$ and $\frac{\langle 1|P_L\rangle}{\langle 1|\mathsf{K}_L|P_L\rangle}$ tend asymptotically to a pair of constant values. This suggests that we must take as our reference an ideal model with N large, instead of the single active side used in the uncorrelated case. We denote by $|\overline{p}_D^{eq}\rangle$ the limit vector $|P_D^{eq}\rangle$ when $N \to \infty$ and also, $|\overline{p}_L^{eq}\rangle$ for $|P_L^{eq}\rangle$ in the same limit.

After these considerations, we find that in the static limit and for a large number of correlated active sites, constrained means have the following functional form

$$\Delta\vec{t}_{D<}^{(N)}(T) = \frac{1}{N}\frac{\langle 1|\left(I\,\bar{t}_D - \mathsf{K}_D^{-1}\right)\mathsf{K}_L e^{-\mathsf{K}_L T}|\overline{p}_L^{eq}\rangle}{\langle 1|(I - e^{-\mathsf{K}_L T})\mathsf{K}_L|\overline{p}_L^{eq}\rangle}, \tag{2.105}$$

$$\Delta\vec{t}_{D>}^{(N)}(T) = -\frac{1}{N}\frac{\langle 1|\left(I\,\bar{t}_D - \mathsf{K}_D^{-1}\right)\mathsf{K}_L e^{-\mathsf{K}_L T}|\overline{p}_L^{eq}\rangle}{\langle 1|e^{-\mathsf{K}_L T}\mathsf{K}_L|\overline{p}_L^{eq}\rangle}, \tag{2.106}$$

$$\Delta\vec{t}_{L<}^{(N)}(T) = \frac{\langle 1|(I\,\bar{t}_L - \mathsf{K}_L^{-1})\mathsf{K}_D e^{-N\mathsf{K}_D T}|\overline{p}_D^{eq}\rangle}{\langle 1|(I - e^{-N\mathsf{K}_D T})\mathsf{K}_D|\overline{p}_D^{eq}\rangle}, \tag{2.107}$$

$$\Delta\vec{t}_{L>}^{(N)}(T) = -\frac{\langle 1|(I\,\bar{t}_L - \mathsf{K}_L^{-1})\mathsf{K}_D e^{-N\mathsf{K}_D T}|\overline{p}_D^{eq}\rangle}{\langle 1|e^{-N\mathsf{K}_D T}\mathsf{K}_D|\overline{p}_D^{eq}\rangle}, \tag{2.108}$$

From Eq. (2.105) and (2.106) we find that in contrast to the independent model, the amplitudes of $\Delta\vec{t}_{D<}^{(N)}(T)$ and $\Delta\vec{t}_{D>}^{(N)}(T)$ decay as N^{-1}. Besides, from Eq. (2.108) we observe that $\Delta\vec{t}_{L>}^{(N)}$ is N-dependent in opposition to the result for independent active sites (see Eq. (2.92)). Moreover, for $n = 2$ the constrained means in Eq. (2.105)- (2.108) reduce to a single-active-site form with the following differences. First, the substate probabilities ρ_{D_i} and ρ_{L_i} are substituted by their asymptotic limit as N becomes large. Second, $\Delta\vec{t}_{D<}^{(N)}$ and $\Delta\vec{t}_{D>}^{(N)}$ have an additional factor of N^{-1}. Third, the exponents in all the exponential functions in $\Delta\vec{t}_{L<}^{(N)}$ and $\Delta\vec{t}_{L>}^{(N)}$ are rescaled to $N \times k_{D_i}$.

In Fig 2.4, we explore numerically the validity of the approximation in Eq.

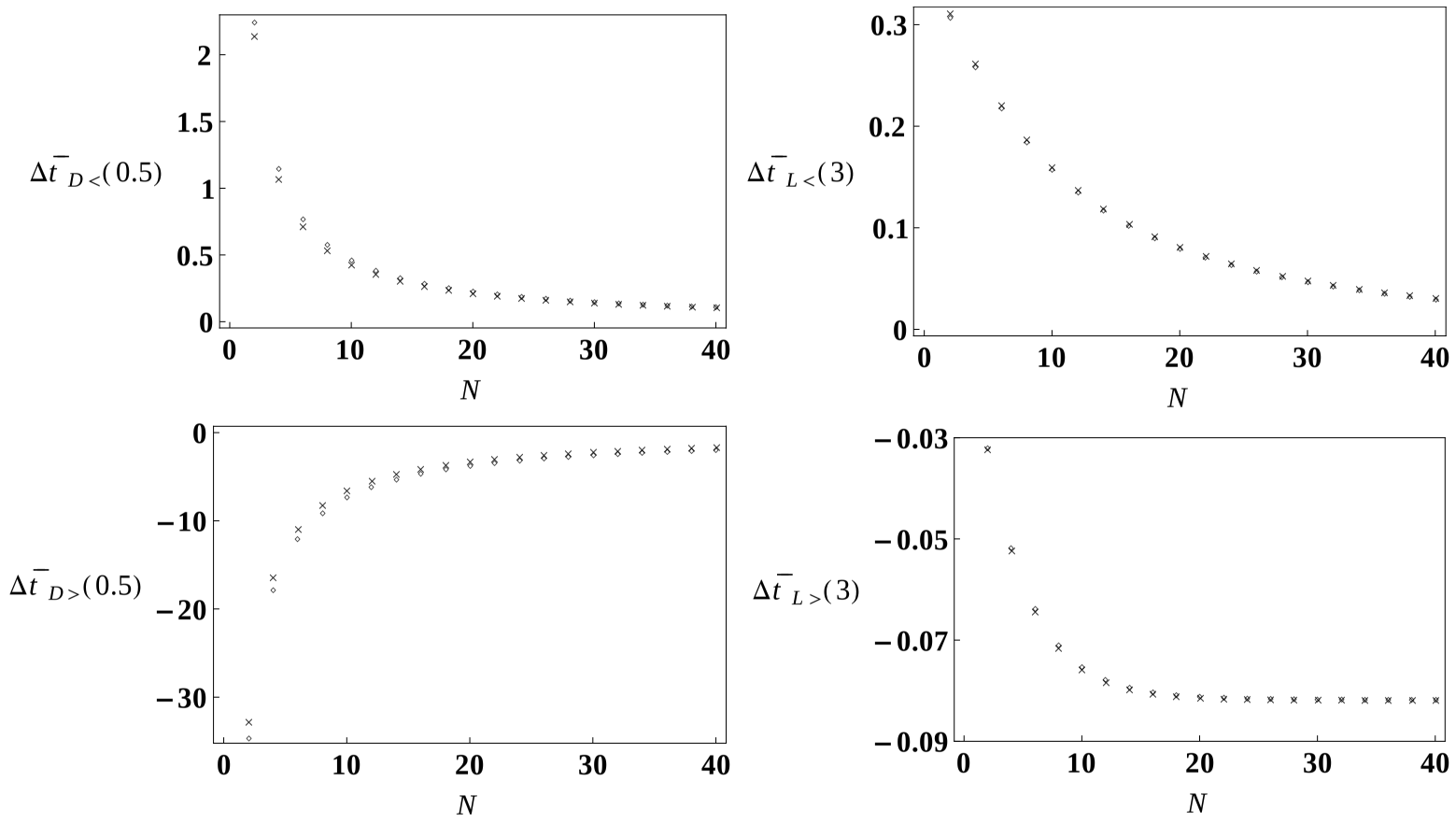

Figure 2.4: Constrained mean dwell times as calculated for a given threshold time T are shown for a catalyst as a function of the number of correlated active sites N. Each active site has two substates. The exact value for each number of active sites N are represented by the symbol $\diamond$, and those calculated approximately from Eq. (2.105)-(2.108) by the symbol $\times$. Rate constants for reaction and desorption have the same values of the solid curves in Fig. 2.1 , $k_{D_1} = 0.1$, $k_{D_2} = 0.01$, $k_{L_1} = 1$, and $k_{L_2} = 10$, as do rate constants for changing site states, $d_{ij} = l_{ij} = 10^{-4}$. Time unit is $k_{L_1}^{-1}$.

(2.105)-(2.108) for a sample model with two substates. We see that our prediction for large values of N is in excellent agreement for a number of correlated active sites as small as 10. In the case of a large separation in the magnitudes of the reaction rate constants and also between the desorption rate constants, we find that the asymptotic decay rates for $\Delta\vec{t}^{(N)}_{D<}$ and $\Delta\vec{t}^{(N)}_{D>}$ are k_L^{small} and k_L^{big}, respectively. This conclusion is exactly the same as we found in the case of a catalyst with independent active sites in Sec. 2.3. On the contrary, the asymptotic decay rates of $\Delta\vec{t}^{(N)}_{L<}$ and $\Delta\vec{t}^{(N)}_{L>}$ are different to those predicted for independent active sites. Specifically, for the model with correlated active sites the asymptotic decay rate for $\Delta\vec{t}^{(N)}_{L<}$ is Nk_D^{small}, and for $\Delta\vec{t}^{(N)}_{L>}$ is Nk_D^{big}; whereas for the model with independent active sites they are Nk_D^{big} and k_D^{big}, respectively. To put it another way, we must observe a faster decay for $\Delta\vec{t}^{(N)}_{L>}$ than for $\Delta\vec{t}^{(N)}_{L<}$ in the case of correlated active sites and, as stated in Sec. 2.3, this situation is reversed for independent active sites. This is a significant characteristic that can qualitatively decide whether a catalyst can be conceived as a set of independent active sites or, whether space correlation or cooperative behavior exists among the active sites. In fact, if a catalyst with many active sites is found to deviate qualitatively from any of the characteristics predicted for the independent model, we must infer that active sites are not independent, as there is only one possible independent model. Furthermore, it only takes one trajectory with statistically meaningful events to find which model describes better a catalyst with many active sites.

In Fig. 2.5 we numerically test how $\Delta\vec{t}^{(N)}_{L<}$ and $\Delta\vec{t}^{(N)}_{L>}$ decay by considering two models, one independent and one correlated, both of them with 256 active sites, all of them identical to the single active site plotted with a solid line in Fig. 2.1. For the independent model, displayed in panel A, $\Delta\vec{t}^{(N)}_{L<}$ decays to zero only near $T_D = 1$ while $\Delta\vec{t}^{(N)}_{L>}$ has reached its asymptote even before $T_D = 0.5$. The correlated

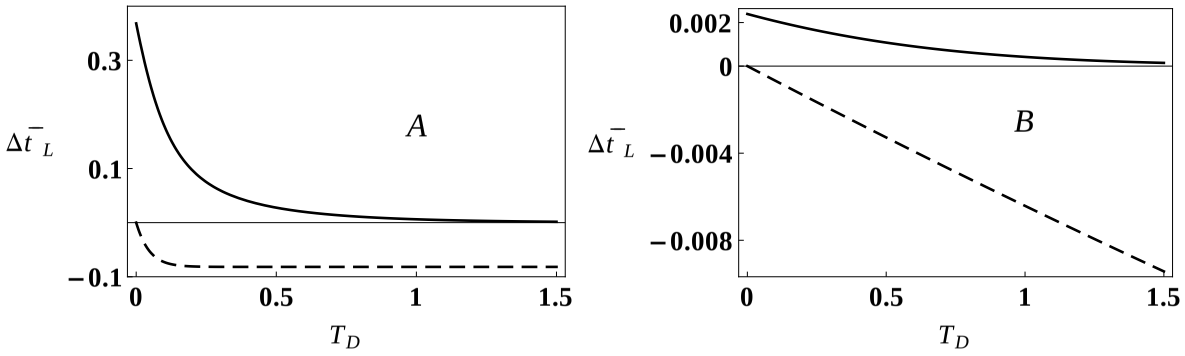

Figure 2.5: Constrained mean dwell times in the fluorescent state are shown for a catalyst with $N = 256$ active sites, each with two internal states. Differences between constrained and unconstrained mean times are plotted. Rate constants for reaction and desorption have the same values of the solid curves in Fig. 2.1 , $k_{D_1} = 0.1$, $k_{D_2} = 0.01$, $k_{L_1} = 1$, and $k_{L_2} = 10$, as do rate constants for changing site states, $d_{12} = l_{12} = l_{21} = 10^{-4}$ and $d_{21} = 0.01$. In panel A, all sites change states simultaneously, while in panel B, sites change states independently. Solid lines show $\Delta\bar{t}_{L<}(\tau_D)$ and dashes show $\Delta\bar{t}_{L>}(\tau_D)$. Time unit is $k_{L_1}^{-1}$.

model, shown in panel B, has a similar decay rate for $\Delta\vec{t}^{(N)}_{L<}$, while $\Delta\vec{t}^{(N)}_{L>}$ reaches its asymptote for $T_D > 1.5$. These observations are consistent with our qualitative characterizations of the constrained means for light times in these two models.

We close this section by emphasizing that, while there may be other possible models with correlation among active sites, we believe that the one introduced in this section is the simplest and, has enough characteristics to be differentiated from the model with independent active sites. In fact, these two models can be used to construct more general scenarios, as will be described in the next section.

2.5 An intermediate model: domains of correlation

The independent model of Sec. 2.3 and the correlated model of Sec. 2.4, are two extreme cases of a more general family of correlated models. It is likely that for certain systems, active sites are only correlated with neighboring active sites defining in this way regions of correlation. Thus, a catalyst with many active sites could be divided i into many different and pairwise independent domains composed of several active sites. Realistically, domains may differ in the number of active sites but, for simplicity, we will assume that the number of active sites S is the same in every domain, and that active sites are chemically identical. If J is the total number of domains, then the total number of active sites N must equal $S\ J$. The model that we will describe below, reduces to the independent model of Sec. **??** when $S = 1$ and $J = N$ and we also recover the model in Sec. 2.4 when $S = N$ and $J = 1$.

We describe correlation in a single domain by restricting the number of possible configurations for the group of S active sites in the same way we did in

Sec. 2.4. As a consequence, the dynamics of a given domain is equivalent to that of a single active site with rescaled reaction rate constants, to wit, k_{D_i} is replaced by $S k_{D_i}$. Because domains are independent, the density functions, their corresponding generating functions and constrained means for a model with domains are those of a model with J independent active sites with reaction rate constants rescaled as the size of our domains. Hence, the constrained mean dwell times for active sites with two substates that are close to the static limit are:

$$\Delta\bar{t}^{(JS)}_{D<}(T) = \frac{(e^{-k_{L_2}T} - e^{-k_{L_1}T})\bar{t}^{(S)}_D k_{L_2}\rho^{(S)}_{L_2}}{J\langle 1|(I - e^{-\mathsf{K}_L T})\mathsf{K}_L|\bar{p}^{eq}_L\rangle}\left(1 - \frac{J}{\bar{t}^{(S)}_D}\int_0^\infty e^{-Sk_{D_2}t}E_D(t)^{J-1}dt\right) \tag{2.109}$$

$$\sim \left(\frac{\bar{t}^{(S)}_D}{JS}\right)^2 S\ \frac{(e^{-k_{L_2}} - e^{-k_{L_1}})(k_{D_2} - k_{D_1})k_{D_2}\rho^{(S)}_{D_2}k_{D_1}\rho^{(S)}_{D_1}}{\langle 1|\mathsf{K}_D|\bar{p}^{eq}_D\rangle\langle 1|(I - e^{-\mathsf{K}_L T})\mathsf{K}_L|\bar{p}^{eq}_L\rangle} + O\left(\frac{1}{J^3S^2}\right) \tag{2.110}$$

$$\Delta\bar{t}^{(JS)}_{D>}(T) = -\frac{(e^{-k_{L_2}T} - e^{-k_{L_1}T})\bar{t}^{(S)}_D k_{L_2}\rho^{(S)}_{L_2}}{J\langle 1|e^{-\mathsf{K}_L T}\mathsf{K}_L|\bar{p}^{eq}_L\rangle}\left(1 - \frac{J}{\langle t^{(S)}_D\rangle}\int_0^\infty e^{-Sk_{D_2}t}E_D(t)^{J-1}dt\right) \tag{2.111}$$

$$\sim \left(\frac{\bar{t}^{(S)}_D}{JS}\right)^2 S\ \frac{(e^{-k_{L_2}} - e^{-k_{L_1}})(k_{D_1} - k_{D_2})k_{D_2}\rho^{(S)}_{D_2}k_{D_1}\rho^{(S)}_{D_1}}{\langle 1|\mathsf{K}_D|\bar{p}^{eq}_D\rangle\langle 1|e^{-\mathsf{K}_L T}\mathsf{K}_L|\bar{p}^{eq}_L\rangle} + O\left(\frac{1}{J^3S^2}\right) \tag{2.112}$$

$$\Delta\bar{t}^{(JS)}_{L<}(T) = E_D(T)^{J-1}\frac{\langle 1|(I\,\bar{t}^{(S)}_L - \mathsf{K}_L^{-1})S\mathsf{K}_D\mathsf{g}_\mathsf{D}(T)|\overline{p}^{eq}_D\rangle}{\langle 1|S\mathsf{K}_D|\overline{p}^{eq}_D\rangle - E_D(T)^{N-1}\langle 1|S\mathsf{K}_D\mathsf{g}_\mathsf{D}(T)|p^{eq}_D\rangle} \tag{2.113}$$

$$= E_D(T)^{J-1}\frac{(k_{L_1} - k_{L_2})(e^{-Sk_{D_1}T} - e^{-Sk_{D_2}T})\rho^{(S)}_{l_1}\rho^{(S)}_{l_2}}{\langle 1|\mathsf{K}_L|\overline{p}^{eq}_L\rangle\langle 1|S\mathsf{K}_D\left(I - E_D(T)^{J-1}\mathsf{g}_\mathsf{D}(T)\right)|\overline{p}^{eq}_D\rangle} \tag{2.114}$$

$$\Delta\bar{t}^{(JS)}_{L>}(T) = \Delta\bar{t}^{(S)}_{L>}(T) \tag{2.115}$$

$$= -\frac{\langle 1|(I\,\bar{t}^{(S)}_L - \mathsf{K}_L^{-1})S\mathsf{K}_D e^{-S\mathsf{K}_D T}|\overline{p}^{eq}_D\rangle}{\langle 1|e^{-S\mathsf{K}_D T}S\mathsf{K}_D|\overline{p}^{eq}_D\rangle} \tag{2.116}$$

Observe that the algebraic sign of the constrained means follows the same rules determined for the uncorrelated and correlated models. On the other hand, the amplitude of $\Delta\bar{t}_{D<}$ and $\Delta\bar{t}_{D>}$ depends on the number of active sites in two different ways: as a function of the size of each domain it decreases as

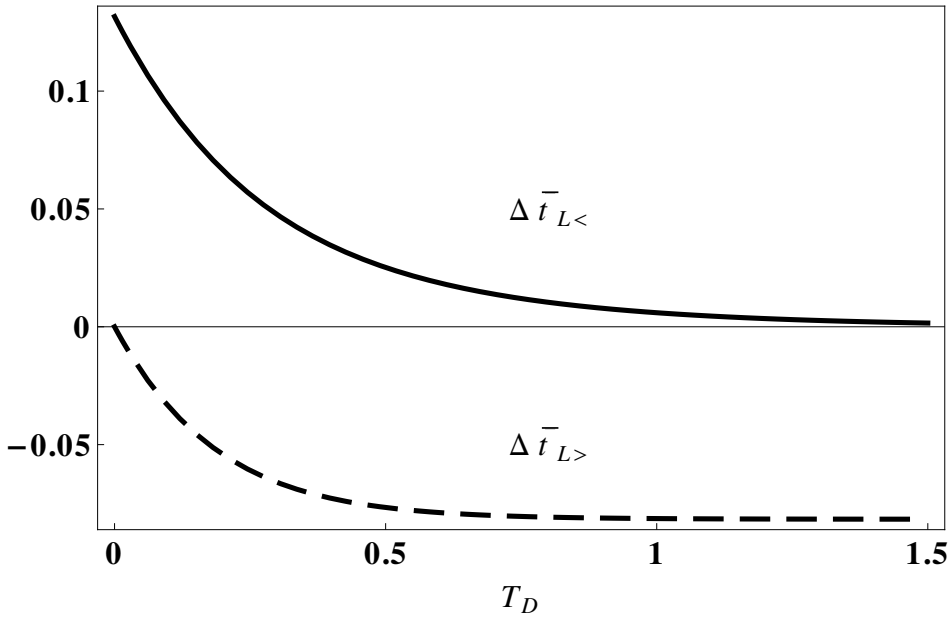

Figure 2.6: Constrained mean dwell times in the fluorescent state are shown for a catalyst with $N = 256$ active sites, each with two internal states. Differences between constrained and unconstrained mean times are plotted. All rate constants are identical to those in Fig. 2.5. The system is composed of 4 domains of 64 sites each, with site fluctuations correlated within a domain and uncorrelated between domains. Time unit is $k_{\mathrm{L_1}}^{-1}$.

S^{-1} and, as a function of the number of domains it decays as J^{-2}. This assertion must hold for a large number of independent domains, each one with a significant number of active sites. On the other hand, we find that $\Delta\bar{t}_{L>}$ is a function only of the size of every domain, and is independent of how many of these exist.

Asymptotic decay rates for models with N active sites and well-separated reaction and desorption rate constants, should transition between the two extreme cases as we go through models with different domain sizes. In Sec. 2.4 we elaborated on the idea that $\Delta\bar{t}_{L>}$ and $\Delta\bar{t}_{L>}$ should decay in different ways for correlated and uncorrelated active sites. While some model with domains may have qualitative decays that are closer to any of the extreme cases, there

is room for unique models where both of these constrained means have similar asymptotic decay rates, to the point that they can be thought as having the same decaying rate. In Fig. 2.6, we study this situation for a model with the same total number of active sites than the correlated and uncorrelated models in Fig. 2.5. In Fig. 2.6, the 256 active sites are partitioned in four independent domains, so that each one has 64 of them. We recognize that for this model $\Delta\bar{t}^{(N)}_{L<}$ and $\Delta\bar{t}^{(N)}_{L>}$ decay to their corresponding asymptotic values around the threshold value $T_D = 1.5$.

2.6 Constrained means for single nanoparticle trajectories

We have calculated constrained mean dwell times from single-turnover fluorescence trajectories measured by Chen and coworkers[51, 58] for the reductive *N*-deoxygenation of the nonfluorescent reactant resazurin to the fluorescent product resorufin, catalyzed by a spherical gold nanoparticle. Constrained mean dwell times were computed from trajectories for individual nanoparticles, and then averaged over the ensemble of trajectories for nanoparticles of the same diameter and with the same reactant concentrations. At least fifty trajectories were averaged for each diameter. The mean dwell times $\bar{t}_{\mathrm{L}}$ and $\bar{t}_{\mathrm{D}}$ show saturation behavior as a function of reactant concentration,[51, 58] and only data in the saturation regime are analyzed here. Results are presented in Figure 2.7 for diameters and resazurin concentrations 6.0 ± 1.7 nm and 1.2 μM (solid lines), 9.1 ± 1.5 nm and 0.4 μM (dotted lines), and 13.7 ±2.4 nm and 0.4 μM (dashed lines). All times are given in seconds. Zhou, et al.[58] observed a significant difference between the catalytic deactivation of particles with the smallest diameter and with the two larger diameters. For particles of the two larger diameters, $\bar{t}_{\mathrm{D}}$ is

found to increase during the course of the measurement on the time scale of tens of minutes, indicating that the catalyst becomes deactivated in time. Since $\bar{t}_{\rm L}$ does not show this time dependence, poisoning of the catalyst by reaction products other than resorufin has been proposed as a cause.[58] For the 6 nm diameter particles, such deactivation occurs detectably only on times longer than three hours, providing a sufficient time window to collect data without significant deactivation. The curves in Fig. 2.7 for the three particle diameters have the same algebraic sign and qualitative appearance. The models of Secs. 2.2-2.5 could be modified to include an irreversible deactivation process when a site is in the dark state. However, to simplify the interpretation, we will focus attention on the data for the particles with 6 nm diameter for which deactivation is negligible.

The data in Fig. 2.7 for particles of diameter 6 nm are replotted as the open squares in Fig. 2.8. As in Fig. 2.7, all times are given in seconds. Dashed curves show fits to empirical functional forms, $\Delta\bar{t}_{j<}(T) = C_1 e^{-k_1 T} + C_2 e^{-k_2 T}$ and $\Delta\bar{t}_{j>}(T) = C_3(1 - e^{-k_3 T})/(C_4 + e^{-k_3 T})$. For j = L, C_1 = 0.0426 s, C_2 = 0.104 s, C_3 = −0.0744 s, C_4 = 2.00, k_1 = 0.217 s^{-1}, k_2 = 1.18 s^{-1}, k_3 = 1.835 s^{-1}. For j = D, C_1 = 0.373 s, C_2 = 0.926 s, C_3 = −0.0287 s, C_4 = 0.0477, k_1 = 1.66 s^{-1}, k_2 = 7.83 s^{-1}, k_3 = 9.37 s^{-1}. In Sec. 2.4, we demonstrated that constrained mean dwell times are sensitive to correlations among dynamic fluctuations at different active sites in a catalyst with multiple active sites. In particular, we showed that for N sites with completely correlated fluctuations, $\Delta\bar{t}_{\rm L>}(T_{\rm D})$ decays more rapidly than $\Delta\bar{t}_{\rm L<}(T_{\rm D})$, while for completely independent fluctuations, $\Delta\bar{t}_{\rm L>}(T_{\rm D})$ decays more slowly than $\Delta\bar{t}_{\rm L<}(T_{\rm D})$.

A qualitative comparison of these two quantities indicates the importance of

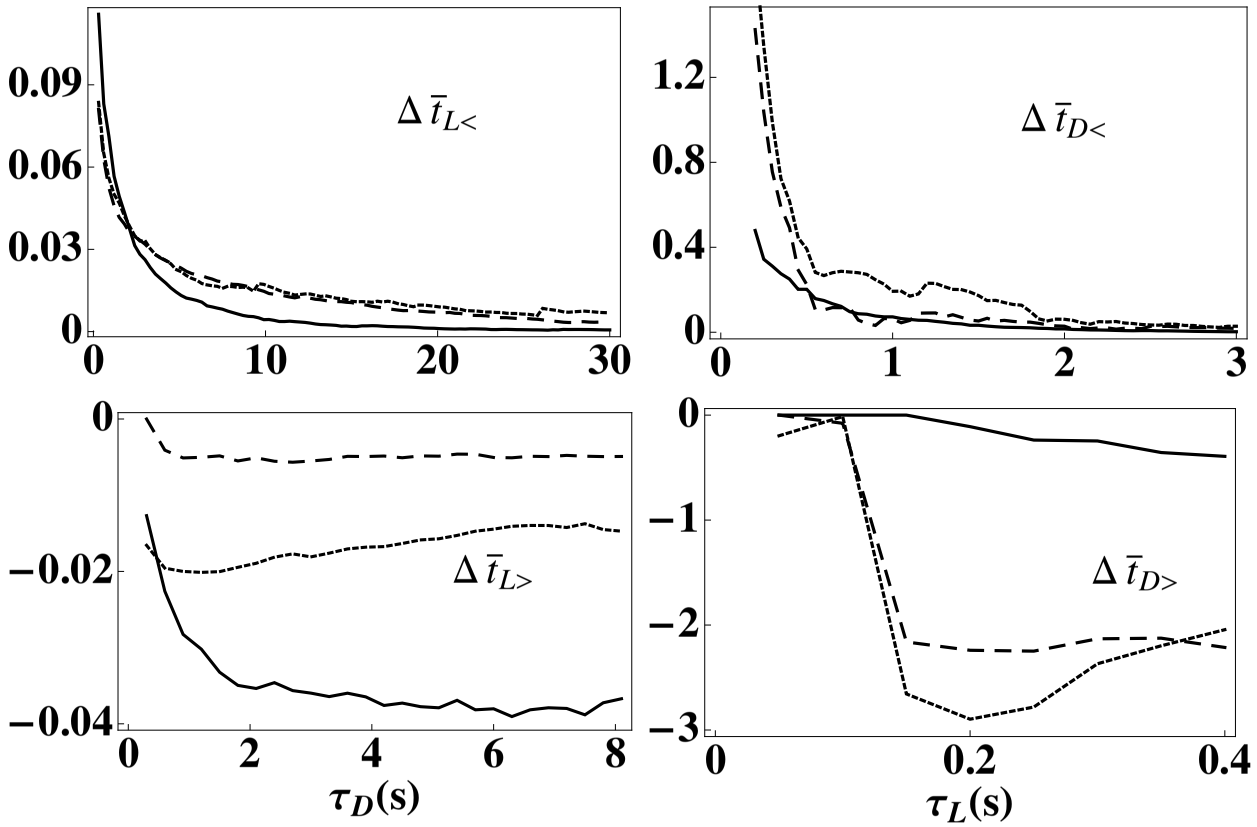

Figure 2.7: Constrained mean dwell times are calculated from single-turnover measurements of the catalysis by spherical gold nanoparticles of the conversion of resazurin to resorufin. The nanoparticle diameter is varied from 6.0 nm (solid lines) to 9.1 nm (dotted lines) to 13.7 nm (dashed lines).

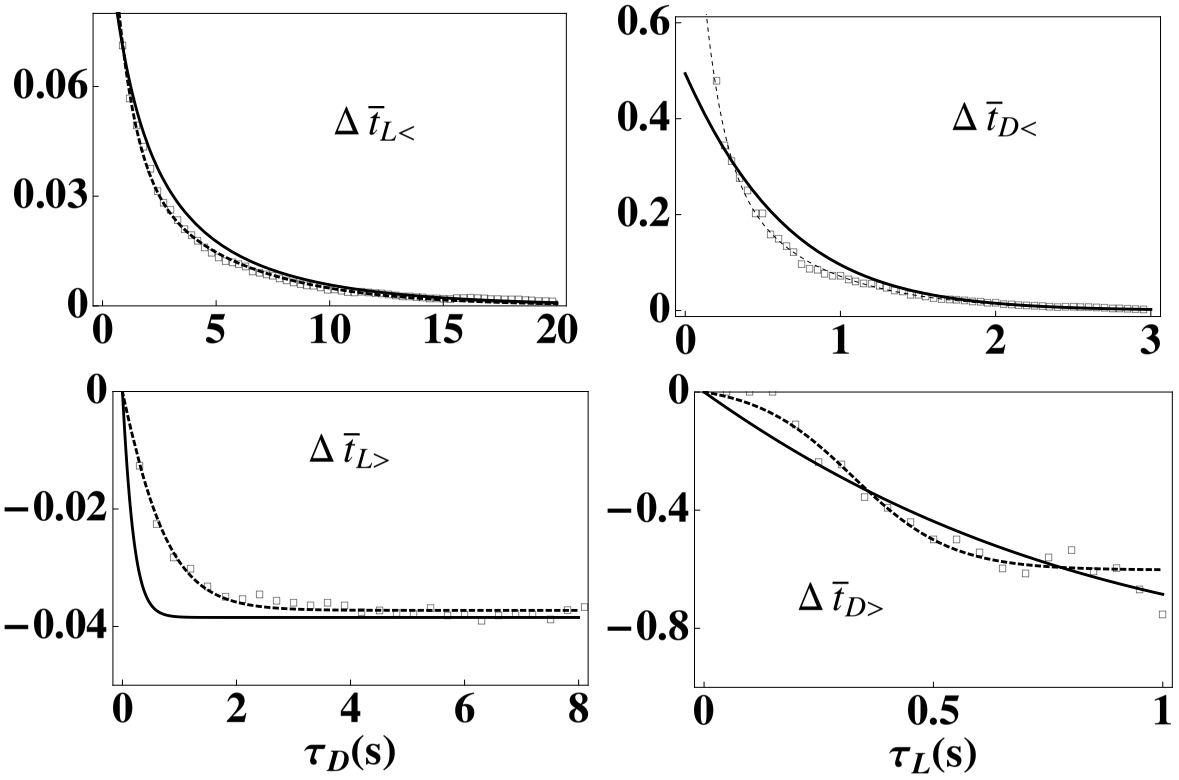

Figure 2.8: Constrained mean dwell times are shown as open squares for gold nanoparticles of diameter 6 nm. Dashed lines show empirical fits and solid lines show fits to a two-state kinetic model with dynamic disorder.

dynamic correlations among events at different active sites. These two quantities for 6 nm particles are shown in the two left-hand panels of Fig. 2.8, which demonstrate that $\Delta\bar{t}_{L>}(T_D)$ decays more rapidly than $\Delta\bar{t}_{L<}(T_D)$. Similar trends are also clear for gold nanoparticles of diameter 9 and 14 nm, as shown in Fig. 2.7.

These data are thus more consistent with a scenario in which active sites are correlated, than with a picture in which the substate fluctuations occur entirely independently. In Sec. 2.4, we showed that in the model of completely correlated fluctuations, the number of active sites N enters only as a scaling factor multiplying reaction rate constants, so that in principle the data in Fig. 2.8 are also consistent with the case of $N = 1$, with each nanoparticle having a single active site. However, this is not the case, since several product molecules are occasionally observed[51] simultaneously on single 6 nm nanoparticles, indicating the presence of a multiplicity of sites. The present analysis therefore indicates correlated dynamics at active sites on gold nanoparticles.

The solid curves in Fig. 2.8 show least-squares fits to the prediction of the kinetic model of Sec. 2.4 with $n = 2$, N sites, and completely correlated fluctuations. The limit of static disorder is not assumed to hold, so that, for example, $\Delta\bar{t}_{L<}(T_D)$ is calculated from the general form in Eq. (2.39) rather than from the simplified static limit in Eq. (2.107). The resulting parameter values are $Nk_{D_1} = 6.30\ s^{-1}, Nk_{D_2} = 0.175\ s^{-1}, k_{L_1} = 1.45\ s^{-1}, k_{L_2} = 2.48\ s^{-1}, d_{12} = 0, d_{21} = 0.147\ s^{-1}, l_{12} = 0.516\ s^{-1}, l_{21} = 0.860\ s^{-1}$. The fit was carried out subject to the conditions that the unconstrained mean dwell times be near to the experimental values $\bar{t}_L = 0.48$ s and $\bar{t}_D = 4.28$ s. The solid curves in Fig. 2.8 yield unconstrained mean times $\bar{t}_L = 0.47$ s and $\bar{t}_D = 4.31$ s, close to the correct values. The fitted rate constant values describe a system near to the limit of static disorder, in which rate

constants for site state changes, l_{ij} and d_{ji} are small compared to rate constants for reaction k_{D_i} and product desorption k_{L_j}. In particular, the rate constant for leaving a particular state because of changes in site state is smaller than the rate constant for leaving that state because of reaction or desorption, for example, $l_{12} < k_{L_2}$. Figure 2.8 demonstrates that a two-state model provides qualitatively reasonable agreement but not a quantitative fit to constrained mean dwell times for single nanoparticles.

Constrained mean dwell times calculated from the nanoparticle data support the interpretation of the autocorrelation function results in Ref.[51] that adsorption sites exist in several functionally different types. Figures 2.7 and 2.8 show that $\Delta t_{\mathrm{L}<}(\tau_{\mathrm{D}})$ and $\Delta t_{\mathrm{D}<}(\tau_{\mathrm{L}})$ decay to zero from positive values and that $\Delta t_{\mathrm{L}>}(\tau_{\mathrm{D}})$ and $\Delta t_{\mathrm{D}>}(\tau_{\mathrm{L}})$ decay from zero to negative asymptotes. As shown by the calculations in Fig. 2.1, these signs indicate that the rate at which a reactant molecule undergoes the catalytic reaction is inversely correlated with the rate of desorption of the resulting product molecule; a relatively rapid reaction event produces a relatively slowly desorbing product molecule. This qualitative conclusion is supported by the values of the rate constants used to generate the solid curves in Fig. 2.8. In these fits to the $S = 2$ model, $k_{\mathrm{D}_1} > k_{\mathrm{D}_2}$, so site state 1 has the more rapid reaction, but $k_{\mathrm{L}_1} < k_{\mathrm{L}_2}$ so site state 1 has slower desorption. This finding is consistent with a scenario in which reactions with lower activation barriers produce more stable surface-bound species.

The constrained mean dwell times also confirm the interpretation of the autocorrelation functions[51, 58] in indicating the presence of dynamical processes that alter the condition of adsorbed reactants and products. These dynamics may arise in principle either from a mechanism in which the adsorption sites

change identity through surface reconstruction of the nanoparticle[23, 13, 42, 47] or from a mechanism in which the sites are static, but mobile adsorbates can sample sites of different types,[43] or from some combination of these two limiting cases. The present analysis does not distinguish between dynamics of the nanoparticle and dynamics of adsorbates. Xu, et al.[51] have measured the dependence of decay times of $C_{\mathrm{L}}(n)$ and $C_{\mathrm{D}}(n)$ on turnover rate. These autocorrelation functions decay increasingly rapidly as the reactant concentration is increased, consistent with a scenario of adsorbate-induced surface restructuring and not with dynamics arising from motion of reactant molecules. Raising reactant concentration increases the fraction of filled sites, hindering possible relaxation through translational motion. This interpretation of dynamic disorder arising from surface reconstruction is further supported by the observation that autocorrelation function decay rates decrease with increasing particle diameter.[58] Our finding that dynamical fluctuations at different active sites are correlated is also consistent with the surface reconstruction mechanism, as surface dynamics in metal nanoparticles can involve the entire particle, and are thus nonlocal.[47] The constrained mean dwell time analysis of single nanoparticle fluorescence turnover trajectories quantifies the role of disorder and of dynamical fluctuations in these kinetics.

2.7 Conclusion

Constrained mean dwell times have proven to be excellent instruments when one is to determine the dynamic heterogeneity and complexity arising from single-molecule measurements. In particular, they can 1) select and filter information coming from different reaction paths, discerning between fast and slow

processes 2) compare between chemically-identical catalysts that differ only in the number of active sites, providing a relative measure of the number of sites 3) account for the existence of cooperative behavior among multiple active sites.

We have found that the constrained means for single nanoparticle measurements in a gold nanoparticle of 6 nm diameter, are qualitatively described by a model with multiple chemically-identical active sites that have correlated fluctuations between two different substates. In this system fast reactions, as compared to the mean reaction time, occur most likely in the same nanoparticle substate that is responsible for most of the slowest product desorptions. According to this model, the nanoparticle acts as a single unit with many reaction centers on its surface and the speed of the catalytic transformation is enhanced by the number of active sites.

All along this chapter, we have put aside the evidence coming from dwell-time correlation functions only invoking them to motive our study of the static limit. We will investigate these functions in the next Chapter and we will find how they connect and complement with the constrained mean dwell times.

APPENDIX A

APPENDICES CHAPTER 2

A.1 The equation of evolution for many independent active sites

In this section we determine the explicit form of the evolution equation Eq. (2.50) for the model with N independent and identical active sites, described in Sec. 2.3.

For a catalyst with N independent active sites, each one admitting n states, we can write the probability of a given configuration as a product of the substate probabilities assigned by the configuration to every active site. The collection of these products defines a vector that can be thought as an ordered set with the following ordering relation

$$\rho^{(1)}_{D_{i_1}}(t)\ldots\rho^{(N)}_{D_{i_N}}(t) < \rho^{(1)}_{D_{j_1}}(t)\ldots\rho^{(N)}_{D_{j_N}}(t) \text{ if } \begin{cases} i_1 < j_1 & or \\ i_k < j_k & i_1 = j_1, \ldots, i_{k-1} = j_{k-1} \end{cases}$$

Thus, we can find the i-th element of the vector $|P_D(t)\rangle$ after writing i in the n basis, i.e., for $i = i_1 m^{N-1} + i_2 m^{N-2} + \cdots + i_{N-1} m^1 + i_N m^0$ we have that the i-th element is $\rho^{(1)}_{D_{i_1}}(t)\rho^{(2)}_{D_{i_2}}(t)\ldots\rho^{(N-1)}_{D_{i_{N-1}}}(t)\rho^{(N)}_{D_{i_N}}(t)$.

In a similar way we define vectors $|P^{(s)}_L\rangle$ for s counting the active sites, and varying between 1 and N. The elements of $|P^{(s)}_L\rangle$ have the form $\rho^{(1)}_{D_{i_1}}(t)\ldots\rho^{(s)}_{L_{i_s}}(t)\ldots\rho^{(N)}_{D_{i_N}}(t)$ and can be ordered as we did for the elements of $|P_D\rangle$. Our total probability vector $|P(t)\rangle$ can be defined in terms of these vectors as

follows

$$|P(t)\rangle = \left(|P_D(t)\rangle, |P_L^{(1)}(t)\rangle, \ldots, |P_L^{(N)}(t)\rangle\right)^T .$$

Now we must establish the differential equation that determines $|P(t)\rangle$. This will arise naturally from the differential equations defining the time evolution of every active site. First, consider the time derivative of an element of $|P_D\rangle$

$$\frac{d}{dt}\left(\rho_{D_{i_1}}^{(1)}(t)\ldots\rho_{D_{i_N}}^{(N)}(t)\right) = \sum_s \rho_{D_{i_1}}^{(1)}(t)\ldots\overline{\rho_{D_{i_s}}^{(s)}(t)}\ldots\rho_{D_{i_N}}^{(N)}(t)\frac{d}{dt}\rho_{D_{i_s}}^{(s)}(t), \tag{A.1}$$

where the line on top of the $\rho_{D_{i_s}}^{(s)}$ probability means that we have removed this term from the product. For the sake of clarity, we are going to omit the explicit time dependence in the probabilities $\rho_{D_{i_k}}^{(k)}$. Given the D_{i_s} substate in the s active site, the time dependence in its probability is given by the differential equation

$$\frac{d}{dt}\rho_{D_{i_s}}^{(s)} = -k_{D_{i_s}}^{(s)}\rho_{D_{i_s}}^{(s)} - \sum_{r\neq i_s} d_{r\,i_s}^{(s)}\rho_{D_{i_s}}^{(s)} + \sum_{r\neq i_s} d_{i_s\,r}^{(s)}\rho_{D_r}^{(s)} + k_{L_{i_s}}^{(s)}\rho_{L_{i_s}}^{(s)}, \tag{A.2}$$

which lets us write expression (A.1) as follows

$$\begin{aligned}\frac{d}{dt}\left(\rho_{D_{i_1}}^{(1)}(t)\ldots\rho_{D_{i_N}}^{(N)}(t)\right) = \sum_s \Bigg[&-\left(k_{i_s}^{(s)} + \sum_{r\neq i_s} d_{r\,i_s}^{(s)}\right)\rho_{D_{i_1}}^{(1)}(t)\ldots\rho_{D_{i_s}}^{(s)}(t)\ldots\rho_{D_{i_N}}^{(N)}(t) + \\ &\sum_{r\neq i_s} d_{i_s\,r}^{(s)}\rho_{D_{i_1}}^{(1)}(t)\ldots\rho_{D_r}^{(s)}\ldots\rho_{D_{i_N}}^{(N)}(t) + k_{L_{i_s}}^{(s)}\rho_{D_{i_1}}^{(1)}(t)\ldots\rho_{L_{i_s}}^{(s)}\ldots\rho_{D_{i_N}}^{(N)}(t)\Bigg]\end{aligned} \tag{A.3}$$

$$\begin{aligned}= &-\sum_{s=1}^{N}\left(k_{i_s}^{(s)} + \sum_{r\neq i_s} d_{r\,i_s}^{(s)}\right)\rho_{D_{i_1}}^{(1)}(t)\ldots\rho_{D_{i_N}}^{(N)}(t) + \\ &\sum_{s=0}^{N}\sum_{r\neq i_s}^{m-1} d_{i_s\,r}^{(s)}\rho_{D_{i_1}}^{(1)}(t)\ldots\rho_{D_r}^{(s)}\ldots\rho_{D_{i_N}}^{(N)}(t) + \sum_{s=0}^{N} k_{L_{i_s}}^{(s)}\rho_{D_{i_1}}^{(1)}(t)\ldots\rho_{L_{i_s}}^{(s)}\ldots\rho_{D_{i_N}}^{(N)}(t)\end{aligned} \tag{A.4}$$

Expressions of the form of Eq. (A.4) for every configuration can be collected in a matrix equation after defining appropriate $n^N \times n^N$ matrices K_D, Γ_D, K_L and Γ_L. We introduce these matrices by writing their matrix elements. For $i, j < n^N$, one

writes i and j in the n basis and uses this expansion to identify the rate constants that determine the element in the ith row, jth column of each matrix. Explicitly

$$[K_D]_{ij} = \sum_{s=1}^{N} k^{(s)}_{D_{i_s}} \delta_{ij} \tag{A.5}$$

$$[K^{(s)}_D]_{ij} = \delta_{ij} k^{(s)}_{D_{j_s}} \tag{A.6}$$

$$[K^{(s)}_L]_{ij} = \delta_{ij} k^{(s)}_{L_{j_s}} \tag{A.7}$$

$$K_L = \bigoplus_{s=1}^{N} K^{(s)}_L \tag{A.8}$$

In addition,

$$[\Gamma_D]_{ij} = \left(\delta_{ij} \sum_{s=1}^{N} \sum_{r \neq i_s} d^{(s)}_{r\, i_s} \right) - \sum_{s=1}^{N} \left(d^{(s)}_{i_s\, j_s} (1 - \delta_{i_s, j_s}) \prod_{v \neq s} \delta_{j_v i_v} \right) \tag{A.9}$$

$$[\Gamma_L]_{ij} = \left(\delta_{ij} \sum_{s=1}^{N} \sum_{r \neq i_s} l^{(s)}_{r\, i_s} \right) - \sum_{s=1}^{N} \left(l^{(s)}_{i_s\, j_s} (1 - \delta_{i_s, j_s}) \prod_{v \neq s} \delta_{j_v i_v} \right) \tag{A.10}$$

$$[\Gamma^{(s)}_D]_{ij} = \left(\delta_{ij} \sum_{r \neq i_s} d^{(s)}_{r\, i_s} \right) - d^{(s)}_{i_s\, j_s} (1 - \delta_{i_s, j_s}) \prod_{v \neq s} \delta_{i_v j_v} \tag{A.11}$$

$$[\Gamma^{(s)}_L]_{ij} = \left(\delta_{ij} \sum_{r \neq i_s} l^{(s)}_{r\, i_s} \right) - l^{(s)}_{i_s\, j_s} (1 - \delta_{i_s, j_s}) \prod_{v \neq s} \delta_{i_v j_v} \tag{A.12}$$

Observe that we always have that $d^{(s)}_{rr} = l^{(s)}_{rr} = 0$. With these definitions we can write the complete set of expressions of the form Eq. (A.4) for the dark configurations as follows

$$\frac{d}{dt} |P_D(t)\rangle = \left(-K_D - \Gamma_D \,,\, K^{(1)}_L \,,\, \ldots \,,\, K^{(N)}_L \right) |P(t)\rangle. \tag{A.13}$$

On the other hand, for a given light configuration

$$\begin{aligned} \frac{d}{dt} \left(\rho^{(1)}_{D_{i_1}} \cdots \rho^{(s)}_{D_{i_s}} \cdots \rho^{(v)}_{L_{i_v}} \cdots \rho^{(N)}_{D_{i_N}} \right) = \sum_{\substack{s=1 \\ s \neq v}}^{N} & \rho^{(1)}_{D_{i_1}} \cdots \overline{\rho^{(s)}_{D_{i_s}}} \cdots \rho^{(v)}_{L_{i_v}} \cdots \rho^{(N)}_{D_{i_N}} \frac{d}{dt} \rho^{(s)}_{D_{i_s}} \\ & + \rho^{(1)}_{D_{i_1}} \cdots \rho^{(s)}_{D_{i_s}} \cdots \overline{\rho^{(v)}_{L_{i_v}}} \cdots \rho^{(N)}_{D_{i_N}} \frac{d}{dt} \rho^{(v)}_{L_{i_v}}, \end{aligned} \tag{A.14}$$

and since our model does not allow more than one active site in any light configuration, in this case the following expressions determine the dynamics in the s active site in a way that is consistent with the condition of probability conservation:

$$\frac{d}{dt}\rho^{(s)}_{D_{i_s}}(t) = 0, \tag{A.15}$$

$$\frac{d}{dt}\rho^{(v)}_{L_{i_v}}(t) = \sum_{r\neq i_v}\left(l^{(v)}_{i_v r}\rho^{(v)}_{L_r} - l^{(v)}_{r i_v}\rho^{(v)}_{L_{i_v}}\right) + k_{D_{i_v}}\rho_{D_{i_v}} - k_{L_{i_v}}\rho_{L_{i_v}}. \tag{A.16}$$

By substituting Eqs. (A.15) and (A.16) into Eq. (A.14) we obtain

$$\begin{aligned}\frac{d}{dt}\left(\rho^{(1)}_{D_{i_1}}\cdots\rho^{(s)}_{D_{i_s}}\cdots\rho^{(v)}_{L_{i_v}}\cdots\rho^{(N)}_{D_{i_N}}\right) = &+\sum_{r\neq i_v} l^{(v)}_{i_v r}\rho^{(1)}_{D_{i_1}}\cdots\rho^{(s)}_{D_{i_s}}\cdots\rho^{(v)}_{L_r}\cdots\rho^{(N)}_{D_{i_N}}\\ &-\sum_{r\neq i_v} l^{(v)}_{r i_v}\rho^{(1)}_{D_{i_1}}\cdots\rho^{(s)}_{D_{i_s}}\cdots\rho^{(v)}_{L_{i_v}}\cdots\rho^{(N)}_{D_{i_N}}\\ &+k_{D_{i_v}}\rho^{(1)}_{D_{i_1}}\cdots\rho^{(s)}_{D_{i_s}}\cdots\rho^{(v)}_{D_{i_v}}\cdots\rho^{(N)}_{D_{i_N}}\\ &-k_{L_{i_v}}\rho^{(1)}_{D_{i_1}}\cdots\rho^{(s)}_{D_{i_s}}\cdots\rho^{(v)}_{L_{i_v}}\cdots\rho^{(N)}_{D_{i_N}}\end{aligned}$$

or in the matrix form

$$\frac{d}{dt}|P^{(s)}_L(t)\rangle = -\left(-K^{(s)}_D,\, 0,\ldots,0,\, K^{(s)}_L+\Gamma^{(s)}_L,\,\ldots,0\right)|P(t)\rangle,$$

for all s. Finally, the differential equation of evolution for the state vector $|P(t)\rangle$ is

$$\frac{d}{dt}|P(t)\rangle = -\begin{bmatrix} K_D+\Gamma_D & -K^{(1)}_L & \cdots & -K^{(s)}_L & \cdots & -K^{(N)}_L \\ -K^{(1)}_D & K^{(1)}_L+\Gamma^{(1)}_L & \cdots & 0 & \cdots & 0 \\ \vdots & \vdots & \ddots & \vdots & \vdots & \vdots \\ -K^{(s)}_D & 0 & \cdots & K^{(s)}_L+\Gamma^{(s)}_L & \cdots & 0 \\ \vdots & \vdots & \vdots & \vdots & \ddots & \vdots \\ -K^{(N)}_D & 0 & \cdots & 0 & \cdots & K^{(N)}_L+\Gamma^{(N)}_L \end{bmatrix}|P(t)\rangle \tag{A.17}$$

At equilibrium, the following relations between state vectors hold

$$(K_D + \Gamma_D)|P_D^{eq}\rangle = \sum_{s=1}^{N} K_L^{(s)}|P_L^{(s),eq}\rangle \tag{A.18}$$

$$K_D^{(s)}|P_D^{eq}\rangle = (K_L^{(s)} + \Gamma_L^{(s)})|P_L^{(s),eq}\rangle. \tag{A.19}$$

This is indeed in agreement with the condition of probability conservation at each active site. From Eq. (A.17) we can define the following matrices

$$W_{DD} = K_D + \Gamma_D \qquad W_{DL} = \begin{bmatrix} K_L^{(1)} & \cdots & K_L^{(s)} & \cdots & K_L^{(N)} \end{bmatrix} \tag{A.20}$$

$$W_{LD} = \begin{bmatrix} K_D^{(1)} \\ \vdots \\ K_D^{(s)} \\ \vdots \\ K_D^{(N)} \end{bmatrix} \qquad W_{LL} = \begin{bmatrix} K_L^{(1)} + \Gamma_L^{(1)} & \cdots & 0 & \cdots & 0 \\ \vdots & \ddots & \vdots & \vdots & \vdots \\ 0 & \cdots & K_L^{(s)} + \Gamma_L^{(s)} & \cdots & 0 \\ \vdots & \vdots & \vdots & \ddots & \vdots \\ 0 & \cdots & 0 & \cdots & K_L^{(N)} + \Gamma_L^{(N)} \end{bmatrix} \tag{A.21}$$

The matrix W_{LD} contains all the kinetic rate constants for transitions from any D substate to any L substate. W_{DD}, W_{DL} and W_{LL} could be interpreted similarly. Furthermore, the following equalities should hold at equilibrium

$$W_{DD}|P_D^{eq}\rangle = W_{DL}|P_L^{eq}\rangle \tag{A.22}$$

$$W_{LL}|P_L^{eq}\rangle = W_{LD}|P_D^{eq}\rangle \tag{A.23}$$

$$\langle 1|W_{DD}|P_D^{eq}\rangle = \langle 1|K_D|P_D^{eq}\rangle = \sum_{s=1}^{N}\langle 1|K_L^{(s)}|P_L^{(s),eq}\rangle = \langle 1|W_{LL}|P_L^{eq}\rangle \tag{A.24}$$

A.2 Relation between $G_D(t_D)$ and $g_D(t_D)$.

In this section we derive Eq. (2.76) and (2.77) for the model of N uncorrelated active sites. First observe that

$$\begin{aligned}
\langle 1|W_{DD}|P_D\rangle =&\langle 1|K_D+\Gamma_D|P_D^{eq}\rangle = \langle 1|K_D|P_D^{eq}\rangle \\
&= \sum_{i=1}^{2^N}\sum_{s=1}^{N} k^{(s)}_{D_{i_s}}\rho_{D_{i_1}}\dots\rho_{D_{i_s}}\dots\rho_{D_{i_N}} \\
&= \sum_{p=0}^{N}\binom{N}{p}(pk_{D_1}+(N-p)k_{D_2})\rho_{D_1}^{p}\rho_{D_2}^{N-p} \\
&= \sum_{p=0}^{N}\binom{N}{p}pk_{D_1}\rho_{D_1}^{p}\rho_{D_2}^{N-p}+\sum_{p=0}^{N}\binom{N}{p}(N-p)k_{D_2}\rho_{D_1}^{p}\rho_{D_2}^{N-p} \\
&=Nk_{D_1}\rho_{D_1}\sum_{p=1}^{N}\frac{(N-1)!}{(p-1)!(N-p)!}\rho_{D_1}^{p-1}\rho_{D_2}^{N-p}+ \\
&\qquad Nk_{D_2}\rho_{D_2}\sum_{p=0}^{N-1}\frac{(N-1)!}{p!(N-(p+1))!}k_{D_2}\rho_{D_1}^{p}\rho_{D_2}^{N-(p+1)} \\
&=N(k_{D_1}\rho_{D_1}+k_{D_2}\rho_{D_2})(\rho_{D_1}+\rho_{D_2})^{N-1} \\
&=N\langle 1|\mathsf{K}_D|p_D^{eq}\rangle\langle 1|p_D^{eq}\rangle^{N-1}
\end{aligned}$$

Now, consider the eigenvalue equations $(\mathsf{K}_D+\Gamma_D)|r_\alpha\rangle = \lambda_\alpha|r_\alpha\rangle$ and $\langle l_\alpha|(\mathsf{K}_D+\Gamma_D) = \lambda_\alpha\langle l_\alpha|$. Thus, for $\overline{\alpha}=\alpha_1\dots\alpha_N$, we let $|R_{\overline{\alpha}}\rangle$ be a vector of dimension n^N whose i-th component is given by $r^{(1)}_{\alpha_{(1)},i_1}\dots r^{(N)}_{\alpha_{(N)},i_N}$. $|R_{\overline{\alpha}}\rangle$ is then an eigenvector of W_{DD} as we

will show next:

$$
\begin{aligned}
[(K_D+\Gamma_D)|R_{\overline{\alpha}}\rangle]_i &= \sum_{s=1}^{N}\left(k_{D_{i_s}}+\sum_{r\neq i_s} d^{(s)}_{r\,i_s}\right) r^{(1)}_{\alpha_1,i_1}\dots r^{(s)}_{\alpha_s,i_s}\dots r^{(N)}_{\alpha_N,i_N} - \\
&\qquad \sum_{j=0}^{2^N-1}\sum_{s=1}^{N}\left(d^{(s)}_{i_s\,j_s}(1-\delta_{i_s,j_s})\prod_{v\neq s}\delta_{j_v i_v}\right) r^{(1)}_{\alpha_1,j_1}\dots r^{(N)}_{\alpha_N,j_N} \\
&= \sum_{s=1}^{N} r^{(1)}_{\alpha_1,i_1}\dots \overline{r^{(s)}_{\alpha_s,i_s}}\dots r^{(N)}_{\alpha_N,i_N}\left(k_{D_{i_s}}+\sum_{r\neq i_s} d^{(s)}_{r\,i_s}\right) r^{(s)}_{\alpha_s,i_s} - \\
&\qquad \sum_{s=1}^{N} r^{(1)}_{\alpha_1,i_1}\dots \overline{r^{(s)}_{\alpha_s,i_s}}\dots r^{(N)}_{\alpha_N,i_N}\sum_{r\neq i_s} d^{(s)}_{i_s\,r} r^{(s)}_{\alpha_s,r} \\
&= \sum_{s=1}^{N} r^{(1)}_{\alpha_1,i_1}\dots \overline{r^{(s)}_{\alpha_s,i_s}}\dots r^{(N)}_{\alpha_N,i_N}\left(\left(k_{D_{i_s}}+\sum_{r\neq i_s} d^{(s)}_{r\,i_s}\right) r^{(s)}_{\alpha_s,i_s} - \sum_{r\neq i_s} d^{(s)}_{i_s\,r} r^{(s)}_{\alpha_s,r}\right) \\
&= \sum_{s=1}^{N} \lambda^{(s)}_{\alpha_s} r^{(1)}_{\alpha_1,i_1}\dots r^{(N)}_{\alpha_N,i_N} \\
&= \left(\sum_{s=1}^{N}\lambda^{(s)}_{\alpha_s}\right)|R_{\overline{\alpha}}\rangle_i .
\end{aligned}
$$

We can use this fact to rewrite the denominator and numerator in $g_D(t)$ as follows

$$
\begin{aligned}
\langle 1|e^{-(K_D+\Gamma_D)t}|P^{eq}_D\rangle &= \sum_{\alpha}\langle 1|R_\alpha\rangle e^{-\lambda_\alpha t}\langle L_\alpha|P^{eq}_D\rangle \\
&= \sum_{\alpha}\langle 1|R_\alpha\rangle\left(\prod_{i=1}^{N} e^{-\lambda_{\alpha_i} t}\right)\langle L_\alpha|P^{eq}_D\rangle
\end{aligned}
$$

and after some algebra

$$
=\langle 1|e^{-(\mathsf{K}_D+\Gamma_D)t}|p^{eq}_D\rangle^N = \langle 1|\mathsf{g}_\mathsf{D}(t)|p^{eq}_D\rangle^N .
$$

A.3 $\Delta\bar{t}_{D<}(T)$ for a catalyst with N independent active sites

In this Appendix we illustrate the derivation of Eq. (2.84).

$$\Delta\bar{t}_{D<}(T) = \frac{\frac{\langle 1|P_D^{eq}\rangle}{\langle 1|W_{DD}|P_D^{eq}\rangle}\frac{\langle 1|\mathsf{G}_\mathsf{L}(T)W_{LL}|P_L^{eq}\rangle}{\langle 1|W_{LL}|P_L^{eq}\rangle} - \int_0^\infty dt_D \frac{\langle 1|\mathsf{G}_\mathsf{D}(t_D)W_{DL}\mathsf{G}_\mathsf{L}(T)|P_L^{eq}\rangle}{\langle 1|W_{LL}|P_L^{eq}\rangle}}{1 - \frac{\langle 1|\mathsf{G}_\mathsf{L}(T)W_{LL}|P_L^{eq}\rangle}{\langle 1|W_{LL}|P_L^{eq}\rangle}} \tag{A.25}$$

$$= \frac{\frac{\langle 1|P_D^{eq}\rangle}{\langle 1|W_{DD}|P_D^{eq}\rangle}\langle 1|\mathsf{G}_\mathsf{L}(T)W_{LL}|P_L^{eq}\rangle - \int_0^\infty dt_D \langle 1|\mathsf{G}_\mathsf{D}(t_D)W_{DL}\mathsf{G}_\mathsf{L}(T)|P_L^{eq}\rangle}{\langle 1|W_{LL}|P_L^{eq}\rangle - \langle 1|\mathsf{G}_\mathsf{L}(T)W_{LL}|P_L^{eq}\rangle} \tag{A.26}$$

$$= \frac{\frac{\langle 1|P_D^{eq}\rangle}{\langle 1|W_{DD}|P_D^{eq}\rangle}\langle 1|\mathsf{G}_\mathsf{L}(T)W_{LL}|P_L^{eq}\rangle - \langle 1|W_{DD}^{-1}W_{DL}\mathsf{G}_\mathsf{L}(T)|P_L^{eq}\rangle}{\langle 1|W_{LL}|P_L^{eq}\rangle - \langle 1|\mathsf{G}_\mathsf{L}(T)W_{LL}|P_L^{eq}\rangle} \tag{A.27}$$

$$= \frac{\frac{\langle 1|P_D^{eq}\rangle}{\langle 1|W_{DD}|P_D^{eq}\rangle}\langle 1|W_{DL}\mathsf{G}_\mathsf{L}(T)|P_L^{eq}\rangle - \langle 1|W_{DD}^{-1}W_{DL}\mathsf{G}_\mathsf{L}(T)|P_L^{eq}\rangle}{\langle 1|(I - \mathsf{G}_\mathsf{L}(T))W_{LL}|P_L^{eq}\rangle} \tag{A.28}$$

$$= \frac{\langle 1|(I\bar{t}_D^{(N)} - W_{DD}^{-1})W_{DL}\mathsf{G}_\mathsf{L}(T)|P_L^{eq}\rangle}{\langle 1|(I - \mathsf{G}_\mathsf{L}(T))W_{LL}|P_L^{eq}\rangle}. \tag{A.29}$$

A.4 $\Delta\vec{t}^{(N)}_{D<}(T)$ close to the static limit

In this section we derive the expression for $\Delta\vec{t}^{(N)}_{D<}(T)$, in the case $m = 2$ presented in Eq. (2.85) from Eq. (2.84). First observe that the denominator of Eq. (2.84) in the static limit is

$$\langle 1|(I - \mathsf{G}_{\mathsf{L}}(T))W_{LL}|P^{eq}_L\rangle = \left(\langle 1|(I - e^{K^{(1)}_L})K^{(1)}_L), \ldots, \langle 1|(I - e^{K^{(N)}_L})(K^{(N)}_L)\right)|P^{eq}_L\rangle \tag{A.30}$$

$$= \sum_{s=1}^{N}\langle 1|(I - e^{K^{(s)}_L})(K^{(s)}_L)|P^{(s)}_L\rangle \tag{A.31}$$

$$= \sum_{s=1}^{N}\sum_{i=1}^{2^N}(1 - e^{-k^{(s)}_{L_{i_s}}t})(k^{(s)}_{L_{i_s}})\rho_{D_{i_1}}\ldots\rho_{L_{i_s}}\ldots\rho_{D_{i_N}} \tag{A.32}$$

$$= \sum_{s=1}^{N}\left((1 - e^{-k_{L_1}T})k_{L_1}\rho_{L_1} + (1 - e^{-k_{L_2}T})k_{L_2}\rho_{L_2}\right) \tag{A.33}$$

$$\times \sum_{i=1}^{2^{N-1}}\rho^{(1)}_{D_{i_1}}(t)\ldots\overline{\rho^{(s)}_{D_{i_s}}(t)}\ldots\rho^{(N)}_{D_{i_N}}(t) \tag{A.34}$$

$$= \sum_{s=1}^{N}\left((1 - e^{-k_{L_1}T})k_{L_1}\rho_{L_1} + (1 - e^{-k_{L_2}T})k_{L_2}\rho_{L_2}\right) \tag{A.35}$$

$$\times \sum_{p=0}^{N-1}\binom{N-1}{p}\rho^{p}_{D_1}\rho^{N-1-p}_{D_2} \tag{A.36}$$

$$= N\langle 1|(I - e^{-\mathsf{K}_L T})\mathsf{K}_L|p^{eq}_L\rangle\langle 1|p^{eq}_D\rangle^{N-1}. \tag{A.37}$$

For the numerator of Eq. (2.84) we have that

$$\langle 1|(I\langle t_D\rangle - W_{DD}^{-1})W_{DL}\mathsf{G}_{\mathsf{L}}(T)|P_L^{eq}\rangle \to \langle 1|(I\langle t_D\rangle - K_D^{-1})(I,\ldots,I)|K_L e^{-K_L T}|P_L^{eq}\rangle \tag{A.38}$$

$$= \langle 1|(I\langle t_D\rangle - K_D^{-1})(K_L^{(1)}e^{-K_L^{(1)}T},\ldots,K_L^{(N)}e^{-K_L^{(N)}T}|P_L^{eq}\rangle \tag{A.39}$$

$$= \langle 1|(I\langle t_D\rangle - K_D^{-1})\sum_{v=1}^{N} K_L^{(v)}e^{-K_L^{(v)}T}|P_L^{(v)eq}\rangle \tag{A.40}$$

$$= \sum_{v=1}^{N}\sum_{i=1}^{2^N}\left(\langle t_D^{(N)}\rangle - \left(\sum_{s=1}^{N} k_{D_{i_s}}\right)^{-1}\right)\times \tag{A.41}$$

$$k_{L_{i_v}}^{(v)}e^{-k_{L_{i_v}}^{(v)}T}\rho_{D_{i_1}}^{(1)}\ldots\rho_{L_{i_v}}^{(v)}\ldots\rho_{D_{i_N}}^{(N)}. \tag{A.42}$$

Observe that when $T = 0$ this expression vanishes. We define p_i as the number of $i_s = 0$ when we write i in basis 2 and $x_0 = \rho_{D_1}/\langle 1|\rho_D\rangle$ then

$$\sum_{v=1}^{N}\sum_{i=1}^{2^N}\left(\frac{\langle t_D^{(1)}\rangle}{N} - \frac{1}{p_i k_{D_1} + (N-p_i)k_{D_2}}\right)k_{L_{i_v}}^{(v)}\rho_{L_{i_v}}\rho_{D_{i_1}}^{(1)}\ldots\overline{\rho_{D_{i_v}}^{(v)}}\ldots\rho_{D_{i_N}}^{(N)} \tag{A.43}$$

$$= \sum_{v=1}^{N}\sum_{i=1}^{2^N}\frac{k_{L_{i_v}}^{(v)}\rho_{L_{i_v}}\rho_{D_{i_1}}^{(1)}\ldots\overline{\rho_{D_{i_v}}^{(v)}}\ldots\rho_{D_{i_N}}^{(N)}}{Nx_0k_{D_1} + (N-Nx_0)k_{D_2}} - \sum_{v=1}^{N}\sum_{i=1}^{2^N}\frac{k_{L_{i_v}}^{(v)}\rho_{L_{i_v}}\rho_{D_{i_1}}^{(1)}\ldots\overline{\rho_{D_{i_v}}^{(v)}}\ldots\rho_{D_{i_N}}^{(N)}}{p_i k_{D_1} + (N-p_i)k_{D_2}} \tag{A.44}$$

$$= \sum_{v=1}^{N}\sum_{i=1}^{2^{N-1}}\frac{(k_{L_1}^{(v)}\rho_{L_1} + k_{L_2}^{(v)}\rho_{L_2})\rho_{D_{i_1}}^{(1)}\ldots\overline{\rho_{D_{i_v}}^{(v)}}\ldots\rho_{D_{i_N}}^{(N)}}{Nx_0k_{D_1} + (N-Nx_0)k_{D_2}} - \sum_{v=1}^{N}\sum_{i=1}^{2^N}\frac{k_{D_{i_v}}^{(v)}\rho_{D_{i_1}}^{(1)}\ldots\rho_{D_{i_N}}^{(N)}}{p_i k_{D_1} + (N-p_i)k_{D_2}} \tag{A.45}$$

$$= \sum_{v=1}^{N}\sum_{i=1}^{2^{N-1}}\frac{(\rho_{D_1} + \rho_{D_2})\rho_{D_{i_1}}^{(1)}\ldots\overline{\rho_{D_{i_v}}^{(v)}}\ldots\rho_{D_{i_N}}^{(N)}}{N} - \sum_{i=1}^{2^N}\frac{(p_i k_{D_1} + (N-p_i)k_{D_2})\rho_{D_{i_1}}^{(1)}\ldots\rho_{D_{i_N}}^{(N)}}{p_i k_{D_1} + (N-p_i)k_{D_2}} \tag{A.46}$$

$$= N\frac{\langle 1|p_D^{eq}\rangle^N}{N} - \langle 1|p_D^{eq}\rangle^N = 0. \tag{A.47}$$

In light of this result, we can write

$$\langle 1|(I\langle t_D\rangle - W_{DD}^{-1})W_{DL}\mathsf{G}_{\mathsf{L}}(T)|\rho_L^{eq}\rangle \rightarrow \tag{A.48}$$

$$\sum_{v=1}^{N}\sum_{i=1}^{2^{N-1}}\left(\vec{t}_D^{(N)} - \left(\sum_{s=1}^{N} k_{D_{i_s}}\right)^{-1}\right) k_{L_{i_v}}^{(v)} e^{-k_{L_{i_v}}^{(v)}T}\rho_{D_{i_1}}^{(1)}\ldots\rho_{L_{i_v}}^{(v)}\ldots\rho_{D_{i_N}}^{(N)} \tag{A.49}$$

$$= \sum_{v=1}^{N}\sum_{i=1}^{2^{N-1}}\left(\vec{t}_D^{(N)} - \frac{1}{(1+p_i)k_{D_1} + (N-p_i-1)k_{D_2}}\right) k_{L_1}^{(v)} e^{-k_{L_1}^{(v)}T}\rho_{D_{i_1}}^{(1)}\ldots\rho_{L_1}^{(v)}\ldots\rho_{D_{i_N}}^{(N)} \tag{A.50}$$

$$+ \sum_{v=1}^{N}\sum_{i=1}^{2^{N-1}}\left(\vec{t}_D^{(N)} - \frac{1}{p_i k_{D_1} + (N-p_i)k_{D_2}}\right) k_{L_2}^{(v)} e^{-k_{L_2}^{(v)}T}\rho_{D_{i_1}}^{(1)}\ldots\rho_{L_2}^{(v)}\ldots\rho_{D_{i_N}}^{(N)} \tag{A.51}$$

$$= \sum_{v=1}^{N}(e^{-k_{L_2}^{(v)}T} - e^{-k_{L_1}^{(v)}T})\sum_{i=1}^{2^{N-1}}\left(\vec{t}_D^{(N)} - \frac{1}{p_i k_{D_1} + (N-p_i)k_{D_2}}\right) k_{L_2}^{(v)}\rho_{D_{i_1}}^{(1)}\ldots\rho_{L_2}^{(v)}\ldots\rho_{D_{i_N}}^{(N)} \tag{A.52}$$

$$= N(e^{-k_{L_2}T} - e^{-k_{L_1}T})k_{L_2}\rho_{L_2}\sum_{p=0}^{N-1}\binom{N-1}{p}\left(\frac{\vec{t}_D^{(1)}}{N} - \frac{1}{pk_{D_1} + (N-p)k_{D_2}}\right)\rho_{D_1}^{p}\rho_{D_2}^{N-1-p} \tag{A.53}$$

$$= (e^{-k_{L_2}T} - e^{-k_{L_1}T})(k_{D_2} - k_{D_1})\vec{t}_D^{(1)}k_{L_2}\rho_{L_2}\sum_{p=0}^{N-1}\binom{N-1}{p}\frac{Nx_0 - p}{(N-p)k_{D_2} + pk_{D_1}}\rho_{D_1}^{p}\rho_{D_2}^{N-1-p} \tag{A.54}$$

We can further simplify this expression by writing the polynomial as the integral of an appropriate function. We use the following identity

$$\frac{1}{a} = \int_0^\infty dt e^{-at}. \tag{A.55}$$

Therefore

$$
\begin{aligned}
(k_{D_2}-k_{D_1})&\sum_{p=0}^{N-1}\binom{N-1}{p}\frac{Nx_0-p}{(N-p)k_{D_2}+pk_{D_1}}\rho_{D_1}^{p}\rho_{D_2}^{N-1-p}\\
&=(k_{D_2}-k_{D_1})Nx_0\sum_{p=0}^{N-1}\binom{N-1}{p}\frac{1}{(N-p)k_{D_2}+pk_{D_1}}\rho_{D_1}^{p}\rho_{D_2}^{N-1-p}\\
&\quad+\langle 1|p_D^{eq}\rangle^{N-1}-\sum_{p=0}^{N-1}\binom{N-1}{p}\frac{Nk_{D_2}}{(N-p)k_{D_2}+pk_{D_1}}\rho_{D_1}^{p}\rho_{D_2}^{N-1-p}\\
&=(k_{D_2}-k_{D_1})Nx_0\sum_{p=0}^{N-1}\binom{N-1}{p}\int_0^\infty e^{-[(N-p)k_{D_2}+pk_{D_1}]t}dt\rho_{D_1}^{p}\rho_{D_2}^{N-1-p}\\
&\quad+\langle 1|p_D^{eq}\rangle^{N-1}-Nk_{D_2}\sum_{p=0}^{N-1}\binom{N-1}{p}\int_0^\infty e^{-[(N-p)k_{D_2}+pk_{D_1}]t}dt\rho_{D_1}^{p}\rho_{D_2}^{N-1-p}\\
&=(k_{D_2}-k_{D_1})Nx_0\int_0^\infty e^{-k_{D_2}t}\langle 1|e^{-\mathsf{K}_D t}|p_D^{eq}\rangle^{N-1}dt+\langle 1|p_D^{eq}\rangle^{N-1}\\
&\quad-Nk_{D_2}\int_0^\infty e^{-k_{D_2}t}\langle 1|e^{-\mathsf{K}_D t}|p_D^{eq}\rangle^{N-1}dt\\
&=-\frac{N}{\vec{t}_D^{(1)}}\int_0^\infty e^{-k_{D_2}t}\langle 1|e^{-\mathsf{K}_D t}|p_D^{eq}\rangle^{N-1}dt+\langle 1|p_D^{eq}\rangle^{N-1}
\end{aligned}
\tag{A.56}
$$

to finally obtain

$$
\Delta\vec{t}_{D<}^{(N)}(T)=\frac{(e^{-k_{L_2}T}-e^{-k_{L_1}T})\vec{t}_D^{(1)}k_{L_2}\rho_{L_2}}{N\langle 1|(I-e^{-\mathsf{K}_L T})\mathsf{K}_L|p_L^{eq}\rangle}\left(1-\frac{N}{\vec{t}_D^{(1)}}\int_0^\infty e^{-k_{D_2}t}E_D(t)^{N-1}dt\right). \tag{A.57}
$$

Observe also that

$$
\begin{aligned}
\frac{Nx_0-p}{(N-p)k_{D_2}+pk_{D_1}}&=\frac{x_0-\frac{p}{N}}{(1-\frac{p}{N})k_{D_2}+\frac{p}{N}k_{D_1}} &\text{(A.58)}\\
&<\frac{x_0}{(1-\frac{p}{N})k_{D_2}+\frac{p}{N}k_{D_1}} &\text{(A.59)}\\
&<\frac{\rho_{D_1}}{\langle 1|\rho_D\rangle}\frac{N}{k_{D_2}}, &\text{(A.60)}
\end{aligned}
$$

which after substitution implies that

$$
\Delta\vec{t}_{D<}^{(N)}(T)<\Delta\vec{t}_{D<}^{(1)}(T). \tag{A.61}
$$

CHAPTER 3

DWELL-TIME CORRELATION ANALYSIS

In the two previous chapters we learned that the analysis of density functions, mean dwell times and their constrained counterparts can provide evidence of the existence of intermediate states, conformers and other species that are inaccessible from a traditional macroscopic kinetic experiment. We learned that the statistical analysis of fluorescence trajectories can reveal complex kinetic schemes with multiple reaction paths for the same chemical process. In particular, we found in Chapter 2 that we can filter the information content of the fluorescence trajectories collected in experiments, such as the catalytic transformation by single nanoparticles studied by Chen[51], by calculating the mean value of a selected group of dwell times. The difference between the total mean and any of the constrained mean dwell times is an indicator of the memory along the trajectory. Here, we understand memory as the dependence of one event (reaction, emission, desorption, ...) on its history and preceding events. Traditionally, memory effects have been measured by studying several indicator functions among which the intensity and dwell-time correlation functions have been extensively implemented [51, 29].

In the present chapter we will study the dwell-time correlation function in single-molecule fluorescence spectroscopy for the system with two states that we investigated in Chapters 1 and 2. To our knowledge, the first formal treatment of the correlation functions was undertaken by Cao [10] in 2000, motivated by the experiments on single-enzyme catalysis done by Lu, Xie and coworkers [29]. From his calculations for the on-time correlation function for the two-conformational-channel model Cao was able to observe that the value of this

function is sensitive not only to the reaction rate constants for transitions from the *on* to the *off* but also to those for the opposite transition. In fact, in a subsequent work[54], Cao found that for the same model the correlation function decays as the powers of a ratio of rate constants (see in Ref. [54] section IV A, Eq. (32)). Working from a different perspective, Gopich and Szabo [20] were able to find a more general result. To obtain the statistics of transitions, Gopich and Szabo considered the probability that no monitored transitions (i.e. reactions leading to a change in the state) occur in a time interval. This probability was calculated by making the monitored probability irreversible, as shown in Eq. (2.3) in reference [20]. The mathematical formulation of this problem differs from that described in Chapters 1 and 2, in that the rate constants of the monitored transitions removed from the equation of evolution for the *total* probability vector. From this, Gopich and Szabo calculated the correlation function of a two-channel model (in section VI B of Ref. [20]). This correlation function is found to decay to zero as the powers of ratios of rate constants (See Eq. (6.16) in this reference). These two results are very close to our findings in Sec. 3.3.1 and, in fact, they can be obtained as limiting cases of the expression in Eq. (3.20).

Experimentally[51, 29], time correlation functions are fitted to exponential functions of the form e^{-m/m_0} where m is the number of events separating two dwell times and m_0 is a constant. Associated with a correlation function there is a correlation time, which is measure of time length of memory effects. Several definitions are possible. In any case, a universal measure of the correlation time is the constant m_0. Actually m_0 can be considered as having for units "number of events" and those can be transformed in seconds by multiplying this constant by the mean time of the event. We will find in this Chapter that we can interpret in several instances the parameter m_0 in terms of the rate parameters of the

model by simple relations.

While several other authors have studied this indicator [51, 29] to some extent and for different models and experimental systems [49], we found that none of them is in place to describe the complete set of qualitative and quantitative properties observed in single nanocatalysis. For one reason we can anticipate this: nanoparticles as heterogeneous catalysts are different from enzymes in that they have a multitude of active sites that, as we concluded in Chapter 2, are correlated. Since our work will essentially extend and further improve previous findings from Cao[10] and others, connections with results in the literature are expected. For this reason, it is important to mention the work of Vlad and Ross[45] on intensity correlation functions of the fluorescence signal. In their treatment of the kinetic equations, solution are given in terms of Green functions. These Green functions are determined by the spectra of a stochastic matrix and, as a consequence, the correlation on fluorescence intensity is a function of the eigenvalues of the same stochastic matrix. This is perhaps, the first instance in the literature where elements of theory of Markov process are put in the description of single-molecule dynamics. But not the last, as Ha et. al. [38] have analyzed single-molecule FRET trajectories using hidden Markov modeling in 2006. More recently Kou and coworkers[12] have studied both dwell-time and intensity correlations from a theoretical perspective. In Sec. 3.2 of Ref. [12] the correlation of turnover times is described by a stochastic matrix and Eq. (3.4) shows that this correlation should decay as the powers of these eigenvalues. Interesting from this study is that it explores the role that substrate concentration can play on the correlation properties of Michaelis-Menten mechanism for a single enzyme subject to conformal fluctuations.

Our investigations will begin in Sec. 3.1 with the introduction of density functions for arbitrary pair of dwell times and the definition of the turnover matrix. Then, in Sec. 3.2 we start our study of dwell-time correlations by inferring some generalities about them. Next in Secs. 3.3, 3.4 and 3.5 we study the two and three-channel models for a catalyst with a single site and also models with many active sites, each one with two substates. After this, in Sec. 3.5 we explore how the correlation function and the constrained mean dwell times are related, at the same time we extend our understanding of the qualitative properties of the constrained means, this time for models fluctuating among three substates.

3.1 More about joint density functions

From a single-molecule fluorescence trajectory with two states, it is possible to construct a bidimensional histogram for any dwell-time pair, with the condition that the two dwell times in consideration are distant a fixed number of events and the trajectory is long enough to provide good statistics. Correspondingly, we must be able to define a joint density function describing the same properties as such histogram. In chapter 2, in Eqs. (2.4) and (2.5) or more generally for many-active-site systems in Eqs. (2.64) and (2.65), we defined joint density functions only for consecutive dwell. The definitions of these functions, as described in Sec. 2.1, take into account the propagation of the system along a sequence of events. Multivariate density functions are expressions for the propagation of the initial vector along a sequence of events, with propagators given by $\mathsf{G}_{\mathsf{D}}(t_D)$ and $\mathsf{G}_{\mathsf{L}}(t_L)$ and matrices for changes in the state W_{DL} and W_{LD}. As we can consider non-consecutive events, four are the number of dwell-time pairs for which

we can define joint density functions, to wit, (t_D, t_D), (t_D, t_L), (t_L, t_D) and (t_L, t_L).

For a sequence of m events, say $D_1 \to L_2 \to \cdots \to D_m \to L_{m+1} \to D_{m+1}$, we can define the multidimensional density function

$$F_{(DL)^m D}(t_{D_1}, t_{L_2}, \ldots, t_{L_{m+1}}, t_{D_{m+1}}) = \frac{\langle 1|W_{LD}\mathsf{G}_\mathsf{D}(t_{D_{m+1}})\left(\prod_{i=1}^{m} W_{DL}\mathsf{G}_\mathsf{L}(t_{L_i})W_{LD}\mathsf{G}_\mathsf{D}(t_{D_i})\right) W_{DL}|p_L\rangle}{\langle 1|W_{DD}|P_D\rangle}, \quad (3.1)$$

and from this, we can obtain the joint density function for the dwell times $t_D^{(m+1)}$ and $t_D^{(1)}$ after integration over all the intermediate events. This amounts to summing over all possible realizations of the same sequence of events, with different times. As a result, the joint density functions for two dark dwell times that are separated by m turnovers and their corresponding generating functions are given by

$$F_D^{(m)}(t_D^{(m+1)}, t_D^{(1)}) = \frac{\langle 1|W_{DD}e^{-W_{DD}t_D^{(m+1)}}S_L M_L^{m-1} W_{LD}e^{-W_{DD}t_D^{(1)}}W_{DD}|P_D^{eq}\rangle}{\langle 1|W_{DD}|P_D^{eq}\rangle} \quad (3.2)$$

$$= \frac{\langle 1|W_{DD}e^{-W_{DD}t_D^{(m+1)}}M_D^{m-1} S_L W_{LD}e^{-W_{DD}t_D^{(1)}}W_{DD}|P_D^{eq}\rangle}{\langle 1|W_{DD}|P_D^{eq}\rangle}, \quad (3.3)$$

and

$$G_D^{(m)}(t_D^{(m+1)}, t_D^{(1)}) = \frac{\langle 1|e^{-W_{DD}t_D^{(m+1)}}S_L M_L^{m-1} W_{LD}e^{-W_{DD}t_D^{(1)}}|P_D^{eq}\rangle}{\langle 1|W_{DD}|P_D^{eq}\rangle} \quad (3.4)$$

$$= \frac{\langle 1|e^{-W_{DD}t_D^{(m+1)}}M_D^{m-1} S_L W_{LD}e^{-W_{DD}t_D^{(1)}}|P_D^{eq}\rangle}{\langle 1|W_{DD}|P_D^{eq}\rangle}, \quad (3.5)$$

for $m \geq 1$. In these expressions we have introduced two new matrices: the turnover matrix for the dark state M_D and the turnover matrix for the light state M_L. They are important elements of the theory that we will develop here to understand dwell-time correlation in the catalytic transformations on single nanoparticles. We have also introduce the auxiliary matrices S_D and S_L, as they

will frequently appear in this study. In terms of the set of rate constants associated with the chemical process these new elements are given by

$$M_D = W_{DL} W_{LL}^{-1} W_{LD} W_{DD}^{-1}, \tag{3.6}$$

$$S_D = W_{LD} W_{DD}^{-1}, \tag{3.7}$$

and M_L, S_L are obtained after index substitution $D \iff L$. Observe that $M_D = S_L S_D$. In the next section we will show how these matrices are useful in the description of the qualitative properties of the correlation function.

3.2 Dwell-time correlation functions

Dwell times are random variables whose stochastic properties are given by multiexponential density functions. The correlation function between two different dwell times has been used as a measure of memory effects[29]. Formally this coefficient estimates the linear dependence between two different times and can vary continuously between -1 and 1. For the case of the dark dwell time, with mean value $\overline{t_D}$, a positive value in the correlation coefficient between two subsequent times, say $t_D^{(1)}$ and $t_D^{(2)}$, predicts that if $t_D^{(1)} > \overline{t_D}$ is observed, then it is most likely that a $t_D^{(2)} > \overline{t_D}$ is also observed. In contrast, a negative value in the correlation coefficient implies that in the second case the most likely event is the opposite, to wit, $t_D^{(2)} < \overline{t_D}$.

In general, the correlation for two dark dwell times $t_D^{(1)}$, $t_D^{(m+1)}$ that are distant apart m turnovers is given by

$$C_D(m) = \frac{\overline{t_D^{(1)} t_D^{(m+1)}} - \overline{t_D}^2}{\overline{t_D^2} - \overline{t_D}^2}, \tag{3.8}$$

with $m \geq 1$. We can calculate these means in terms of the joint density function $F_D^{(m)}$ in eq. (3.2) and the density function F_D in Eq. (2.58) according to the following expressions

$$\overline{t_D^{(1)} t_D^{(m+1)}} = \int_0^\infty dt_D^{(1)} \int_0^\infty dt_D^{(m+1)}\ t_D^{(1)} t_D^{(m+1)}\ F_D^{(m)}(t_D^{(1)}, t_D^{(m)}), \tag{3.9}$$

$$\overline{t_D} = \int_0^\infty dt_D\ t_D\ F_D(t_D), \tag{3.10}$$

and conclude that the difference $\overline{t_D^{(1)} t_D^{(m+1)}} - \overline{t_D}^2$ depends on the powers of either the turnover matrix M_D or the turnover matrix M_L. A noticeable fact is that Eq. (3.8) is independent of whether we use M_D or M_L in its computation, as M_D and M_L are similar matrices with similarity transformation

$$S_D^{-1} M_L S_D = M_D. \tag{3.11}$$

While similar matrices have the same eigenvalues[32], their eigenvectors are different but they can be transformed into each other by means of the similarity relation (3.11). For instance, if $M_D|R_i^D\rangle = \lambda_i |R_i^D\rangle$ and $M_L|R_i^L\rangle = \lambda_i |R_i^L\rangle$, then $|R_i^L\rangle \propto S_D |R_i^D\rangle$. We can find the spectral decomposition of M_D after choosing eigenvectors that are normalized according to the rule $\langle L_i^D | R_j^D \rangle = \delta_{ij}$, and then we can write

$$M_D = \sum_i |R_i^D\rangle \lambda_i \langle L_i^D|. \tag{3.12}$$

It follows that $C_D(m)$ is a function of the power of the eigenvalues of the turnover matrix. In particular, one should notice that

$$\langle 1|M_D = \langle 1|, \tag{3.13}$$

$$M_D W_{DL}|p_L\rangle = W_{DL}|p_L\rangle, \tag{3.14}$$

and therefore 1 is always an eigenvalue of the turnover matrix. In the cases that will be discussed below, W_{DD} and W_{LL} are M-matrices[4] and we can use this

fact to show that M_D and M_L are positive matrices[6]. As a consequence, we can state that these turnover matrices are left-stochastic[5] and they model single-nanoparticle trajectories as Hidden Markov process. Besides, we can appeal to the Perron-Frobenius theorem to say that every eigenvalue of the turnover matrix is less that or equal to one, in norm. We elaborate on the above statements in Appendix B.1. These properties turn out to be very nice tools for the study of correlation functions in simple models, as we will illustrate in next sections.

3.3 Catalyst with one active site

We start our discussion about correlation in different kinetic models by assuming that our system has only one active site. This is the case of many enzymes. As we assumed before, the active site undergoes transformations between a dark and a light state and each state has n substates. Under these conditions, equations (2.50)-(2.63) are written in terms of the matrices $W_{DD} = \mathsf{K}_D + \Gamma_D$, $W_{LL} = \mathsf{K}_L + \Gamma_L$, $W_{DL} = \mathsf{K}_L$ and $W_{LD} = \mathsf{K}_D$. After some algebraic manipulation(see Appendix B.2), we obtain the following expressions for the covariance of two dwell times corresponding to the same or different states:

$$\overline{t_D^{(1)} t_D^{(m+1)}} - \overline{t_D}^2 = \frac{1}{\langle 1|\mathsf{K}_D|p_D\rangle} \sum_{i=1}^{N-1} l_i \lambda_i^{m+1} \langle 1|\mathsf{K}_D^{-1}|R_i^L\rangle \langle L_i^D|p_D\rangle \tag{3.15}$$

$$\overline{t_L^{(1)} t_L^{(m+1)}} - \overline{t_L}^2 = \frac{1}{\langle 1|\mathsf{K}_L|p_L\rangle} \sum_{i=1}^{N-1} r_i \lambda_i^{m+1} \langle 1|\mathsf{K}_L^{-1}|R_i^D\rangle \langle L_i^L|p_L\rangle \tag{3.16}$$

$$\overline{t_D^{(1)} t_L^{(m+1)}} - \overline{t_D}\,\overline{t_L} = \frac{1}{\langle 1|\mathsf{K}_D|p_D\rangle} \sum_{i=1}^{N-1} \lambda_i^{m+1} \langle 1|\mathsf{K}_L^{-1}|R_i^D\rangle \langle L_i^D|p_D\rangle \tag{3.17}$$

$$\overline{t_L^{(1)} t_D^{(m+1)}} - \overline{t_D}\,\overline{t_L} = \frac{1}{\langle 1|\mathsf{K}_D|p_D\rangle} \sum_{i=1}^{N-1} \lambda_i^{m+1} \langle 1|\mathsf{K}_D^{-1}|R_i^L\rangle \langle L_i^L|p_L\rangle \tag{3.18}$$

where $l_i = 1/\langle L_i^D|S_L|R_i^L\rangle$, $r_i = 1/\langle L_i^L|S_D|R_i^D\rangle$ and $\lambda_i r_i l_i = 1$. Correlation functions can be written as a ratio between a covariance and the standard deviation of each variable. An interesting conclusion can be drawn at this point about these correlation functions: In the absence of heterogeneity in the reaction rate constants for transitions from the dark to the light state (i.e. $k_{D_i} = k_D$), one has that $\langle 1|\mathsf{K}_D^{-1}|R_i^L\rangle = k_D^{-1}\langle 1|R_i^L\rangle = 0$ for all i and, as a consequence, $\overline{t_D^{(1)} t_D^{(m+1)}} - \overline{t_D}^2 = 0$ and $C_D(m) = 0$ for all $m \geq 1$. This fact indicates that correlation is due not only to the existence of multiple channels or reaction paths, but also as a result of the differences in the kinetic properties among them. Besides, it is also the case that the correlation function will be independent of m in the limit of multiple channels without substate-substate transformation. We will make more precise this statement below when we study in detail some explicit models.

3.3.1 Two-channel model

We consider the kinetic scheme for one active site and two substates described in Figure (1.7). This is the smallest model for which we can expect correlation(see

Appendix B.4). After substitution of Eq. (3.15) into Eq. (3.8) with $n = 2$ we obtain

$$C_D(m) = \lambda^{m+1} \frac{\langle 1|\mathsf{K}_D^{-1}|R^L\rangle\langle L^D|P_D\rangle}{\langle 1|\mathsf{K}_D|P_D\rangle\langle L_D|S_L|R^L\rangle\sigma_D^2}. \tag{3.19}$$

Similar expressions follow for other correlation functions. Here, we notice again that the decay in the correlation function is given by the powers of the unique nontrivial eigenvalue λ of the turnover matrix $M_D = \mathsf{K}_L(\mathsf{K}_L + \Gamma_L)^{-1}\mathsf{K}_D(\mathsf{K}_D + \Gamma_D)^{-1}$. In fact, we can verify that

$$\lambda = \frac{1}{\left(1 + \frac{d_{21}}{k_{D_1}} + \frac{d_{12}}{k_{D_2}}\right)\left(1 + \frac{l_{21}}{k_{L_1}} + \frac{l_{12}}{k_{L_2}}\right)}, \tag{3.20}$$

and thus we expect to find correlation when the time scales associated with transitions from the dark to the light state and vice versa are much shorter than the time scales of internal transformations. When this is the case, we can approximate to an exponential function the decay of the correlation function, i.e.

$$\lambda^{m+1} \sim e^{-\left(\frac{d_{21}}{k_{D_1}} + \frac{d_{12}}{k_{D_2}} + \frac{l_{21}}{k_{L_1}} + \frac{l_{12}}{k_{L_2}}\right)(m+1)}. \tag{3.21}$$

This prediction is in agreement with the phenomenological observation in some systems that $C_D(m) \sim e^{-m/m_D}$, where m_D is a constant[29, 51, 21]. However, we must stress that as the rates of internal dynamics increase the exponential approximation to the decay deviates from the exact rate of decay. In Figure 3.1, we have investigated this numerically. We observe that the exponential decay approximation, as presented in eq. (3.21), is in excellent agreement with the exact decay for slowly decaying correlation functions ($\lambda > 0.8$).

The constant m_D has been experimentally measured before in nanoparticles[51] and enzymes[29]. This parameter is strongly associated with the concept of correlation time. Here we give a physical interpretation for it that is valid when this parameter is large and a 2-channel model is describes all the correlation

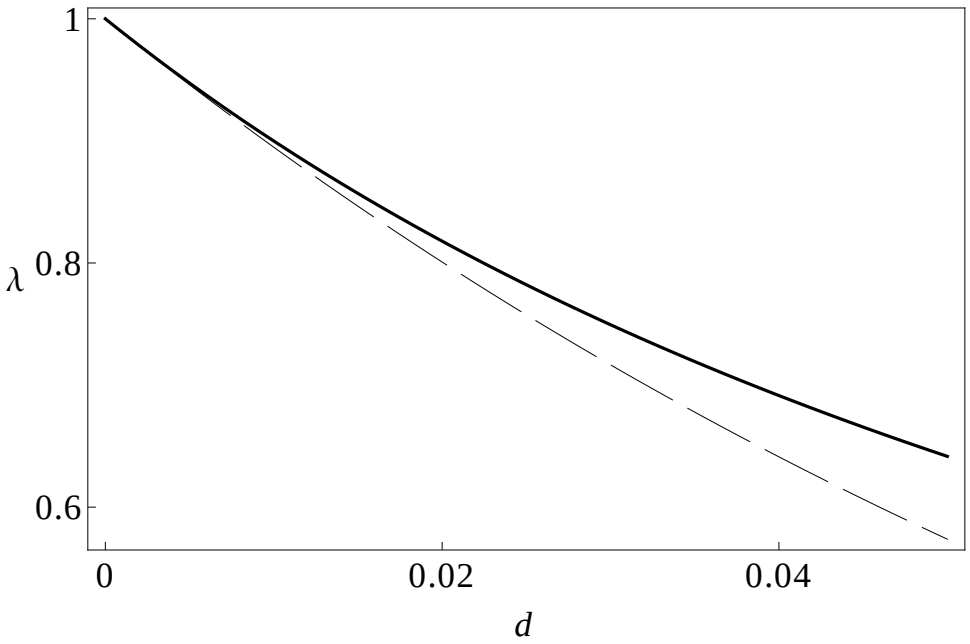

Figure 3.1: Eigenvalue λ as defined in Eq. (3.20) for a 2-channel model as a function of the rate constant for internal transformation d. The exact decay is presented in solid line and the exponential approximation is represented by a dashed line. Parameters for this model are $k_{D_1} = 1$, $k_{D_2} = 1/10$, $k_{L_1} = 10$, $k_{L_2} = 100$ and $d_{ij} = l_{ij} = d$.

properties:

$$\frac{1}{m_D} = \frac{d_{21}}{k_{D_1}} + \frac{d_{12}}{k_{D_2}} + \frac{l_{21}}{k_{L_1}} + \frac{l_{12}}{k_{L_2}}. \tag{3.22}$$

One should also notice that $m_D = m_L = m_{DL} = m_{LD}$ for every model with two substates. This is a simple consequence of all four rate constants decaying as the powers of the same parameter λ. Therefore a two-channel model does not describe any system in which the correlation functions show different decays.

The amplitude of the correlation function is the limiting value that the correlation coefficient takes when m goes to zero. We notice again that the explicit computation of the factor $\langle 1|\mathsf{K}_D^{-1}|R_i^l\rangle$ leads to the conclusion that in the absence of heterogeneity in the channels (i.e. $k_{D_1} = k_{D_2}$), the dark-dwell-time correla-

tion should vanish as well as one of the crosscorrelation functions, independent of the heterogeneity that might exist in the rate constants k_{L_1} and k_{L_2}. A similar conclusion holds in the absence of dynamic heterogeneity in the transitions from the light to the dark state for the corresponding correlation functions.

Another interesting property of two channel systems is that a large amplitude in the autocorrelation function for the dark and light dwell times, with slow rate of decay, necessary implies crosscorrelation between these times. This remark is an interpretation of the following relation among correlation functions

$$C_D(m)C_L(m) = \frac{1}{\lambda}C_{LD}(m)C_{DL}(m), \tag{3.23}$$

that is valid for every two channel model. Expression (3.23) provides another way to test if an experimental system can be fully described by a model with two substates.

The static limit approximation is an idealization of the dynamical evolution of systems for which internal transformations are significantly slower than those that lead to transitions to different states. In this limit, we neglect the internal dynamics by setting the corresponding rate constants to zero in the time propagation of the state vectors $|p_D\rangle$ and $|p_L\rangle$. We will find soon how this assumption simplifies our treatment of correlation functions at the same time revealing interesting aspects of them. Under the static limit approximation, the equilibrium condition for the vector of probabilities is given by $\mathsf{K}_D|p_D\rangle = \mathsf{K}_L|p_L\rangle$, which implies detailed balance for every channel.

From Eqs. (3.21) and (3.22), we infer that systems exhibiting long correlation time can be well described by considering the static limit approximation. In that

limiting case the correlation function takes the form (see Appendix B.3)

$$C_D(m) = \frac{1}{(\rho_{D_1} k_{D_1} + \rho_{D_2} k_{D_2})^2} \frac{\lambda^m}{\sigma_D^2} \left(\frac{\rho_{D2}\rho_{D1}}{k_{D1}k_{D2}} (k_{D2} - k_{D1})^2 \right), \tag{3.24}$$

where σ_D^2 is given by Eq. (1.32). We immediately see that $C_D(m)$ is a quadratic function of the difference $k_{D_1} - k_{D_2}$ when this difference is small, and that $C_D(m)$ is always positive. Similarly, $C_L(m)$ is proportional to $(k_{L_2} - k_{L_1})^2$. In Fig. 3.2, we show for a sample model the value of the dark-dwell-time correlation coefficient for dwell times that occur immediately one after the other, as calculated from the exact expression given by Eq. (3.19) with $m = 1$ and the static limit case described in Eq. (3.24). Notice that we have set three of the rate constants of internal transformations to the same value, and we have estimated the fourth rate constant so as to satisfy the condition of microscopic reversibility. Although this choice of the rate constants may not be close to the conditions demanded in the static limit when the value of k_{D_1} is small, we observe that eq. (3.24) is in excellent agreement with the exact solution. Deviations are only evident when the difference in the k_D constants are large. We have not included our calculations for smaller values in the internal rate constant, as they are nearly indistinguishable from the exact solution for the set of parameters considered.

The reader should notice that both crosscorrelation functions are proportional to the product $(k_{D2} - k_{D1})(k_{L2} - k_{L1})$ and as a consequence, their sign is a measure of the relative proportion of the four reaction rate constants in the model. For instance, we expect negative crosscorrelations in the case that fast transitions from the dark to the light state are coupled to slow reactions from the light to the dark state. In such a case, we can say that the relative proportion among reaction rate constants is $k_{D_1} < k_{D_2}$ and $k_{L_1} > k_{L_2}$. On the contrary, if slow reactions happen through the same channel then positive crosscorrelation should be observed. Another interesting observation about crosscorrelations in

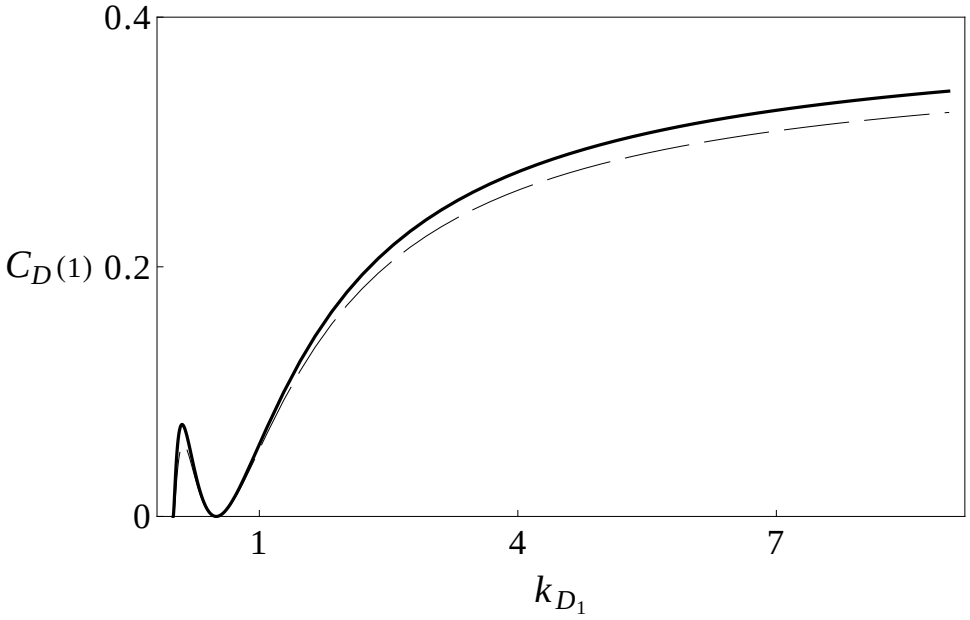

Figure 3.2: $C_D(1)$ for a 2-channel model as a function of the rate constant k_{D_1}. The solid line corresponds to the exact value for the correlation, calculated according to (3.19). The dashed line shows the static limit estimation (see Eq. (3.24)). Parameters for this model are $k_{D_2} = 1/2$, $k_{L_1} = 1$, $k_{L_2} = 2$, $d_{21} = d_{12} = l_{12} = 1/10$ and $l_{21} = 1/(40k_{D_1})$.

the static limit is that they should be almost the same, i.e. $C_{LD}(m) \sim C_{DL}(m)$.

We close this section by presenting numerical calculations in Fig. 3.3 that display some of the characteristics that we have just described. The dwell-time correlation functions have been calculated without approximations and one of the internal rate constants has been set so that the condition of microscopic reversibility holds for this model. Notice that we can interpret the qualitative properties of the correlation functions for this models based on our study of models close to the static limit.

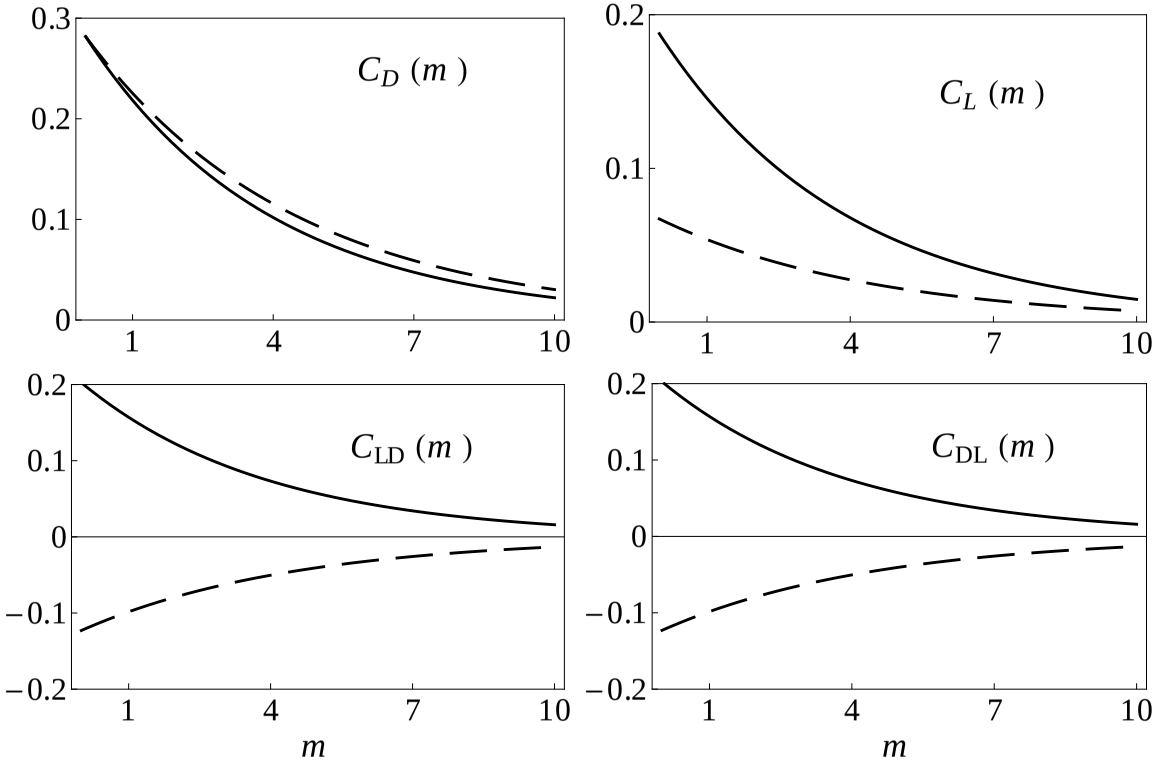

Figure 3.3: Dwell-time correlation functions for two-channel models with slow internal dynamics. Parameters for the model shown in a solid line are $k_{D_1} = 1/10$, $k_{D_2} = 1/2$, $k_{L_1} = 1$, $k_{L_2} = 3$, $d_{21} = d_{12} = l_{12} = 1/50$ and $l_{21} = 1/30$. Parameters for the model showed in dashed line are $k_{D_1} = 1/2$, $k_{D_2} = 1/10$, $k_{L_1} = 1$, $k_{L_2} = 3$, $d_{21} = d_{12} = l_{12} = 1/50$ and $l_{21} = 1/750$.

3.3.2 Three-channel model

Autocorrelation functions for the dark and light dwell times decay with different rates[51], as we pointed out in Chapter 1, Sec. 1.2 and in Fig. 1.6. In light of our discussion above in Sec. 3.3.1 we must conclude that a two channel model is not sifficient for the complete description of the dwell-time correlation properties observed in single nanoparticle catalysis. The assumption of the existence of an additional light or dark substate, but not in both, does not break the symmetry that a two-channel system imposes in the rates of decay of each correlation function. This can be anticipated by using the same ideas as in Appendix B.4.

For a system with 3 substates, M_D is now a 3×3 matrix with two eigenvalues λ_1 and λ_2 different from 1. In terms of these parameters the dark-dwell-time correlation function is

$$C_D(m) = \frac{1}{\langle 1|\mathsf{K}_D|p_D\rangle\sigma_D^2}\left(\lambda_1^m \frac{\langle 1|\mathsf{K}_D^{-1}|R_1^L\rangle\langle L_1^D|p_D\rangle}{\langle L_1^D|S_L|R_1^L\rangle} + \lambda_2^m \frac{\langle 1|\mathsf{K}_D^{-1}|R_2^L\rangle\langle L_2^D|p_D\rangle}{\langle L_2^D|S_L|R_2^L\rangle}\right). \tag{3.25}$$

In general the decay of these functions is multiexponential. However, it is possible to find some three-channel models for which these functions have a nearly monoexponential decay in both $C_D(m)$ and $C_L(m)$, with $m_D \neq m_L$. We stress the fact that crosscorrelation is not observed in catalytic transformations by single spherical nanoparticles. For a three channel system, Eq. (3.23) no longer holds, opening the door for us to find autocorrelated systems without crosscorrelation or, perhaps, negligible crosscorrelation. In Fig. 3.4 we show dwell-time correlation functions for a model that has all these properties.

Rate constants for the model in Fig. 3.4 have been chosen so that the turnover matrix has eigenvectors for which $\langle 1|\mathsf{K}_D^{-1}|R_2^L\rangle$, $\langle L_2^D|p_D\rangle$, $\langle 1|\mathsf{K}_L^{-1}|R_1^D\rangle$ and $\langle L_1^L|p_L\rangle$ are

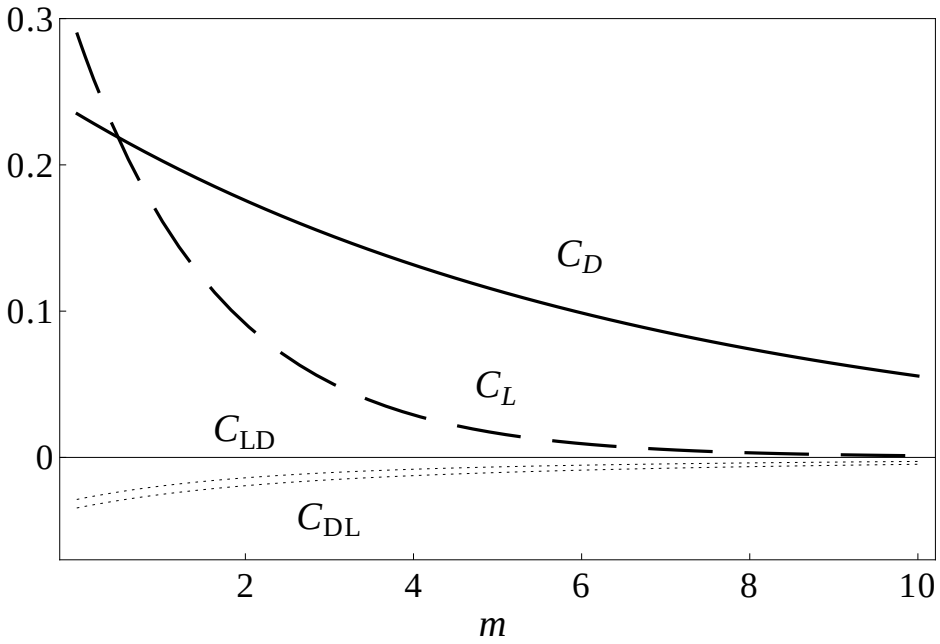

Figure 3.4: Dwell-time correlation functions for a three-channel model. The solid line is the correlation function for dark dwell times, the dashed line plots the correlation function for light dwell times and plots in dotted lines are crosscorrelation functions. Reaction rate constants for this model are $k_{D_1} = 0.7$, $k_{D_2} = 0.7$, $k_{D_3} = 8000$, $k_{L_1} = 0.5$, $k_{L_2} = 8$, $k_{L_3} = 0.941$ and rate constants for internal transformations are $d_{21} = 0.25$, $d_{32} = 0.05$, $d_{13} = 0$, $d_{12} = 0.117$, $d_{23} = 0.8$, $d_{31} = 0$, $l_{21} = 0.05$, $l_{32} = 0.01$, $l_{13} = 0$, $l_{12} = 0.375$, $l_{23} = 0.1$ and $l_{31} = 0$.

identically zero, or very small (less that 10^{-3})[1]. Details on how these parameter can be chosen are elaborated in Appendix B.5. When these factors are zero, the autocorrelation functions decay given as the powers of different eigenvalues, to wit, $C_D(m) \sim \lambda_1^{(m+1)}$ and $C_L(m) \sim \lambda_2^{(m+1)}$, with the additional consequence of setting to zero the amplitude of both crosscorrelation functions. For the example in Fig. 3.4 we have that $\lambda_1 = 0.866$ and $\lambda_2 = 0.560$. Numerical explorations reveal that it is possible to find more than one set of rate constants for a three-channel system with similar correlation functions. This lack of determinacy is

[1]Observe that the turnover matrix M_D, λ, $|R_i^D\rangle$ and $\langle L_i^D|$ are dimensionless.

due to the size of the parameter space, that can have as many as 18 different rate constants. Put another way, dwell-time correlation analysis does not provide a unique model but gives information about the smallest number of substates in which the system fluctuates, even when particular properties, such as null crosscorrelations, are imposed in the model.

Other correlation scenarios are possible for three-channel systems, such as autocorrelated models with $C_{LD}(m) = 0$ and $C_{DL}(m) > 0$ or, models that are cross-correlated having zero autocorrelation. As we discussed in the previous section, many of these scenarios are impossible for systems with two substates. In the following, we will concentrate on the study of two specific cases: models with negative autocorrelation and models with oscillations in one of the correlation functions. While at the present moment we do not know of chemical systems showing any of these characteristics, we want to understand under which conditions or properties on the kinetic scheme they are possible. Below, we will find that they are not expected to be very common as they demand very particular conditions in the set of rate constants that at the same time lead to very low amplitudes or fast rates of decay. In Fig. 3.5 we present a model with negative dark-dwell-time autocorrelation and positive light-dwell-time autocorrelation, each with different rates of decay. This particular model also exhibits low cross-correlation when compared with the light autocorrelation function and these crosscorrelation functions have opposite signs. Each one of these characteristics is only possible in a system that has at least three substates. Numerically, we have found that in order to achieve negative correlations internal transformations should happen at the same rate of the reactions. In this example, this is reflected in our choice of the magnitude for the nonzero internal rate constants, which are comparable to the reaction rate constants of the same state.

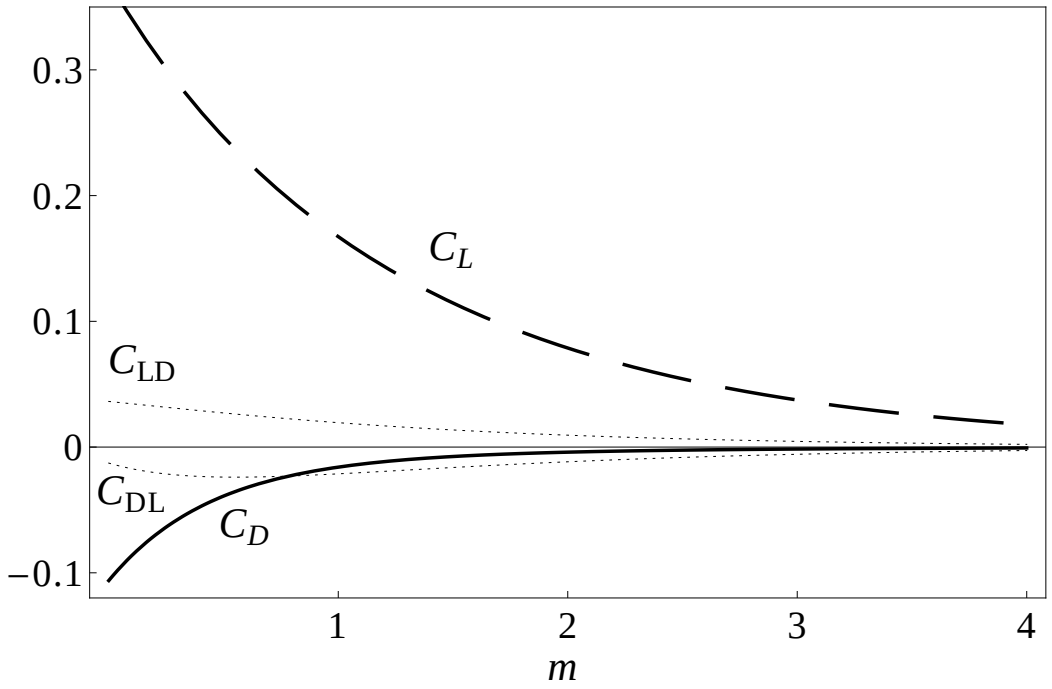

Figure 3.5: Dwell-time correlation functions for a three-channel model. The solid line is the correlation function for dark dwell times, the dashed line plots the correlation function for light dwell times and plots in dotted lines are crosscorrelation functions. Reaction rate constants for this model are $k_{D_1} = 5.5$, $k_{D_2} = 5$, $k_{D_3} = 10$, $k_{L_1} = 0.333$, $k_{L_2} = 12$, $k_{L_3} = 0.366$ and rate constants for internal transformations are $d_{21} = d_{32} = d_{13} = 5$, $d_{12} = d_{23} = d_{31} = 0$, $l_{21} = l_{32} = l_{13} = 0$, $l_{12} = l_{23} = l_{31} = 1.4$.

Essentially, models with negative correlation are systems in which the internal dynamics competes with those processes that lead to a change in the state. However, as we have numerically tested, not every model with competing dynamics exhibits negative correlation. In addition, under these conditions a fast rate of decay is expected in every correlation plot. In order to experimentally access these very low correlations, the experimentalist may have to collect long trajectories or average over many equivalent trajectories, so as to minimize the statistical error.

The system studied in Fig. 3.5 does not respect the principle of detailed bal-

ance characteristic of systems in equilibrium. As a consequence, this kinetic model can only represent chemical systems that are not in thermodynamic equilibrium. Numerical explorations of three-channel models obeying the detailed balance condition with negative autocorrelation have been found to also exhibit very low amplitude in the correlation, in the order of 0.01 or lower. While our exploration might not be conclusive, given the size of the space parameter of a three channel system; it seems to be the case that microscopic reversibility leads to very low correlations, whenever they are negative. Based on our interpretation of the correlation coefficient, it is possible that if two reactions, say from the dark to the light state, happen through the same channel or reaction path with times $t_D^{(1)}$ and $t_D^{(2)}$, they will most likely be positively correlated as they will most likely have the same deviation from the mean: either $t_D^{(1)} < \bar{t}_D$ and $t_D^{(2)} < \bar{t}_D$ or, $t_D^{(1)} > \bar{t}_D$ and $t_D^{(2)} > \bar{t}_D$. On the other hand, if these two reactions occur through different channels and one of them has short reaction times while the other one has long reaction times it is likely to observe a negative correlation coefficient, as in this case we could observe either $t_D^{(1)} < \bar{t}_D$ and $t_D^{(2)} > \bar{t}_D$ or, $t_D^{(1)} > \bar{t}_D$ and $t_D^{(2)} < \bar{t}_D$. That is why internal dynamics have to be of the same order of magnitude than the reaction rates, otherwise it would not be possible to change from one channel to the other. But microscopic reversibility implies that the average rate of every process is equal to the average rate of its reverse process, and this reduces the probability of a biased transition from one channel to another.

Correlation functions of three-channel models may decay with damped oscillations, as illustrated in Fig. 3.6. We have numerically found that oscillations can be observed in models with internal dynamics of the same order of magnitude as the reaction rates. However, as we discussed above, this also leads to correlation functions with fast decays. If loops or cycles exist in the set of

internal transformations, it is also possible that the eigenvalues of the turnover matrix can be complex. We investigate this scenario by analyzing Eq. (3.25) assuming that the turnover matrix M_D has complex eigenvalues. In this case, a basic consequence of the fundamental theorem of algebra tells us that $\lambda_1^* = \lambda_2$. The eigenvectors for different eigenvalues can be obtained by conjugation: If $M_D|R_i^D\rangle = \lambda_i|R_i^D\rangle$, then

$$\left(M_D|R_i^D\rangle\right)^* = \left(\lambda_i|R_i^D\rangle\right)^* = \lambda_i^*|R_i^{D\,*}\rangle \tag{3.26}$$

$$= M_D|R_i^{D\,*}\rangle. \tag{3.27}$$

Therefore, coefficients in eq. (3.25) can be complex numbers as well, and in that case they are the complex conjugate of each other. We can write

$$\lambda_1 = re^{-i\phi} \quad \lambda_2 = re^{+i\phi} \tag{3.28}$$

$$\frac{\langle 1|\mathsf{K}_D^{-1}|R_1^L\rangle\langle L_1^D|p_D\rangle}{\langle L_1^D|S_L|R_1^L\rangle} = ae^{-i\theta} \quad \frac{\langle 1|\mathsf{K}_D^{-1}|R_2^L\rangle\langle L_2^D|p_D\rangle}{\langle L_2^D|S_L|R_2^L\rangle} = \frac{\langle 1|\mathsf{K}_D^{-1}|R_1^{L\,*}\rangle\langle L_1^{D\,*}|p_D\rangle}{\langle L_1^{D\,*}|S_L|R_1^{L\,*}\rangle} = ae^{+i\theta} \tag{3.29}$$

with $0 \leq r \leq 1$, $a > 0$, $0 \leq \phi < 2\pi$ and $0 \leq \theta < 2\pi$; we find that the dark correlation function for models with λ_1 and λ_2 complex, can be written as follows:

$$C_D(m) = 2\,a\,r^{m+1}\cos\left(\phi(m+1) + \theta\right) \tag{3.30}$$

While Eq. (3.30) suggests that one should observe damped oscillations in the correlation function when the turnover matrix for the model has complex eigenvalues, we observe in Fig. 3.7 that this is not always the case, as we have $\lambda_1 = 0.417e^{-0.17i}$ for this model, with $r = 0.417$ and $\phi = 0.17$. In the upper panel of Fig. 3.7 we observe that for this model powers of r decay to zero before an oscillation takes place, which will be induced by the factor $\cos(\phi(m+1))$. Put another way, the correlation time for this model, that is given by r^{m+1} is much shorter than its period of oscillation (given by $2\pi/\phi$). The lower panel in Fig. 3.7 shows the four correlation plots for this model. We will find below an explanation for this difference between the correlation time and the period of oscillation

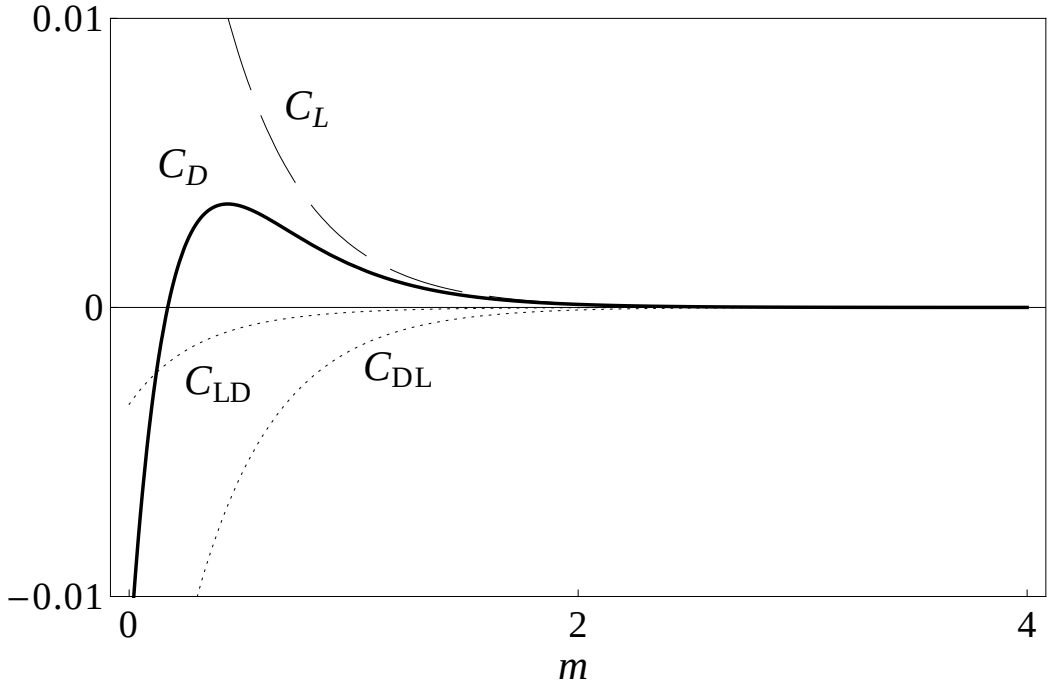

Figure 3.6: Oscillations in the dark-dwell-time correlation for three-channel model. $C_D(m)$ Solid line, $C_L(m)$ dashed, $C_{LD}(m)$ and $C_{DL}(m)$ dotted. Reaction rate constants for this model are $k_{D_1} = 3.1$, $k_{D_2} = 1$, $k_{D_3} = 4$, $k_{L_1} = 1$, $k_{L_2} = 5$, $k_{L_3} = 2$ and rate constants for internal transformations are $d_{21} = d_{32} = d_{13} = 2.5$, $d_{12} = d_{23} = d_{31} = 0$, $l_{21} = l_{32} = l_{13} = 0$, $l_{12} = l_{23} = l_{31} = 55$.

once we have introduced a different form of the turnover matrix (see Eq. (3.31)). Before we proceed, we should go back to Fig. (3.6) and note that in this case λ_1 and λ_2 are real, which means that nonmonotonic behavior are not exclusive to systems with complex eigenvalues.

3.4 A perturbative analysis of the turnover matrix

While we can interpret the exponential decay of the correlation function in a simple fashion and calculate the decay constant m_D in terms of the rate constants

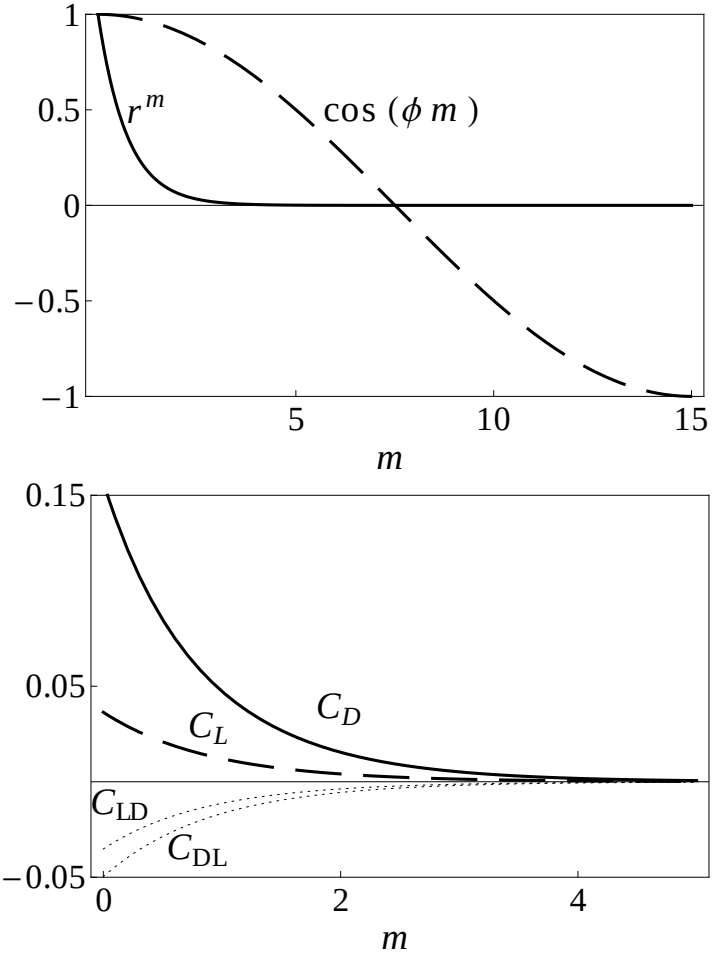

Figure 3.7: The top panel shows the norm r (solid line) and the cosine of the argument ϕ (dashed line) for a three channel model with complex eigenvalues. The bottom panel shows the dwell-time correlation functions for the same model. Notice that there are no oscillations. Reaction rate constants for this model are $k_{D_1} = 3$, $k_{D_2} = 1$, $k_{D_3} = 4$, $k_{L_1} = 1$, $k_{L_2} = 5$, $k_{L_3} = 2$ and rate constants for internal transformations are $d_{21} = d_{32} = d_{13} = 1/20$, $d_{12} = d_{23} = d_{31} = 0$, $l_{21} = l_{32} = l_{13} = 0$, $l_{12} = l_{23} = l_{31} = 3/2$. The eigenvalues for this model are $\lambda_1 = 0.416e^{-0.17i}$ and $\lambda_1 = 0.416e^{+0.17i}$.

defining the two-channel scheme, the decay for a general three-channel system does not have a simple form that can be predicted in a simple way from its set of parameters. Only in some particular cases, such as chemical systems with monoexponential decays in the autocorrelation functions, can we get some qualitative understanding of the factors in the model that dominate the observed decays. This requires the introduction of perturbation theoretical methods to calculate the eigenvalues of M_D and we will undertake this task next.

First, we observe that the turnover matrix M_D can be written as follows:

$$M_D = (I + V_D)^{-1}, \tag{3.31}$$

where $V_D = \Gamma_L \mathsf{K}_L^{-1} + \Gamma_D \mathsf{K}_D^{-1} + \Gamma_L \mathsf{K}_L^{-1} \Gamma_D \mathsf{K}_D^{-1}$. V_D has a simpler structure when compared with M_D, as all the inverse matrices involved in its definition are diagonal matrices. In fact, every matrix element V_D is a simple combination of ratios of rate constants of internal transformations and rate constants of reaction. In addition, V_D and M_D have the same set of eigenvectors.

If α_i is an eigenvalue of V_D, then

$$\lambda_i = \frac{1}{1 + \alpha_i} \tag{3.32}$$

is an eigenvalue of M_D. Close to the static limit, we can write these eigenvalues as exponential functions: $\lambda_i^m \sim e^{-\alpha_i m}$. Hence, constants determining the exponential decay are the eigenvalues of V_D, in this limit. Besides, one has that α_i is in general a function of ratios of rate constants for internal transformations and reaction rate constants. These observations hold for every n-channel system.

When the internal dynamics (given by Γ_D and Γ_L) are significantly slower than the reaction dynamics (given by K_D and K_L), M_D can be written as a series

in powers of V_D

$$M_D = \sum_n (-1)^n V_D^n, \tag{3.33}$$

and in a first-order approximation to this series we have

$$M_D^{(1)} = I - \Gamma_L \mathsf{K}_L^{-1} - \Gamma_D \mathsf{K}_D^{-1} = I - V_D^{(1)}, \tag{3.34}$$

where we have introduced the super index $^{(1)}$ to indicate that M_D has been approximated by Eq. (3.34). For an n-channel system admitting only internal transformations between neighbor substates (i.e. $A_i \to A_j$ possible only if $i = j + 1$ or $i = j - 1$), we observe that $V_D^{(1)}$ is a tri-diagonal matrix with matrix elements

$$[V_D^{(1)}]_{ij} = \delta_{ij}\left(\frac{\sum_{k\neq i} d_{ki}}{k_{D_j}} + \frac{\sum_{k\neq i} l_{ki}}{k_{L_j}}\right) - (\delta_{i\,j+1} + \delta_{i\,j-1})\left(\frac{d_{ij}}{k_{D_j}} + \frac{l_{ij}}{k_{L_j}}\right) \tag{3.35}$$

In the next example we illustrate how the approximation in eq. (3.34) can be used to study some systems.

3.4.1 Example: A three-channel system as a perturbation of a two-channel system

For a two channel system

$$V_{D(2)} = \begin{pmatrix} x_1 & y_1 \\ z_2 & x_2 \end{pmatrix} \tag{3.36}$$

where we have introduced the subindex (2) to remind us that this is is the representation of V_D for a system with two substates. Notice that in Eq. (3.36) with $x_1 + z_2 = 0$ and $y_1 + x_2 = 0$. The exact elements of this matrix can be easily determined. For example,

$$x_1 = \frac{d_{21}}{k_{D_1}} + \frac{l_{21}}{k_{L_1}} + \frac{l_{21}}{k_{L_1}}\frac{d_{21}}{k_{D_1}} + \frac{l_{12}}{k_{L_2}}\frac{d_{21}}{k_{D_1}}. \tag{3.37}$$

Here, the first two terms in the right hand side are the elements that would be considered in a first order approximation. For a three channel system with slow substate transformations we can write

$$V^{(1)}_{D(3)} = \begin{pmatrix} x_1 & y_1 & 0 \\ z_2 & \tilde{x}_2 & y_2 \\ 0 & z_3 & x_3 \end{pmatrix} \tag{3.38}$$

and in this case $y_1 + \tilde{x}_2 + z_3 = 0$. From this or just by direct computation we can see that $\tilde{x}_2 = x_2 - z_3$. Observe that if z_3 vanishes then the eigenvalues of $V_{D(3)}$ are those of $V_{D(2)}$ and x_3. Also, observe that the exact value of z_3 is given by

$$z_3 = -\frac{l_{32}}{k_{L_2}} - \frac{d_{32}}{k_{D2}} - \frac{d_{32}}{k_{D_2}}\left(\frac{l_{12} + l_{32}}{k_{L_2}}\right) - \frac{d_{23}}{k_{D_3}}\frac{l_{32}}{k_{L_2}}. \tag{3.39}$$

We can take z_3 as a perturbation parameter since its magnitude is controlled by that of the rate constants that involve transitions from the two channel model and an additional substate. Our goal is to describe the eigenvalues of $V^{(1)}_{D(3)}$ as a perturbation of those corresponding to a two-channel system and one term associated with the kinetic parameters of the additional channel. Observe that $\alpha = x_1 + x_2$ is the eigenvalue of $V_{D(2)}$ different to zero. For the eigenvalues of $V^{(1)}_{D(3)}$ we have

$$\alpha_1 = x_1 + x_2 - z_3\frac{(x_2)}{(x_1 - x_3 + \tilde{x}_2)} + O(z_3^2) \tag{3.40}$$

$$\alpha_2 = x_3 - z_3\frac{(x_1 - x_3)}{(x_1 - x_3 + \tilde{x}_2)} + O(z_3^2) \tag{3.41}$$

where z_3 is small. In the same fashion, we can describe the eigenvectors of $V^{(1)}_{D(3)}$ as series of z_3 which should provide a simple description for small values on z_3. This perturbative approach to the eigenvectors of $V^{(1)}_{D(3)}$, and at the end, to the factors defining the amplitude of the correlation functions, can be understood

after defining the matrices

$$V_{D(3)}^{(0)} = \begin{pmatrix} x_1 & -x_2 & 0 \\ -x_1 & x_2 & -x_3 \\ 0 & 0 & -x_3 \end{pmatrix} \qquad P = \begin{pmatrix} 0 & 0 & 0 \\ 0 & -z_3 & 0 \\ 0 & z_3 & 0 \end{pmatrix} \tag{3.42}$$

in such a way that $V_{D(3)}^{(1)} = V_{D(3)}^{(0)} + P$. Observe that the eigenvalues for $V_{D(3)}^{(0)}$ are 0, $x_1 + x_2$ and x_3 with the corresponding left eigenvectors

$$\begin{pmatrix} 1 & 1 & 1 \end{pmatrix} \qquad \begin{pmatrix} x_1 & -x_2 & \frac{x_2 x_3}{x_1 + x_2 - x_3} \end{pmatrix} \qquad \begin{pmatrix} 0 & 0 & 1 \end{pmatrix}. \tag{3.43}$$

The corresponding right eigenvectors are

$$\begin{pmatrix} x_2 \\ x_1 \\ 0 \end{pmatrix} \qquad \begin{pmatrix} 1 \\ -1 \\ 0 \end{pmatrix} \qquad \begin{pmatrix} \frac{1}{x_1 - x_3} \\ \frac{1}{x_2} \\ -\frac{(x_1 + x_2 - x_3)}{x_2 (x_1 - x_3)} \end{pmatrix}. \tag{3.44}$$

In Fig. 3.8, we numerically explore a system satisfying the conditions demanded by the perturbative approach described above. A two-channel system with correlation only between the dark dwell times, as presented in the upper panel of Fig. 3.8, is considered as a subsystem of a three-channel system (see lower panel of Fig. 3.8). Substates in one of the channels of the subsystem transform into the substates of the third channel with small rate constants. This is the condition that we have imposed in our perturbative analysis of three-channel systems. By contrasting both panels, we conclude that the dark-dwell-time correlation function is well described only by the kinetic rate constants of the two-channel system that is taken as a subsystem of the total kinetic model. In fact, the exact m_D^{-1} for the two channel system is 0.325 and for the total three-channel system is 0.330. One can also calculate m_D^{-1} according to Eq. (3.22) and obtain a value of 0.36, after what we find that m_D^{-1} is very close to α_1 as predicted in Eq.

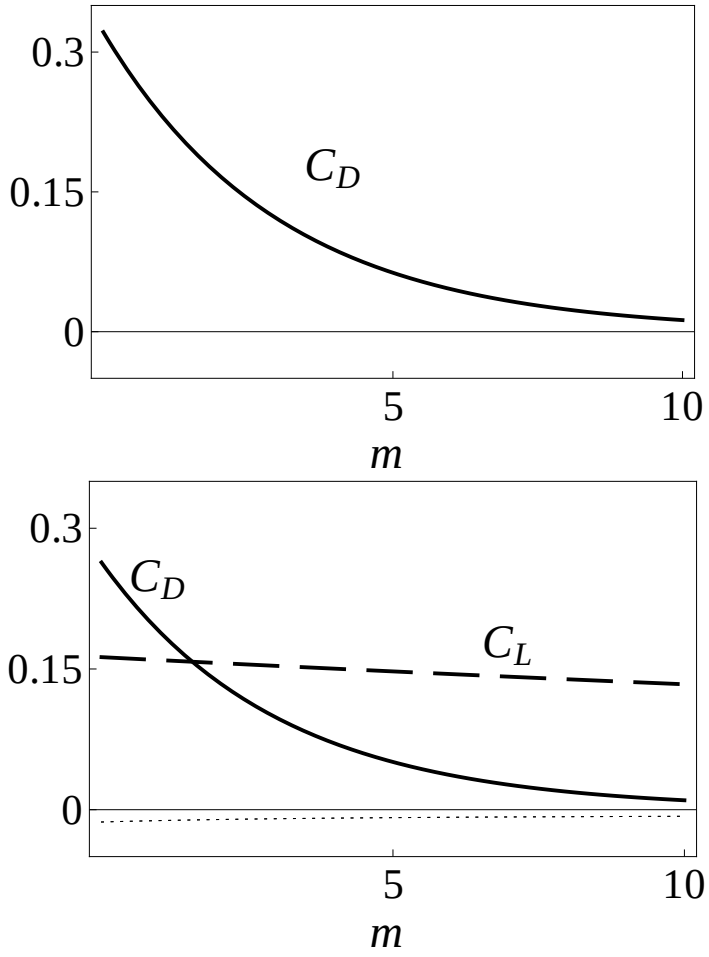

Figure 3.8: The top panel shows C_D for a two channel model with vanishing C_L, C_{LD} and C_{DL}. The bottom panel shows a C_D, C_L, C_{LD} and C_{DL} for three-channel model that is the result of expanding the model of the top by introducing a third substate with slow internal transformations to the two-channel subsystem. Reaction rate constants for this model are $k_{D_1} = 1/10$, $k_{D_2} = 5$, $k_{D_3} = 10/51$, $k_{L_1} = k_{L_2} = 1$, $k_{L_3} = 9/2$ and rate constants for internal transformations are $d_{21} = 0.015$, $d_{12} = 0.6$, $d_{32} = 0.01$, $d_{23} = 1/2295$, $l_{21} = 5/100$, $l_{12} = 4/100$, $l_{32} = 1/100$, $l_{23} = 1/20$. The two-channel model in the top panel is the subsystem composed by channels 1 and 2.

(3.40). On the other hand, the third channel introduces heterogeneity in the reaction rate constants associated with transitions from the light to the dark state with consequent existence of correlation between light dwell times. As anticipated by our perturbative analysis, the decay of the light correlation function is dominated by the rate constants in the third channel: The exact value of m_L^{-1} is 0.0195 and the one predicted by Eq. (3.41) is 0.0133. Notice that in the above model we have chosen the values for some of the rates constants in such a way that crosscorrelation is negligible.

3.4.2 Example: Oscillations in a three-channel model

In our treatment of the three-channel system we stated that oscillations in the correlation functions are actually seldom, even in the case that M_D has complex eigenvalues. In that case we found numerically that the period for an oscillation is expected to be longer than the correlation time. We will support this conclusion by considering the argument and the norm of the eigenvalues in Eq. (3.28) based on their form according to Eq. (3.32). Assuming that λ_1 and α_1 are complex numbers, we can write $\alpha_1 = a + bi$ with a and b real to find that

$$r = \frac{1}{(1+a)^2 + b^2}, \tag{3.45}$$

$$\phi = \arctan\left(\frac{-b}{1+a}\right). \tag{3.46}$$

The coefficients a and b are functions of different ratios between rate constants of internal transformation and rate constants of reaction. Both of them are expected to be small when the internal dynamics is small, and so $r \sim 1 - 2a$ and $\phi \sim b$. This will lead to a long period of oscillation of $2\pi/b$.

3.5 Many active sites

Our treatment of correlation functions through this Chapter has consider only case of catalysts with one active site. Nanoparticles, as pointed out Sec. 1.2, have many active sites. As a consequence, we must determine the effects that multiple active sites may have on the dwell-time correlation functions that are measured from a single trajectory. As we found in Chapter 2, Secs. 2.3-2.5, whether the active sites are independent or spatially correlated can make a difference in the qualitative properties of the constrained means. Thus, we should also include cooperative effects among active sites in our study of dwell-time correlation functions and, we will do this in the following two sections.

3.5.1 Active sites with correlated fluctuations

Under saturating conditions and in the presence of multiple active sites, we can hypothesize that internal transformations in a single active site influence the internal dynamics of nearby active sites and vice verse. As discussed in Chapter 2 and as reported in[35], this in fact the case for gold nanoparticles of 6 nanometers diameter. In order to understand how this cooperative behavior is manifest in the fluorescence trajectory, we introduced a model for many-active-site nanoparticles that restricts the configuration space, i.e. the number of possible substates that every active site can take at any time. In the absence of space resolution, it is plausible to assume that every active site has the same number of substates, and also that the set of rate constants is the same. To further simplify our model, we assume that when the nanoparticle is in the dark state every active site is in the same substate. In addition, whenever the nanoparti-

cle is the light configuration L_i, any active site in the dark substate D_i remains in that substate until the dark configuration is recovered. In accordance to the experimental observations for nanoparticles, only one active site at a time is allowed to experience a transition from the dark to the bright state. One can also consider the case of a nanoparticle with independent active sites, and we will do this in the next section. Intermediate cases can be described by considering independent domains of active sites that act cooperatively, as studied in Sec. 2.5, Chapter 2.

For the model with spatially correlated active sites we found [35] that the dynamic equations are equivalent to those of one active site with enhanced reaction rate constants from the dark to the light state (i.e., $k_{D_i} \rightarrow N \times k_{D_i}$) and, if every state admits only two substates, then we have that

$$\lambda = \frac{1}{\left(1 + \frac{d_{21}}{Nk_{D_1}} + \frac{d_{12}}{Nk_{D_2}}\right)\left(1 + \frac{l_{21}}{k_{L_1}} + \frac{l_{12}}{k_{L_2}}\right)}, \tag{3.47}$$

which indeed suggests that a significant increase in the correlation time should be observed for N spatially correlated active sites, when compared to the decay observed for an individual active site. In fact, if two nanoparticles differ only in the number of active sites and they have active sites with spatially correlated fluctuations, then the correlation time should be larger for the system with the bigger number of active sites. In addition, one should also observe that as N increases the decay constant, and therefore the correlation time, increases and we should expect to find that rate of decay is controlled by the rate constants associated with the light substate. This assertion follows from the asymptotic behavior of λ for large N:

$$\lambda_{N\rightarrow\infty} \rightarrow \frac{1}{\left(1 + \frac{l_{21}}{k_{L_1}} + \frac{l_{12}}{k_{L_2}}\right)}. \tag{3.48}$$

The dark correlation function for a set of N spatially correlated active sites close to the static limit is given by

$$C_D(m) = \frac{1}{N^2(k_{D_1}\rho_{D_1} + k_{D_2}\rho_{D_2})^2} \frac{\lambda^{m+1}}{\sigma_D^{2\,(N)}} \left(\frac{\rho_{D2}\rho_{D1}}{k_{D1}k_{D2}} (k_{D2} - k_{D1})^2 \right). \tag{3.49}$$

While Eq. (3.49) suggests a simple relation between the amplitude and the number of active sites, one should notice that this is not the case, for the equilibrium probabilities are rational functions of the number of active sites and the variance depends on N as well. In general, this leads to a non-monotonic behavior of the amplitude of the C_D. However, this change in the amplitude is small close to the static limit. First, notice that in this case the variance scales as N increases as follows

$$\sigma_D^{2\,(N)} = \frac{1}{N^2} \left(\frac{\langle 1|(\mathsf{K}_D + N^{-1}\Gamma_D)|\rho_D\rangle}{\langle 1|\mathsf{K}_D|\rho_D\rangle} - \frac{\langle 1|\rho_D\rangle^2}{\langle 1|\mathsf{K}_D|\rho_D\rangle}^2 \right), \tag{3.50}$$

$$\sim \frac{1}{N^2}\sigma_D^{2\,(1)}, \tag{3.51}$$

and therefore $C_D(0)$ should be nearly independent of N[2]. In Figs. 3.9 and 3.10 we have explored numerically the above assertions. Notice that these models differ only in the values that we have assign to the internal rate constants: The system in Fig. 3.9 is close to the static limit while the one in Fig. 3.10 is not. We find, as anticipated, that the amplitude is independent from the number of active sites for models that are close to the static limit, but certainly dependent on N when the system experiences fast internal dynamics. Besides, in both cases the correlation time becomes longer as the number of active site increases.

[2]Remember that the eigenvalue λ depends on N according to Eq. 3.47. The value obtained for these correlation functions by extrapolation at $m = -1$ must be independent of N, but m is only defined for $m \geq 1$.

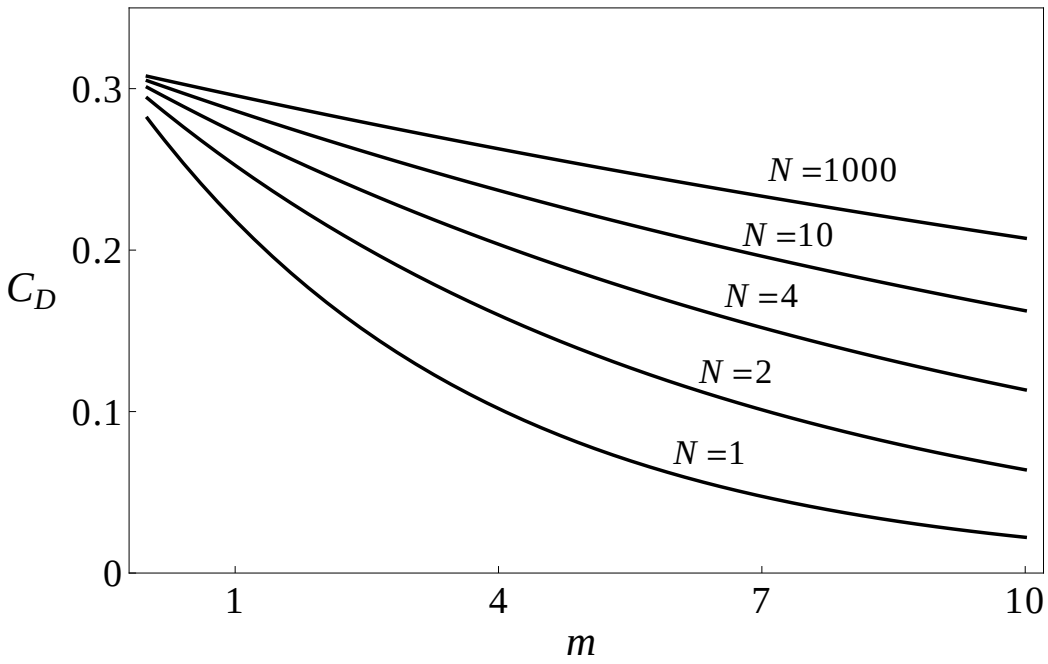

Figure 3.9: $C_D(m)$ for many correlated active sites. Parameters for these models are $k_{D_1} = 1/10, k_{D_2} = 1/2, k_{L_1} = 1, k_{L_2} = 3$, $d_{21} = d_{12} = l_{12} = 1/50$ and $l_{21} = 1/30$. Time unit is $(k_{L_1})^{-1}$.

3.5.2 Independent active sites

A full treatment of the correlation functions for a set of N independent active sites based only on the analysis of the turnover matrix might be cumbersome. As illustrated in our treatment of constrained mean dwell times, introducing appropriate generating functions helps to avoid these complications. In the following, we will center our discussion around the dependence of dark dwell-time correlation on the number of independent active sites N, as it serves for illustration. Similar conclusions to those that we will find below can be drawn for the case of the light dwell-time correlation after considering the multiple incidents that can contribute to the correlation coefficient. We will come back to this point once we have introduced the general treatment of dwell-time correla-

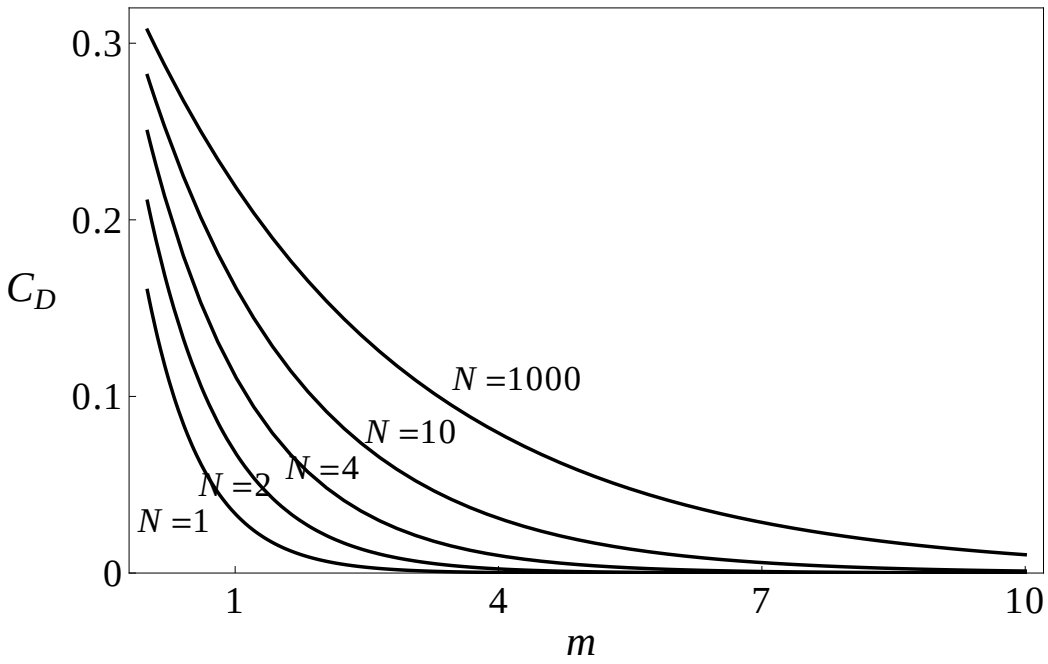

Figure 3.10: $C_D(m)$ for many correlated active sites. Parameters for these models are $k_{D_1} = 1/10, k_{D_2} = 1/2, k_{L_1} = 1, k_{L_2} = 3$, $d_{21} = d_{12} = l_{12} = 1/5$ and $l_{21} = 1/3$

tion functions in terms of generating functions.

First, consider two dark states in a fluorescence trajectory. If $t_D^{(1)}$ and $t_D^{(m+1)}$ are dark dwell times that are spaced m turnovers apart ($m \geq 1$), the generating function for their density function is given by Eq. (3.4). In terms of this generating function the mean value of the product of these dwell times is given by

$$\overline{t_D^{(1)} t_D^{(m+1)}} = \int_0^\infty dt_D^{(1)} \int_0^\infty dt_D^{(m+1)} G_{DD}^{(m)}(t_D^{(1)}, t_D^{(m+1)}). \tag{3.52}$$

We want to illustrate here that a system of N independent active sites is less correlated than a single active site. To achieve this goal, it will be enough to illustrate the dependence on the number of active sites for the correlation when $m = 1$, since the correlation function is strictly decreasing for systems with two substates. In this case, $t_D^{(1)}$ and $t_D^{(2)}$ are dark dwell times that are separated by a

single event in a single active site. In contrast, if we were to consider dwell times $t_D^{(1)}$ and $t_D^{(3)}$, we would find that the generating function $G_{DD}^{(2)}(t_D^{(1)}, t_D^{(3)})$ has contributions from events that occur in the same active site but also contributions from events that happen at two different active sites (with dwell times $t_L^{(2)}$ and $t_L^{(3)}$). An equivalent expression for Eq. (3.52) can be derived for the mean value of the products $t_L^{(1)} t_L^{(m+1)}$, $t_D^{(1)} t_L^{(m+1)}$ and $t_L^{(1)} t_D^{(m+1)}$. Also, their generating functions have multiple contributions from sequences of events occurring in one, two, ..., m active sites.

Thus if $m = 1$, Eq. (3.52) can be written in terms of the generating function for a single active site as follows

$$\overline{t_D^{(1)} t_D^{(2)}} = \int_0^\infty dt_D^{(1)} \int_0^\infty dt_D^{(2)} (E_D(t_D^{(1)} + t_D^{(2)}))^{N-1} g_{DD}^{(2)}(t_D^{(1)}, t_D^{(2)}). \tag{3.53}$$

with $E_D(t_D)$ is as defined in Eq. (2.80) and $g_{DD}^{(2)}(t_D^{(1)}, t_D^{(2)})$ is equal to $G_{DD}^{(2)}(t_D^{(1)}, t_D^{(2)})$ for a single active site. One can see that $E(t_D) < 1$ for all $t_D > 0$ and therefore, the mean of the product $t_D^{(1)} t_D^{(2)}$ should decrease as the number of active sites increases. For the sake of calculating the $C_D(1)$ we should notice the following equalities:

$$\overline{t_D^2} = 2 \frac{\langle 1 | W_{DD}^{-1} | \rho_D \rangle}{\langle 1 | W_{DD} | \rho_D \rangle}, \tag{3.54}$$

$$= 2 \overline{t_D} \int_0^\infty dt \, (E_D(t))^N, \tag{3.55}$$

$$\sigma_D^2 = \overline{t_D} \left(2 \int_0^\infty dt \, (E_D(t))^N - \overline{t_D} \right). \tag{3.56}$$

By substituting Eqs. (3.56), (3.55) and (3.53) into Eq. (3.8) with $m = 1$, we find an integral expression for $C_D(1)$ with explicit dependence on N. The resulting expression is investigated numerically in Fig. 3.11. There, we have also included the corresponding values for $C_D(1)$ for the equivalent model with spatially correlated active sites. First we notice that both models coincide at $N = 1$ and that

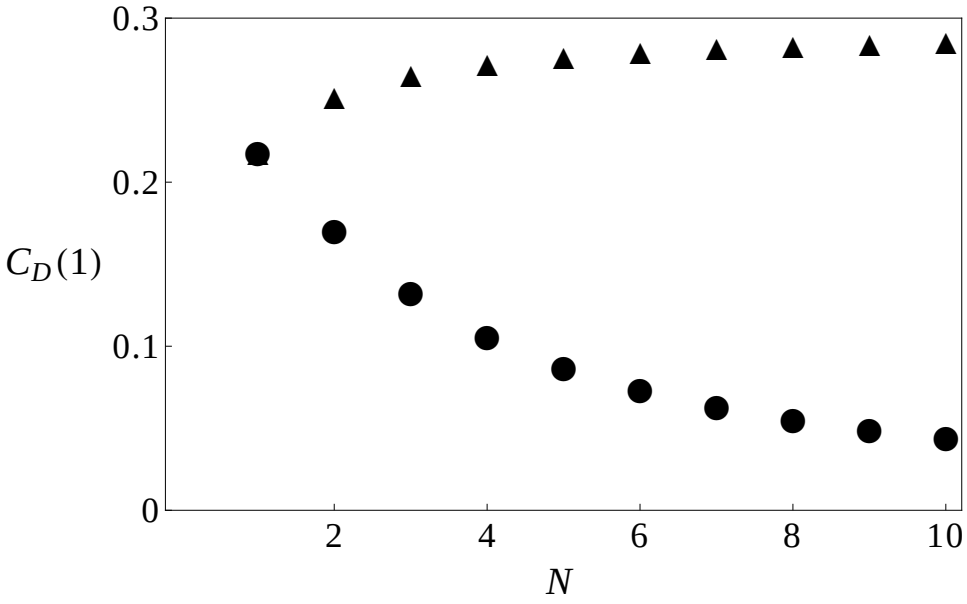

Figure 3.11: A comparison between $C_D(1)$ for a model with spatially correlated (triangles) and independent (circles) actives sites as function of the number of active sites. Parameters for these models are $k_{D_1} = 1/10, k_{D_2} = 1/2, k_{L_1} = 1, k_{L_2} = 3$, $d_{21} = d_{12} = l_{12} = 1/50$ and $l_{21} = 1/30$. Time unit is $(k_{L_1})^{-1}$.

this correlation coefficient decreases as the number of independent active sites increases.

We would like to estimate how this decrease in the $C_D(1)$ scales as N increases. For large N one can calculate the integral Eq. (3.56) after considering the cumulant expansion for $E_D(t)$ in Eq. (2.86). This way, we can conclude that

$$\sigma_D^2 \to \frac{1}{N}\bar{t}_D^2(onesite), \tag{3.57}$$

for large N. On the other hand the covariance $Cov(1) = \overline{t_D^{(1)} t_D^{(m+1)}} - \bar{t}_D^2$ can also be calculated using the cumulant expansion and, after a change of variables given by $t_D^+ = t_D^{(1)} + t_D^{(2)}$ and $t_D^- = t_D^{(1)} - t_D^{(2)}$, i.e.

$$C_D(1) = \frac{\frac{1}{2}\int_{-\infty}^{-\infty} dt_D^- \int_0^{-\infty} dt_D^+ E_D(t_D^+)^{N-1} g_{DD}^{(2)}\left(\frac{t_D^+ + t_D^-}{2}, \frac{t_D^+ - t_D^-}{2}\right) - \overline{t_D}^2}{\sigma_D^2}. \tag{3.58}$$

In order to simplify eq (3.58), we first note from eq. (3.4), for one active site, that $g^{(2)}_{DD}$ is a multiexponential function of t^+_D and t^-_D, and that this function can be written in the general form

$$g^{(2)}_{DD}\left(\frac{t^+_D + t^-_D}{2}, \frac{t^+_D - t^-_D}{2}\right) = \sum_i e^{-\phi_i t^+_D} b_i(t^-_D), \tag{3.59}$$

where ϕ_i and b_i are functions of the rate constants for our model. Using this and the cumulant expansion of $E_D(t^+_D)$, we find that for systems with a large number of independent active sites $C_D(1)$ decays as follows

$$C_D(1) = \frac{\overline{\mathbf{t}_D}}{N}\left(\int_{-\infty}^{\infty} \sum_i b_i(t^-_D)\sigma^2_{wD} dt^-_D \; - 1\right). \tag{3.60}$$

In the derivation of eq. (3.60), we have made use of the fact that $\overline{\mathbf{t}^+_D} = 2\,\overline{\mathbf{t}_D}$, which is a simple consequence of the properties of the joint density function.

Finally, we can conclude that our model for many active sites with spatially correlated fluctuations has a longer dark correlation time, as manifested in decreased rate of decay, when compared to a single active site. In contrast, a nanoparticle with many independent active sites should have a shorter dark correlation time, as compared again to a single active site.

3.6 Interlude: constrained mean dwell times as calculated from the turnover matrix

In Chapter 2 and in our paper[35], we investigated the interdependence in the fluctuations among active sites on the surface of a nanoparticle by means of difference between unconstrained and constrained mean dwell times. Our main conclusion was that gold nanoparticles have active sites that are *correlated*, in

the sense that there is an interdependence in the fluctuations among active sites. On the other hand, in this chapter we are studying the dwell-time correlation functions as indicators of memory. In order to avoid any potential misunderstandings, in the following we will talk about independent and spatially correlated instead of uncorrelated and correlated active sites, saving this adjective for the C_D, C_L, C_{DL} and C_{LD} functions.

For simplicity, we assumed in chapter 2 that every active site was able to fluctuate between two substates. However, as we discussed above, a nanoparticle with spatially correlated fluctuations among active sites, each one with two substates, does not exhibit the dwell-time correlation properties that have been observed in single nanoparticle catalysis, to wit, C_D and C_L decay with different rates and crosscorrelation is not detected. We know that these properties indicate that every active site fluctuates among three or more different substates. For this reason, we should expand our findings in Chapter 2 to the study of constrained mean dwell times for spatially correlated active sites that fluctuate among three substates.

Most of our results in Chapter 2 and in reference [35] are readily adaptable to models with active sites having three or more substates. For example, one can notice that the difference between the unconstrained and constrained mean light dwell time, for this case and the static limit, can be written simply as

$$\Delta\bar{t}_{L<} = h_{12}^{L<} + h_{13}^{L<} + h_{23}^{L<}, \tag{3.61}$$

where

$$h_{ij}^{L<}(t) = \frac{\rho_{L_i}\rho_{L_j}(k_{L_j} - k_{L_i})(e^{-k_{D_i}t} - e^{-k_{D_j}t})}{\langle 1|\mathsf{K}_D|\rho_D\rangle\ P(t_D < T)}, \tag{3.62}$$

$$P(t_D < T) = \int_0^T f_D(t_D)dt_D. \tag{3.63}$$

This result can be derived from generating functions in the static limit or from by introducing the the partition of unity induced by the eigenspace of M_D into f_{LD}. The last technique is illustrated in Appendix (B.6). By comparison of Eq. (3.62) with Eq. (2.39) in Chapter 2, we find that $h_{ij}^{L<}$ has the form of the constrained mean light dwell time for a two channel model close to the static limit composed only by channels i and j. The only significant difference is that the $h_{ij}^{L<}$ functions involve the probability $P(t_D < T)$ that takes into account the full set of channels of the original model, as well as the total product $\langle 1|\mathsf{K}_D|\rho_D\rangle$. Whenever the conditions are those demanded by the static limit, $P(t_D < T)$ assumes the form

$$P(t_D < T) = 1 - \frac{e^{-k_{D_1}T}k_{D_1}\rho_{D_1} - e^{-k_{D_2}T}k_{D_2}\rho_{D_2} - e^{-k_{D_3}T}k_{D_3}\rho_{D_3}}{k_{D_1}\rho_{D_1} + k_{D_2}\rho_{D_2} + k_{D_3}\rho_{D_3}}. \tag{3.64}$$

On the other hand, $\Delta\bar{t}_{L>}$ is given by

$$\Delta\bar{t}_{L>} = h_{12}^{L>} + h_{13}^{L>} + h_{23}^{L>}, \tag{3.65}$$

with

$$h_{ij}^{L>}(t) = \frac{\rho_{L_i}\rho_{L_j}(k_{L_i} - k_{L_j})(e^{-k_{D_i}t} - e^{-k_{D_j}t})}{\langle 1|\mathsf{K}_D|\rho_D\rangle\ P(t_D > T)}. \tag{3.66}$$

Similar conclusions and definitions follow for constrained mean dark dwell times.

We explore numerically the qualitative behavior of the constrained mean dwell times in Figs. 3.12 to 3.16. Differences in the constrained means for two and three-channel models are enhanced when the time scales of transformations in distinct channels differ in orders of magnitude. In all these plots we have included not only the exact curve for the corresponding constrained mean, but also the static limit prediction (Dashed line) and the different contributions from the functions h_{ij} to the static limit approximation (Dotted lines). We observed

that the static limit predictions are in great agreement in almost every model, with the exception of $\Delta\bar{t}_{L>}$ in Fig. 3.15. And we can see why: the rate constant d_{32} is 0.005, same as k_{D2} giving a ratio equal to 1. Thus, the model in Fig. 3.15 is far from the static limit and deviations from Eq. (3.65) are possible.

In Fig. 3.12 we have a model in which the fastest transition from the dark to the light (k_{D_1}) occurs through the same channel as the slowest transition from the light to the dark (k_{L_1}). It is also true for this model that the smallest k_D and the largest k_L are in the same channel (third channel). This leads to the observation that curves for $\Delta\bar{t}_{D<}$ and $\Delta\bar{t}_{L<}$ are positive and those for $\Delta\bar{t}_{D>}$ and $\Delta\bar{t}_{L>}$ are negative. We can anticipate this behavior from the two-channel decomposition of a three-channel model suggested by Eqs. (3.61) and (3.65), and the corresponding expressions for the constrained means for dark dwell times. For the model in Fig. 3.12 it is true that $(k_{D_i} - k_{D_j})(k_{L_j} - k_{L_i}) > 0$ for every (i, j) pair. We also notice that $\Delta\bar{t}_{D<}$, $\Delta\bar{t}_{L<}$ and $\Delta\bar{t}_{D>}$ are dominated by a single pair of channels and, as a consequence they resemble two-channel-model constrained means. On the contrary, $\Delta\bar{t}_{L>}$ has an unusual decay that can qualitatively be explained by the independent contribution of the three functions $h_{ij}^{L>}$. In Fig. (3.13) $h_{12}^{L>}$, $h_{13}^{L>}$ and $h_{23}^{L>}$ are identified. Observe that two different decay rates are observed. Initially, $\Delta\bar{t}_{L>}$ decays fast ($T_D < 10$) to approach a pseudo-asymptote of approximately 0.25. Later, for threshold values between 50 and 100, $\Delta\bar{t}_{L>}$ decays to a true asymptote with a slower decay rate. This different decay rates can be rationalized by observing that every $h_{ij}^{L>}$ for a large separation in the rate constant values k_{D_i} and k_{D_j} is exponential, with an exponential decay constant of $|k_{D_i} - k_{D_j}|$. Another comment that we can make from Fig. (3.13) is that $h_{12}^{L>}$ approaches zero as a result of $P(t_d > T)$ being dominated by the smallest rate constant[3], i.e. k_{D_3}.

[3]This follows after Eq. 3.64 and the fact that $P(t_d > T) = 1 - P(t_d < T)$.

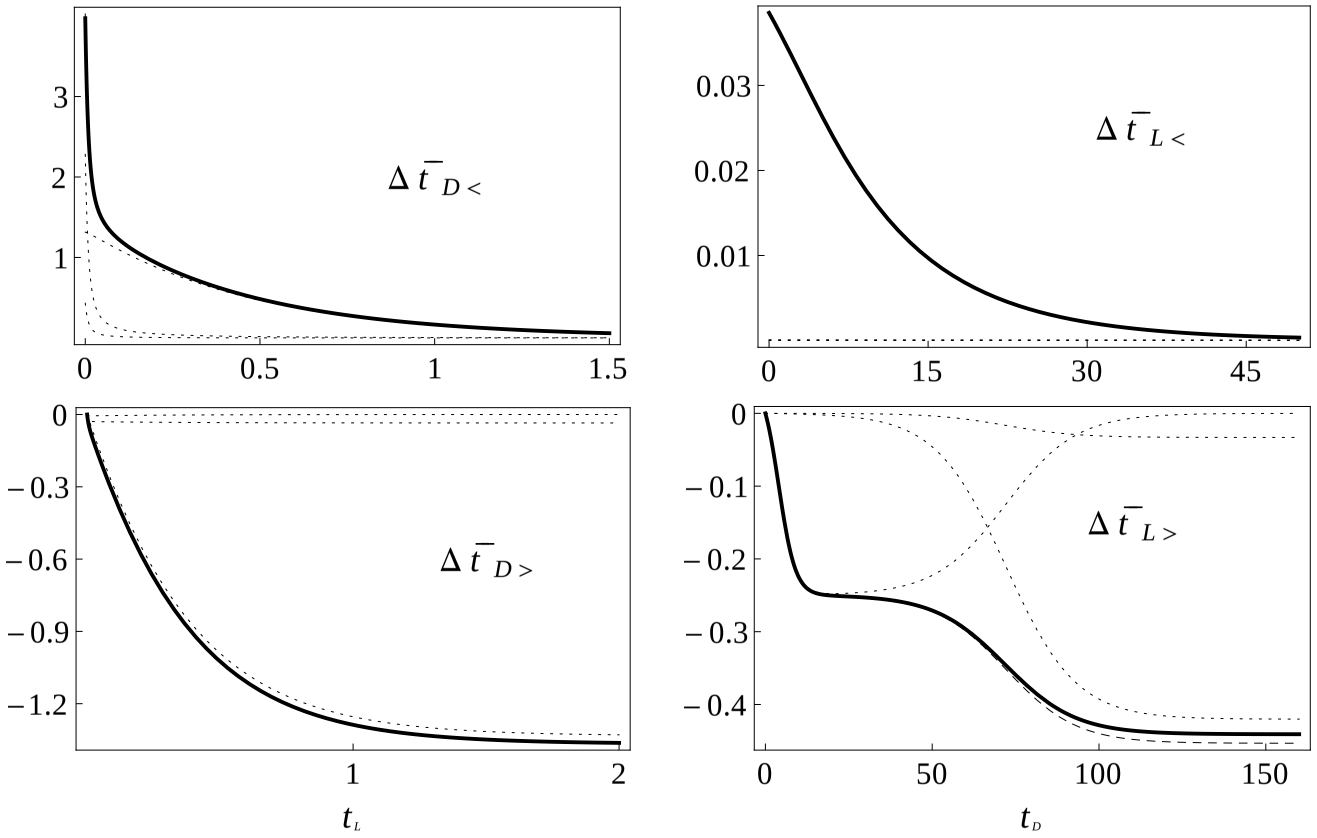

Figure 3.12: Constrained mean dwell times for a system with three substates. The exact value for each constrained mean is shown by a solid line. The approximated constrained mean, calculated according expressions of the form of Eq. (3.61) are dashed. Dotted plots correspond to the different functions h_{ij}. Parameters for this model are $k_{D_1} = 1/2$, $k_{D_2} = 1/10$, $k_{D_3} = 1/200$, $k_{L_1} = 2$, $k_{L_2} = 5$, $k_{L_3} = 200$, $d_{12} = d_{21} = l_{12} = l_{23} = l_{32} = d_{23} = 1/10000$, $l_{21} = 1/125000$ and $d_{32} = 1/8000000$. Time unit is $(2k_{D_1})^{-1}$.

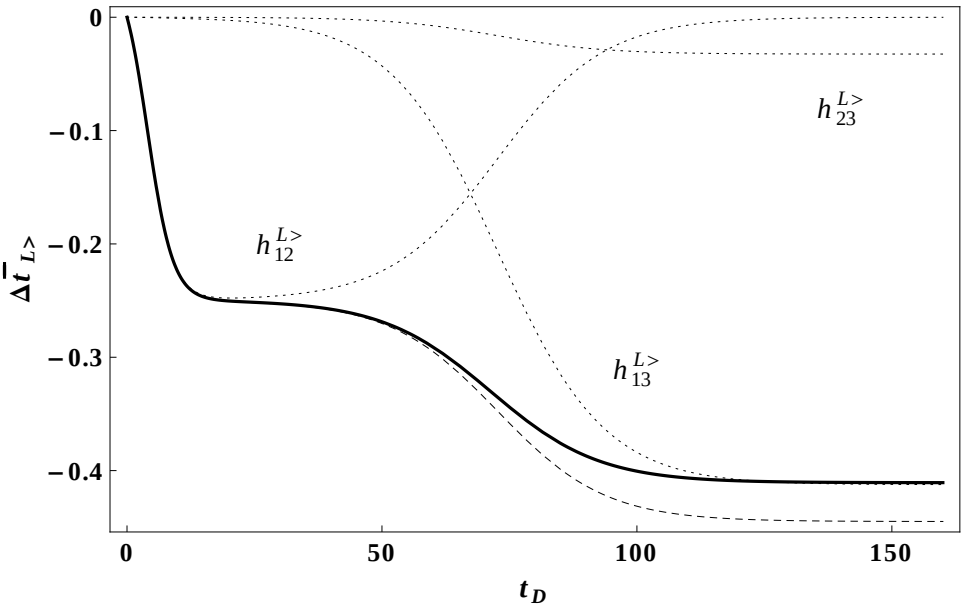

Figure 3.13: Decomposition into different pair that constribute to the total $\Delta\bar{t}_{L>}$ for the system with three substates shown in Fig 3.12. Time unit is $(2k_{D_1})^{-1}$.

.

In summary, we observe close to the static limit in $\Delta\bar{t}_{L>}$ fastest decay rates at short times and, if the separation between rate constants is significant, the rate of decay can change for longer threshold values.

We now consider a slightly different system that is the result of an interchange between the values for the reaction rate constants k_{D_2} and k_{D_3} in Fig. 3.14. Internal rate constants are reassigned in such a way that the condition of microscopic reversibility holds and, we can observe these parameters are in the regime that we consider close to the static limit. In this case we find that $(k_{D_2} - k_{D_3})(k_{L_3} - k_{L_2}) < 0$, while a similar product for the other pair of channels is positive. As a consequence, we see that plots for the h_{23} functions, contribute to the total in a different way, with negative constrained means when h_{12} and h_{13} are positive, and so on. However, this permutation in reaction rate parameters

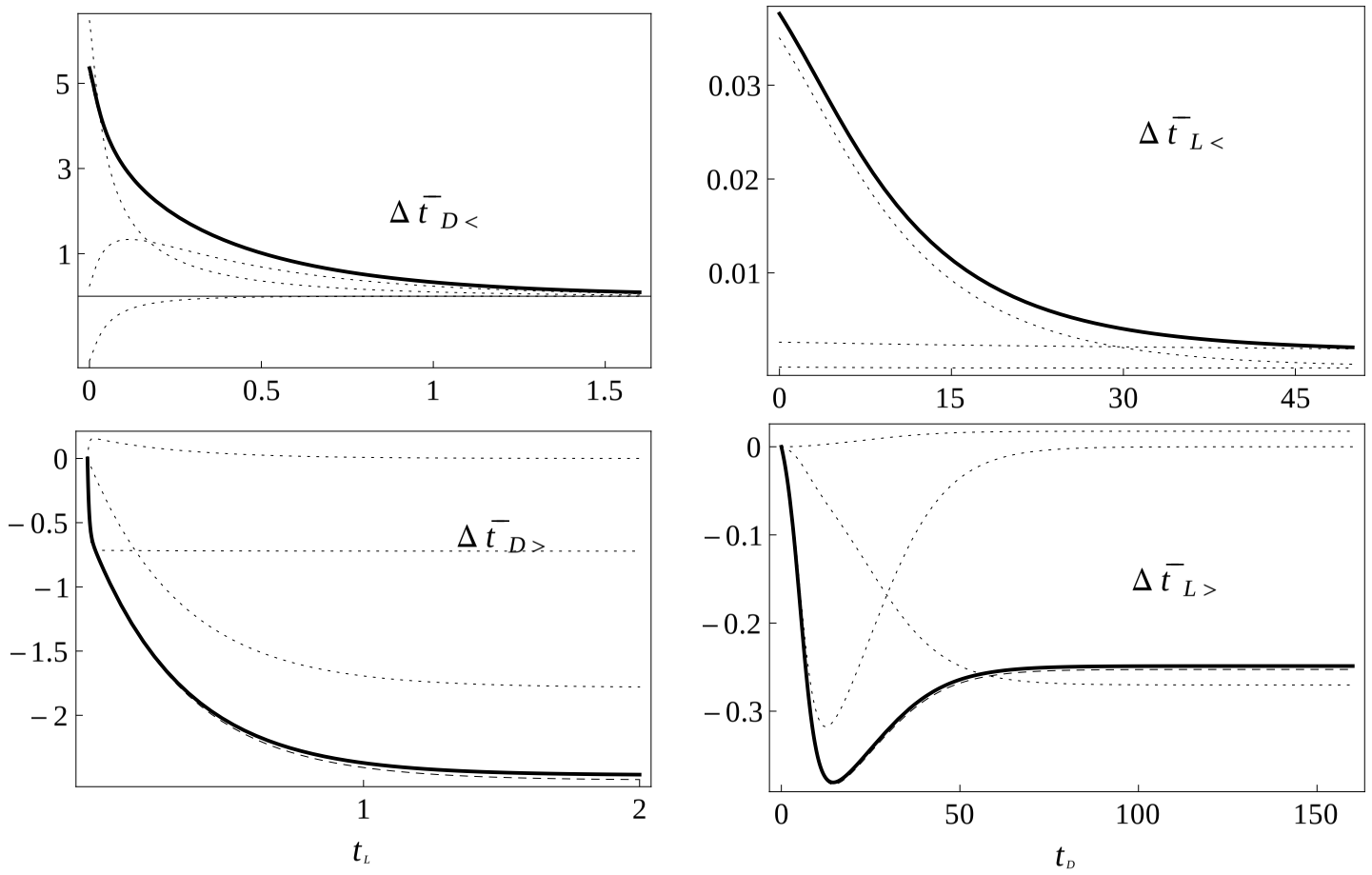

Figure 3.14: Constrained mean dwell times for a system with three substates. The exact value for each constrained mean is shown by a solid line. The approximated constrained mean, calculated according expressions of the form of Eq. (3.61) are dashed. Dotted plots correspond to the different functions h_{ij}. Parameters for this model are $k_{D_1} = 1/2$, $k_{D_2} = 1/200$, $k_{D_3} = 1/10$, $k_{L_1} = 2$, $k_{L_2} = 5$, $k_{L_3} = 200$, $d_{12} = d_{21} = l_{12} = l_{23} = l_{32} = d_{23} = 1/10000$, $l_{21} = 1/2500000$ and $d_{32} = 1/20000$. Time unit is $(2k_{D_1})^{-1}$.

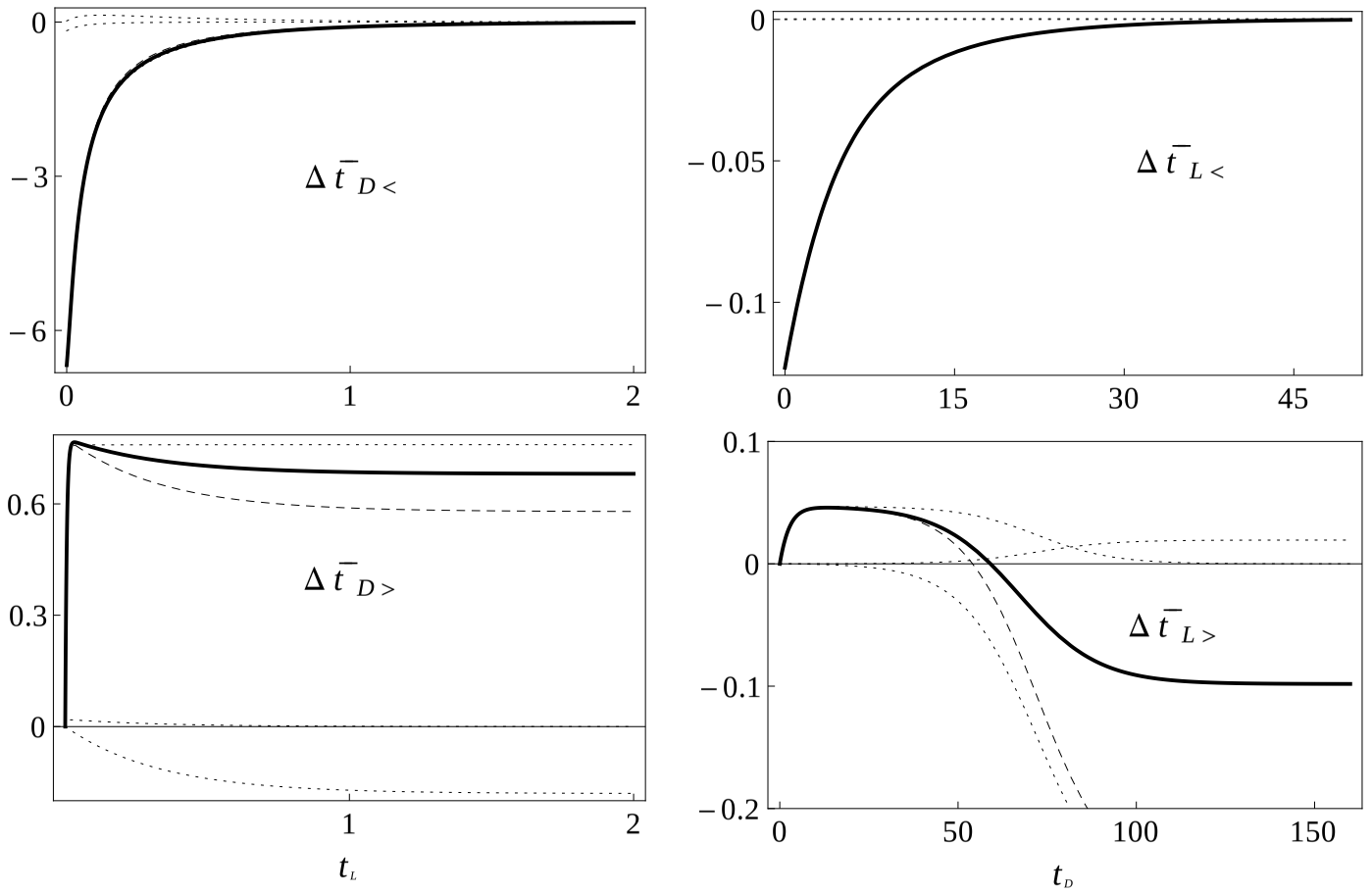

Figure 3.15: Constrained mean dwell times for a system with three substates. The exact value for each constrained mean is shown by a solid line. The approximated constrained mean, calculated according expressions of the form of Eq. (3.61) are dashed. Dotted plots correspond to the different functions h_{ij}. Parameters for this model are $k_{D_1} = 1/2$, $k_{D_2} = 1/200$, $k_{D_3} = 1/10$, $k_{L_1} = 200$, $k_{L_2} = 5$, $k_{L_3} = 2$, $d_{12} = d_{21} = l_{12} = l_{23} = l_{32} = d_{23} = 1/10000$, $l_{21} = 1/2500000$ and $d_{32} = 1/200$. Time unit is $(2k_{D_1})^{-1}$.

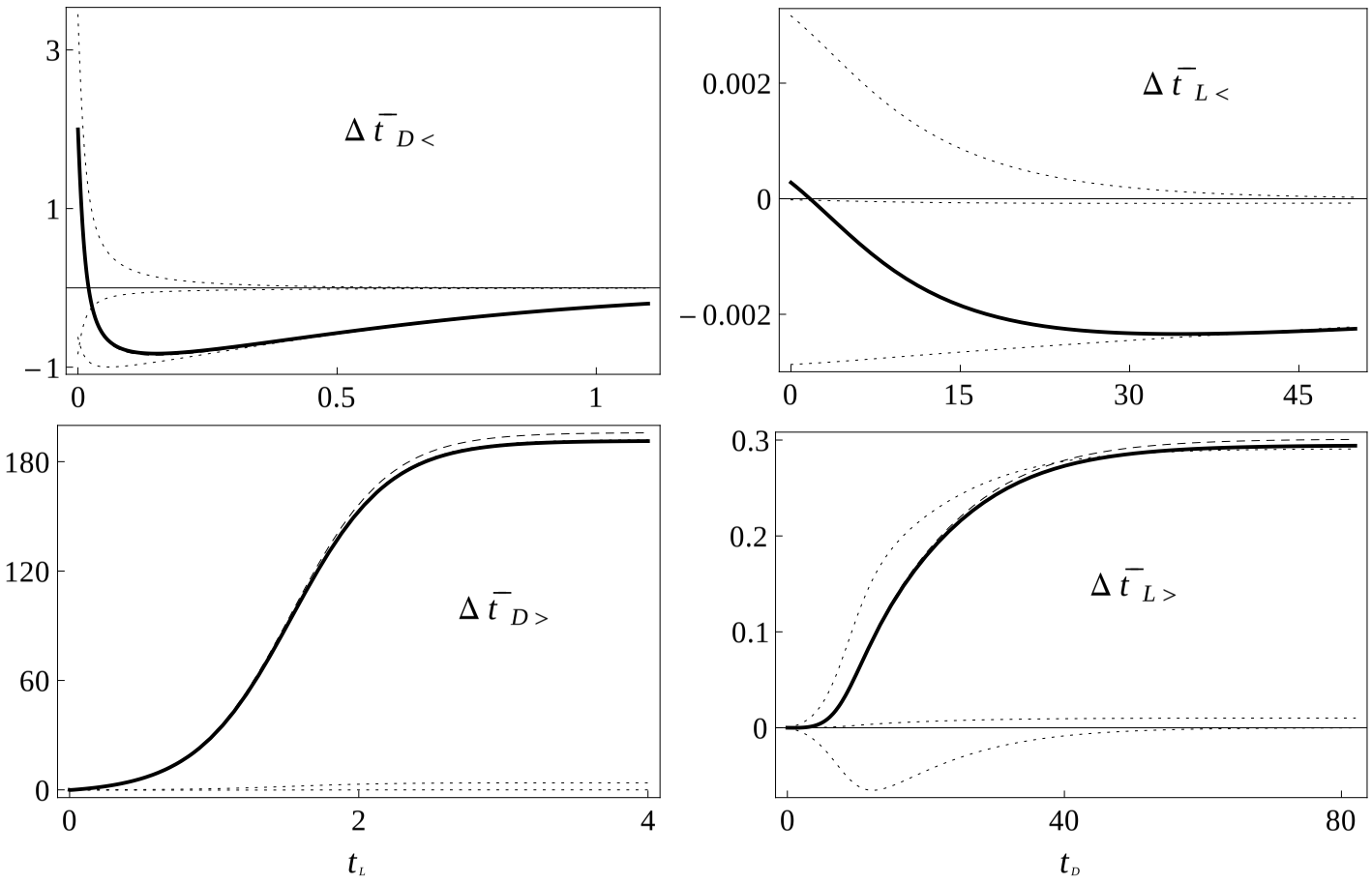

Figure 3.16: Constrained mean dwell times for a system with three substates. The exact value for each constrained mean is shown by a solid line. The approximated constrained mean, calculated according expressions of the form of Eq. (3.61) are dashed. Dotted plots correspond to the different functions h_{ij}. Parameters for this model are $k_{D_1} = 1/200$, $k_{D_2} = 1/2$, $k_{D_3} = 1/10$, $k_{L_1} = 2$, $k_{L_2} = 5$, $k_{L_3} = 200$, $d_{12} = d_{21} = l_{12} = l_{23} = l_{32} = d_{23} = 1/10000$, $l_{21} = 1/25000$ and $d_{32} = 1/2000000$. Time unit is $(2k_{D_2})^{-1}$.

only induces a qualitative change in the form of $\Delta\bar{t}_{L>}$.

A further permutation in the set of reaction rate constants is done in Fig. 3.15, namely, the values of k_{L_1} and k_{L_3} in the model of Fig. 3.14 are interchanged by each other. We now see a dramatic change in the qualitative behavior of this functions. In contrast to the situation in Fig. 3.14, we have that $(k_{D_2} - k_{D_3})(k_{L_3} - k_{L_2}) > 0$ and all other products are negative. As a consequence, the sign of $\Delta\bar{t}_{D<}, \Delta\bar{t}_{L<}$ and $\Delta\bar{t}_{D>}$ has changed. Even more striking is the form of $\Delta\bar{t}_{L>}$ which has now a positive value for short t_D and a negative value when t_D is big. This characteristic is only found in three-channel models or bigger and is not observed in two-channel ones. We can also see larger deviations from the static limit prediction for this model as the internal rate constant d_{32} has become of the same order of magnitude of k_{D_2}. In Fig. 3.16 we show that the nonmonotic behavior observed in Figs. 3.12-3.15 for the constrained means $\Delta\bar{t}_{D>}$ and $\Delta\bar{t}_{L>}$ can also be found in the complementary constrained means, $\Delta\bar{t}_{D<}$ and $\Delta\bar{t}_{L<}$, for certain models.

As stated above, Eq. (3.61) can be demonstrated by using our knowledge of the spectral properties of the turnover matrix. Details can be found in the Appendix B.6 and we only sketch the main steps here. First, we write the identity matrix in term of the eigenvectors of M_D as follows

$$I = \sum_{i=1}^{3} |R_i^D\rangle\langle L_i^D|. \tag{3.67}$$

Then, we insert this form of the identity matrix in $f_{LD}(t_L, t_D)$ defined in Eq. (2.4), and rearrange terms until we find the following expression

$$f_{LD}(t_L, t_D) - f(t_L)f(t_D) = k_{LD}^1(t_L, t_D) + k_{LD}^2(t_L, t_D), \tag{3.68}$$

where

$$k^i_{LD}(t_L, t_D) = \frac{1}{\langle 1|\mathsf{K}_D|\rho_D\rangle}\langle 1|\mathsf{K}_D e^{-(\mathsf{K}_D+\Gamma_D)t_D}|R^D_i\rangle\langle L^D_i|\mathsf{K}_L e^{-(\mathsf{K}_L+\Gamma_D)t_L}\mathsf{K}_D|\rho_D\rangle. \tag{3.69}$$

The result in Eq (3.68) can be generalized to n-channel systems. However, the main obstacle in this procedure lies on the computation of the eigenvectors for $n \times n$ turnover matrices. In this regard, the method of generating functions, introduced in Chapter 2 is better. On the other hand, the approach of this section to the description of the constrained means is appropriate for the understanding of other properties that will be described below.

First, from our definition of the joint density functions for two dwell times that are distant apart m turnovers as for example in Eq. (3.2), we can define additional constrained mean dwell times. If we denote the dark constrained mean dwell time by $\Delta\bar{t}_{D<}(T; m)$, where m is the number of turnovers separating the light and the dark dwell times, then we find for a system with two channels that

$$\Delta\bar{t}_{D<}(T; m) = \lambda^{m-1}\Delta\bar{t}_{D<}(T; 1). \tag{3.70}$$

Second, note that there is a connection between the dwell time crosscorrelation functions and the constrained mean dwell times of Chapter 2. The expression in Eq. (3.68) can be generalized for n-channel systems, and from this we obtain the general result

$$\int_0^\infty dT P(t_L < T)\Delta\bar{t}_{D<}(T) = C_{DL}(1). \tag{3.71}$$

From here, we can infer that if the difference in the constrained mean dwell time is null, crosscorrelation between the light and dark states should vanish. The opposite implication does not hold. However, we may expect that the lack of crosscorrelation between this variables is associated with systems with fast

decay in $\Delta\bar{t}_{D<}$ and low rate of desorption. In this way, it is plausible to find systems with vanishing C_{DL} and $\Delta\bar{t}_{D<} \neq 0$.

At this point, it is questionable whether the difference on the asymptotic decay rates for $\Delta\bar{t}_{L<}$ and $\Delta\bar{t}_{L>}$ can discern between an independent and a spatially correlated model, when active sites fluctuate among three substates. As we will illustrate below, in the static limit and with a significant separation in the values of the reaction rate constants, an equivalent statement about the qualitative decay rates of $\Delta\bar{t}_{L<}$ and $\Delta\bar{t}_{L>}$ that differentiates between these two scenarios exists.

Our model for a spatially correlated catalyst with N active sites is identical to that of a single active site with the same rate constants, but except for k_{D_1}, k_{D_2} and k_{D_3}, which are replaced by the renormalized constant $N \times k_{D_1}$, $N \times k_{D_2}$ and $N \times k_{D_3}$. Thus, close to the static limit, it is possible to describe $\Delta\bar{t}^{(N)}_{L<}$ and $\Delta\bar{t}^{(N)}_{L>}$ as the sum of the functions $h^{L<}_{ij}$ and $h^{L>}_{ij}$ as in Eq. (3.61) and Eq. (3.65), with the rescaled rate constants. If the k_{D_1}, k_{D_2} and k_{D_3} are pairwise significantly different, perhaps by a few orders of magnitude as in Fig. 3.13, then $\Delta\bar{t}^{(N)}_{L<}$ and $\Delta\bar{t}^{(N)}_{L>}$ may show an intricate behavior as T_D increases. However, the initial decay should be dominated by the two largest reaction rate constants. Notice that this is the case in Fig. 3.13, where $h^{L>}_{12}$ dominates for $T_D < 40$. Our claim, which follows from the asymptotic analysis of Eq. (3.62) and Eq. (3.66) is that, $\Delta\bar{t}^{(N)}_{L>}$ must decay initially to the first inflection point exponentially, with decay constant $N \times k^{mid}_D$, while $\Delta\bar{t}^{(N)}_{L<}$ must decay exponentially with decay constant $N \times k^{mid}_D$, where k^{mid}_D represents the second largest reaction rate constant. Observe that the so-called asymptotic analysis that we are considering in this case, does not correspond to the one observed at $T_D \to \infty$. Instead, we consider $\Delta\bar{t}^{(N)}_{L<}$ and $\Delta\bar{t}^{(N)}_{L>}$ as they approach a given time T_{max} that is larger that the time scales of k^{big}_D and k^{mid}_D.

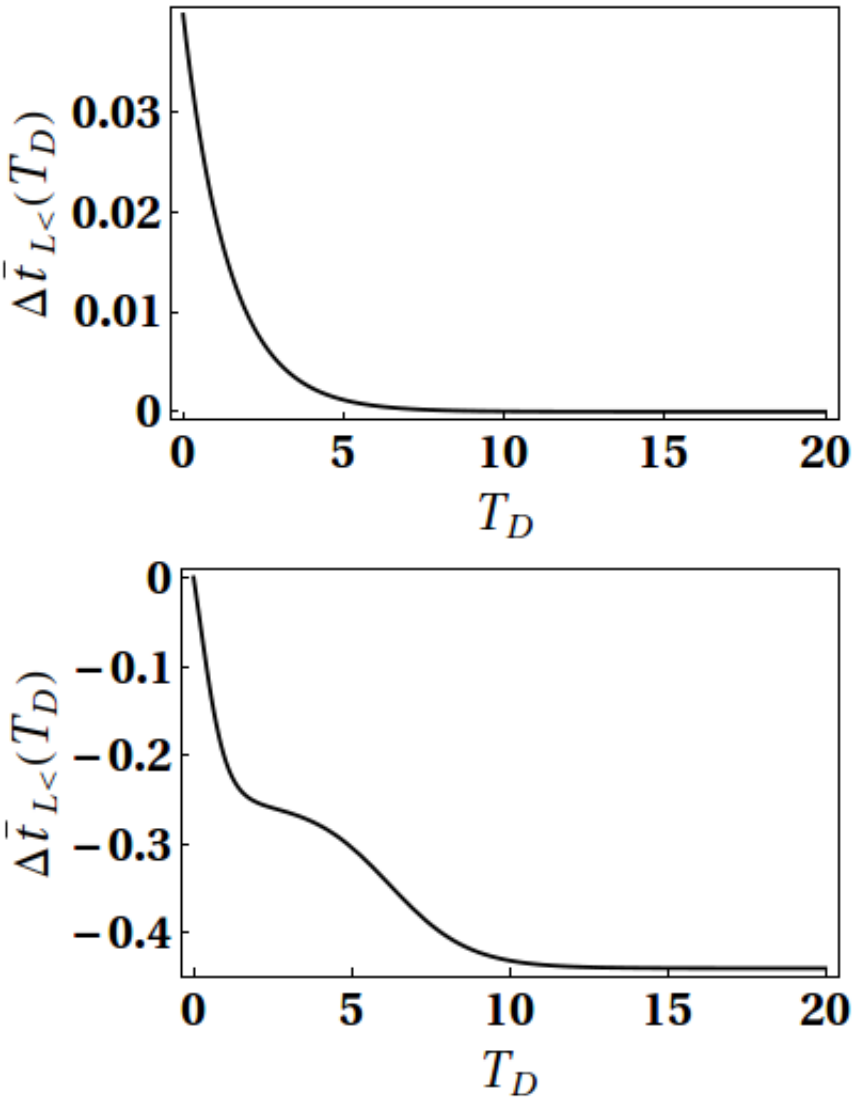

Figure 3.17: $\Delta \bar{t}_{L<}$ and $\Delta \bar{t}_{L>}$ for 8 active sites that are spatially correlated. Each active site has three substates. Parameters for this model are $k_{D_1} = 1/200$, $k_{D_2} = 1/2$, $k_{D_3} = 1/10$, $k_{L_1} = 2$, $k_{L_2} = 5$, $k_{L_3} = 200$, $d_{12} = d_{21} = l_{12} = l_{23} = l_{32} = d_{23} = 1/10000$, $l_{21} = 1/25000$ and $d_{32} = 1/2000000$

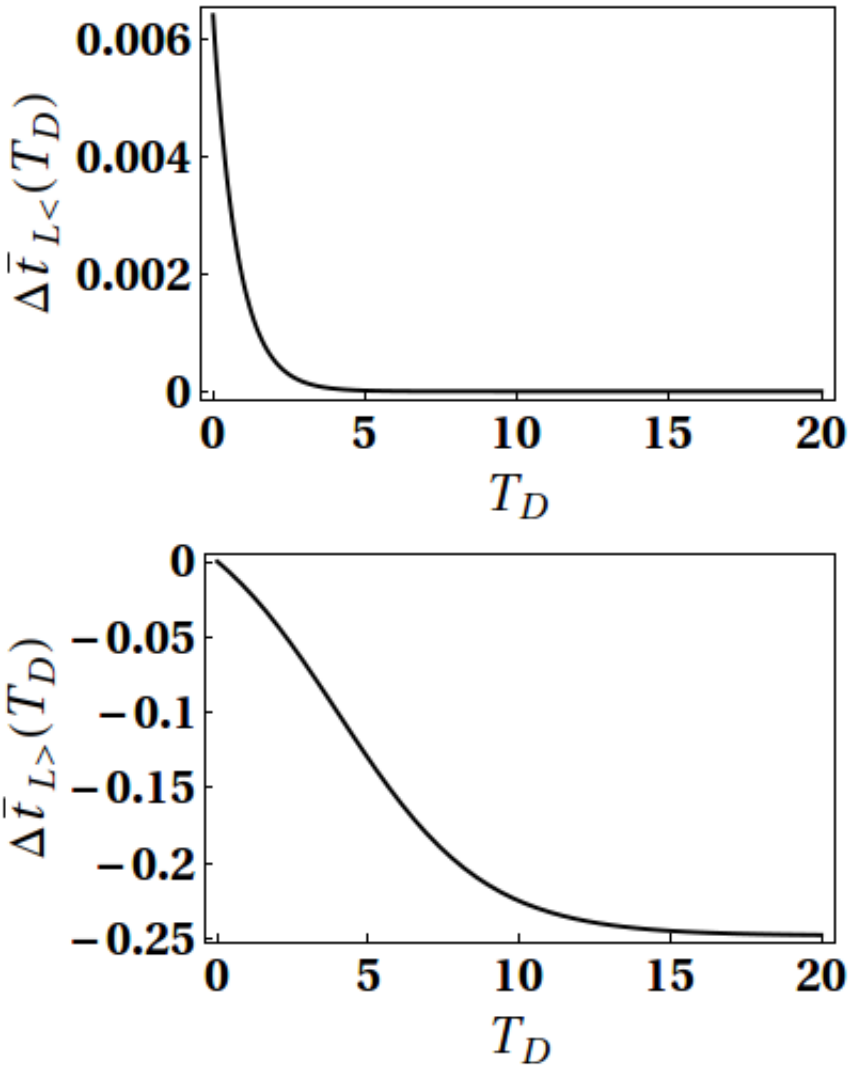

Figure 3.18: $\Delta \bar{t}_{L<}$ and $\Delta \bar{t}_{L>}$ for 8 active sites that are independent. Each active site has three substates. Parameters for this model are $k_{D_1} = 1/200$, $k_{D_2} = 1/2$, $k_{D_3} = 1/10$, $k_{L_1} = 2$, $k_{L_2} = 5$, $k_{L_3} = 200$, $d_{12} = d_{21} = l_{12} = l_{23} = l_{32} = d_{23} = 1/10000$, $l_{21} = 1/25000$ and $d_{32} = 1/2000000$

Once more, in Fig. (3.13) observe that the time scales for k_{D_1} and k_{D_2} are less than 40.

For a system with N independent active sites and three substates, the qualitative decays of the light constrained means are the same as predicted in Chapter 2, i.e. $\Delta\vec{t}^{(N)}_{L<}$ has as decay rate constant $N \times k_D^{big}$ and $\Delta\vec{t}^{(N)}_{L>}$ has as decay rate constant k_D^{big}. In brief, this statement is a consequence of the factor $E_D(t)^{N-1}$ in Eq. (2.94), that $\vec{t}_D^{(N)} \sim (k_D^{big})^{-1}$ and the result in Eq. (2.96). Numerical calculations also support the idea that $\Delta\vec{t}^{(N)}_{L<}$ and $\Delta\vec{t}^{(N)}_{L>}$ can differetiate between independent and spatially correlated models, for active sites admitting three substates. In Fig. 3.17 and Fig. 3.18 we show light constrained means for two models with 8 active sites corresponding to the spatially correlated and independent active sites. Each active site in this model is equivalent to the model in Fig 3.12 and Fig. 3.13. Amazingly, our prediction is correct even when the number of active sites is as small as 8.

3.7 Conclusion

For a catalyst with a single active site, dwell-time correlation functions can differentiate among systems with one, two or three substates. In the case of a catalyst that fluctuates between two substates, the correlation time, measured as the inverse of the decay rate, is the same for each correlation function. Besides, if dark and light dwell times are autocorrelated, they are crosscorrelated. In the presence of a third substate correlation times can be different, as correlation functions are, in this case, biexponential. Differences in the correlation times reveal the different time scales of distinct internal processes. A scenario

with autocorrelated dwell times and null crosscorrelation is only possible if the system fluctuates among three substates.

Many-active-site catalysts with correlated fluctuations exhibit larger correlation times as compared to the correlation time of a single active site. Also, when internal fluctuations are slow, the amplitude is not significantly affected by the number of active sites and, therefore, it is of the same magnitude as the amplitude for a single active site. In contrast, a catalyst with independent active sites has a lower dwell-time correlation than a single active site, and the value decays fast as the number of active sites increases.

Constrained mean dwell times for a catalyst with three internal substates also differentiate between active sites that experience correlated fluctuations and those that are independent, based on the pseudo-asymptotic behavior of $\Delta\bar{t}_{L<}$ and $\Delta\bar{t}_{L>}$.

Single-nanoparticle catalytic transformations under saturating conditions exhibit positive autocorrelation, null crosscorrelation and two different correlation times. These findings, together with our conclusions in this chapter, complement our analysis of the experimental constrained means for the same system in Chapter 2. As a consequence, we must reinterpret the experimental evidence for this system with a model that takes into account the existence of a third substate. We will undertake this discussion in Chapter 4.

APPENDIX B

APPENDICES CHAPTER 3

B.1 Properties of the turnover matrix M_D and M_L

In this section we describe some of the most relevant characteristics of the turnover matrices M_D and M_L for a single active site that has to n channels. In this case, $S_D = \mathsf{K}_D(\mathsf{K}_D+\Gamma_D)^{-1}$ and $S_L = \mathsf{K}_L(\mathsf{K}_L+\Gamma_L)^{-1}$ and we can write $M_L = S_D S_L$ and also $M_D = S_L S_D$. As long as K_D and K_L are invertible, we can conclude that M_L and M_D are similar matrices, with the following possible similarity transformations

$$M_L = S_D M_D S_D^{-1} = S_L^{-1} M_D S_L, \tag{B.1}$$

$$M_D = S_L M_L S_L^{-1} = S_D^{-1} M_L S_D. \tag{B.2}$$

This fact has as a consequence that the spectrum for these two matrices are the same, as they have the same characteristic polynomial[32]. A similar statement is not true for the eigenvector spaces. Nevertheless, the eigenvectors of M_D and M_L are related by the following transformations. Let $|R_i^D\rangle$ be such that $M_D|R_i^D\rangle = \lambda_i|R_i^D\rangle$, then

$$S_D S_L S_D|R_i^D\rangle = S_D M_D|R_i^D\rangle = \lambda_i S_D|R_i^D\rangle \tag{B.3}$$

$$= M_L S_D|R_i^D\rangle, \tag{B.4}$$

and we infer that $|R_i^L\rangle = r_i S_D|R_i^D\rangle$, for some constant r_i. This expression also leads to the identity $S_L|R_i^L\rangle = r_i\lambda_i|R_i^D\rangle$. In the same fashion we find $\langle L_i^L| = l_i\langle L_i^D|S_L$ and $\langle L_i^L|S_D = l_i\lambda_i\langle L_i^D|$.

There is a relation between r_i and l_i that arises from the conditions used in

the spectral decomposition of M_D and M_L, i.e.,

$$\langle L_i^L | R_i^L \rangle = (l_i \langle L_i^D | S_L)(r_i S_D | R_i^D \rangle) \tag{B.5}$$

$$= l_i r_i \lambda_i \langle L_i^D | R_i^D \rangle, \tag{B.6}$$

then

$$l_i r_i \lambda_i = 1, \tag{B.7}$$

since $\langle L_i^D | R_i^D \rangle = \langle L_i^L | R_i^L \rangle = 1$. Finally, these coefficients are given by the expressions $r_i = 1/\langle L_i^L | S_D | R_i^D \rangle$ and $l_i = 1/\langle L_i^D | S_L | R_i^L \rangle$.

We can say more about the spectrum of the turnover matrix. The fact that $\langle 1 | S_D = \langle 1 | S_L = \langle 1 |$ and also that every element in these matrices is nonnegative, leads immediately to the conclusion that $|\lambda| \leq 1$. In order to see that, we need to understand that the products $\langle 1 | S_D = \langle 1 | S_L = \langle 1 |$ tell us that the sum of all the elements of every column in S_D or S_L is equal to 1. Then, our statement follows from the Frobenius and Perron-Frobenius[18] theorems on nonnegative matrices that we partially present now.

Theorem 1. *Let A be a nonnegative matrix, S_i be the sum of the entries in column i of A, $s = \min_i S_i$, $S = \max_i S_i$ and let r denote the maximal characteristic root of A. Then $s \leq r \leq S$.*

Theorem 2. *[33] Let A be an n-square nonnegative indecomposable matrix. Then:*

- *A has a real positive characteristic root r (the maximal root of A) which is a simple root of the characteristic equation of A. If λ_i is any characteristic root of A, then $|\lambda_i| \leq r$.*
- *There exists a positive characteristic vector corresponding to r.*

- *If A has h characteristic roots of modulus r:* $\lambda_0 = r, \lambda_1, \ldots, \lambda_{h-1}$ *then these are the h distinct roots of* $\lambda^n - r = 0$*. The number h is called the index of imprimitivity of A.*

That S_D and S_L are nonnegative matrices is a consequence of the fact that $\mathsf{K}_D + \Gamma_D$ and $\mathsf{K}_L + \Gamma_L$ are M-matrices: the inverse matrix of an M-matrix has the property that every element in the matrix is greater or equal to zero[4, 18, 6]. Finally, since $r = 1$ for M_D and M_L, we conclude that these matrices are left-stochastic matrices[5, 6].

B.2 Derivation of the general form of C_D, C_L, C_{DL} and C_{LD} for an n-channel system

In this section we derive the forms of correlation functions for a single active site with n channels. We can rewrite Eq. (3.2) in terms of the eigenvectors of the turnover matrix by replacing either M_D or M_L by its corresponding spectral decomposition. In that way, we obtain the following expressions for the joint density functions

$$f_{DD}(t_1, t_{m+1}) = f_D(t_1) f_D(t_{m+1}) + \left(\frac{1}{\mathcal{N}}\right) \sum_i^{n-1} \lambda_i^{m-1} \langle 1|\mathsf{K}_D \mathsf{g}_\mathsf{D}(t_{m+1})\mathsf{K}_L(\mathsf{K}_L + \Gamma_L)^{-1}|R_i^L\rangle \times \langle L_i^L|\mathsf{K}_D \mathsf{g}_\mathsf{D}(t_1)\mathsf{K}_L|p_L\rangle, \quad \text{(B.8)}$$

or,

$$f_{DD}(t_1, t_{m+1}) = f_D(t_1) f_D(t_{m+1}) + \left(\frac{1}{\mathcal{N}}\right) \sum_i^{n-1} \lambda_i^{m-1} \langle 1|\mathsf{K}_D \mathsf{g}_\mathsf{D}(t_{m+1})|R_i^D\rangle \times \langle L_i^D|\mathsf{K}_L(\mathsf{K}_L + \Gamma_L)^{-1}\mathsf{K}_D \mathsf{g}_\mathsf{D}(t_1)\mathsf{K}_L|p_L\rangle, \quad \text{(B.9)}$$

where

$$\mathcal{N} = \langle 1|\mathsf{K}_D|p_D\rangle. \quad \text{(B.10)}$$

In addition,

$$f_{DL}(t_1, t_{m+1}) = f_D(t_1) f_L(t_{m+1}) + \left(\frac{1}{\mathcal{N}}\right) \sum_i^{n-1} \lambda_i^{m} \langle 1|\mathsf{K}_L \mathsf{g}_\mathsf{L}(t_{m+1})|R_i^L\rangle \langle L_i^L|\mathsf{K}_D \mathsf{g}_\mathsf{D}(t_1)\mathsf{K}_L|p_L\rangle, \quad \text{(B.11)}$$

with similar expressions for $f_{LL}(t_1, t_{m+1})$ and $f_{LD}(t_1, t_{m+1})$. The covariance for the dwell times can be calculated from these expressions after integration, taking in account that

$$Q_D \equiv \int_0^\infty t\, \mathsf{g_D}(t)dt = (\mathsf{K}_D + \Gamma_D)^{-2}. \tag{B.12}$$

This indeed leads to a further simplification of the coefficients involved in the spectral expansion of the covariance function. Explicitly,

$$\begin{aligned}\langle 1|\mathsf{K}_D Q_D \mathsf{K}_L(\mathsf{K}_L + \Gamma_L)^{-1}|R_i^L\rangle =& \langle 1|\mathsf{K}_D(\mathsf{K}_D + \Gamma_D)^{-2}\mathsf{K}_L(\mathsf{K}_L + \Gamma_L)^{-1}|R_i^L\rangle \\ =& \lambda_i \langle 1|\mathsf{K}_D(\mathsf{K}_D + \Gamma_D)^{-1}\mathsf{K}_D^{-1}|R_i^L\rangle \\ =& \lambda_i \langle 1|\mathsf{K}_D^{-1}|R_i^L\rangle\end{aligned}$$

also,

$$\begin{aligned}\langle L_i^L|\mathsf{K}_D Q_D \mathsf{K}_L|p_L\rangle =& \langle L_i^L|\mathsf{K}_D(\mathsf{K}_D + \Gamma_D)^{-2}\mathsf{K}_L|p_L\rangle \\ =& \langle L_i^L|\mathsf{K}_D(\mathsf{K}_D + \Gamma_D)^{-1}|p_D\rangle \\ =& l_i\lambda_i\langle L_i^D|p_D\rangle,\end{aligned}$$

$$\begin{aligned}\langle 1|\mathsf{K}_L T_L|R_i^L\rangle =& \langle 1|(\mathsf{K}_L + \Gamma_L)^{-1}|R_i^L\rangle \\ =& r_i\lambda_i\langle 1|\mathsf{K}_L^{-1}|R_i^D\rangle,\end{aligned}$$

$$\begin{aligned}\langle L_i^D|\mathsf{K}_L(\mathsf{K}_L + \Gamma_L)^{-1}\mathsf{K}_D Q_D \mathsf{K}_L|p_L\rangle =& \langle L_i^D|\mathsf{K}_L(\mathsf{K}_L + \Gamma_L)^{-1}\mathsf{K}_D(\mathsf{K}_D + \Gamma_D)^{-2}\mathsf{K}_L|p_L\rangle \\ =& \lambda_i\langle L_i^D|(\mathsf{K}_D + \Gamma_D)^{-1}\mathsf{K}_L|p_L\rangle \\ =& \lambda_i\langle L_i^D|p_D\rangle.\end{aligned}$$

Then,

$$\overline{t_1\, t_{m+1}}_{DD} - \bar{t}_D^2 = \left(\frac{1}{\mathcal{N}}\right)\sum_{i=1}^{n-1} l_i\lambda_i^m\langle 1|\mathsf{K}_D^{-1}|R_i^L\rangle\langle L_i^D|p_D\rangle \tag{B.13}$$

also,

$$\overline{t_1\, t_{m+1}}_{LL} - \bar{t}_L^2 = \left(\frac{1}{\mathcal{N}}\right)\sum_{i=1}^{n-1} r_i \lambda_i^m \langle 1|\mathsf{K}_L^{-1}|R_i^D\rangle\langle L_i^L|p_L\rangle \tag{B.14}$$

$$\overline{t_1\, t_{m+1}}_{DL} - \bar{t}_D\bar{t}_L = \left(\frac{1}{\mathcal{N}}\right)\sum_{i=1}^{n-1} \lambda_i^m \langle 1|\mathsf{K}_L^{-1}|R_i^D\rangle\langle L_i^D|p_D\rangle \tag{B.15}$$

$$\overline{t_1\, t_{m+1}}_{LD} - \bar{t}_L\,\bar{t}_D = \left(\frac{1}{\mathcal{N}}\right)\sum_{i=1}^{n-1} \lambda_i^m \langle 1|\mathsf{K}_D^{-1}|R_i^L\rangle\langle L_i^L|p_L\rangle \tag{B.16}$$

On the other hand,

$$\bar{t}_D = \frac{1}{\mathcal{N}}\langle 1|\mathsf{K}_D Q_D \mathsf{K}_L|p_L\rangle = \frac{1}{\mathcal{N}}\langle 1|p_D\rangle \tag{B.17}$$

$$\begin{aligned}\overline{t^2}_D &= \frac{2}{\mathcal{N}}\langle 1|\mathsf{K}_D(\mathsf{K}_D+\Gamma_D)^{-3}\mathsf{K}_L|p_L\rangle \\ &= \frac{2}{\mathcal{N}}\langle 1|(\mathsf{K}_D+\Gamma_D)^{-1}|p_D\rangle.\end{aligned} \tag{B.18}$$

The variance $\sigma_D^2(t)$ for the dwell time in the dark state is then given by $\overline{t^2}_D - \bar{t}_D^2$. Therefore, we can write the correlation function as

$$C_D(m) = \frac{\sum_{i=1}^{n-1} l_i \lambda_i^{m+1}\langle 1|\mathsf{K}_D^{-1}|R_i^L\rangle\langle L_i^D|p_D\rangle}{\mathcal{N}\sigma_D^2}, \tag{B.19}$$

for all $m \geq 1$. Also, the cross correlation function is given by

$$C_{DL}(m) = \frac{\sum_{i=1}^{n-1} \lambda_i^{m+1}\langle 1|\mathsf{K}_L^{-1}|R_i^D\rangle\langle L_i^D|p_D\rangle}{\mathcal{N}(\sigma_D^2\,\sigma_L^2)^{1/2}}. \tag{B.20}$$

From (B.13)-(B.16), we can conclude that all possible different behaviors of this set of functions can be determined by studying the set of zeros of the functions $\langle 1|\mathsf{K}_D|R_i^L\rangle, \langle 1|\mathsf{K}_L|R_i^D\rangle, \langle L_i^D|p_D\rangle, \langle L_i^L|p_L\rangle$, for every i. We refer to these as the *coefficients of the correlation functions*. In general, $|R_i^\times\rangle$ and $\langle L_i^\times|$, where $\times = D, L$, are vectors of rational functions of all the rate constants of the kinetic scheme, with the important property that they are orthogonal to the vectors $\langle 1|$ and $K_{\square *}|p_*\rangle$, respectively and with $\square = L$ if $\times = D$ and $\square = D$ if $\times = L$.

B.3 Correlation functions for the two-channel model

In this section we derive some of our results in Sec. 3.3.1 for a single active site with two channels. We start by noticing that there is only one eigenvalue λ different to 1 and therefore

$$C_D(m) = \frac{l\lambda^{m+1}\langle 1|\mathsf{K}_D^{-1}|R^L\rangle\langle L^D|\rho_D\rangle}{\mathcal{N}\sigma_D^2}, \tag{B.21}$$

and also,

$$C_{DL}(m) = \frac{\lambda^{m+1}\langle 1|\mathsf{K}_L^{-1}|R^D\rangle\langle L^D|p_D\rangle}{\mathcal{N}(\sigma_D^2\,\sigma_L^2)^{1/2}}. \tag{B.22}$$

Since $\langle 1| = (1,1)$ and $\langle 1|R^D\rangle = \langle 1|R^L\rangle = 0$, then we can choose $|R_D\rangle$ and $|R_L\rangle$ proportional to the vector $(1,-1)^T$, leading to the expression

$$\langle 1|\mathsf{K}_D^{-1}|R^L\rangle = C\left(\frac{1}{k_{D_1}} - \frac{1}{k_{D_2}}\right). \tag{B.23}$$

This shows that $C_{LD}(m)$ and $C_D(m)$ vanish for all m in the case $k_{D_1} = k_{D_2}$, but the same is not necessarily true for $C_{DL}(m)$ and $C_L(m)$.

Moreover, $\langle L^D|\mathsf{K}_L|p_L\rangle = 0$ and we can take $\langle L^D| = C'(k_{L_2}\rho_{L_2}, -k_{L_1}\rho_{L_1})$ for some nonzero constant C'. In fact, we can set $C = 1$ and $C' = 1/\mathcal{N}$ since

$$(k_{L_2}\rho_{L_2}, -k_{L_1}\rho_{L_1}).(1,-1)^T = \mathcal{N},$$

leading in this way to the following expression

$$\langle L^D|p_D\rangle = \frac{1}{\mathcal{N}}(k_{L_2}\rho_{L_2}\rho_{D_1} - k_{L_1}\rho_{L_1}\rho_{D_2}).$$

From the above, we can establish a rule for the qualitative dependence of $\langle L^D|p_D\rangle$ on its parameters. If the ratio $(k_{L_2}\rho_{L_2}\rho_{D_1})/(k_{L_1}\rho_{L_1}\rho_{D_2})$ is greater than, equal to or less than 1, then the coefficient $\langle L^D|p_D\rangle$ is greater than, equal to or less than 0, respectively.

Similar rules are expected for $\langle L^L|p_L\rangle$ and $\langle 1|\mathsf{K}_L^{-1}|R^D\rangle$.

B.4 Models with different substates: nonsymmetric kinetic schemes

In this section we investigate models with a different number of internal states in two possible states, dark and light, and we show that the simplest model with correlation has two substates per state.

A system with a kinetic model such as

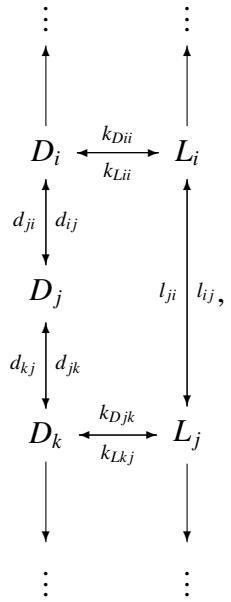

will be denominated as an (n_D, n_L)-channel reaction model, whenever the dark state has n_D different substates and the light state has n_L. Let $|p_D(t)\rangle$ be the probability vector of dimension n_D for the set of all possible conformations for the dark state, and $|p_L(t)\rangle$ be the probability vector of dimension n_L for the light state. Then, the dynamics of the system is given by the set of differential equations,

$$\begin{pmatrix} |\dot{p}_D(t)\rangle \\ |\dot{p}_L(t)\rangle \end{pmatrix} = \begin{pmatrix} \mathsf{K}_D + \Gamma_D & -Z_{DL}\mathsf{K}_L \\ -Z_{DL}\mathsf{K}_L & \mathsf{K}_L + \Gamma_L \end{pmatrix} \begin{pmatrix} |p_D(t)\rangle \\ |p_L(t)\rangle \end{pmatrix} \tag{B.24}$$

where the matrices Z_{DL} and Z_{LD} are the transition matrices that describe the way the different light substates transform into the different dark substates. For a symmetric model, Z_{DL} and Z_{LD} are the identity matrix.

Under equilibrium conditions we have

$$(\mathsf{K}_D + \Gamma_D)|p_D^{eq}\rangle = Z_{DL}\mathsf{K}_L|p_L^{eq}\rangle \qquad \text{and} \tag{B.25}$$

$$(\mathsf{K}_L + \Gamma_L)|p_L^{eq}\rangle = Z_{LD}\mathsf{K}_D|p_D^{eq}\rangle, \tag{B.26}$$

from which we can infer that

$$\mathsf{K}_D|p_D^{eq}\rangle = \mathsf{K}_D(\mathsf{K}_D + \Gamma_D)^{-1}Z_{DL}\mathsf{K}_L(\mathsf{K}_L + \Gamma_L)^{-1}Z_{LD}\,\mathsf{K}_D|p_D^{eq}\rangle, \tag{B.27}$$

$$\mathsf{K}_L|p_L^{eq}\rangle = \mathsf{K}_L(\mathsf{K}_L + \Gamma_L)^{-1}Z_{LD}\mathsf{K}_D(\mathsf{K}_D + \Gamma_D)^{-1}Z_{DL}\,\mathsf{K}_L|p_L^{eq}\rangle. \tag{B.28}$$

It is useful to define

$$M_D = \mathsf{K}_D(\mathsf{K}_D + \Gamma_D)^{-1}Z_{DL}\mathsf{K}_L(\mathsf{K}_L + \Gamma_L)^{-1}Z_{LD} \tag{B.29}$$

and

$$M_L = \mathsf{K}_L(\mathsf{K}_L + \Gamma_L)^{-1}Z_{LD}\mathsf{K}_D(\mathsf{K}_D + \Gamma_D)^{-1}Z_{DL}. \tag{B.30}$$

We also adopt the notation $|1_r\rangle$ for the column vector of length r all of whose entries are 1. Note that $\langle 1_{n_D}|\Gamma_D = \langle 0_{n_D}|$ and $\langle 1_{n_L}|\Gamma_L = \langle 0_{n_L}|$. In addition, the matrices Z_{DL} and Z_{LD} are completely determined by the kinetic model that is assumed. This comes from the fact that Z_{DL} and Z_{LD} reflect the connectivity that different substates have by means of direct reactions. Hence, If $D_i \to L_k$ is a valid transformation in the kinetic model, then the entry in the kth row and ith column of the matrix Z_{LD} is one. If it happens that D_i can transform into multiple light substates (say k of them) with a subdiagram

$$D_i \begin{array}{c} \nearrow \\ \vdots \\ \searrow \end{array} \begin{array}{c} L_{j_1} \\ \vdots \\ L_{j_k} \end{array}, \tag{B.31}$$

then the entry at the j_sth row and ith column of Z_{LD} is given by the fraction

$$\frac{k_{Dj_s\,i}}{\sum_{r=1}^{k} k_{Dj_r\,i}}, \tag{B.32}$$

for every $s = 1, \ldots, k$. Any other entry in that matrix must be zero.

The above shows that the equalities $\langle 1_{n_D}|Z_{DL} = \langle 1_{n_L}|$, $\langle 1_{n_L}|Z_{LD} = \langle 1_{n_D}|$, $\langle 1_{n_D}|M_D = \langle 1_{n_D}|$ and $\langle 1_{n_L}|M_L = \langle 1_{n_L}|$ hold.

Before studying some specific systems, let us explore how the definitions of the density function and the correlation function are extended. Let $f_D(t)$ be the density function given by

$$f_D(t) = \langle 1_{n_D}|\mathsf{K}_D|p_D(t)\rangle = \langle 1_{n_D}|\mathsf{K}_D\mathsf{g}_\mathsf{D}(t)|p_D(0)\rangle \tag{B.33}$$

$$= \frac{1}{\mathcal{N}}\langle 1_{n_D}|\mathsf{K}_D\mathsf{g}_\mathsf{D}(t)Z_{DL}\mathsf{K}_L|p_L^{eq}\rangle, \tag{B.34}$$

where we have assumed that $|p_D(0)\rangle = \frac{1}{\mathcal{N}} Z_{DL}\mathsf{K}_L|p_L^{eq}\rangle$ and $\mathcal{N} = \langle 1_{n_L}|\mathsf{K}_L|p_L^{eq}\rangle$. Also, observe that $\mathcal{N} = \langle 1_{n_D}|\mathsf{K}_D|p_D^{eq}\rangle$. Note that $f_D(t)$ integrates to 1 thanks to equation (B.28). In contrast, the joint density function for the first and $m+1$ dwell times

$$f_{DD}(t_1, t_{m+1}) = \langle 1_{n_D}|\mathsf{K}_D\mathsf{g}_\mathsf{D}(t_m)Z_{DL}\mathsf{K}_L(\mathsf{K}_L + \Gamma_L)^{-1}Z_{LD}M_D^{m-1}\mathsf{K}_D\mathsf{g}_\mathsf{D}(t_1)\frac{\mathsf{K}_L|p_L^e q\rangle}{\mathcal{N}}. \tag{B.35}$$

Similar expressions to Eq. (B.34) and Eq. (B.35) for the light state can be derived. Besides, for the special case of the joint density function for times in different states we have

$$f_{DL}(t_1, t_{m+1}) = \langle 1_{n_L}|\mathsf{K}_L\mathsf{g}_\mathsf{L}(t_m)Z_{LD}M_D^{m-1}\mathsf{K}_D\mathsf{g}_\mathsf{D}(t_1)\frac{\mathsf{K}_L|p_L^{eq}\rangle}{\mathcal{N}}, \tag{B.36}$$

$$f_{LD}(t_1, t_{m+1}) = \langle 1_{n_D}|\mathsf{K}_D\mathsf{g}_\mathsf{D}(t_m)Z_{DL}M_L^{m-1}\mathsf{K}_L\mathsf{g}_\mathsf{L}(t_1)\frac{\mathsf{K}_D|p_D^{eq}\rangle}{\mathcal{N}}, \tag{B.37}$$

from which we could calculate the crosscorrelation of a system.

We now consider some specific small kinetic models. First, for a model with two dark substates and one light substate such as

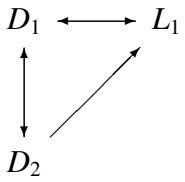

(B.38)

we have

$$\mathsf{K}_D = \begin{pmatrix} k_{D12} & 0 \\ 0 & k_{D11} \end{pmatrix} \qquad \Gamma_D = \begin{pmatrix} d_{21} & -d_{12} \\ -d_{21} & d_{12} \end{pmatrix} \tag{B.39}$$

$$\mathsf{K}_L = (k_{L11}) \qquad \Gamma_L = 0 \tag{B.40}$$

$$Z_{DL} = \begin{pmatrix} 1 \\ 0 \end{pmatrix} \qquad Z_{LD} = \begin{pmatrix} 1 & 1 \end{pmatrix} = \langle 1_2| \tag{B.41}$$

Since $\langle 1_2|Z_{DL} = 1$ then we have $\langle 1_2|M_D = \langle 1_2|$. In fact, for this case $M_D = \mathsf{K}_D(\mathsf{K}_D + \Gamma_D)^{-1}Z_{DL}\langle 1_2|$ and so $\det(M_D) = 0$ ($\det(Z_{DL}\langle 1_2|) = 0$). Finally, this implies that $f_{DD}(t_1, t_m) = f_D(t_m)f_D(t_1)$. Besides, $M_L = \langle 1_2|Z_{DL} = 1$ and so we can also conclude that the dwell times are uncorrelated.

We now consider the system,

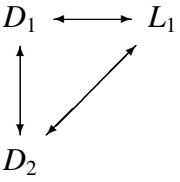

. (B.42)

The dynamical description of this system differs only in the elements

$$\mathsf{K}_L = k_{L11} + k_{L21} \qquad Z_{DL} = \begin{pmatrix} \frac{k_{L11}}{k_{L11}+k_{L21}} \\ \frac{k_{L21}}{k_{L11}+k_{L21}} \end{pmatrix} \tag{B.43}$$

As before, it can be verified that $\det(M_L) = 1$ and $\det(M_D) = 0$. We conclude in both cases that $\lambda = 0$ and therefore they have zero dwell-time correlation.

Next, we should proceed to study models with two substates in both, the dark and the light state. These are (2,2)-system. First, consider the following

kinetic models

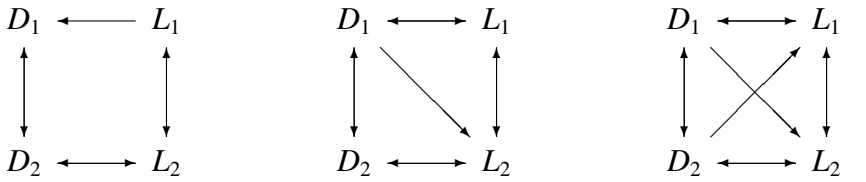

(i) (ii) (iii)

For the kinetic model (i), we can see that

$$\mathsf{K}_D = \begin{pmatrix} 0 & 0 \\ 0 & k_{D22} \end{pmatrix}, \tag{B.44}$$

which implies that $\det(M_D) = \det(M_L) = 0$, since $Z_{DL} = Z_{LD} = I$. Note that this result show us that making $k_{D11} = 0$ breaks the correlation properties observed in a two-channel system.

The kinetic model number (ii) shows additional features. First of all, note that in that case

$$Z_{DL} = \begin{pmatrix} \frac{k_{D11}}{k_{D11}+k_{D21}} & 0 \\ \frac{k_{D21}}{k_{D11}+k_{D21}} & 1 \end{pmatrix}, \qquad Z_{LD} = I. \tag{B.45}$$

The correlation properties for this system are given by the eigenvalue

$$\lambda = \det(M_D) = \left(\frac{k_{D11}}{k_{D11}+k_{D21}}\right) \frac{\det(\mathsf{K}_D)}{\det(\mathsf{K}_D+\Gamma_D)} \frac{\det(\mathsf{K}_L)}{\det(\mathsf{K}_L+\Gamma_L)}. \tag{B.46}$$

Due to the properties of the determinant, it can be shown that $\det(M_D) = \det(M_L)$, meaning that the correlation has the same behavior for both states D and L.

In the case of the kinetic model number (iii)

$$Z_{LD} = \begin{pmatrix} \frac{k_{D11}}{k_{D11}+k_{D21}} & \frac{k_{D12}}{k_{D12}+k_{D22}} \\ \frac{k_{D21}}{k_{D11}+k_{D21}} & \frac{k_{D22}}{k_{D12}+k_{D22}} \end{pmatrix}, \tag{B.47}$$

which leads to a similar expression for the eigenvalue with the factor given by $\det(Z_{LD})$. In the same way as in model (ii), both autocorrelation functions are

given by the same eigenvalue. This is a consequence of the stronger fact that $\det(M_D) = \det(M_L)$ for every (n, n)-system.

B.5 A three-channel system without crosscorrelation

In this section we analyze the three-channel model, with a single active site, introduced in Sec. 3.4.1. We present the line of arguments that led to the choice of the set of rate parameters used in this example.

For the three-channel system described in Sec. 3.4.1, two nontrivial eigenvalues λ_1 and λ_2 and eight different correlation coefficients are possible. We want to understand how these coefficients depend on the whole set of rate constants. Thus, we consider first the orthogonality relations $\langle 1|R_1^D\rangle = \langle 1|R_2^D\rangle = 0$. Then, by setting $|e_1\rangle = (1,-1,0)^T$ and $|e_2\rangle = (1,1,-2)^T$ we can write

$$|R_1^D\rangle = c_{11}^D|e_1\rangle + c_{12}^D|e_2\rangle \tag{B.48}$$

$$|R_2^D\rangle = c_{21}^D|e_1\rangle + c_{22}^D|e_2\rangle \tag{B.49}$$

since the set $\{|1\rangle, |e_1\rangle, |e_2\rangle\}$ is an orthogonal basis for $\mathbb{R}^3$. Similar expressions are expected for $|R_i^L\rangle$. Also, considering $\langle L_1^D|\mathsf{K}_L|p_L\rangle = \langle L_2^D|\mathsf{K}_L|p_L\rangle = 0$ and setting

$$\langle f_1^D| = (k_{L_2}\rho_{L_2}, -k_{L_1}\rho_{L_1}, 0), \tag{B.50}$$

$$\langle f_2^D| = (k_{L_3}\rho_{L_3}\,k_{L_1}\rho_{L_1}\ ,\ k_{L_3}\rho_{L_3}\,k_{L_2}\rho_{L_2}\ ,\ -k_{L_1}^2\rho_{L_1}^2 - k_{L_2}^2\rho_{L_2}^2), \tag{B.51}$$

$$\langle f_1^L| = (k_{D_2}\rho_{D_2}, -k_{D_1}\rho_{D_1}, 0), \tag{B.52}$$

$$\langle f_2^L| = (k_{D_3}\rho_{D_3}\,k_{D_1}\rho_{D_1}\ ,\ k_{D_3}\rho_{D_3}\,k_{D_2}\rho_{D_2}\ ,\ -k_{D_1}^2\rho_{D_1}^2 - k_{D_2}^2\rho_{D_2}^2), \tag{B.53}$$

we can write

$$\langle L_1^\times| = b_{11}^\times\langle f_1^\times| + b_{12}^\times\langle f_2^\times| \tag{B.54}$$

$$\langle L_2^\times| = b_{21}^\times\langle f_1^\times| + b_{22}^\times\langle f_2^\times|. \tag{B.55}$$

for $\times = D, L$. Hence,

$$\langle 1|\mathsf{K}_L^{-1}|R_1^D\rangle = c_{11}^D\left(\frac{1}{k_{L_1}} - \frac{1}{k_{L_2}}\right) + c_{12}^D\left(\frac{1}{k_{L_1}} + \frac{1}{k_{L_2}} - \frac{2}{k_{L_3}}\right) \tag{B.56}$$

$$\begin{aligned}\langle L_1^D|p_D\rangle =& d_{11}^D\left(k_{L_2}\rho_{L_2}\rho_{D_1} - k_{L_1}\rho_{L_1}\rho_{D_1}\right) + d_{12}^D\left(k_{L_3}\rho_{L_3}k_{L_1}\rho_{L_1}\rho_{D_1}\right.\\ &\left.+k_{L_3}\rho_{L_3}k_{L_2}\rho_{L_2}\rho_{D_2} - (k_{L_1}^2\rho_{L_1}^2 + k_{L_2}^2\rho_{L_2}^2)\rho_{D3}\right)\end{aligned} \tag{B.57}$$

We are studying the 3-channel system in order to find a system with vanishing crosscorrelation functions, and autocorrelation functions with different decay in m, a behavior experimentally observed by Chen and coworkers[51] during the single nanoparticle catalytic transformation. Again, this amounts to understanding when the factors involved in the spectral decomposition of the correlation function are zero. From Eq. (B.56), we can see that $\langle 1|\mathsf{K}_L^{-1}|R_1^D\rangle = 0$ if

1. $k_{L_1} = k_{L_2} = k_{L_3}$.
2. $k_{L_1} = k_{L_2}$ and $c_{12}^D = 0$.
3. $k_{L_3}(k_{L_1} + k_{L_2}) - 2k_{L_1}k_{L_2} = 0$ and $c_{11}^D = 0$,

and from Eq. (B.57) we have that $\langle L_1^D|p_D\rangle = 0$ if any of the following set of conditions holds

1. $k_{L_2}\rho_{L_2}\rho_{D_1} - k_{L_1}\rho_{L_1}\rho_{D_1} = 0$ and
   $k_{L_3}\rho_{L_3}k_{L_1}\rho_{L_1}\rho_{D_1} + k_{L_3}\rho_{L_3}k_{L_2}\rho_{L_2}\rho_{D_2} - (k_{L_1}^2\rho_{L_1}^2 + k_{L_2}^2\rho_{L_2}^2)\rho_{D3} = 0$
2. $k_{L_2}\rho_{L_2}\rho_{D_1} - k_{L_1}\rho_{L_1}\rho_{D_2} = 0$ and $b_{12}^D = 0$.
3. $k_{L_3}\rho_{L_3}k_{L_1}\rho_{L_1}\rho_{D_1} + k_{L_3}\rho_{L_3}k_{L_2}\rho_{L_2}\rho_{D_2} - (k_{L_1}^2\rho_{L_1}^2 + k_{L_2}^2\rho_{L_2}^2)\rho_{D3} = 0$ and $b_{11}^D = 0$.

The coefficients $c_{ij}^\times$ and $b_{ij}^\times$ for $i, j \in 1, 2$ and $\times = D, L$, are not independent. In order to see this, we project the eigenvalue equation into the different eigenspaces

of the chosen basis. For example

$$M_D|R_j^D\rangle = \lambda_j|R_j\rangle$$

$$\langle e_i|M_D|R_j^D\rangle = \lambda_j\langle e_i|R_j\rangle$$

$$c_{j1}^D\langle e_i|M_D|e_1\rangle + c_{j2}^D\langle e_i|M_D|e_1\rangle = \lambda_j c_{ji}^D\langle e_i|e_i\rangle,$$

letting $a_{ij=}^e\langle e_i|M_D|e_j\rangle$ and $\mathbf{e}_i = \langle e_i|e_i\rangle$, we end with the expression

$$c_{j1}^D a_{i1+}^e c_{j2}^D a_{i2=}^e \lambda_j c_{ji}^D \mathbf{e}_i. \tag{B.58}$$

These are four equations for four coefficients that can be summarized in a matrix equation. If $j = 1$ then

$$\begin{pmatrix} \frac{a_{11}^e}{\mathbf{e}_1} & \frac{a_{12}^e}{\mathbf{e}_1} \\ \frac{a_{21}^e}{\mathbf{e}_2} & \frac{a_{22}^e}{\mathbf{e}_2} \end{pmatrix} \begin{pmatrix} c_{11}^D \\ c_{12}^D \end{pmatrix} = \lambda_1 \begin{pmatrix} c_{11}^D \\ c_{12}^D \end{pmatrix}. \tag{B.59}$$

The solutions to this eigenvalue problem can be written in terms of the constants

$$x = \frac{a_{11}^e}{\mathbf{e}_1} - \frac{a_{22}^e}{\mathbf{e}_2} \qquad\qquad y = \frac{4a_{21}^e a_{12}^e}{\mathbf{e}_1\mathbf{e}_2}$$

as follows

$$\lambda_1 = \frac{1}{2}\left(\frac{a_{11}^e}{\mathbf{e}_1} + \frac{a_{22}^e}{\mathbf{e}_2} + \sqrt{x^2+y}\right) \tag{B.60}$$

$$c_{11}^D\frac{1}{2}\left(-x + \sqrt{x^2+y}\right) = \frac{a_{12}^e}{\mathbf{e}_1}c_{12}^D \tag{B.61}$$

$$c_{11}^D\frac{a_{21}^e}{\mathbf{e}_2} = \frac{1}{2}\left(x + \sqrt{x^2+y}\right)c_{12}^D \tag{B.62}$$

$$\lambda_2 = \frac{1}{2}\left(\frac{a_{11}^e}{\mathbf{e}_1} + \frac{a_{22}^e}{\mathbf{e}_2} - \sqrt{x^2+y}\right) \tag{B.63}$$

$$\frac{c_{21}^D}{2}\left(-x - \sqrt{x^2+y}\right) = \frac{a_{12}^e}{\mathbf{e}_1}c_{22}^D \tag{B.64}$$

$$c_{21}^D\frac{a_{21}^e}{\mathbf{e}_2} = \frac{c_{22}^D}{2}\left(x - \sqrt{x^2+y}\right) \tag{B.65}$$

from which we can deduce the following rules

$$a^e_{12} = 0 \text{ and } \frac{a^e_{11}}{\mathbf{e}_1} < \frac{a^e_{22}}{\mathbf{e}_2} \Rightarrow c^D_{11} = 0 \tag{B.66}$$

$$a^e_{12} = 0 \text{ and } \frac{a^e_{11}}{\mathbf{e}_1} > \frac{a^e_{22}}{\mathbf{e}_2} \Rightarrow c^D_{21} = 0 \tag{B.67}$$

$$a^e_{21} = 0 \text{ and } \frac{a^e_{11}}{\mathbf{e}_1} < \frac{a^e_{22}}{\mathbf{e}_2} \Rightarrow c^D_{22} = 0 \tag{B.68}$$

$$a^e_{21} = 0 \text{ and } \frac{a^e_{11}}{\mathbf{e}_1} > \frac{a^e_{22}}{\mathbf{e}_2} \Rightarrow c^D_{12} = 0 \tag{B.69}$$

We conclude that the representation of M_D and M_L in the given basis sets contains all the information required to estimate the conditions under which the coefficients cancel without knowing their analytic expressions and before we actually solve the equilibrium problem. Note also that we cannot cancel simultaneously the pairs (c^D_{11}, c^D_{21}) and (c^D_{22}, c^D_{12}). Similar expressions can be obtained for M_L and also with the "f" basis set. However, we must stress that our analysis and the conclusions about the form in which rate constants determine the correlation coefficients, depends on the arbitrary choice of these basis sets. Put another way, there might be other possible sets of rate constants for a three-channel model, without crosscorrelation and exhibiting different autorrelation times, that are not anticipated by the rules we found.

B.6 A derivation of the constrained means from the turnover matrix

In this section we describe how we calculate constrained mean dwell times for a single active site with n substates from its corresponding turnover matrix M_D or M_L. This section demonstrates that the static limit is not a equivalent to a model composed of independent channels. We will also provide general forms for the constrained mean dwell times out of the static limit and, in particular, we will present the expressions of these functions for a three-channel model implemented in Sec. 3.6.

Let us consider a single reaction path or substate $D_i \rightarrow L_i$ in an n-channel system. The density function for the dwell times for the D_i state due to its transformation into L_i will be a simple Poisson process[25] with density

$$f_{D_i}(t) = k_{D_i} e^{-k_{D_i} t}. \tag{B.70}$$

General laws of probability provide a connection between the density function of individual channels and the density function for dark dwell times:

$$f_D(t) = \sum_{i=1}^{N} f_{D_i}(t) P(X_t = D_i), \tag{B.71}$$

where $P(X_t = D_i)$ is the probability that the transition happens through the ith channel at time t. In Eq. (B.71) we assume that transitions in different channels are independent, a condition that only valid in the static limit. Under these conditions, we have

$$\bar{t}_D = \sum_i \bar{t}_{D_i} P(X_t = D_i). \tag{B.72}$$

As a matter of fact, Eq. (B.71) in the static limit is equivalent to

$$f_D(t) = \sum_{i=1}^{N} k_{D_i} e^{-k_{D_i} t} \frac{k_{L_i} \rho_{L_i}}{\mathcal{N}}, \tag{B.73}$$

from which we infer that $P(X_t = D_i) = k_{L_i}\rho_{L_i}/\mathcal{N}$.

In the same fashion for two subsequent dwell times for the states L and D we have

$$f_{LD}(t_L, t_D) = \sum_i \sum_j f_{Li\,Dj}(t_{Li}, t_{Dj}) P(X_{t_L} = i \wedge X_{t_D} = j) \tag{B.74}$$

$$= \sum_i \sum_j f_{Li}(t_{Li}) f_{Dj}(t_{Dj}) P(X_{t_L} = i) P(X_{t_D} = j), \tag{B.75}$$

where $P(X_{t_L} = i \wedge X_{t_D} = j) = P(X_{t_L} = i)P(X_{t_D} = j)$ will hold if these two event are independent. Then

$$\overline{t_D t_L} = \sum_i \sum_j \bar{t}_{Li}\, \bar{t}_{Dj} P(X_{t_L} = i) P(X_{t_D} = j) \tag{B.76}$$

and as a consequence $\overline{t_D t_L} - \bar{t}_D \bar{t}_L = 0$. Similarly, this model lacks any autocorrelation. In addition, using the definition of conditional probability we have

$$f(t_D | t_L < T) = \frac{\int_0^T f_{LD}(t_L, t_D) dt_L}{\int_0^T f_b(t_L) dt_L} \tag{B.77}$$

$$= \frac{\sum_i \int_0^T f_{Li}(t_L) P(X_{t_L} = i) dt_L \;\; \sum_j f_{Dj}(t_{Dj}) P(X_{t_D} = j)}{\sum_i \int_0^T f_{Li}(t_L) P(X_{t_L} = i) dt_L} \tag{B.78}$$

$$= \sum_j f_{Dj}(t_{Dj}) P(X_{t_D} = j) \tag{B.79}$$

$$= f_D(t_D). \tag{B.80}$$

Observe that with the introduction of the conditional density function $f(t_D | t_L < T)$ one can also obtain $\bar{t}_{D<}$ as follows

$$\bar{t}_{D<}(T) = \int_0^\infty dt_D\, t_D\; f(t_D | t_L < T), \tag{B.81}$$

and therefore in the independent case we have that $\Delta\bar{t}_{D<}(T) = 0$.

Now we will show that for a two-channel system close to the static limit $P(X_{t_L} = i, X_{t_D} = j) \neq P(X_{t_L} = i)P(X_{t_D} = j)$, showing that even in this case the two channels are correlated. First, we consider the original expression for f_{LD} in Eq. (2.5) :

$$f_{LD}(t_L, t_D) = \frac{1}{\mathcal{N}}\langle 1|\mathsf{K}_D\mathsf{g}_\mathsf{D}(t_D)\mathsf{K}_L\mathsf{g}_\mathsf{L}(t_L)\mathsf{K}_D|p_D\rangle$$

Introducing the identity matrix in terms of the eigenvectors of the turnover matrix (i.e. $I = \mathsf{K}_L|p_L\rangle\mathcal{N}^{-1}\langle 1| + |R_2\rangle\langle L_2|$) we obtain

$$\begin{aligned} f_{LD}(t_L, t_D) = \frac{1}{N}\langle 1|\mathsf{K}_D\mathsf{g}_\mathsf{D}(t_D)\mathsf{K}_L|p_L\rangle\frac{1}{N}\langle 1|\mathsf{K}_L\mathsf{g}_\mathsf{L}(t_L)\mathsf{K}_D|p_D\rangle \\ + \langle 1|\mathsf{K}_D\mathsf{g}_\mathsf{D}(t_D)|R_2\rangle\langle L_2|\mathsf{K}_L\mathsf{g}_\mathsf{L}(t_L)\mathsf{K}_D|p_D\rangle \end{aligned} \tag{B.82}$$

$$\begin{aligned} f_{LD}(t_L, t_D) = f_D(t_D)f_L(t_L) \\ + \frac{k_{L1}k_{L2}}{\mathcal{N}^2}\left(k_{D1}e^{-k_{D1}t} - k_{D2}e^{-k_{D2}t}\right)\times \\ \left(\rho_{L2}e^{-k_{L1}t}k_{D1}\rho_{D1} - \rho_{L1}e^{-k_{L2}t}k_{D2}\rho_{D2}\right) \end{aligned} \tag{B.83}$$

The second term vanishes when $k_{D1} = k_{D2}$ or when $k_{L1} = k_{L2}$[1]. If any of these conditions hold, then we would have that

$$P(X_{t_D} = i \wedge X_{t_L} = j) = \frac{k_{Li}\rho_{Li}}{N}\frac{k_{Dj}\rho_{Dj}}{N} \tag{B.84}$$

$$= P(X_{t_D} = i)P(X_{t_L} = j). \tag{B.85}$$

Thus, in the absence of dynamic heterogeneity among transitions from the dark to the light state (i.e. $k_{D_1} = k_{D_2}$), the constrained and the unconstrained means are the same and dwell times are independent. Now we assume $k_{D_1} \neq k_{D_2}$ and

[1]Observe that $\rho_{D1} = c_1k_{L1}/(k_{D1} + k_{L1})$ and $\rho_{D2} = c_2k_{L2}/(k_{D2} + k_{L2})$ for some constants c_1 and c_2.

$k_{L_1} \neq k_{L_2}$. Then

$$f_{LD}(t_L, t_D) = k_{D1} e^{-k_{D1} t} k_{L1} e^{-k_{L1} t} P(X_{t_D} = 1) + k_{D2} e^{-k_{D2} t} k_{L2} e^{-k_{L2} t} P(X_{t_D} = 2). \tag{B.86}$$

From the last expression, Eq. (B.77) and Eq. (B.81) we can calculate $\bar{t}_{D<}(T)$ and also

$$\Delta\bar{t}_{D<}(T) = \left(\frac{1}{k_{D1}} - \frac{1}{k_{D2}}\right) \frac{(1 - e^{-k_{L1}T}) P_{D2} P_{L1} - (1 - e^{-k_{L2}T}) P_{D1} P_{L2}}{(1 - e^{-k_{L1}T}) P_{L1} + (1 - e^{-k_{L2}T}) P_{L2}}. \tag{B.87}$$

$$= \left(\frac{k_{D_2} - k_{D_1}}{k_{D_1} k_{D_2}}\right) \frac{P_{D2} P_{L1} (e^{-k_{L2}T} - e^{-k_{L1}T})}{(1 - e^{-k_{L1}T}) P_{L1} + (1 - e^{-k_{L2}T}) P_{L2}}. \tag{B.88}$$

Similar considerations and definitions also lead to

$$\Delta\bar{t}_{D<}(T) = \left(\frac{k_{D_1} - k_{D_2}}{k_{D_1} k_{D_2}}\right) \frac{P_{D2} P_{L1} (e^{-k_{L2}T} - e^{-k_{L1}T})}{e^{-k_{L1}T} P_{L1} + e^{-k_{L2}T} P_{L2}}. \tag{B.89}$$

In the above expressions we have introduced the notation P_{zn} for $P(X_z = n)$. Finally, the reader should notice that the same line of argument can be used to derive expressions for $\Delta\bar{t}_{L<}$ and $\Delta\bar{t}_{L>}$, in the static limit.

We now generalize the above analysis to cases that are not close to the static limit. For this, the diagonalization of $\mathsf{g_D}(t)$ and $\mathsf{g_L}(t)$ will be important together with the partition in terms of the "D" and "L" eigenspaces.

$$I_D = \sum_i |R_i^D\rangle\langle L_i^D| \qquad\qquad I_L = \sum_i |R_i^L\rangle\langle L_i^L| \tag{B.90}$$

$$M_D|R_i^D\rangle = \lambda_i |R_i^D\rangle \qquad\qquad M_L|R_i^L\rangle = \lambda_i |R_i^L\rangle \tag{B.91}$$

$$\langle L_i^D| M_D = \lambda_i \langle L_i^D| \qquad\qquad \langle L_i^L| M_L = \lambda_i \langle L_i^L| \tag{B.92}$$

also

$$U_D = \mathsf{K}_D + \Gamma_D \qquad\qquad U_L = \mathsf{K}_L + \Gamma_L \tag{B.93}$$

$$\tilde{I}_D = \sum_i |r_i^D\rangle\langle l_i^D| \qquad\qquad \tilde{I}_L = \sum_i |r_i^L\rangle\langle l_i^L| \tag{B.94}$$

$$U_D|r_i^D\rangle = \alpha_i |r_i^D\rangle \qquad\qquad U_L|r_i^L\rangle = \beta_i |r_i^L\rangle \tag{B.95}$$

$$\langle l_i^D| U_D = \alpha_i \langle l_i^D| \qquad\qquad \langle l_i^L| U_L = \beta_i \langle l_i^L| \tag{B.96}$$

The density function for the dwell times in the D state is

$$f_D(t) = \frac{1}{N}\langle 1|\mathsf{K}_D \mathsf{g}_\mathsf{D}(t)\mathsf{K}_L|p_L\rangle \tag{B.97}$$

$$= \frac{1}{N}\langle 1|\mathsf{K}_D \sum_i |r_i^D\rangle e^{-\alpha_i t}\langle l_i^D|\mathsf{K}_L|p_L\rangle \tag{B.98}$$

$$= \frac{1}{N}\langle 1|U_D \sum_i |r_i^D\rangle e^{-\alpha_i t}\langle l_i^D|\mathsf{K}_L|p_L\rangle \tag{B.99}$$

$$= \sum_i \alpha_i e^{-\alpha_i t}\frac{1}{N}\langle 1|r_i^D\rangle\langle l_i^D|\mathsf{K}_L|p_L\rangle \tag{B.100}$$

$$= \sum_i f_{\alpha i}(t)P(X_D = i) \tag{B.101}$$

where

$$f_{\alpha i}(t) = \alpha_i e^{-\alpha_i t} \tag{B.102}$$

$$P(X_D = i) = \frac{1}{N}\langle 1|r_i^D\rangle\langle l_i^D|\mathsf{K}_L|p_L\rangle \tag{B.103}$$

$$= \frac{1}{N}\alpha_i\langle 1|r_i^D\rangle\langle l_i^D|p_D\rangle \tag{B.104}$$

Note that in the static limit $\langle 1|r_i^D\rangle = 1$, $\langle l_i^D|p_D\rangle = \rho_{D_i}$ and Eq. (B.104) reduces to $k_{D_i}\rho_{D_i}/\mathcal{N} = k_{L_i}\rho_{L_i}/\mathcal{N}$.

For the joint density function $f_{LD}(t_L, t_D)$, we write the identity matrix in the in terms of the eigenvectors of the turnover matrix M_D to insert it in the joint density function as follows.

$$f_{LD}(t_L, t_D) = \frac{1}{N}\langle 1|\mathsf{K}_D \mathsf{g}_\mathsf{D}(t_D)(\sum_{k=1} |L_k^D\rangle\langle R_k^D|)\mathsf{K}_L \mathsf{g}_\mathsf{L}(t_L)\mathsf{K}_D|p_D\rangle \tag{B.105}$$

$$= f_D(t_D) f_L(t_L) + \frac{1}{N} \sum_{k=2} \langle 1 | \mathsf{K}_D \mathsf{g}_\mathsf{D}(t_D) | R_k^D \rangle \langle L_k^D | \mathsf{K}_L \mathsf{g}_\mathsf{L}(t_L) \mathsf{K}_D | p_D \rangle \tag{B.106}$$

$$= f_D(t_D) f_L(t_L) + \frac{1}{N} \sum_{k=2} \langle 1 | \mathsf{K}_D \Big(\sum_{i=1} |r_i^D\rangle e^{-\alpha_i t_D} \langle l_i^D| \Big) |R_k^D\rangle \times \langle L_k^D | \mathsf{K}_L \Big(\sum_{j=1} |r_j^L\rangle e^{-\beta_j t_L} \langle l_j^L| \Big) \mathsf{K}_D | p_D \rangle \tag{B.107}$$

Thus,

$$f_{LD}(t_L, t_D) - f_D(t_D) f_L(t_L) = \sum_{i=1} \sum_{j=1} f_{\alpha i}(t_D) f_{\beta j}(t_L) P(X_D = i | X_L = j), \tag{B.108}$$

with

$$P(X_D = i | X_L = j) = \frac{1}{N} \sum_{k=2} \langle 1 | r_i^D \rangle \langle l_i^D | R_k^D \rangle \langle L_k^D | \mathsf{K}_L | r_j^L \rangle \langle l_j^L | p_L \rangle \tag{B.109}$$

and $f_{\alpha i}(t_D)$ and $f_{\beta j}(t_L)$ given by Eq. (B.102). Now observe that

$$P(t_L < T) = \int_0^T \sum_i f_{\beta i}(t) P(X_L = i) \tag{B.110}$$

$$= \sum_i P_{\beta i}(t_L < T) P(X_L = i) \tag{B.111}$$

and

$$f_D(t_D | t_L < T) - f_D(t_D) P(t_L < T) = \sum_{i=1} \sum_{j=1} f_{\alpha i}(t_D) P_{\beta i}(t_L < T) P(X_D = i | X_L = j), \tag{B.112}$$

implying that

$$\Delta \bar{t}_{D<}(T) = \frac{\sum_{i=1} \sum_{j=1} (\alpha_i)^{-1} P_{\beta j}(t_L < T) P(X_D = i | X_L = j)}{\sum_i P_{\beta i}(t_L < T) P(X_L = i)}. \tag{B.113}$$

Eq. (B.113) is valid for any set of rate constants and also for any number of substates. For a two channel system, Eq. (B.113) is

$$\begin{aligned}\Delta\bar{t}_{D<}(T) =& \frac{1}{\alpha_1}\frac{(1-e^{-\beta_1 T})P_{D1L1}+(1-e^{-\beta_2 T})P_{D1L2}}{(1-e^{-\beta_1 T})P_{L1}+(1-e^{-\beta_2 T})P_{L2}} \\ &+\frac{1}{\alpha_2}\frac{(1-e^{-\beta_1 T})P_{D2L1}+(1-e^{-\beta_2 T})P_{D2L2}}{(1-e^{-\beta_1 T})P_{L1}+(1-e^{-\beta_2 T})P_{L2}}\end{aligned} \tag{B.114}$$

where $P_{DiLj} = P(X_D = i|X_L = j)$. Observe that $\sum_{i,j} P_{DiLj} = 0$ and also $P_{D1L1} = -P_{D2L1}$ and $P_{D2L1} = -P_{D2L1}$. In fact, for any n-channel model we have

$$\sum_{i=1}^{n} P_{DiLj} = 0 \qquad\qquad \sum_{j=1}^{n} P_{DiLj} = 0, \tag{B.115}$$

therefore,for a two-channel system

$$\Delta\bar{t}_{D<}(T) = \Big(\frac{1}{\alpha_1}-\frac{1}{\alpha_2}\Big)\frac{e^{-\beta_1 T}P_{D2L1}-e^{-\beta_2 T}P_{D1L2}}{(1-e^{-\beta_1 T})P_{L1}+(1-e^{-\beta_2 T})P_{L2}} \tag{B.116}$$

$$= \Big(\frac{\alpha_2-\alpha_1}{\alpha_1\alpha_2}\Big)\frac{P_{D1L2}(e^{-\beta_2 T}-e^{-\beta_1 T})}{(1-e^{-\beta_1 T})P_{L1}+(1-e^{-\beta_2 T})P_{L2}}. \tag{B.117}$$

Using a similar argument we can show that

$$\Delta\bar{t}_{D>}(T) = \Big(\frac{\alpha_2-\alpha_1}{\alpha_1\alpha_2}\Big)\frac{P_{D1L2}(e^{-\beta_1 T}-e^{-\beta_2 T})}{e^{-\beta_1 T}P_{L1}+e^{-\beta_2 T}P_{L2}}. \tag{B.118}$$

Eq. (B.113) can be immediately applied to the three-channel system to give the following result

$$\begin{aligned}\Delta\bar{t}_{D<}(T) =& \Big(\frac{1}{\alpha_1}-\frac{1}{\alpha_3}\Big)\frac{-e^{-\beta_1 T}P_{D1L1}-e^{-\beta_2 T}P_{D1L2}-e^{-\beta_3 T}P_{D1L3}}{1-e^{-\beta_1 T}P_{L1}-e^{-\beta_2 T}P_{L2}-e^{-\beta_3 T}P_{L3}} \\ &+\Big(\frac{1}{\alpha_2}-\frac{1}{\alpha_3}\Big)\frac{-e^{-\beta_1 T}P_{D2L1}-e^{-\beta_2 T}P_{D2L2}-e^{-\beta_3 T}P_{D2L3}}{1-e^{-\beta_1 T}P_{L1}-e^{-\beta_2 T}P_{L2}-e^{-\beta_3 T}P_{L3}}\end{aligned} \tag{B.119}$$

$$\begin{aligned}\Delta\bar{t}_{D>}(T) =& \Big(\frac{1}{\alpha_1}-\frac{1}{\alpha_3}\Big)\frac{e^{-\beta_1 T}P_{D1L1}+e^{-\beta_2 T}P_{D1L2}+e^{-\beta_3 T}P_{D1L3}}{e^{-\beta_1 T}P_{L1}+e^{-\beta_2 T}P_{L2}+e^{-\beta_3 T}P_{L3}} \\ &+\Big(\frac{1}{\alpha_2}-\frac{1}{\alpha_3}\Big)\frac{e^{-\beta_1 T}P_{D2L1}+e^{-\beta_2 T}P_{D2L2}+e^{-\beta_3 T}P_{D2L3}}{e^{-\beta_1 T}P_{L1}+e^{-\beta_2 T}P_{L2}+e^{-\beta_3 T}P_{L3}},\end{aligned} \tag{B.120}$$

which can be simplified to the forms equivalent to Eq. (3.61) only in the static limit, because in that case $P_{DiLj} = P_{DjLi}$ for $i \neq j$. On a final note, observe that in

the limit of $\Delta\bar{t}_{D<}(T)$ when $T \to 0$ for a two-channel model is

$$\lim_{T\to 0} \Delta\bar{t}_{D<}(T) = \Big(\frac{1}{\alpha_1} - \frac{1}{\alpha_2}\Big)\frac{\beta_1 P_{D1L1} + \beta_2 P_{D1L2}}{\beta_1 P_{L1} + \beta_2 P_{L2}}, \tag{B.121}$$

and for a three channel system

$$\begin{aligned}\lim_{T\to 0} \Delta\bar{t}_{D<}(T) = &\Big(\frac{1}{\alpha_1} - \frac{1}{\alpha_3}\Big)\frac{\beta_1 P_{D1L1} + \beta_2 P_{D1L2} + \beta_3 P_{D1L3}}{\beta_1 P_{L1} + \beta_2 P_{L2} + \beta_3 P_{L3}} \\ &+ \Big(\frac{1}{\alpha_2} - \frac{1}{\alpha_3}\Big)\frac{\beta_1 P_{D2L1} + \beta_2 P_{D2L2} + \beta_3 P_{D2L3}}{\beta_1 P_{L1} + \beta_2 P_{L2} + \beta_3 P_{L3}}\end{aligned} \tag{B.122}$$

CHAPTER 4

INTERPRETING SINGLE NANOPARTICLE MEASUREMENTS

We found in Chapter 2 that the catalytic transformation of resazurin to resorufin on the surface of a single nanoparticle has constrained mean dwell times that are well described by a model with many chemically-identical active sites, each one fluctuating between two substates and, spatially correlated. As a stronger finding, we determined that a system with many independent active sites fails to reproduce the qualitative differences that in the asymptotic decay rates of $\Delta\bar{t}_{L<}$ and $\Delta\bar{t}_{L>}$ are observed for nanoparticles of 6, 9.1 and 13.7 nanometer diameter. We conclude again that the correct description of these experimental systems has to include spatial correlation among active sites, as there is only one model with n-independent active sites. In the last statement, we implicitly assumed two substates per active site.

In Chapter 3, we found that two states are not enough and that a third substate is required to predict the qualitative properties observed in the dwell-time correlation functions C_D, C_L, C_{LD} and C_{DL}, for the same experimental system. We are now in a good place to discuss and analyze simultaneously dwell-time correlations and constrained mean dwell times observed during the catalytic transformation by single nanoparticles studied by Chen [51, 49, 11].

4.1 Kinetic scheme and fitted rate constants

For the fluorescence trajectory reported by Chen and coworkers in Ref. [51] measured on a single nanoparticle of 6 nanometer diameter, we have numerically determined an optimal three-channel model that qualitatively reproduces the

experimentally observed constrained means and dwell-time correlation functions. We present the predictions for these quantities for this model in Figs. 4.1 and 4.2, and we also include the experimental values for comparison. Parameters for this model are $k_{D_1} = 2.47s^{-1}$, $k_{D_2} = 0.175s^{-1}$, $k_{D_3} = 0.156s^{-1}$, $k_{L_1} = 1.43s^{-1}$, $k_{L_2} = 2.80s^{-1}$, $k_{L_3} = 0.0766s^{-1}$, $d_{21} = 0.0043s^{-1}$, $d_{12} = 1.69 \times 10^{-4}$, $l_{12} = 0.045s^{-1}$, $l_{21} = 0.042s^{-1}$, $l_{23} = 0.040s^{-1}$, $l_{32} = 0.0185$, $d_{32} = 0.00018s^{-1}$ and $d_{23} = 0.012s^{-1}$. For this model d_{21} and l_{32} were determined by the condition of detailed balance. An initial inspection of Fig. 4.1 reveals that for this trajectory $\Delta\bar{t}_{L>}$ decays much faster than $\Delta\bar{t}_{L<}$: $\Delta\bar{t}_{L<}$ numerically vanishes as $T_D \sim 16$ while $\Delta\bar{t}_{L>}$ reaches its first pseudo asymptote close to $T_D = 2$. Based on our discussion in Sec. 3.6, we must conclude that the multiple active sites located on the surface on the 6nm nanoparticle are spatially correlated and they can be described by the model introduced in Sec. 2.4 with fluctuations among three substates. In this way, we must reinterpret our fitting and say that it provides numerical values for every rate constant, including the rescaled constants of reaction. Hence, $N \times k_{D_1} = 2.47s^{-1}$, $N \times k_{D_2} = 0.175s^{-1}$, $N \times k_{D_3} = 0.156s^{-1}$ for this system. These constants are effective rate constants and they may also include the saturation factor, given as the ratio of occupied active sites, predicted in Ref. [11].

The reader should notice the difference between the experimental data analyzed in this section and the data in Sec. 2.6. In this chapter we are considering constrained means and correlation plots as calculated from the single fluorescence trajectory reported in Ref. [51] (see Figs. 4.1 and 4.2), while we have previously analyzed constrained means for a collection of more than fifty trajectories and reported the average constrained means in Fig. 2.7. As we want to emphasize that the analysis of constrained mean dwell times and dwell-time correlation function only requires a single trajectory with a statistically mean-

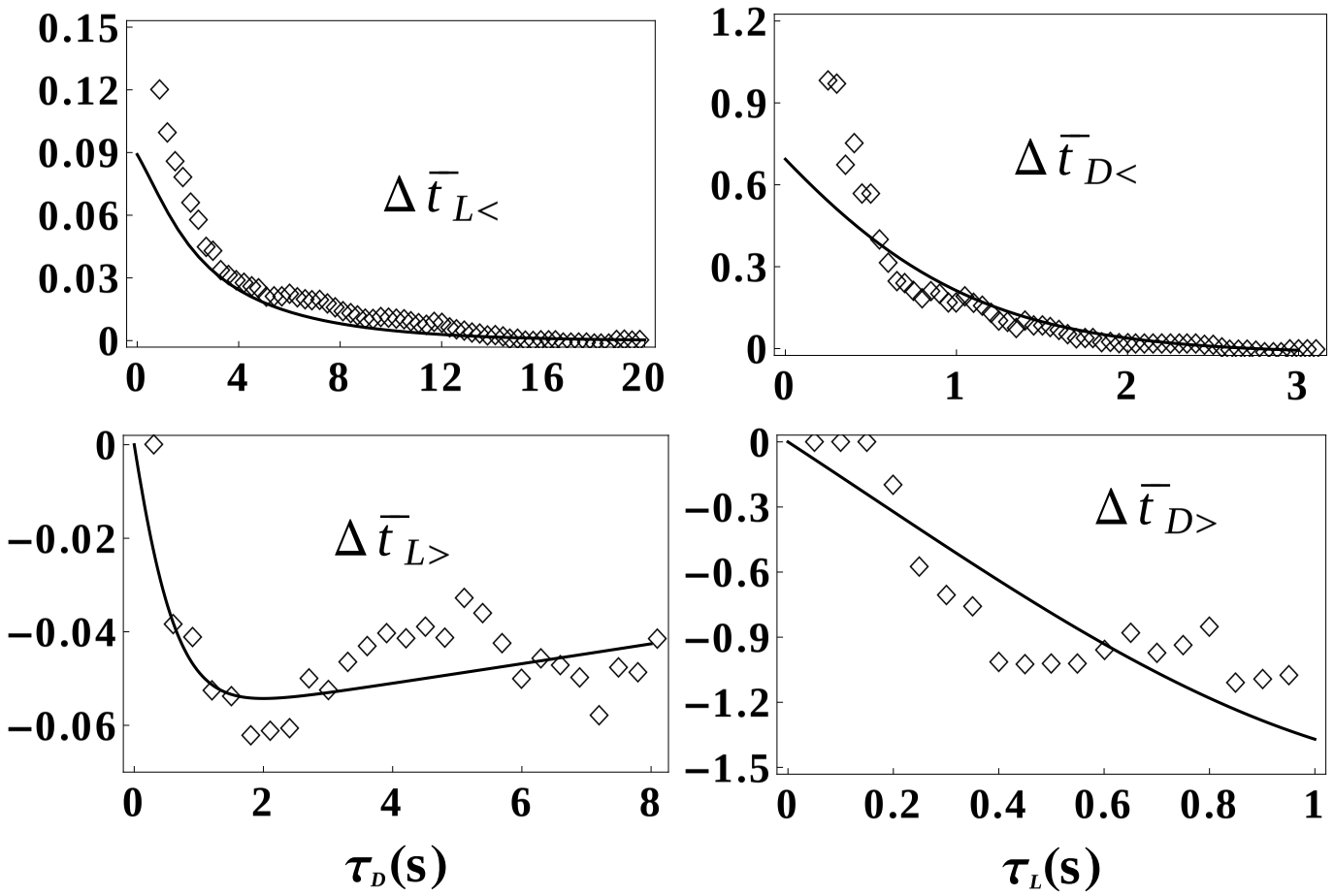

Figure 4.1: Experimental constrained mean dwell times for a 6 nanometer nanoparticle. Parameters for this model are $k_{D_1} = 2.47s^{-1}$, $k_{D_2} = 0.175s^{-1}$, $k_{D_3} = 0.156s^{-1}$, $k_{L_1} = 1.43s^{-1}$, $k_{L_2} = 2.80s^{-1}$, $k_{L_3} = 0.0766s^{-1}$, $d_{21} = 0.0043s^{-1}$, $d_{12} = 1.69 \times 10^{-4}$, $l_{12} = 0.045s^{-1}$, $l_{21} = 0.042s^{-1}$, $l_{23} = 0.040s^{-1}$, $l_{32} = 0.0185$, $d_{32} = 0.00018s^{-1}$ and $d_{23} = 0.012s^{-1}$. The last two internal rate constants were determined by detailed balance. Time is given in seconds.

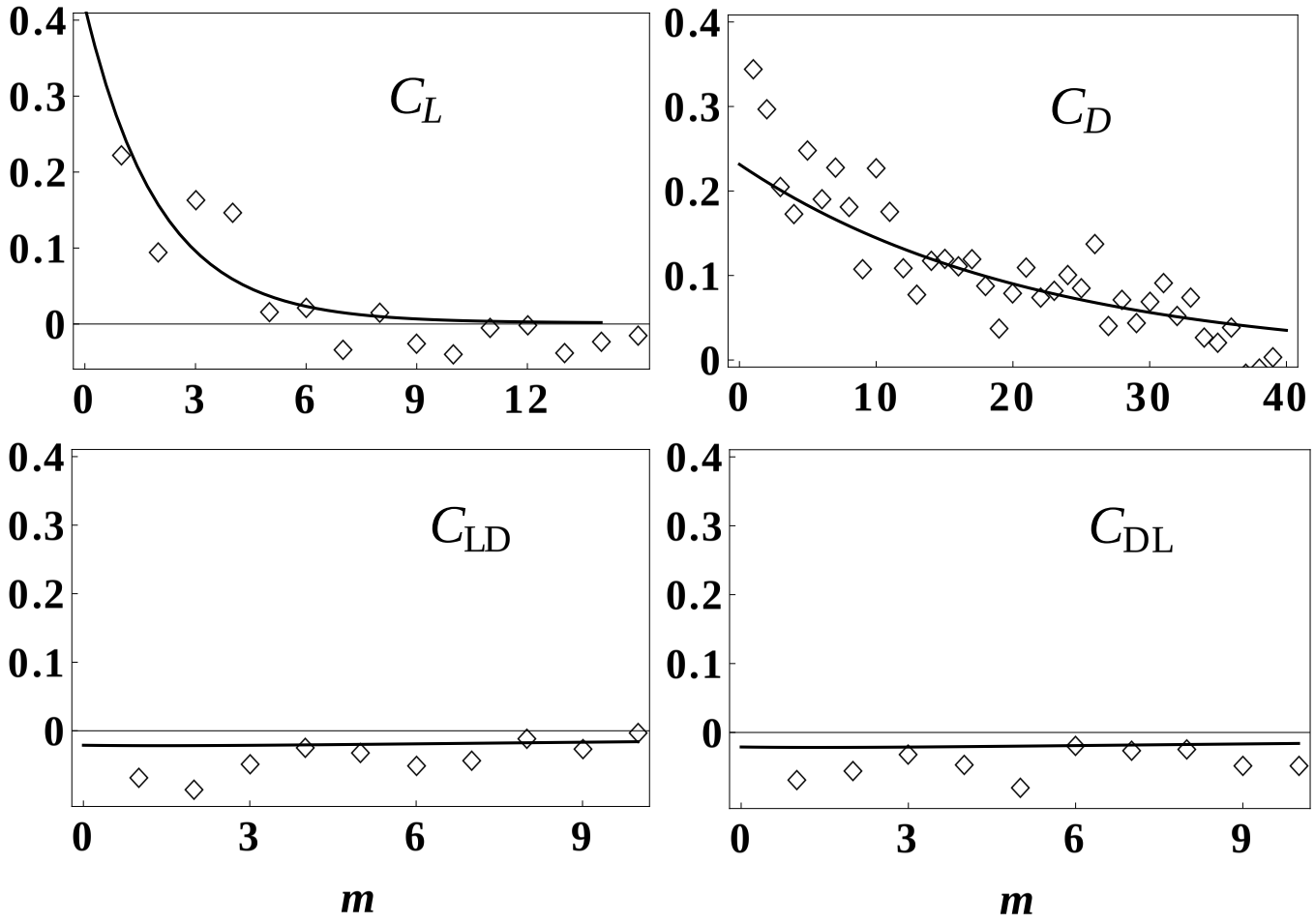

Figure 4.2: Experimental dwell time correlations for a 6 nanometer nanoparticle. Solid lines correspond to a fitted three channel model with parameters: $k_{D_1} = 2.47s^{-1}$, $k_{D_2} = 0.175s^{-1}$, $k_{D_3} = 0.156s^{-1}$, $k_{L_1} = 1.43s^{-1}$, $k_{L_2} = 2.80s^{-1}$, $k_{L_3} = 0.0766s^{-1}$, $d_{21} = 0.0043s^{-1}$, $d_{12} = 1.69 \times 10^{-4}$, $l_{12} = 0.045s^{-1}$, $l_{21} = 0.042s^{-1}$, $l_{23} = 0.040s^{-1}$, $l_{32} = 0.0185$, $d_{32} = 0.00018s^{-1}$ and $d_{23} = 0.012s^{-1}$.

ingful number of events; we have decided to study the trajectory measured from a single nanoparticle. This trajectory has about 800 turnovers, providing in this way a good sample for the calculation of constrained means and correlation functions. Moreover, the discussion in this section also applies to the data analyzed in Sec. 2.6. For instance, in Fig. 2.7 we noticed that $\Delta\bar{t}_{L>}$ decays much faster than $\Delta\bar{t}_{L<}$ to the respective asymptotic values. In light of the discussion in Sec. 3.6, we can still state that this is an indicator of correlation among active sites.

Rate constants for this model have been determined by an optimization strategy for large systems[27] that partitions the variables of the system into smaller subsets and optimizes one group at a time, while parameters in other subsets are unchanged during the optimization. This leads to a cascade of constrained minima that must approach to a local minimum. In every step, we minimized the sum of the squares of the offsets ("the residuals") of the predicted points from the experimentally measured values. Moreover, in order to avoid trapping in sub-optimal positions, we have introduced in the course of the optimization weighting coefficients that enhance the contribution to the minimization function of those experimental values that are more relevant in the determination of the qualitative properties of the fitted model. For example, in the case of C_L the experimental values at $m = 1, \ldots, 5$ are relevant to determine the decay that the fitted dwell-time correlation should have. Thus, we have multiplied the residuals for C_L at $m = 1, \ldots, 5$ by weighting factors that increment their contribution to the total function. As this optimization algorithm is sensitive to the way in which variables are distributed in the different subsets, we cannot guarantee that we have reached a global minimum. Our optimal model has been determined by starting with two partitions: a two channel system and an additional

channel. The initial set of parameters for the two-channel submodel was determined by fitting this subsystem to the constrained mean dwell times in Fig. 4.1, and the experimental C_D. Next, initial parameters for the third channel were assigned by fitting the whole set of unconstrained and constrained means, and also the time correlation functions, with the three-channel model that has the parameters for the previous two channel submodel included. These parameters are not allowed to change in the course of this optimization step. Once we have a complete set of initial values for rate constants, we redistribute the set of parameters into two different subsets and then repeat the previous strategy many times, until we reach a point in which no further minimization is possible even after considering all possible partitions of the set of variables.

4.2 Insights into the catalytic properties of a single nanoparticle

In this section we investigate how the optimal model described in Sec. 4.1 provides further insight into the dynamical heterogeneity observed in single nanoparticle catalysis. Internal rate constants in Fig. 4.1 and Fig. 4.2 are significantly smaller than the reaction and product desorption rate constants and we can say that this model is close to the static limit. In fact, as illustrated in Fig. 4.3 the static limit prediction for this model for the constrained mean dwell times, calculated according to Eq. (3.62) and Eq. (3.66) and displayed in dashed lines, is numerically correct. This observation validates the following analysis of the qualitative characteristics of the constrained means in terms of the pairwise decomposition introduced in Sec. 3.6, and summarized in Eqs. (3.61) and(3.65).

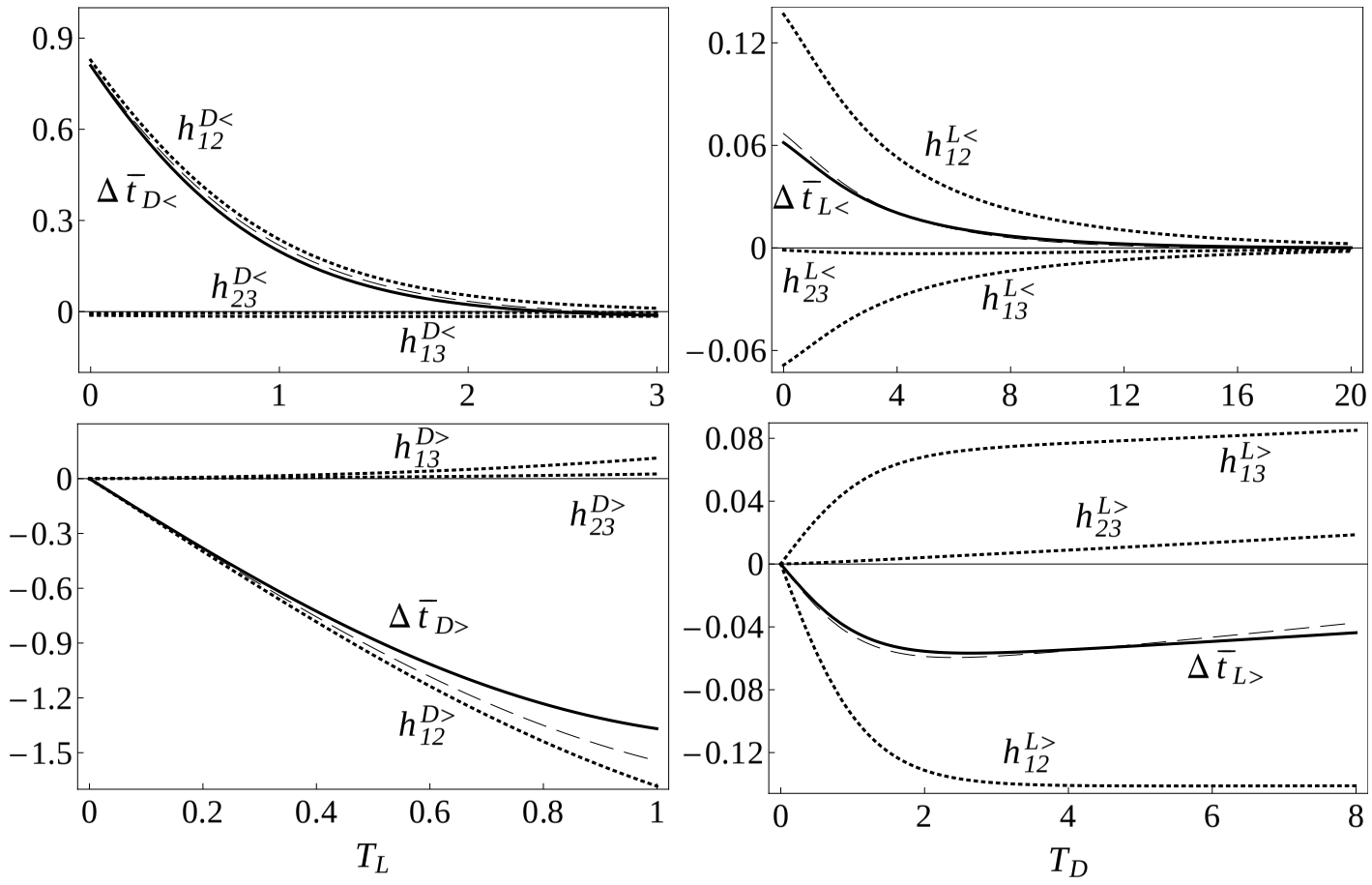

Figure 4.3: Decomposition of the predicted constrained mean dwell times into the independent contributions of pairs of channels. Solid lines correspond to a fitted three channel model with parameters $k_{D_1} = 2.47s^{-1}$, $k_{D_2} = 0.175s^{-1}$, $k_{D_3} = 0.156s^{-1}$, $k_{L_1} = 1.43s^{-1}$, $k_{L_2} = 2.80s^{-1}$, $k_{L_3} = 0.0766s^{-1}$, $d_{21} = 0.0043s^{-1}$, $d_{12} = 1.69 \times 10^{-4}$, $l_{12} = 0.045s^{-1}$, $l_{21} = 0.042s^{-1}$, $l_{23} = 0.040s^{-1}$, $l_{32} = 0.0185$, $d_{32} = 0.00018s^{-1}$ and $d_{23} = 0.012s^{-1}$. Dashed lines are the static limit prediction of each constrained mean for this set of parameters. Dotted lines represent contributions of every two-channel subsystem to the static limit prediction. Time is given in seconds.

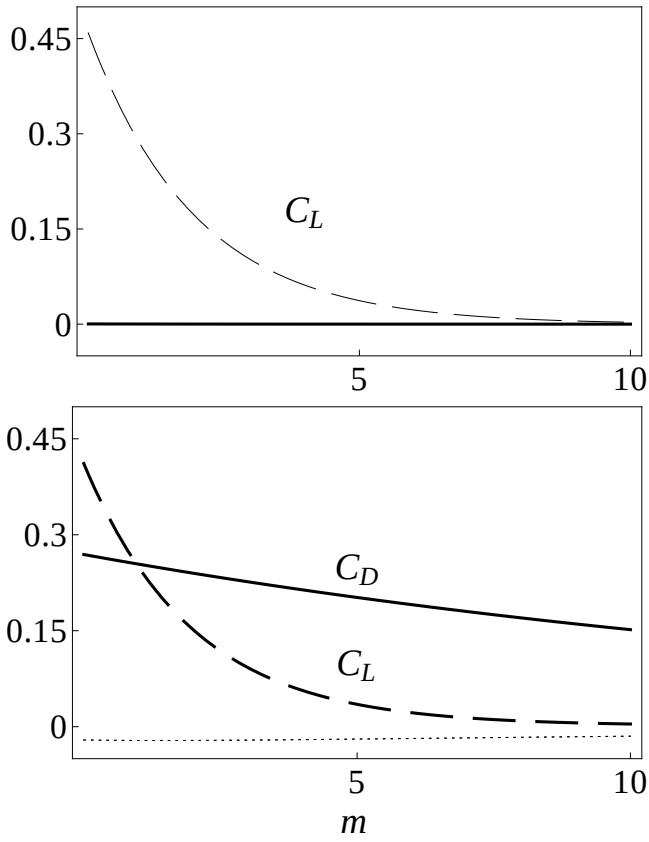

Figure 4.4: The top panel shows C_L (Dashed line) and C_D (Solid line) for the two-channel submodel composed of channels 2 and 3. This model exhibits small C_D, C_{LD} and C_{DL}. The bottom panel shows C_D (Solid line), C_L (Dashed line), C_{LD} (Dotted line) and C_{DL} (Dotted line) for the full three-channel model that is the result of expanding the model of the top by introducing a third substate with slow internal transformations to the two-channel subsystem. This model is the same as the one used to fit experimental data in Fig. 4.2. Parameters for this model are $k_{D_1} = 2.47s^{-1}$, $k_{D_2} = 0.175s^{-1}$, $k_{D_3} = 0.156s^{-1}$, $k_{L_1} = 1.43s^{-1}$, $k_{L_2} = 2.80s^{-1}$, $k_{L_3} = 0.0766s^{-1}$, $d_{21} = 0.0043s^{-1}$, $d_{12} = 1.69 \times 10^{-4}$, $l_{12} = 0.045s^{-1}$, $l_{21} = 0.042s^{-1}$, $l_{23} = 0.040s^{-1}$, $l_{32} = 0.0185$, $d_{32} = 0.00018s^{-1}$ and $d_{23} = 0.012s^{-1}$.

We observe that the behavior of $\Delta\bar{t}_{D<}$ and $\Delta\bar{t}_{D>}$ is dominated by the set of transformations taking place through the first and second channel, and that the third channel does not contribute significantly to these observables in the range of times that is experimentally accessible. Notice that these two channels correspond to the two fastest desorption paths (k_{L_1} and k_{L_2} are larger than k_{L_3}), and therefore they are responsible for the shorter light dwell times. In contrast, $\Delta\bar{t}_{L<}$ and $\Delta\bar{t}_{L>}$ have contributions from each one of the three channels, and the decay is dominated by both h_{12} and h_{13}. This is a consequence of the existence of two reaction paths, corresponding to channels two an three, that have reaction constants k_D that are very similar, namely, $k_{D_2} = 0.175s^{-1}$ and $k_{D_3} = 0.156s^{-1}$. This also implies that h_{12} and h_{13} have similar decay rates, both dominated by k_{D_1}, and that $\Delta\bar{t}_{L<}$ and $\Delta\bar{t}_{L>}$ behave as constrained functions for a two-channel system in the range of times that is experimentally accessible. These observations serve to justify why we were able to qualitatively describe with a two-channel model the complete set of constrained means for the same system in Chapter 2, Sec. 2.6. Put another way, the two-channel subsystem composed by channels one and two, have the minimum qualitative properties that would be required to describe the experimentally-measured constrained mean dwell times. In fact, the reaction rate constants for the second channel of the model described in this chapter are about the same to those obtained for the second channel in Sec. 2.6, and this statement also holds when we compare rate constants for the first channel in both models with the exception of the rate constant $N \times k_{D_1}$. However, the value determined for $N \times k_{D_1}$ is of the same order of magnitude in both models. Notice that this difference is also due to the difference in the data analyzed in each case.

Another interesting characteristic of this model is presented in Fig. 4.4, based

on the fitted correlation plots. Different decay rates in C_D and C_L are only possible in a system as big as a three-channel model. From our analysis in Sec. 3.4 and our finding in Fig. 4.4, we observe that C_L is dominated by reactions and desorptions that happen through channels two and three, which correspond to the fastest and the slowest desorption events. Moreover, C_D is small for the subsystem composed only by these two channels, and we can expect this since the numerical values of k_{D_2} and k_{D_3} are very similar. On the other hand, we observe that the first channel dominates the decay of C_D, as illustrated in the bottom panel of Fig. 4.4. In order to better appreciate this result, we now consider the analytic expressions for C_D and C_L derived from our optimal model

$$C_L(m) = 2.14\left(0.0015 \times 0.954^{m+1} + 0.319 \times 0.608^{m+1}\right) \tag{4.1}$$

$$\sim 0.683 \times 0.608^{m+1} \tag{4.2}$$

$$C_D(m) = 0.16\left(1.51 \times 0.954^{m+1} + 0.00082 \times 0.608^{m+1}\right) \tag{4.3}$$

$$\sim 0.243 \times 0.954^{m+1} \tag{4.4}$$

From here we observe that the two nontrivial eigenvalues are $\lambda_1 = 0.608$ and $\lambda_2 = 0.954$. As Fig. 4.4 suggests, the decay rate of C_L is dominated by the subsystem of channels two and three and we can use perturbation theory[1] to estimate the contribution of this subsystem to the decay of C_L as follows. If we let $\lambda_1^{(1)}$ be the first order correction to the eigenvalue λ_1 predicted in Sec. 3.4, then

$$\lambda_1^{(1)} = \left(1 + \frac{l_{23}}{k_{L_3}} + \frac{l_{32}}{k_{L_2}} + \frac{d_{23}}{k_{D_3}} + \frac{d_{32}}{k_{D_2}}\right)^{-1} \tag{4.5}$$

$$= 0.544, \tag{4.6}$$

from where we observe that $\lambda_1^{(1)}$ amount to about 90 % of the fitted value of λ_1.

[1] In this case, the perturbation parameter is dominated by the sum $l_{12}/k_{L_2} + d_{12}/k_{D_2} = 0.016$ corresponding to z_2 in Sec. 3.4.

Likewise,

$$\lambda_2^{(1)} = \left(1 + \frac{l_{21}}{k_{L_1}} + \frac{d_{21}}{k_{D_1}}\right)^{-1} \tag{4.7}$$

$$= 0.970 \tag{4.8}$$

differs from the fitted value for λ_2 by less that 1.7%. While we do not have a perfect separation into two different sets of rate constants and distinct functions for these two decays, the fact that we can understand C_D and C_L as manifestations of the dynamical properties of different groups of channels or reaction paths, leads us to the conclusion that the different decays of the autocorrelation plots, given by $1/m_D$ and $1/m_L$ are measurements of the relative time scales of two different internal process. This fact is better appreciated from Eq. (3.40) and Eq. (3.41), where such a difference in the $1/m_D$ and $1/m_L$ is determined to a first order, to wit,

$$\frac{1}{m_D^{(1)}} = \frac{l_{21}}{k_{L_1}} + \frac{d_{21}}{k_{D_1}} = 0.0160 \tag{4.9}$$

$$\frac{1}{m_L^{(1)}} = \frac{l_{23}}{k_{L_3}} + \frac{l_{32}}{k_{L_2}} + \frac{d_{23}}{k_{D_3}} + \frac{d_{32}}{k_{D_2}} = 0.838\ . \tag{4.10}$$

These values should be compared to those experimentally reported in Ref. [51] which are $m_D^{-1} = 0.0800$ and $m_L^{-1} = 0.385$.

These different internal transformations can then be interpreted as two different forms of surface reconstruction or, as two different processes that are induced on the nanoparticle by the substrate molecules, as they change from docking place. While Chen [51] has reported experimental evidence supporting the first idea, our model is not able to differentiate among these two scenarios.

4.3 Answers provided by this thesis to the questions posed in Chapter 1

We close this chapter by listing the answers to our research has found to the questions posed in Sec. 1.3.

1. The single-molecule kinetic theory developed by Cao[10] predicts that dwell-time density functions are multiexponential in the presence of internal transformations, such as conformational fluctuations or surface-reconstruction processes.
2. Constrained mean dwell times and dwell-time correlation functions are robust statistical indicators that can expose different but complementary information about the time scale and the number of internal processes that give rise to the memory effects observed in a single-molecule fluorescence trajectory.
3. Our qualitative analysis of the experimental constrained mean light dwell times for a nanoparticle of 6nm diameter led us to the conclusion that active sites on the surface of the nanoparticle are spatially correlated.
4. We have demonstrated that the decay rates of the light and dark dwell time autocorrelation functions in the absence of crosscorrelation, measure the relative time scale of two distinct internal process occurring on the nanoparticle surface. The time scale is found to be orders of magnitude smaller than the time scale associated transitions from a state of low to a high emission intensity.
5. While at this point our analysis do not let us determine a unique model for the quantitative description of the whole set of constrained means and

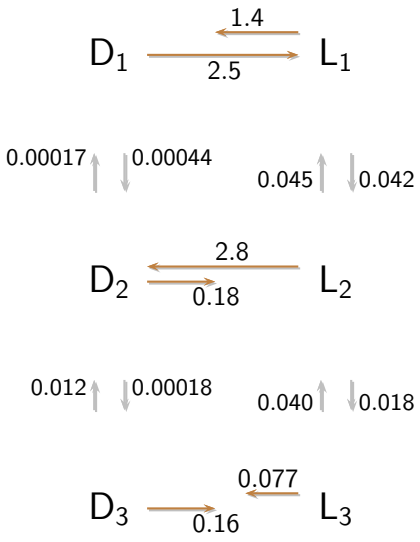

Figure 4.5: A kinetic scheme for the catalytic transformation of resazurin into resorufin on the surface of a gold nanoparticle of 6nm diameter. Parameters for this model are $k_{D_1} = 2.47s^{-1}$, $k_{D_2} = 0.175s^{-1}$, $k_{D_3} = 0.156s^{-1}$, $k_{L_1} = 1.43s^{-1}$, $k_{L_2} = 2.80s^{-1}$, $k_{L_3} = 0.0766s^{-1}$, $d_{21} = 0.0043s^{-1}$, $d_{12} = 1.69 \times 10^{-4}$, $l_{12} = 0.045s^{-1}$, $l_{21} = 0.042s^{-1}$, $l_{23} = 0.040s^{-1}$, $l_{32} = 0.0185$, $d_{32} = 0.00018s^{-1}$ and $d_{23} = 0.012s^{-1}$.

dwell-time correlation function; it is indeed possible to qualitatively characterize the kinetic scheme that must describe these statistical indicators for single nanoparticle catalytic process under substrate-saturating conditions. Our research has shown that the nanoparticle must fluctuate among at least three different substates and, fast product desorptions must happen through the same reaction path as slow activation processes and vice versa. We can then provide a kinetic scheme, with numerical values for every rate constant, that qualitatively describes all the properties that we found in the statistical indicators that we studied. As an example, Fig. 4.5

presents the kinetic scheme for the fitted model obtained in Sec. 4.1.

BIBLIOGRAPHY

[1] A.V. Akimov and A. Kolomeisky. Dynamics of Single-Molecule Rotations on Surfaces that Depend on Symmetry, Interactions and Molecular Sizes . *J. Phys. Chem. C*, 115:125–131, 2011.

[2] W. P. Ambrose, P. M. Goodwin, R. A. Keller, and J. C. Martin. Alterations of Single Molecule Fluorescence Lifetimes in Near-Field Optical Microscopy . *Science*, 265:364367, 1994.

[3] A. Ashkin, J.M. Dziedzic, J.E. Bjorkholm, and S. Chu. Observation of a single-beam gradient force optical trap for dielectric particles . *Opt. Lett.*, 11:288290, 1986.

[4] R. B. Bapat and T. E. S. Raghavan. *Nonnegative matrices and applications* . Cambridge University Press, New York, 1997.

[5] R. Bellman. *Introduction to Matrix Analysis* . SIAM, second edition, 1997.

[6] A. Berman and N. Shaked-Monderer. *Completely positive Matrices* . World Scientific, Singapore, 2003.

[7] E. Betzig and R.J. Chichester. Single Molecules Observed by Near-Field Scanning Optical Microscopy . *Science*, 262:14221425, 1993.

[8] S. M. Block, L. S. B. Goldstein, and B. J. Schnapp. Bead movement by single kinesin molecules studied with optical tweezers . *Nature*, 348:348352, 1990.

[9] F.L.H. Brown. Generating Function Methods in Single-Molecule Spectroscopy . *Acc. Chem. Res.*, page 0500281, 2006.

[10] J. Cao. Event-averaged measurements of single molecule kinetics . *Chem. Phys. Letts.*, 327:38–44, 2000.

[11] P. Chen, W. Xu, X. Zhou, D. Panda, and A. Kalininskiy. Single-Nanoparticle Catalysis at Single-Turnover Resolution . *chem. phys. lett.*, 470:151–157, 2009.

[12] C. Du and S. Kou. Correlation Analysis of Enzymatic Reaction of a Single Protein Molecule. *Ann. App. Stat.*, in press, 2012.

[13] G. Ertl. Dynamics of surface reactions . *Faraday Discuss.*, 121:1–15, 2002.

[14] D. Feldman and M. Fox. *Probability: the mathematics of uncertainty* . Marcel Dekker, INC., USA, 1991.

[15] M. Fisher and A. Kolomeisky. Molecular motors and the forces they exert . *Phys. A*, 274:24166, 1999.

[16] M. Fisher and A. Kolomeisky. The force exerted by a molecular motor. *Proc. Natl. Acad. Sci. USA*, 96:6597602, 1999.

[17] O. Flomenbom and R. J. Silbey. Utilizing the information content in two-state trajectories . *Proc. Natl. Acad. Sci.*, 103(29):10907–10910, 2006.

[18] F. R. Gantmacher. *Applications of the theory of Matrices*. Interscience publishers, Inc., New york, 1959.

[19] I. Gopich. and A. Szabo. Single-macromolecule fluorescence resonance energy transfer and free-energy profiles. *J. Phys. Chem. B*, 107:5058–5063, 2003.

[20] I. Gopich and A. Szabo. Statistics of transition in single molecule kinetics . *J. Chem. Phys.*, 118:454–55, 2003.

[21] K.-S. Han, G. Liu, X. Zhou, R. E. Medina, and P. Chen. How does A Single Pt Nanocatalyst Behave in Two Different Reactions? A Single-Molecule Study . *Nano Letters*, 12:1253–1259, 2012.

[22] G. Hummer and A. Szabo. Kinetics from nonequilibrium single-molecule pulling experiments. *Biophys J*, 85:5–15, 2003.

[23] R. Imbihl and G. Ertl. Oscillatory Kinetics in Hetergeneous Catalysis. *Chem. Rev.*, 95:697–733, 1995.

[24] J. Jansesen and R. Manca. *Applied semi-Markov processes.* Springer, USA, 2006.

[25] J. F. Kingman. *Poisson Processes* . Oxford university Press Inc., New York, 1993.

[26] S.S. Konyukhov, I.V. Kupchenko, A.A. Moskovsky, A.V. Nemukhin, A.V. Akimov, and A.B Kolomeisky. Rigid-Body Molecular Dynamics of the Fullerene-Based Nanocars on the Metallic Surfaces. *J. Chem. Theor. Comp.*, 6:2581–2590, 2010.

[27] S. L. Lasdon. *Optimization theory for large systems*. Dover Publication Inc., Mineola, New york, 2002.

[28] P. Lu and S. Xie. Single-Molecule Kinetics of Interfacial Electron Transfer Temperature. *J. Phys. Chem.*, 101:2753, 1997.

[29] P. Lu, L. Xun, and S. Xie. SingleMolecule Enzymatic Dynamics . *Science*, 282:1877, 1998.

[30] P. H. Lu and S. Xie. Single-Molecule Spectral Fluctuations at Room Temperature. *Nature*, 385:143, 1997.

[31] J.J. Macklin, J.K. Trautman, T.D. Harris, and L.E. Brus. Fluorescence intermittency in single cadmium selenide nanocrystals . *Science*, 272:255258, 1996.

[32] M. Marcus and H. Minc. *Introduction to linear algebra*. Dover publications, Inc., New York, 1965.

[33] M. Marcus and H. Minc. *A suvey of matrix theory and matrix inequalities* . Dover publications Inc., New York, 1969.

[34] W. E. Moerner and L. Kador. Optical detection and spectroscopy of single molecules in a solid . *Phys. Rev. Lett.*, 62:25352538, 1989.

[35] M. A. Ochoa, X. Zhou, P. Chen, and R. F. Loring. Interpreting single turnover catalysis measurements with constrained mean dwell times . *J. Chem. Phys.*, 135:174509, 2011.

[36] M. Orrit and J. Bernard. Single pentacene molecules detected by fluorescence excitation in a p-terphenyl crystal. *Phys. Rev. Lett.*, 65:27162719, 1990.

[37] Y. Peng, S. Xie, Y. Zheng, and F. L. H. Brown. Single-molecule photon emission statistics for systems with explicit time-dependence: generating function approach. *J. Chem. Phys.*, 131:214107, 2009.

[38] C. Joo S.A. McKinney and T. Ha. Analysis of single molecule FRET trajectories using hidden Markov modeling . *Biophys. J.*, 91(5):1941–1951, 2006.

[39] J. W. Shaevitz, S. M. Block, and M. J. Schnitzer. Statistical Kinetics of Macromolecular Dynamics . *Biophys J.*, 89(4):22772285, 2005.

[40] H. Shen, W. Xu, and P. Chen. Single-Molecule Nanoscale Electrocatalysis . *Phys. Chem. Chem. Phys.*, 12:6555–6563, 2010.

[41] S.B. Smith, Y. Cui, and C. Bustamante. Overstretching B-DNA: the elastic response of individual double-stranded and single-stranded DNA molecules . *Science*, 271:795799, 1996.

[42] G. A. Somorjai and J. Y. Park. Molecular Factors of Catalytic Selectivity . *Angew. Chem., Int. Ed.*, 47:9212–9228, 2008.

[43] B. C. Stipe, M. A. Rezaei, and W. Ho. Atomistic studies of O_2 dissociation on Pt(111) induced by photons, electrons, and by heating . *J. Chem. Phys.*, 107:6443–6447, 1997.

[44] J. Taylor, D. Makarov, and C. Landes. Denoising Single-Molecule FRET Trajectories with Wavelets and Bayesian Inference . *Biophys. J.*, 98:164–173, 2010.

[45] M. O. Vlad, F. Moran, F. W. Schneider, , and J. Ross. Memory effects and oscillations in single-molecule kinetics. *PNAS*, 99:12548–12555, 2002.

[46] J. Witkoskie and J. Cao. Single molecule kinetics I. Analysis of indicators . *J. Chem. Phys.*, 121:6361, 2004.

[47] S. Wunder, Y. Lu, M. Albrecht, and M. Ballauff. Catalytic activity of faceted gold nanoparticles studied by a model reaction: evidence for substrate-induced surface restructuring . *ACS Catalysis*, 1:908–916, 2011.

[48] S. Xie and R. C. Dunn. Probing Single Molecule Dynamics . *Science*, 265:361, 1994.

[49] W. Xu, J. S. Kong, and P. Chen. Probing the Catalytic Activity and Heterogeneity of Au-Nanoparticles at the Single-Molecule Level . *Phys. Chem. Chem. Phys.*, 11:2767–2778, 2009.

[50] W. Xu, J. S. Kong, and P. Chen. Single-Molecule Kinetic Theory of Heterogeneous and Enzyme Catalysis . *J. Phys. Chem. C*, 113:2393–2404, 2009.

[51] W. Xu, J. S. Kong, Y.-T. E. Yeh, and P. Chen. Single-Molecule Nanocatalysis Reveals Heterogeneous Reaction Pathways and Catalytic Dynamics . *Nature Materials*, 7:992–996, 2008.

[52] W. Xu, H. Shen, G. Liu, and P. Chen. Single-Molecule Kinetics of Nanoparticle Catalysis . *Nano Research*, 2:911–922, 2009.

[53] X. Xue, F. Liu, and O. Ou-Yang. Single molecule Michaelis-Menten equation beyond quasistatic disorder . *Phys. Rev. E*, 74:030902(R), 2006.

[54] S. Yang and J. Cao. Two-event echos in single molecule kinetics: A signature of conformational fluctuations . *J. Phys. Chem.*, 105:6535, 2001.

[55] S. Yang and J. Cao. Direct measurements of memory effects in single molecule kinetics . *J. Chem. Phys.*, 117:10996, 2002.

[56] C. G. Yin and Z. Qian. *Continuous Time Markov Chains and applications: A singular perturbation approach* . Springer-Verlag, New York, 1991.

[57] X. Zhou, N. M. Andoy, G. Liu, E. Choudhary, K.-S. Han, H. Shen, and P. Chen. Quantitative Super-resolution Imaging Uncovers Reactivity Patterns on Single Nanocatalyst . *Nature Nanotechnology*, 7:237241, 2012.

[58] X. Zhou, W. Xu, G. Liu, D. Panda, and P. Chen. Size Dependent Catalytic Activity and Dynamics of Gold Nanoparticles at the Single-Molecule Level . *J. Am. Chem. Soc.*, 132:138–146, 2010.

[59] R. Zwanzig. Dynamical disorder: Passage through a fluctuating bottleneck . *J. Chem. Phys.*, 97:3587, 1992.